Piezoelectric transformer based power converters; design and control

Rødgaard, Martin Schøler

Publication date:
2012

Document Version
Publisher's PDF, also known as Version of record

Technical University of Denmark

Martin Schøler Rødgaard

Piezoelectric transformer based power converters; design and control

PhD thesis, September 2012

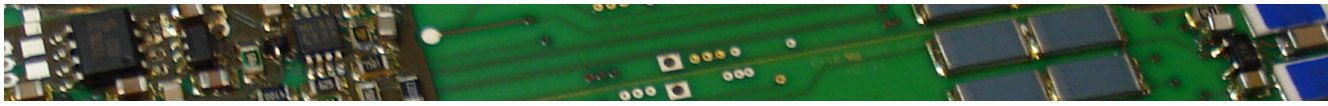

DTU Electrical Engineering
Department of Electrical Engineering

PhD thesis

Piezoelectric transformer based power converters; design and control

Author:
Martin Schøler Rødgaard

Supervisors:
Michael A. E. Andersen (*DTU*)
Erik Bruun (*DTU*)

Department of Electrical Engineering
Electronics Group
Technical University of Denmark
Ørsteds Plads
Building 348
DK-2800 Kgs. Lyngby
Denmark
`www.elektro.dtu.dk`
Tel: (+45) 45 25 38 00
Fax: (+45) 45 93 16 34

Preface

This PhD thesis is the culmination of my PhD project, which was carried out under the PhD school at DTU Elektro at the Technical University of Denmark in Kongens Lyngby and was conducted in the period of July 2009 to September 2012. The PhD project was funded by the Advanced Technology Foundation (HTF) and has been part of the HTF project "A miniature high-voltage piezoelectric power supply for driving a dielectric electro active polymer actuator", which was a joint research project between *Danfoss PolyPower A/S*, *Noliac A/S* and *DTU Elektro*, and the project has been carried out in close collaboration with involved parties.

During the PhD project a research visit at *Fairchild semiconductors* was carried out in Munchen, Germany.

During the PhD project I have had the pleasure to meet and discuss with many specialists in the field and I am grateful to all of those who has supported and helped me.

Acknowledgements

This project would never have been possible and I would never have managed to succeed, if I haven't had the support of the people around me and I would therefore like to extend my gratitude to the following people:

- My supervisors Prof. Michael A. E. Andersen and Prof. Erik Bruun, for their support, inspiration and encouragement, guiding me through the project.
- My colleagues of the "Electronics Group", especially Assoc. Prof. Ole Cornelius Thomsen, Ziwei Ouyang, Assistant Prof. Arnold Knott, Dennis Nielsen and Kaspar Sinding Meyer, for their valuable discussions and inspiration. And group secretary Henriette D. Wolff, for her kindly assistance and care.
- Thomas Andersen, with whom I have had a great collaboration and countless discussions regarding technical and non-technical matters, as well as I have enjoyed his company, he has always been good for a couple of laughs.
- The involved parties *Danfoss PolyPower A/S* and *Noliac A/S*, for a good and rewarding collaboration, especially Kim Lorenzen, Hans-Erik Kiil, Jean Bruland and Charles Mangeot.
- *Fairchild semiconductors*, especially Michael Weirich and Fredrik Jeppsson for making the research visit possible and supporting me through my stay.
- My family and friends, for their love, endless support, encouragements and indulgence during this endeavor.

Abstract

The last two decades of research into piezoelectric transformer (PT) based power converters have led to some extensive improvements of the technology, but it still struggles to get its commercial success. This calls for further research and has been the subject of this work, in order to enable the utilization of the PT technology advantages, reduce cost and increase competitiveness.

First of all an overview of the basic PT technology used in general power converters is given, including the basic piezoelectric nature, converter topologies and control methods. Compared to traditional magnetic technology based power conversion, the PT technology has some obvious advantages, being the electromechanical energy conversion, low EMI profile, a compact and low profile design, as well as a high potential of high efficiency and power density.

The utilized inductor-less half-bridge topology is investigated in detail, revealing its strong points, as well as some shortcomings. As a result of this investigation, a soft switching factor (ZVS factor) is derived, which describes the maximal achievable soft switching capability of the PT, as well as it is related to the structure of the PT, through the effective electromechanical coupling factors.

In order to exploit the advantages of the inductor-less half-bridge, research into soft switching optimized PT's has been conducted. Several innovative PT solutions have been proposed, simulated and optimized, using Finite Element Modeling (FEM) tools, all with the main goal of achieving soft switching capabilities. The proposed designs have been manufactured, tested and evaluated. The main achievement has been the development of an Interleaved interdigitated electrode (IDE) PT, which retains some of the easy manufacturing advantages, combined with the high efficiency of the thickness mode vibration.

The main focus of this research has been control methods, due to the high control requirements of PT based power converters and the inductor-less half-bridge, as well as the shortcomings of the prior-art solutions, and has led to several innovative solutions. A self-oscillating control method is proposed that has a very tight and precise frequency control, which ensures optimal and soft switching operation at all times. Furthermore a forward conduction mode control method is proposed, which resembles a PLL control and ensures a constant and optimal operation, as well as having the advantage of being purely primary side based. A revolutionary bi-directional control method is proposed, which utilizes active phase shift of the output rectifier that enables bi-directional power flow. Soft switching operation is maintained over the full power flow modulation range, ensuring optimal and efficient operation. Furthermore, it enables line and load regulation.

Dansk resumé

De sidste to årtiers forskning i Piezoelektriske Transformer (PT) baserede strømforsyninger har ført til omfattende forbedringer af teknologien, men teknologien kæmper stadig for at få sit kommercielle gennembrud. For at kunne udnytte fordelene ved PT-teknologien, reducere omkostningerne og øge konkurrenceevnen, er yderligere forskning på området påkrævet, hvilket har været formålet med dette arbejde.

Først og fremmest bliver den grundlæggende anvendelse af PT-teknologi i strømforsyninger gennemgået, herunder den grundlæggende piezoelektriske effekt, konverter topologier og kontrolmetoder. Sammenlignet med traditionelle magnetisk baseret strømforsyninger, har PT-teknologien nogle åbenlyse fordele, så som den elektromekaniske energikonvertering, lav udstrålet støj, et kompakt og lav-profil design, samt et stort potentiale for høj effektivitet og effekttæthed.

Der er blevet udført en dybdegående undersøgelse af den anvendte spole-løse halv-bro topologi, hvor dens styrker og svagheder bliver fremhævet. Et resultat af denne undersøgelse er udledelsen af en soft-switching factor (ZVS factor), som beskriver den maksimale opnåelige soft-switching evne for PT'en, såvel som den vil blive relateret til strukturen af PT'en igennem de effektive elektromekaniske koblingsfaktorer.

For at udnytte fordelene ved den spole-løse halv-bro, er der blevet forsket i soft switching optimerede PT'er. Ved hjælp af Finite Element Modeling (FEM) værktøjer er der opnået flere innovative PT-løsninger, som er simuleret og optimeret, alle med det primære mål at opnå soft-switching evner. De foreslåede designs er blevet produceret, testet og evalueret. Udviklingen af en Interleaved InterDigiteret Elektrode (IDE) PT er et af hovedresultaterne og bevarer nogle af de produktionsmæssige fordele, kombineret med den høje effektivitet ved anvendelsen af tykkelses mode vibrationer.

Forskningen i dette arbejde har primært været fokuseret på kontrolmetoder, på grund af de høje kontrolkrav til PT strømforsyninger og den spole-løse halv-bro, samt manglerne ved de nuværende løsninger, hvilket har ført til flere innovative løsninger. En selvsvingende kontrolmetode er blevet foreslået, som har en meget snæver og præcis frekvens kontrol, der sikrer optimal og soft-switching drift til enhver tid. Endvidere foreslås en forward conduction mode kontrolmetode, der minder om faselåst sløjfe kontrol og sikrer en konstant og optimal drift, der ydmere udelukkende er primærside baseret. Et revolutionerende tovejs kontrolmetode foreslås, som anvender aktiv faseforskydning af udgangsensretteren, hvilket muliggør tovejs effektflow. Soft-switching drift er endvidere sikre over hele effektflow modulationsområdet, hvilket sikrer optimal og effektiv drift. Endvidere muliggøres forsynings- og ballast-regulering.

Contents

Chapter 1

Introduction

1.1 Scope

The scope of this thesis is to present the research conducted during this PhD project, which was carried out at DTU Elektro. Most of the research has been presented and published as conference papers, journal papers and patent applications. The publications compose the major part of this thesis and are included in Appendix D and are referenced to as [D.1]-[D.9].

The objectives of this thesis is to complement and summarize the publications, providing a condensed and more complete overview of the research work and results obtained during this project.

1.2 Scope of project

As mentioned in the preface this PhD project is part of the Advanced Technology Foundation (HTF) project "A miniature high-voltage piezoelectric power supply for driving a dielectric electro active polymer actuator", which is a joint research project between *Danfoss PolyPower A/S*, *Noliac A/S* and *DTU Elektro*.

As the title reveals, the goal of the HTF project is to develop a miniature high voltage (HV) piezoelectric transformer (PT) based power converter, suited for driving a dielectric electro active polymer (DEAP) actuator. The DEAP actuator is a HV device (several kV's) and the HV interface is a drawback for general use due to safety concerns and regulations. The objective is to develop a miniature power converter, small enough to be integrated into the core of the DEAP actuator, forming a low voltage (24V) interfaced DEAP actuator and hence avoiding the HV interface and its challenges.
Furthermore, the use of magnetic components is avoided thus enabling the utilization of DEAP actuators in environments subjected to high magnetic fields, where magnetic components are exposed to saturation and malfunctioning. In addition, the elimination of the magnetic components potentially minimizes the component count of the power converter.

This PhD research is focused on the electrical part, being the PT based power converter, whereas *Danfoss PolyPower A/S* is researching on the DEAP actuator and

Noliac A/S researching on the PT. Furthermore, the PhD project has been focused on the control and operation of the PT based power converter, but has also involved development of PT's, as the PT is utilized as an electrical power component and is essential to the functionality and operation of the power converter.

1.3 Background and motivation

The field of electro active polymers (EAP) emerged as far back as 1880, but it is not until the early 1990s the technology really starts to evolve, demonstrating electro active properties far superior to previous EAP's [1]. EAP or DEAP devices are based on polymer materials and change shape as the result of electrostatic forces, when a voltage is applied. The shape change is proportional to the square of the applied voltage and the current technology requires a relative high voltage, in order to achieve a satisfying shape change. The DEAP devices are often referred to as "artificial muscles" and the technology is explained in more detail in section 2.2. Within the last decade new high performing and low cost DEAP materials have emerged that enables the commercialization of the technology, in products such as actuators for various mechanical components, like gripers and valves for example. But the technology is still dependent on a relative high applied voltage (several kV's), in order to fully utilizes the material and calls for high performing drivers, in order for the technology to reach its potential.

Conventional electromagnetic power converters are the only available HV sources to drive DEAP actuators, but they suffer from high and inconvenient parasitic (at high conversion ratios), have poor efficiency, are bulky and provide limited opportunities for miniaturization. The drawbacks of the electromagnetic transformer are pronounced at high conversion ratios and high voltage, where large creep distances and higher winding and inter winding isolation are required, which leads to bad magnetic coupling, large parasitic components and a bulky transformer.

The PT technology and PT based power converters emerged in the late 1950s, where C. Rosen was a pioneer and invented and patented the Rosen type transformer [2, 3]. Since then, the technology has evolved and there has been a lot of research in this field. The technology has struggled to get its commercial success, but in one application of high step-up and low power it has succeeded, namely for the power supply for cathode back-lighting for LCD displays [4, 5, 6]. But it is still limited to these simple applications of resistive high frequency AC loads. The PT is not limited by the same drawbacks as the electromagnetic transformer; on the contrary it excels at high step-up and high voltage applications. Furthermore, the PT based power converter is compact, has a low profile design and offers potentially high efficiency and power density, making it a perfect match for the DEAP technology.

As opposed to the cathode back-lighting for LCD displays, which is a DC/AC application, the DEAP actuator is a DC/DC application, with a controlled variable output voltage. The PT based DC/DC power converter is still somewhat immature. It has been treated a lot in the literature, but the commercial breakthrough has yet to come. With the high potential of the PT based DC/DC power convert, the partners have a clear vision of the unique and highly competitive solutions, which are achievable. This specific application takes advantage of the PT's strong points, at high step-up and high voltage, but it is envisioned that the research will contribute towards the development and commercialization of the PT based DC/DC power converter in general.

1.4 Project objectives

As described in Scope of project, the main objective is to develop a miniature high voltage PT based power converter, suited for driving a DEAP actuator. This PhD research is focused on the electrical part, the control and operation of the PT based power converter, but has also involved development of PT's and the research have the following main objectives:

- Research the PT based power converters in general, especially in relation to the inductor-less half-bridge topology, for DC/DC applications.
- The utilized inductor-less half-bridge has some obvious advantages, but it also introduces some new challenges, primarily related to the PT and the challenge of designing suitable PT. This demands a better understanding of the PT's properties, especially how native soft switching capability can be achieved and a investigation of the PT's properties and nature is performed in this study. Furthermore several suitable PT designs is proposed, manufactured, evaluated and utilized through the project.
- The capacitive nature of the DEAP actuator calls for a bi-directional power converter, in order to regenerate and reuse the electrically energy stored in the DEAP actuator. This is one of the main goals of this project and demands the research of bi-directional PT based power converters, topologies and control methods, as well as bi-directional enabling PT's.
- The research of control methods suited for soft switching optimized PT based converters is key. As the PT is operated close to its resonance frequency and is of very high quality factor, the band of optimal and efficient operation is very narrow, hence a tight control of the operating frequency is essential. Obviously the control methods should take advantage of the PT nature, as well as avert and/or compensate the challenging parts and shortcomings of its nature.

1.5 Thesis structure and content

The following flow chart illustrates the structure and content of the PhD thesis, starting out with the Introduction and Overview and State of the art. These introducing chapters are followed by the three main chapters, breaking down the subject to the PT based power converter, PT design and control methods. The thesis is finalizing with a conclusion and future work, providing a condensed and more complete overview of the research work and results obtained during this project. Most of the research has been published through conference papers, journal papers and patent applications. The publications are linked to the relevant chapters and sections, where some publications are relevant in more than one chapter.

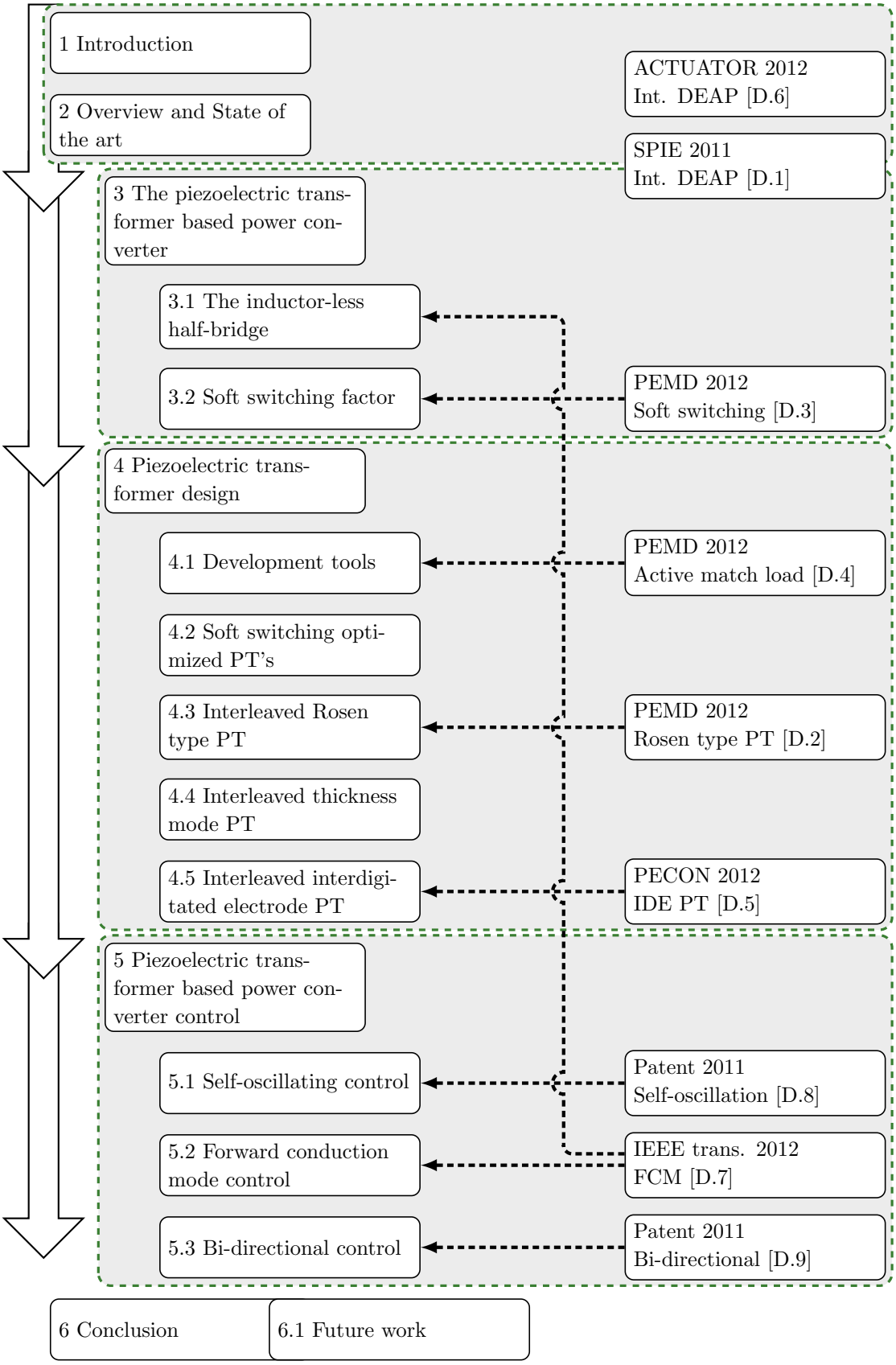
1 Introduction
2 Overview and State of the art
ACTUATOR 2012
Int. DEAP [D.6]
SPIE 2011
Int. DEAP [D.1]
3 The piezoelectric transformer based power converter
3.1 The inductor-less half-bridge
3.2 Soft switching factor
PEMD 2012
Soft switching [D.3]
4 Piezoelectric transformer design
4.1 Development tools
PEMD 2012
Active match load [D.4]
4.2 Soft switching optimized PT's
4.3 Interleaved Rosen type PT
PEMD 2012
Rosen type PT [D.2]
4.4 Interleaved thickness mode PT
4.5 Interleaved interdigitated electrode PT
PECON 2012
IDE PT [D.5]
5 Piezoelectric transformer based power converter control
5.1 Self-oscillating control
Patent 2011
Self-oscillation [D.8]
5.2 Forward conduction mode control
IEEE trans. 2012
FCM [D.7]
5.3 Bi-directional control
Patent 2011
Bi-directional [D.9]
6 Conclusion
6.1 Future work

Chapter 2

Overview and State of the art

In this chapter an overview of the topics of the study is given. Starting out with a description of the application itself, which is followed by an overview of the involved technologies, being the Electro Active Polymer, the Piezoelectric transformer and the available Control methods.

2.1 The application

As described in the Introduction, the objectives is to research a miniature high voltage PT based power converter, suited for driving a DEAP actuator and the application is also described in general in [D.1][D.6]. The challenge is to drive a highly capacitive DEAP load, which is described in further detail in the following sections, with the objective of performing a controlled voltage modulation of the DEAP load, to voltages as high as 2.5 kV. Figure 2.1 illustrates a conceptual block diagram of the application and the power converter, and as it can be seen the driver is supplied from a 24 V DC line, giving it a very high step-up conversion ratio of more than 100.

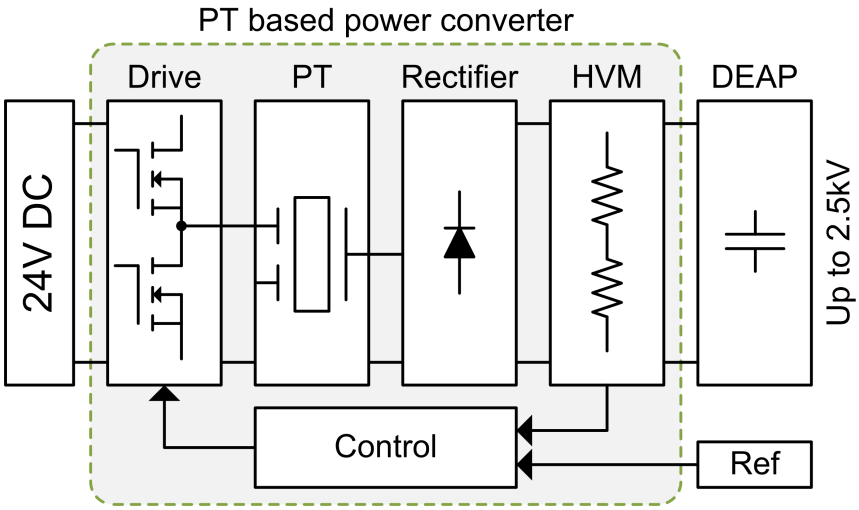

Figure 2.1: Conceptual block diagram of the PT based DEAP driver, initially without bi-directional power flow support. Composing a MOSFET based driver, the PT, a output rectifier, a control circuit and a high voltage measurement (HVM) circuit.

The driver is to be controlled by an external reference voltage that is related linearly to the output voltage. The DEAP actuator displacement or stroke is directly proportional to the square of the applied voltage, so by applying a specific voltage of up

to 2.5 kV, a desired stroke by the actuator can be achieved, which is the essence of an actuator.

The control of the driver should ensure a optimal operation of the PT, maximizing efficiency and power conversion, as well as it compares the reference voltage and the output voltage, which is obtained through a high voltage measurement (HVM) circuit. The high impedance and capacitive nature of the DEAP makes it quite difficult to measure the voltage, without discharging and dissipating the electrical energy of the DEAP. A very high impedance HVM circuit is needed and the circuit considerations and design is described and discussed in [D.1]. The DEAP actuator itself is a coreless cylindrical structure, having an outer and inner diameter of approximately 32 mm and 13 mm, it is 110 mm high and is illustrated in Figure 2.2. It is intended that the driver should be so small that it fits inside the cylindrical DEAP actuator, giving it at low voltage interface, essentially making it a low voltage device. The low voltage interface will make the device much more applicable and practically useful, as all the high voltage concerns are contained inside the device. Figure 2.3 illustrates a conceptual drawing of the driver integrated in to the DEAP actuator, as a matter of fact, the illustrated driver is one of the developed prototype PT based drivers [D.1,D.6] and the full schematic can be found in

Figure 2.2: Danfoss PolyPower cylindrical DEAP actuator (110 mm x 32 mm).

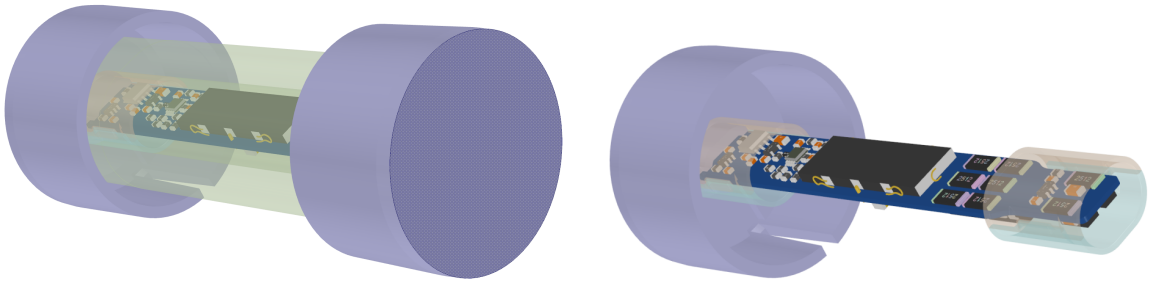

Figure 2.3: Illustration of the DEAP actuator with integrated driver (left) and the integrated driver (right). The actuator has a height/length of 110 mm and an outer and inner diameter of approximately 32 mm and 13 mm.

Appendix B. As the illustration reveals, the space for the driver is very limited and leads to quit high requirements for minimization, as well as pushing the limits of high voltage clearance and routing in the electrical circuits.
As the DEAP actuator is a highly capacitive load, with very low leakage, the power requirement of the driver is more a consideration of how fast the DEAP actuator should respond. Initially, a 30 ms response from relaxation to full stroke was desired (0 V to 2.5 kV) and with a capacitance of approximately 110 nF, an average power of 11.5 W is required.

11.5 W at 2.5 kV translate into a very small current (4.6 mA), which challenges the design in terms of high output impedance and potential high impact of parasitic components on the output side. Furthermore, the high voltage and impedance pose a challenge if any level-shifting is needed, such as gate signal to a high-side switch. The major part of the energy supplied to the DEAP actuator is stored as electrical energy and only a small part is converted to mechanical work (2-5 %). To date, the stored electrical energy is just dissipated when the DEAP actuator is discharged and if this electrical energy could be regenerated, the overall performance could be greatly improved. Achieving energy recovery is one of the main goals and challenges of this project and can be achieved by having two converters, one for each direction or by having a bi-directional power converter. To date, no bi-directional PT based power converter exists and it will be applicable and have a huge potential in various other applications.

Concerning the efficiency of the drive, the unique features of the PT is expected to improve the efficiency compared to a magnetic solution and in general as a high efficiency as possible is desired. And in relation to the energy recovery, it is desired to recover 90 % of the DEAP actuator stored electrical energy, which leads to a required driver efficiency of at least 90 %.

From an electrical point of view, the driver has the following main specification:

- 24 V input voltage.
- Up to 2.5 kV controllable output voltage.
- Up to 11.5 W average output power.
- An efficiency of at least 90 %.
- Bi-directional power flow and/or energy recovery.
- Avoid magnetic based components.

2.2 Electro Active Polymer

The field of electro active polymers (EAP) emerged as far back as 1880, where Wilhelm Röntgen designed an experiment, testing the effect of an electrical current on the mechanical properties of a rubber band [1, 7]. In the early 1990s, the technology really started to evolve, demonstrating electro active properties far superior to previous EAP materials and within the last decade new high performing and low cost EAP materials have emerged, enabling the commercialization of the technology. EAP's consist of two electrodes and an intermediate material (polymer) and based on their activation mechanism, there are two general types of EAP's: Electronic EAP's and Ionic EAP's [1, 7, 8, 9].

Electronic EAP's are driven by Coulomb forces, and includes electrostrictive, electrostatic, piezoelectric and ferroelectric forces. This type of EAP materials change shape as the result of the electrical field strength, when a voltage is applied to the electrodes and they can be made to hold the induced displacement. However, they require a high activation field (>100 V/μm) that may be close to the breakdown level of air, as well as it pose challenges to generate and handle voltages as high a 2-10 kV.

Ionic EAP's are materials that involve mobility or diffusion of ions, and includes gels, polymer-metal composites, conductive polymers and carbon nanotubes. The activation voltage of the Ionic EAP is much lower than Electronic EAP and can be as low as 1-2 V, but the disadvantages are that they need to maintain wetness and they pose difficulties to sustain constant displacement under activation.

As the EAP construction resembles a simple plate capacitor, this type of load is also highly and almost purely capacitive, seen from an electrical point of view. EAP devices are often referred to as "artificial muscles", as the polymer material is flexible and tensile compared to traditional mechanical actuators and is comparable to the biological muscle.

2.2.1 Dielectric Electro Active Polymer

Dielectric electro active polymer (DEAP) is an Electric EAP materials and the operational principle is quite simply to explore the electrostatic force in between two electrodes, inducing a deformation of the intermediate material. The pressure on the material generated by the electrostatic force is described by Maxwell pressure (2.1), where the pressure p is proportional to the square of the electrical field strength E, and is dependent on the permeability of the material ϵ_r.

$$p = \epsilon_0 \epsilon_r E^2 \tag{2.1}$$

The intermediate material is a soft dielectric polymer, which is soft enough for the electrostatic force to be comparable to the spring force of the material, allowing

a deformation of the material. Figure 2.4 illustrates the basic DEAP structure, consisting of two electrodes placed on each side of a thin dielectric polymer film. As it can be seen, the polymer film is squeezed thinner when a voltage is applied,

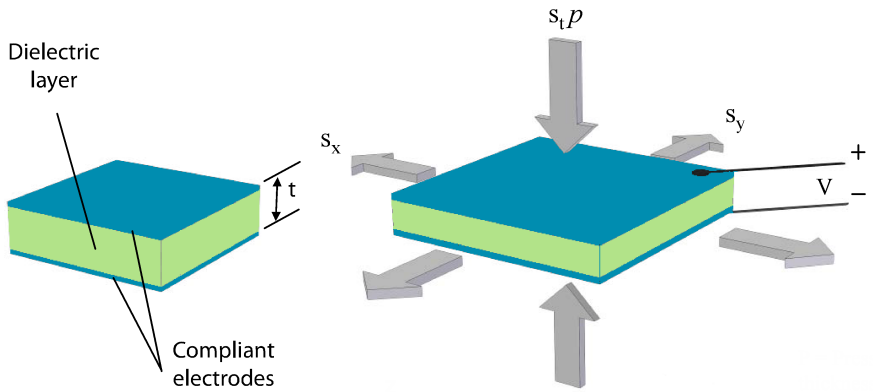

Figure 2.4: Basic DEAP structure, in relaxation with no voltage applied (left) and in deformation with a DC voltage applied (right).

which results in a deformation and elongation of the polymer film in the directions perpendicular to the electrical field. The thickness squeeze or strain is dependent on Young's modulus Y and is inversely proportional to the applied pressure (2.2).

$$S_t = \frac{-p}{Y} = \frac{-\epsilon_0 \epsilon_r E^2}{Y} \tag{2.2}$$

Both the thickness reduction and the elongation can be utilized, but the elongation is more pronounced as the polymer film is very thin, where there are no really limits of the length or size of the film. A very thin film is desirable, as the thinner the film is, the lower an applied voltage is needed, in order to obtain the required electrical field. Some other desired properties of the polymer are a high insulation and high breakdown voltage. A high insulation ensures a low leakage current and minimizes the electrical loss. A high breakdown voltage enables the use of high electrical fields, which is very desirable since the higher an applied field the higher an generated electrostatic force.

2.2.2 Danfoss PolyPower DEAP actuator

The DEAP actuator developed by *Danfoss PolyPower A/S* is based on a DEAP material as described in the previous section, with some unique features, which greatly improves performance and eases production. The PolyPower DEAP is based on a silicone dielectric material, it has a corrugated surface and metallic electrodes. The metallic electrode is very stiff in comparison to the silicone material and the electrostatic force, and does not allow the silicone to deform and elongate. But with the PolyPower patented corrugated surface [10, 11, 12, 13, 14], the DEAP structure is

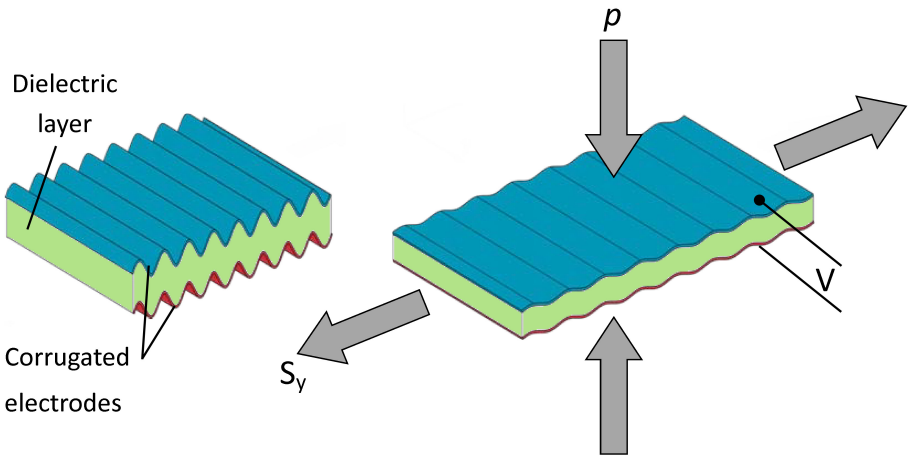

Figure 2.5: Danfoss PolyPower DEAP material, in relaxation with no voltage applied (left) and in deformation with a DC voltage applied (right).

compliant in one direction, allowing the silicone to deform and elongate, as illustrated in Figure 2.5. The corrugated surface does not only enable the silicone to deform, but it also forces the elongation in one direction, as the electrode still is stiff in the other direction. This increases the performance further by doubling elongation, as a result of the silicone being limited to expand in only one direction and the strain (2.2) is directed directly in this direction. Furthermore, the DEAP material is easy to manufacture, where a thin single side silicone sheet if formed during a roll coating process, typically as thin as 40 μm. This single side silicone sheet has a corrugated surface structure, on which a thin electrode is applied (100 nm range). Two of these sheets with electrodes are then laminated together, forming a DEAP film, having two electrodes with corrugated surfaces in the same direction.

PolyPower DEAP unique features:

- Extremely low electrical losses.
- Uni-directional elongation, due to the corrugated surface.
- High breakdown voltage of 40 kV/mm, allowing applied electrical fields of up to 31 kV/mm.
- Very robust; suitable for demanding industrial applications.
- Scalable roll-to-roll volume manufacturing made possible.

With a DEAP film thickness of 80 μm, the film can withstand a voltage of 2.5 kV and will produce up to 2% ellongation of the material [10, 11, 12, 13, 14]. The DEAP actuator is buildup by wounding two layers of film around a collapsible winding mandrel, forming a cylindrical actuator as illustrated in Figure 2.6. The coreless DEAP

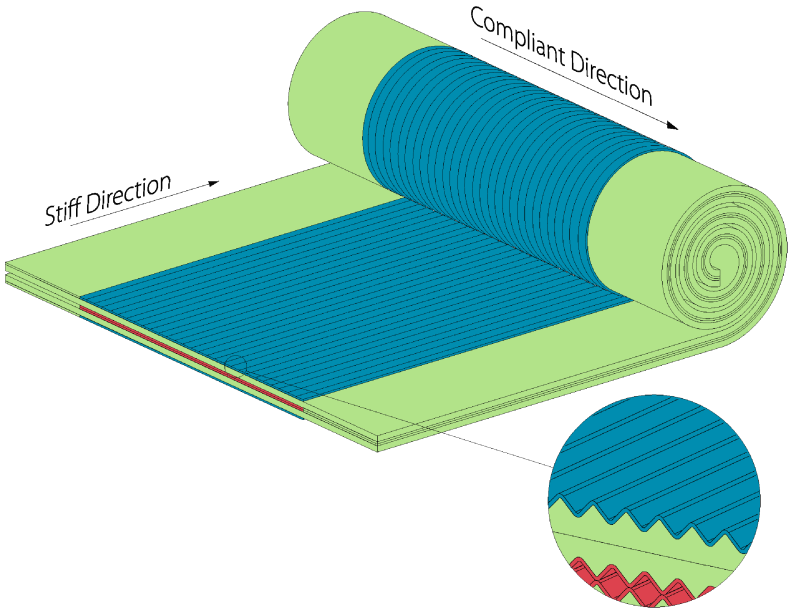

Figure 2.6: Danfoss PolyPower coreless DEAP actuator build-up, consisting of 0.1x7 m, 80 μm DEAP film.

actuator is wounded from 7 m of DEAP film and the structure is self-supporting. The final device is illustrated in Figure 2.3 and has an outer and inner diameter of approximately 32 mm and 13 mm and a height of 110 mm. The film has a height of 100 mm and have 2x20 mm of inactive area, where only one electrode is present, in order to make the electrical connections, as well as ensuring isolation between the two electrodes.

PolyPower DEAP actuator specifications:

- 110 mm high and a outer diameter of approximately 32 mm.
- Build-up of 0.1x7 m, 80 μm PolyPower DEAP film.
- Electrically highly capacitive, with a capacitance of approximately 110 nF.
- Rated for voltages of up to 2.5 kV.
- Maximal force of 7 N or maximal elongation of 1.1 mm (1.7%).

2.3 Piezoelectric transformer technology

In the late 1950s C. Rosen invented the first PT [2, 3], which was named the *Rosen type PT* after him. He was a pioneer within PT technology and PT based power converter, and since then there has been a lot of research in this field and as a result the technology has also evolved a lot. The technology has struggled to get

its commercial success, but in one application of high step-up and low power it has succeeded, namely for the power supply for cathode back-lighting for LCD displays [4, 5, 6]. But as the LCD display has evolved away from the PT based converter, it is mainly only commercially available for special low yield applications. The PT based converter is still somewhat limited to these simple applications of resistive high frequency AC loads. The pending challenge is to enable usage of PT based converters in DC/DC applications, in low voltage applications, as well as it is desirable to increase the power level above 5-10 W. The PT is not limited by the same drawbacks as the electromagnetic transformer and has some clear advantages, which is especially pronounced in high step-up and high voltage applications.

2.3.1 Piezoelectricity

The word *piezoelectricity* means electricity resulting from pressure and was discovered in 1880 by the French physicists Jacques Curie and Pierre Curie [15]. The piezoelectric effect is an interaction between the mechanical and the electrical state in crystalline materials, such as crystals and ceramics, giving them an electromechanical coupling. Through the direct piezoelectric effect an electrical charge displacement is generated as a resulting of an applied mechanical force [15, 16, 17, 18, 19, 20, 21]. The piezoelectric effect is reversible and through the reverse piezoelectric effect mechanical strain is generated as a resulting of an applied electrical field. The generated mechanical strain is typically very small and for lead zirconate titanate (PZT) based materials it is approximately 0.1 % [15], but they have a very precise positioning and can generate large forces. Furthermore piezoelectric devices are one of the few devices which can carry out mechanical work at very low temperatures (close to 0^o K).

During World War I, piezoelectric devices found its first practical application, with the development of sonar. The sonar system utilized piezoelectric quartz crystals as the transducer, which generates a sound wave pulse that would be reflected by a submerged submarine. By measuring the time of the sound wave travel, the distance to the object can be calculated.

In newer times, new and high performing piezoelectric materials have been developed, such as the PZT based materials. It has found its usage in various applications, such as actuators with the qualities of being very precise and rapid, for application like fuel injectors, loudspeakers and piezoelectric motors. Through the direct piezoelectric effect, it has found its usage as positioning and vibration sensors. One of the most widespread utilization of piezoelectricity is crystal oscillators, which is present in a lot of electronic applications, such as radios, digital circuits and microprocessor circuits, where a precise clock frequency is needed.

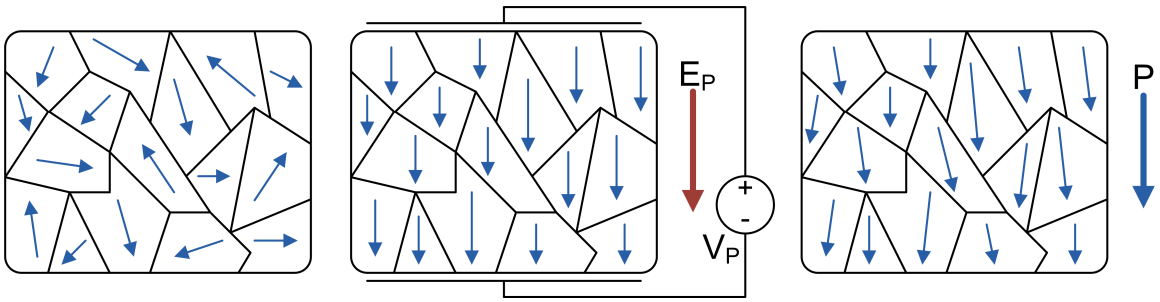

(a) Unpolarized crystals. (b) Polarization process. (c) Polarized crystals.

Figure 2.7: Polarization of piezoelectric material, where the blue arrows indicate the polarization direction.

Polarization

The direction of the piezoelectric effect is related to the direction (polarization) of the electric dipole moments in the piezoelectric material and dipoles near each other tend to be aligned in regions called domains. When a piezoelectric material is heated above a certain temperature, it loses its polarization, which is called the Curie temperature [15, 17, 18, 22]. The material restores its polarization when the temperature drops below the Curie temperature and if no external electrical field is applied, the domains are polarized randomly. In single domain structures, the piezoelectric effect can be observed and excited externally. But in multi domain structures, the random polarization results in a total dipole moment of zero, which results in no piezoelectric effect that can be observed or excited on macro scale. Figure 2.7(a) illustrates the random polarization of a multi domain structures, but by applying a high external electrical field (usually at elevated temperatures), the domains can be forced in one direction, as illustrated in Figure 2.7(b). After the polarization process, all the domains are aligned in one direction, giving the structure a total non-zero dipole moment, as illustrated in Figure 2.7(c). The polarization field strength is several decades higher than what the material usually is operated under, but the material can be de-polarized or re-polarized (total dipole moment), when exposed to high fields or high stress.

2.3.2 The piezoelectric transformer

The PT is basically just two piezoelectric elements joined together, forming a joined transformer structure. The operational principle is that the primary element or section of the transformer is excited by an electrical AC voltage, which induces a deformation of the joined structure. The deformation of the secondary element or section will generate a charge displacement and an electrical output voltage. And through the PT design (structure, section size, layer thickness), a desired voltage conversion can be achieved, matching a specific load and application. PT's are built from piezoelectric ceramics, such as the PZT based ceramics [19, 20], and are build-

up utilizing tape casting technology [17, 18], which is the same technology used for building multilayer ceramic capacitors. Figure 2.8 illustrates the three most common PT types, which utilizes three different structures, as well as electromechanical couplings [16, 17, 18, 19, 20]. The electromechanical coupling is a measure of how strong the piezoelectric effect is and relates the mechanical stored energy to the applied electrical energy or the other way around. The square of electromechanical coupling expresses the fraction of the electrical energy converted in to mechanical energy (2.3) or the other way around [16, 17, 18, 19, 20].

$$k^2 = \frac{W_{mechanical\ stored}}{W_{electrical\ applied}} \quad or \quad k^2 = \frac{W_{electrical\ stored}}{W_{mechanical\ applied}} \tag{2.3}$$

In order to obtain an efficient transmission of the mechanical energy from the primary to the secondary section, the PT is operated in one of its resonance modes [4, 22, 23, 24, 25, 26, 27, 28]. The PT resonates each time it is possible to generate a standing acoustical sound wave in the structure. In a resonance mode the two sections are well mechanical coupled, in terms of transferring mechanical energy, as the primary section is capable of exciting the resonance of the joined structure. As one can imagine, an excitation at low frequency (close to DC), the primary section will just move the secondary section, without deforming and inducing any charge displacement. Furthermore the PT is typically optimized for one specific resonance mode, in order to achieve the highest efficiency [4, 22, 23, 24, 26, 27, 28]. In this manner, electrical energy is converted through the electromechanical domain, which has some advantages and disadvantages.
PT main advantages and potentials:

- Electromechanical energy conversion.
- No magnetic field generation, as well as immunity to magnetic fields.
- Low EMI profile, due to the nature of resonance converter and soft switching.
- Potential high efficiency and power density.
- Potential low price, due to simple build-up and manufacturing utilizing tape casting technology [17, 18].

PT main drawbacks:

- Best suited for constant resistive AC loads.
- Mechanical mounting of PT, without restricting the free mechanical movement.
- Low thermal conductivity of ceramics, limiting heat dissipation.
- Limited current carrying capacity, due to thin electrodes.
- Limited to lower power levels (<100 W), due to physical and efficiency limitations [21, 29].

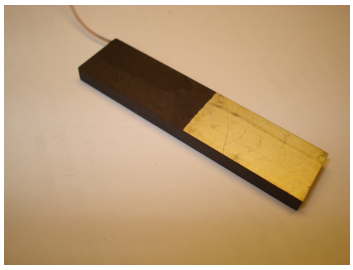

(a) Rosen type PT.

(b) Radial mode PT.

(c) Ring shaped Thickness mode PT.

Figure 2.8: Three different types of PT's, utilizing three different operation principles and electromechanical couplings.

Rosen type PT

In the classical Rosen type PT [2, 3, 30, 31, 32] (Figure 2.8(a)), the primary and secondary sections each occupy half of the rod shaped PT. The operational resonance is along the longitudinal direction, where a standing sound wave occurs in the length of the rod. The primary section is polarized perpendicular to the direction of the vibration, which is the transverse mode electromechanical coupling k_{31} and the section can be configured with several layers. The secondary section is polarized in the same direction as the vibration, which is the thickness mode electromechanical coupling k_{33} and it has only one layer. It can be operated in its first mode shape, with a standing half wave sound wave, but also its second mode shape, with a standing full wave sound wave.

Radial mode PT

In the radial mode PT [26, 33, 34, 35, 36, 37, 38] (Figure 2.8(b)), the primary and secondary sections occupy a certain part in the height of the disc shaped structure, which can be configured with several layers. It is operates in the radial mode, where a standing sound wave occurs across the element. It is operated in its first mode shape of a standing half wave sound wave and is generated through the planar mode electromechanical coupling k_p.

Thickness mode PT

The thickness mode PT [39, 40, 41, 42, 43, 44, 45, 46, 47] (Figure 2.8(c)) operates in the thickness mode, where a standing wave occurs in the hight of the element and the same direction as the polarization. The primary and secondary sections occupy a certain part in the height of the structure, which can be configured with several layers. It is usually, but not limited to, operated in its first mode shape of a standing half wave sound wave and has a significant higher resonance frequency, due to the small thickness. The thickness mode electromechanical coupling k_{33} is approximately

twice as large as the transverse mode k_{31}, which gives it a much higher potential for high efficiency and high power density.

2.3.3 Modeling of piezoelectric transformers

The electromechanical structure of the PT resembles a distributed network and one of the most used PT models is the lumped parameter model, which was derived by Mason in 1946 [22, 24, 26, 27, 28, 48]. The lumped parameter model is illustrated in Figure 2.9 and describes the behavior of the PT in a narrow band around the resonance mode of interest. For simplicity and mathematical representation, normally only the resonance mode of interest is included in the model, but the model can represent several resonance modes, by adding branches of each resonance mode [22, 24, 26, 27, 28]. However the resonance mode of interest is usually the most pronounced mode, as the design is optimized for this mode, and in practice a modeling of a single mode is sufficient. The model is basically an electrical LCC resonance tank and

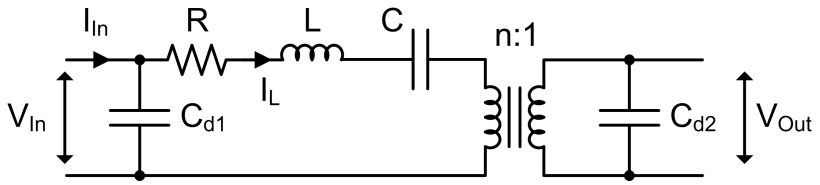

Figure 2.9: Lumped parameter model, which describes the behavior of the PT in a narrow band around the operating resonance mode.

describes the mechanical resonance circuit. The behavior of a PT based converter is also quite similar to a traditional resonance converter [49]. As the PT is operated close to the resonance frequency and the PT resonance is of very high quality, the band of optimal and efficient operation is very narrow [22, 23, 24, 26, 27, 28, 50, 51], which is expanded further in section 3.2. In order to maximize the power transfer of the resonance tank, the load is usually matched to the output capacitance C_{d2} of the PT, or the other way around (2.4) [24, 26, 27, 49].

$$R_{match} = \frac{1}{C_{d2}\omega_r} \quad \Rightarrow \quad C_{d2} = \frac{1}{R_{match}\omega_r} \tag{2.4}$$

Model parameter determination

The lumped parameters can either be calculated from its dimensions and material parameters for some of the known PT types [24, 26, 30, 32, 36, 38, 45, 52, 53] or be determined from a impedance measurements or simulations [25, 53, 54, 55]. Finite element method (FEM) can be a huge asset in terms of simulating PT structures, especially when developing new PT's, which are not well described yet. FEM has been used through the development of the PT's in chapter 4, from which the primary and secondary impedance can be extracted, which is used for calculating the lumped

parameters, using the method of [25, 54]. Furthermore, the lumped parameters of prototype PT's can be obtained in the same manner, by measuring the primary and secondary impedance. Figure 2.10 illustrates a FEM simulated primary and secondary impedance, of the developed interleaved Rosen type PT of section 4.3 [D.2], from which the lumped parameters are calculated.

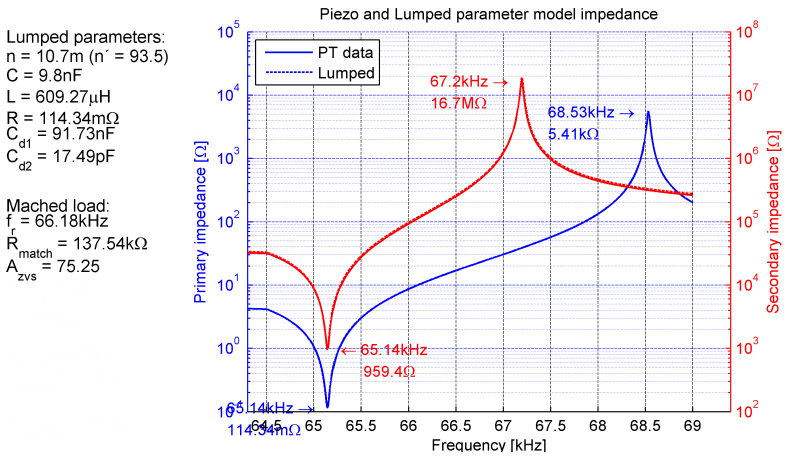

Figure 2.10: FEM simulated primary and secondary impedance, of the interleaved Rosen type PT (section 4.3 [D.2]).

2.4 Control methods

As described in the previous section the PT is operated close to its primary resonance mode, in order to obtain optimal and efficient operation. But as the PT resonance is of very high quality factor, the band of optimal and efficient operation is very narrow. Ensuring an optimal operating frequency is one of the main objectives of control methods for PT based converters, as the resonance frequency is subject to variations, as a result of internal or external influences, such as temperature, load variations, aging etc. When employing inductor-less topologies (chapter 3), that utilizes PT's with native soft switching capabilities (chapter 4), the band of operation is even further reduced and small variations in the resonance frequency can easily totally destroy the operation and efficiency. Hence a tight control of the operating frequency is essential.

In terms of load regulation, classical pulse width modulation (PWM) [49] is not really an option, especially not in connection with inductor-less topologies, as it demands a 50 % duty cycle. Pulse frequency modulation (PFM) on the other hand, can be used for load regulation, assuming a relative wide band of optimal and efficient operation of the PT. This is usually not the case when utilizing inductor-less topologies, due to the utilization of soft switching operation, and PFM is therefore not really an option.

2.4.1 Controlled oscillator

The most basic type of PFM is a controlled oscillator, typically a voltage controlled oscillator (VCO), which is controlled directly or indirectly by a feedback signal. This method is primarily used in continuous and constant load application, but is applicable both for AC and DC loads, such as fluorescent lamp ballast [56] or LED loads [57, 58]. The feedback is typically a measurement of the load current or voltage, which is held up to a reference, resulting in an error signal that adjusts the operating frequency [23, 44, 56, 57, 58, 59, 60], as illustrated in figure 2.11.

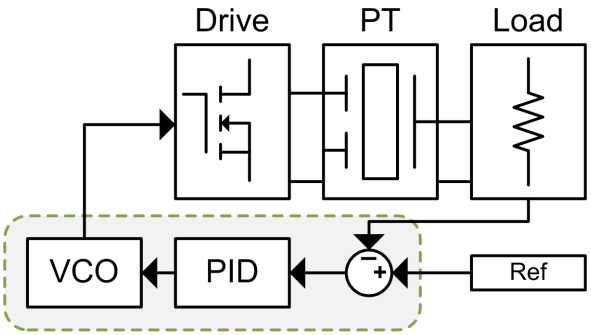

Figure 2.11: Basic principle of PFM based on a VCO, which compares a load current or voltage feedback to a reference and adjusts the operating frequency.

2.4.2 Phase lock loop

The phase lock loop (PLL) approach is basically also a controlled oscillator, but the feedback here is not a load state measurement, it is a measurement of the phase lag coursed by the PT. As the PT acts as a band pass filter, there will be a certain phase lag at the desired operating frequency, between the applied primary voltage and the secondary output voltage. This phase lag is measured by the PLL, as illustrated in figure 2.12, from which the operating frequency is adjusted, as the PLL seek to lock

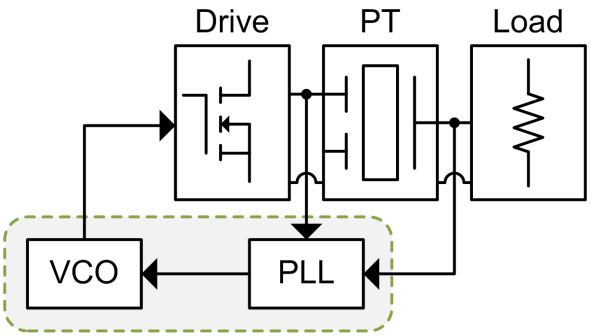

Figure 2.12: Basic principle of PFM based on a PLL, which compares the phase lag and adjusts the operating frequency.

the phase [5, 23, 61, 62, 63, 64, 65], hence the name. The method is applicable both for AC and DC loads, as well as it is possible to implement the control digitally [5].

2.4.3 Self-oscillating control

The phase lag of a band pass filter can be utilized in another manner, by forming a phase shifted self-oscillating closed loop. The idea is to have a phase shift in the loop of a multiple of 360^o, at the desired operating frequency, making it highly unstable, which induces self-oscillation [42, 66]. A clear benefit of this approach is its very fast response to track and "hit" the resonance frequency at startup, which is beneficial when utilizing burst-mode control for load regulation, which is described in the next section. Despite its excellence to "hit" the resonance frequency at start up, it can have difficulties to start, as the loop needs a "spark", noise or distortion, in order to initiate the self-oscillation.

2.4.4 Burst-mode modulation

Load regulation becomes necessary when the load is variable and the transferred energy need to be modulated in order to maintain a desired DC output voltage, as an example. The classical PWM control is typically not applicable for load regulation when utilizing inductor-less topologies, as well as neither of the previous described methods, although they are capable of maintaining a constant operating point and hence achieving control of the output power of a predefined load. An option is to use burst-mode modulation, also known as quantum-mode control, with the relatively simple principle of transferring energy in modulated bursts, which is done by switching the power converter ON and OFF [42, 53, 66, 67, 68]. The power converter is operated at full power and by modulating the ratio of the ON and OFF period, a controlled output can be achieved.

2.5 Summary

In this chapter the principle of the targeted application, Electro Active Polymer, piezoelectricity, the piezoelectric transformer and control methods, have been described, giving an overview of the subjects. As the nature of this chapter is to summarize and present the technological advances of the technologies, it is difficult to summarize and compress the contents even further. As an alternative the literature has been summarized, by sorting it by subject. Table 2.1 lists the relevant reference by subject, with the intentions of helping the reader to quickly find literature on the subjects. Some references might be relevant in several subjects and hence are listed several times, as well as the table includes subject of the remaining chapters.

Subject	References
Electro Active Polymer	[1, 7, 8, 9]
Dielectric Electro Active Polymer	[7, 8, 9]
Danfoss PolyPower DEAP actuator	[10, 11, 12, 13, 14]
The piezoelectric transformer (PT)	[4, 16, 21, 22, 23, 27]
Piezoelectricity	[15, 16, 17, 18, 19, 20, 21]
Modeling of piezoelectric transformers	[22, 24, 26, 27, 28, 48, 50, 51]
Model parameter determination	[24, 26, 30, 32, 36, 38, 45, 52, 53]
Piezoelectric loss and PT loss	[16, 17, 18, 21, 29, 69, 70]
Piezoelectric transformer design	[26, 53]
Rosen type PT	[2, 3, 30, 31, 32]
Radial mode PT	[26, 33, 34, 35, 36, 37, 38]
Thickness mode PT	[39, 40, 41, 42, 43, 44, 45, 46, 47]
Soft switching optimized PT's	[36, 38, 39, 40, 71],[D.2,D.5]
The PT based power converter	[23, 50]
Topologies	[23]
Push-pull	[4, 72]
Class-E	[58, 60, 68]
Half-bridge	[5, 66, 67, 73, 74]
The inductor-less half-bridge	[40, 50, 51, 54, 63, 64, 74, 75, 76],[D.7]
Soft switching factor	[26, 36, 50, 51, 54],[D.3]
Control methods	[23]
Controlled oscillator	[23, 44, 56, 57, 58, 59, 60]
Phase lock loop (PLL)	[5, 23, 61, 62, 63, 64, 65],[D.7]
Self-oscillating control	[42, 66],[D.8]
Burst-mode modulation	[42, 66, 67, 68],[D.1,D.6]
Bi-directional control	[D.9]

Table 2.1: Relevant reference sorted by subject.

Chapter 3

The piezoelectric transformer based power converter

The PT based power converter is basically a resonant converter [49], with the distinction of converting the electrical energy through an electromechanical resonant tank, contrary to the traditional resonant converter, which utilizes an electromagnetic and capacitive resonant tank. One of the qualities of resonant converters is the opportunity to exploit soft switching operation, which significantly reduces switching loss and switching stress. As a side product, the switching loss and stress reduction will also lead to a reduced EMI profile, due to the elimination of high frequency switching noise.

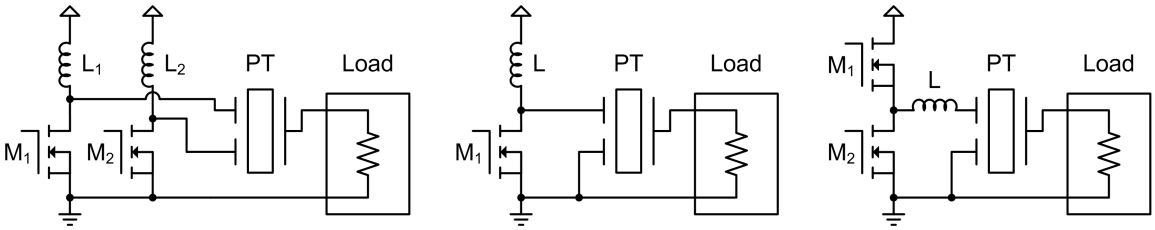

Figure 3.1: Some of the most popular topologies for driving PT's. The topologies are as follows, seen from the left: the push-pull, the class-E and the half-bridge. An output rectifier is also applicable for DC loads.

The PT can be driven by various converter topologies, where the most popular topologies [23] are the push-pull [4, 72], Class-E [58, 60, 68] and half-bridge [5, 66, 67, 73, 74] and is illustrated in Figure 3.1. The push-pull topology is primarily used for step-up applications, due to a higher step-up ratio and simple control requirements [23]. The Class-E and half-bridge topology are more suitable for step-down applications, where the half-bridge handles high power levels better than the Class-E [77]. But they all suffer the drawback of requiring additional inductive components in order to achieve soft switching operation. There are also various charge-pump topologies, which offers soft switching and power factor correction (PFC) capabilities [56, 71, 78, 79, 80, 81], but they have very demanding requirements for the PT.

The inductor-less half-bridge topology however, offers soft switching capabilities, through the utilization of soft switching optimized PT's [40, 50, 51, 54, 63, 64, 74, 75, 76]. The elimination of bulky series inductors reduces complexity and component

count, which leads to a smaller and cheaper power converter and the inductor-less half-bridge is treated in detail in the following section.

3.1 The inductor-less half-bridge

Figure 3.2 illustrates the inductor-less half-bridge topology and the lumped parameter model, where the absence of a series inductance reduces component count, size and price of the converter. Usually a series inductor is required in the half-bridge topology, in order to achieve soft switching operation of the switches and avoid large hard switching losses, in connection to the parasitic input capacitor of the PT C_{d1} [22, 23, 66, 74]. The parasitic input capacitance can easily lead to hard switching losses in the same range as the output power, resulting in a very poor efficiency. In order to achieve sustained soft switching of the switches, the inductor-less half-bridge utilizes soft switching optimized PT's [36, 38, 39, 40],[D.2,D.5], which possess native soft switching capabilities, without requiring auxiliary inductive components. Furthermore, the PT is operating slightly above its operating resonant frequency, where the series resonant network becomes inductive and contains enough resonating energy to charge and discharge C_{d1}. And as it will be shown in section 3.2, there is an optimum where the inductive behavior and energy of the resonant network is maximized, making the largest energy transfer to C_{d1}. Moreover the dead time in-between the two switches should be sufficiently large, in order to let the charge and discharge occur. A detailed description of the operational principle is conducted in the following section.

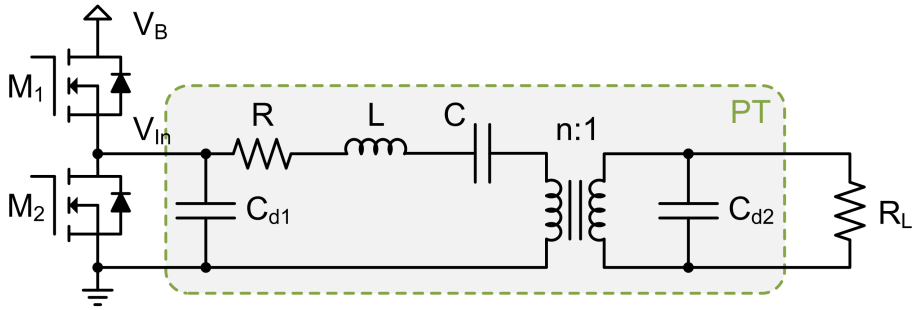

Figure 3.2: Schematic diagram of the inductor-less half-bridge topology and the lumped parameter model.

3.1.1 Operational principle

Figure 3.3 illustrates the steady-state operation of the inductor-less half-bridge, which is operated slightly above its operational resonant frequency, maximizing inductive behavior and resonating energy. As it can be seen the resonant current possesses sufficient phase shift (inductive behavior) and magnitude to achieve soft switching, where the switches are operated under zero voltage switching (ZVS). Furthermore

sufficient dead time is supplied in-between the switches, clearly allowing the resonant current to charge and discharge C_{d1}, making the input voltage V_{in} reach the supply rails, before the switches is turned ON.

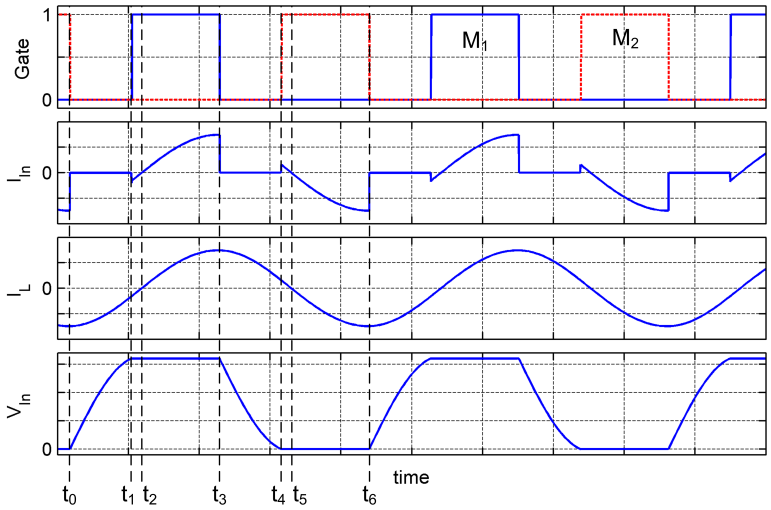

Figure 3.3: Operational waveforms of the inductor-less half-bridge topology, operated slightly above its operational resonant frequency, where ZVS is obtained.

The circuit (Figure 3.2) has 6 modes of operation, divided into the following periods:

$t_0 - t_1$: Both switches are turned OFF in this period and the reverse resonant current I_L charges the input capacitor C_{d1}.

$t_1 - t_2$: When the input capacitor C_{d1} is charged to the supply voltage the body diode of M_1 conducts the reverse resonant current I_L and it is in this period M_1 is switched ON, achieving ZVS.

$t_2 - t_3$: At t_2 the resonant current I_L is inverted, switch M_1 conducts the resonant current I_L and transfers energy to the resonant tank.

$t_3 - t_4$: At t_3 switch M_1 is turned OFF and the resonant current I_L discharges the input capacitor C_{d1}.

$t_4 - t_5$: When the input capacitor C_{d1} is totally discharged the body diode of M_2 conducts the resonant current I_L and it is in this period M_2 is switched ON, achieving ZVS.

$t_5 - t_6$: At t_5 the resonant current I_L is reversed and the resonant current I_L is freewheeling through switch M_2. The period ends at t_6, where M_2 is switched OFF and a new cycle begins.

As mentioned the switches should be turned ON in-between the time periods $t_1 - t_2$ and $t_4 - t_5$, so sufficient dead-time should be supplied to the gate signals, in order to utilize the ZVS capability.

3.2 Soft switching factor

The inductor-less half-bridge topology is quite simple, making it easy to understand the subject of soft switching. But the soft switching principle and the requirements for the PT for a bit more advance topologies, like the full-bridge, are the same. However for the more advanced PFC charge pump topologies, the requirements to the soft switching capability of the PT is higher, as the apparent parasitic input capacitance is increased.

From a design point of view, it is desirable to get a measure of soft switching capability, in order to evaluate PT designs and meet the requirement for achieving soft switching operation. The PT soft switching capability can be derived from the lumped parameter model and several attempts of doing so, have been made [26, 36, 50, 51, 54]. They all succeed to derive expressions, but suffer from complexity and are not transparent or accurate. In [54] a simple and transparent expression is derived (3.1), but it lacks accuracy, by being too optimistic.

$$V'_{P\text{-}[54]} = \frac{1}{n^2}\frac{C_{d2}}{C_{d1}}\frac{36\sqrt{6}}{9\pi^2}\eta \tag{3.1}$$

The expression assumes a matched load as this maximizes the power transfer of the resonant network, as well as this is the worst case condition for soft switching capability [54]. What the expression states is the maximal obtainable soft switching capability, for a given set of PT model parameters, also known as the soft switching factor or ZVS factor. As the expression reveals only a few parameters of the model affect the ZVS factor, making it very simple and transparent. As the expression is too optimistic, a ZVS factor of at least 1.4 is required, in order to achieve soft switching operation. This expression (3.1), is used as a starting point for the empirical search for a simple, transparent and accurate expression of the soft switching capability, which is conducted in [D.3] and described in the following section.

3.2.1 Derivation of soft switching factor

Due to the lack of a simple and transparent measure of soft switching capability, an investigation has been conducted in [D.3], seeking to express the maximal obtainable soft switching capability (ZVS factor). The approach has been to perform an empiric series of parametric sweep time domain simulations of the inductor-less half-bridge and the lumped parameter model, searching for linearization opportunities in respect to the soft switching capability. The simulations have been performed using *OrCad*

PSpice, with at least 100 cycles before any measurements were made, in order to ensure steady-state operation. Furthermore the simulated circuit utilizes idealized switches and body diodes, as well as a matched load is employed. But it also uses an adaptive dead-time, which ensures an optimal dead-time for any given operation point. The measurement of the soft switching capability, i.e. the maximal charging and discharging of C_{d1}, has been performed by a circuit arrangement that enables a measurement of the peak voltage across C_{d1}. The simulated circuit can be found in Appendix A, where the peak voltage is measured in the V_Cd1 node. This makes it possible to measure the overshoot, which is a measure of the soft switching capability. Or the simulation will reveal a lack of overshoot, where the limited voltage is a measure of the lacking soft switching capability. Figure 3.4 illustrates two simulation cases, at 56.5 kHz, showing a soft switching and hard switching case.

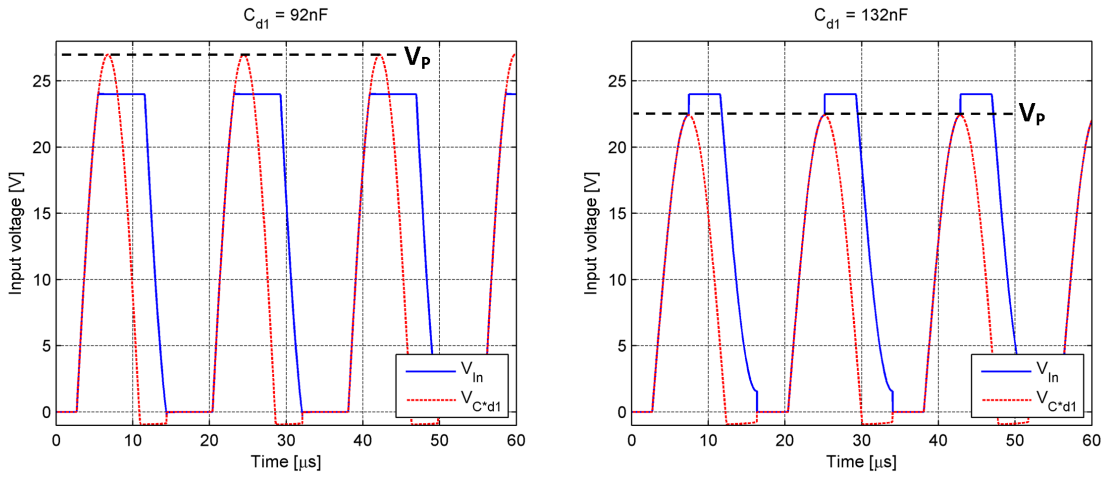

Figure 3.4: Simulated PT soft switching capability, at 56.5 kHz, with two different input capacities C_{d1}, using the simulation circuit of Appendix A.

As (3.1) revealed, the soft switching capability is strongly dependent on the input and output capacitor. Figure 3.5 illustrates a series of simulations, sweeping the frequency above and in the vicinity of the operational resonant frequency. Furthermore the swept frequency simulations has been performed with a linearly increment of the input capacitor C_{d1}, while keeping the remaining model fixed[1].
As anticipated the simulations confirm a clear and strong dependency on the frequency and the input capacitor C_{d1}, as well as the frequency profile matches what is seen in prior art [26, 50, 51, 54]. The simulations unveil an optimal point in operating frequency, where the soft switching capability is maximized. This maximal obtainable soft switching capability or ZVS factor (V_P'), can then be plotted in relation

[1]The PT and model parameters used for the simulations, are from the developed Interleaved Rosen type PT [D.2], but as the lumped parameter mode is independent of PT design, the results are general.

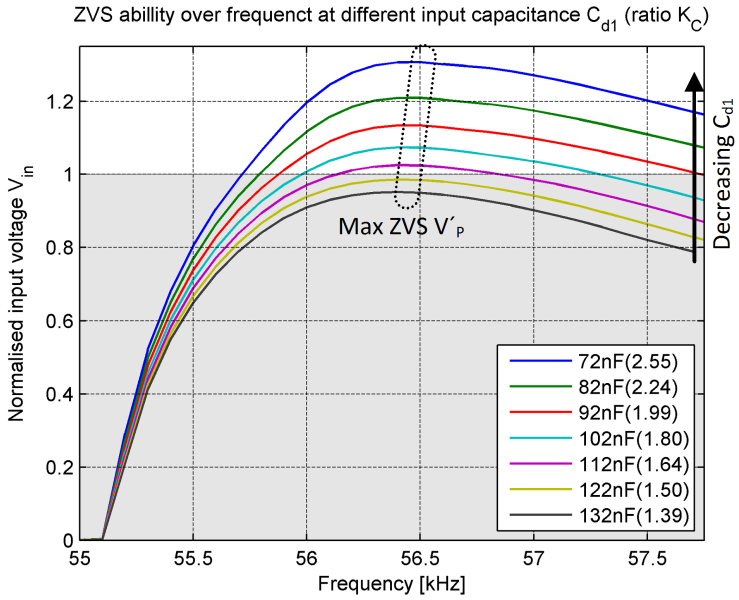

Figure 3.5: Simulated PT soft switching capability over frequency, with different input capacities C_{d1} (capacitor ratio K_C), using the lumped parameters of [D.2] and having a series resistance of 98 mΩ (98.7% efficiency).

to the swept input capacitor C_{d1} or, more interestingly, in relation to the input and output capacitor ratio K_C (3.2).

$$K_C = \frac{1}{n^2}\frac{C_{d2}}{C_{d1}} \tag{3.2}$$

The ZVS factors of Figure 3.5, at varying capacitor ratio K_C, resembles the second top most line in Figure 3.6, which illustrates the ZVS factors dependency on the capacitor ratio K_C, as well as ZVS factors at different efficiencies are included (increasing series resistance R).
And as it can be observed there is a fine linear relation between the capacitor ratio K_C and the ZVS factor V'_P and by performing a linear regression of the topmost line ($\eta \approx 100\%$), the most simplified expression of the ZVS factor is found (3.3).

$$\boxed{V'_{P\ \eta\approx 100\%} = 0.304\frac{1}{n^2}\frac{C_{d2}}{C_{d1}} + 0.538} \tag{3.3}$$

The expression is very handy and as simple as it gets, it holds for high efficient PT's, which in the end is the ultimate goal of the PT technology.

The efficiency dependency should be taken in to account, when working with less efficient PT's (approximately $< 97\%$), in order to get an acurate result. The ZVS factor $V'_{P\ \eta\approx 100\%}$ (3.3) can be adjusted by an efficiency dependent factor, which is derived in the same manner of a linear regression of the normalized ZVS factor ($V'_P/V'_{P\ \eta\approx 100\%}$) dependency on the efficeincy. This linearization leads to the final expressing of the

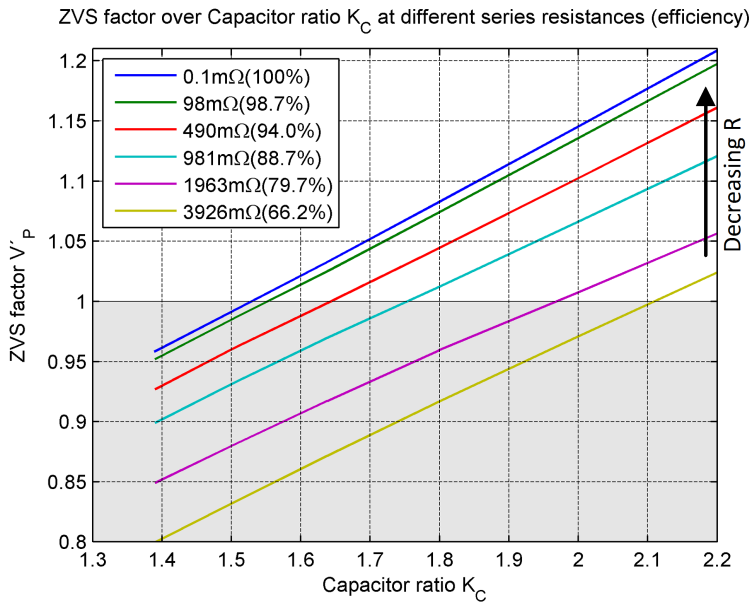

Figure 3.6: Simulated maximal PT soft switching capability (ZVS factor V_P') in relation to the capacitor ratio K_C, at different efficiencies.

ZVS factor V_P' (3.4), which describes the maximal obtainable soft switching capability of the lumped parameter PT model, for any given model parameters.

$$V_P' = \left(0.304\frac{1}{n^2}\frac{C_{d2}}{C_{d1}} + 0.538\right)(0.585\eta + 0.414) \tag{3.4}$$

In section 4.2 the ZVS factor will be related to the physical structure of the PT, which enables a much more intuitive design process.

3.2.2 Experimental verification

The derived ZVS factor is verified up against experimental measurements on one of the developed 30x10x2 mm prototype Interleaved Rosen type PT's. The approach has been to make a stepwise increment of the input capacitor C_{d1} and measure the drop in soft switching capability, just as performed in the simulations. Two sets of ZVS factor measurements have been collected, where the half-bridge has been operated at two different supply voltages, 10 V and 20 V respectively. The increase in voltage should reflect a decrease in efficiency, as a result of the nonlinear nature of the piezoelectric loss [16, 17, 18, 21, 29, 69, 70].

In Figure 3.7 the experimental measurements is plotted, together with the prediction of (3.4). As it can be observed the experimental results are not perfectly linear as anticipated, but the ZVS factor drops when employing a higher half-bridge supply voltage, just as expected. Furthermore the prediction is a bit more optimistic than the experimental results, where a 3-6% deviation can be observed. This is mainly

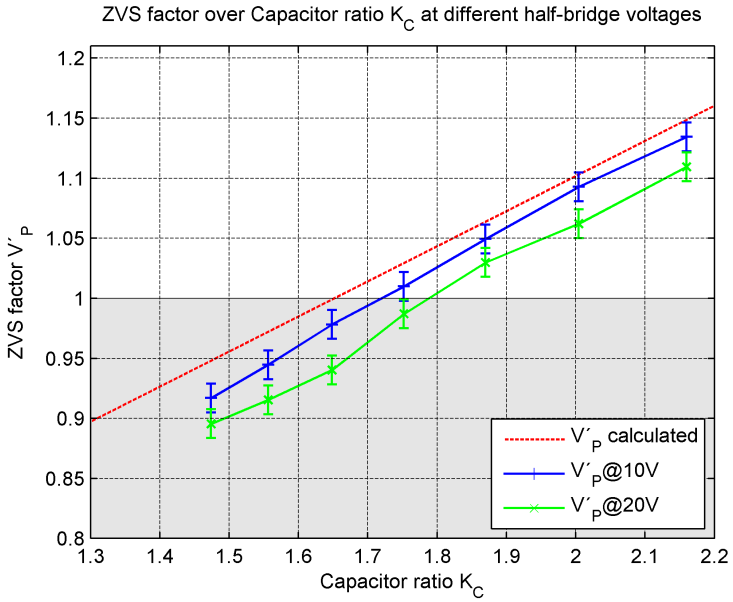

Figure 3.7: ZVS factor measurement of prototype PT in relation to the capacitor ratio K_C, compared with the ZVS factor expression. The utilized PT is a 30x10x2 mm Interleaved Rosen type PT [D.2] (section 4.3).

due to the fact that the PT efficiency drops as the half-bridge voltage increases and gets heavily loaded. As the lumped parameters of the prototype PT are measured by a impedance analyzer, which only applies a small signal, in order to perform an impedance measurement. The result is that the measure loss resistance R is also only a measure of efficiency at light or no load, which results in a too optimistic prediction. In order to get an accurate prediction, the loaded PT efficiency should be used, which in fact is quite difficult to obtain, as it involves precision measurements of relative high frequency voltages and currents, as well as the input voltage is non-sinusoidal. Furthermore the experimental results are extracted "by hand" from oscilloscope plots, which can lead to some deviation, as well as the prototype unavoidably adds parasitic components, such as the highly nonlinear semiconductor parasitic capacitances.

Nonetheless an accurate, simple and transparent ZVS factor has been derived, with the intentions of forming a fundamental measure of soft switching capability and basic tool to assist through the development of soft switching optimized PT's.

3.2.3 Operation point of maximal soft switching capability

As described in the previous section, there is an optimal point of operation, where inductive behavior and resonating energy is maximized, which maximizes soft switching capability of the PT. This point is located slightly above the operational resonant frequency, as illustrated in Figure 3.5. By plotting the soft switching capability of Figure 3.5 ($K_C = 1.8$), in relation to the voltage gain (3.5) and resonant current transfer

function (3.6) of the PT[2], some valuable operation conditions can be derived.

$$\frac{V_{Out}}{V_{In}} = \frac{\frac{1}{j\omega C_{d2}} \| R_L}{(R + j\omega L + \frac{1}{j\omega C})/n^2 + (\frac{1}{j\omega C_{d2}} \| R_L)} \frac{1}{n} \tag{3.5}$$

$$I_L = \frac{V_{In}}{Z_{In}} = \frac{V_{In}}{R + j\omega L + \frac{1}{j\omega C} + (\frac{1}{j\omega C_{d2}} \| R_L) n^2} \tag{3.6}$$

In Figure 3.8 the soft switching capability is related to the transfer functions and as it reveals, there is a clear connection between the operational point of optimal soft switching capability and the phase and magnitude of the transfer functions. As it can be seen the PT voltage gain magnitude is reduced to 57% and has a phase lag of 102^o, whereas the resonant current magnitude also is reduced to 57% and has a phase lag of 56^o, which is summarised in (3.7).

$$A_{ZVS} = 57\% \cdot A_{max} \ \angle 102^o \qquad I_{L\_ZVS} = 57\% \cdot I_{max} \ \angle 56^o \tag{3.7}$$

The results are general for ZVS optimized PT's as the gain and phase characteristic of the resonant tank can be considered as constant within a reasonable ZVS range (ZVS factor of 1 to 1.5). This operational information is key in connection to controlling and maintaining optimal and sustained soft switching operation of the inductor-less half-bridge topology, as well as through the design of PT's, as the voltage gain is one of the design criterion. Control methods such as PLL relies on the phase information, as it seek to locking the operation to a certain phase shift [5, 23, 61, 62, 63, 64, 65]. In chapter 5 the phase information will become valuable, as several control method are presented, which relies on the phase response of the PT.

3.3 Summary

In this chapter the utilized inductor-less half-bridge topology is presented, as well as the most popular PT based topologies are introduced. The operational principle of the inductor-less half-bridge is described in detail, where it:

- Relies on soft switching optimized PT's, which possess native soft switching capabilities, without requiring auxiliary inductive components.
- Is operated slightly above its operational resonant frequency, where inductive behavior and resonating energy is maximized, enabling ZVS of the half-bridge switches.
- Require a sufficiently large dead-time in-between the two switches, in order to allow the resonant current to charge and discharge of input capacitor C_{d1}, enabling the utilization of soft switching.

[2]The input capacitor C_{d1} is excluded in the derivation of these equations, as it does not have any influence on the frequency domain transfer functions.

The inductor-less half-bridge topology is described in detail in [D.3] and [D.7], but is the target or utilized topology of this study and all the publications of Appendix D.

An expression of the ZVS factor V_P' (3.4) has been derived, which describes the maximal obtainable soft switching capability of the lumped parameter PT model, for any given model parameters, assuming a matched load. The derived expression demonstrates good correlation with the experimental results, although having a too optimistic result of 3-6%, but this is mainly the result of using a too optimistic efficiency for the predicted ZVS factor. Which leads to the conclusion that an accurate, simple and transparent ZVS factor has been derived, with the intentions of forming a basic tool to assist through the development of soft switching optimized PT's. As a closing conclusion on soft switching capability, the derived ZVS factor leads to the rule of thumb, that a capacitor ratio K_C of at least 1.55 is needed, in order to achieve soft switching capability for high efficient PT's:

$$1.55 < \frac{1}{n^2}\frac{C_{d2}}{C_{d1}}$$

An in-depth analysis of the topic of soft switching and derivation of the ZVS factor is presented in [D.3][3].

Moreover the study of the soft switching capability, revealed an operational point of optimal soft switching capability, which is closely connected to the transfer functions of the PT. It was shown how this optimal operational point was related to a certain magnitude decrease and phase lag of the PT.

[3]The ZVS factor will be related to the physical structure of the PT in section 4.2, which enables a much more intuitive design process.

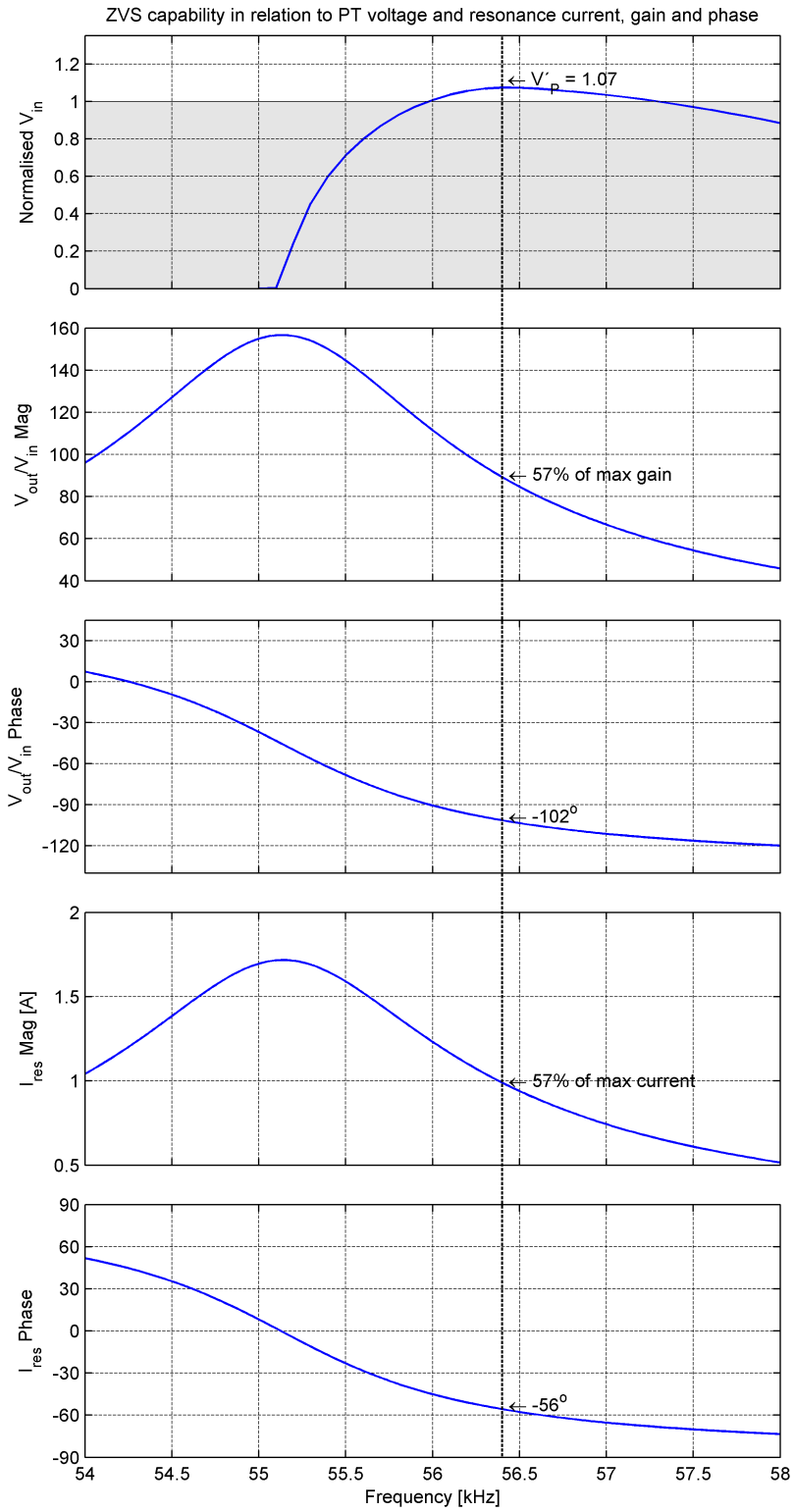

Figure 3.8: ZVS capability over frequency, in relation to voltage gain and resonant current, gain and phase, for the 30x10x2 mm Interleaved Rosen type PT [D.2] (section 4.3), but the results are general for ZVS optimized PT's.

Chapter 4

Piezoelectric transformer design

During this study several PT designs and PT's were developed, in order to accommodate the need of high gain and soft switching capabilities, which enables the utilization of the inductor-less half-bridge topology. As described in Overview and State of the art chapter 2, the target application is to drive a high voltage DEAP actuator from a low 24 V supply voltage, which leads to the following main specification for the PT:

- High step-up conversion ratio within the vicinity of 100.
- A desired output power of up to 11.5 W.
- Optimized for soft switching and the inductor-less half-bridge.

4.1 Development tools

One of the challenges of developing PT's is to make a good evaluation of PT designs and PT structures, as well as evaluating the manufactured prototypes.
A good evaluation tool of the soft switching capability is derived in section 3.2, that enables the determination of PT's soft switching capability from its lumped parameter model. The ZVS factor is further improved in section 4.2, where it is related to the physical structure of the PT, enabling a much more intuitive design process. Furthermore the gain and power can also be determined from the lumped parameter model [22, 27, 53]. When designing PT's one of the objectives is to match the output of the PT to the load, as this maximizes power and efficiency, but as a drawback this is also the worst case condition for soft switching capability. Another benefit of utilizing a matched load is that the design is evaluated at the same load conditions, making it possible to make a fair comparison of different designs, even though the designs are for different power and voltage levels, or the targeted application does not resemble a match load, like DC/DC applications.

4.1.1 Finite element method

Through this study the development has relied heavily on finite element method (FEM) simulations. FEM has proved to be a good evaluation tool, in terms of determining the lumped parameter model values, from which matched load, gain, ZVS factor and power can be determined. It has demonstrated fairly good correlation with manufactured prototypes, but with some shortcomings, primarily in terms of determining the efficiency. The shortcomings is likely more due to bad correlation

of the material parameters used, as well as an incomplete implementation of the loss mechanism of piezoelectric material. All in all FEM has proven as a good development tool, with the lack of a good loss and efficiency determination.

4.1.2 Active match load

In this work with PT's of high output voltage and output impedance, it is quite difficult to make its matched load, as the availability of high impedance power resistors is very limited. Furthermore the match load changes for PT designs and design variations, requiring the manufacturing of a matched load for every new design, which typically is a resistor matrix of standard 1/4 W resistors. Therefore as a development tool, an active high impedance load has been developed [D.4], which makes it easy to adjust the load impedance, without having to solder a resistor matrix of standard 1/4 W resistors and without having any significant inductive component in the load.

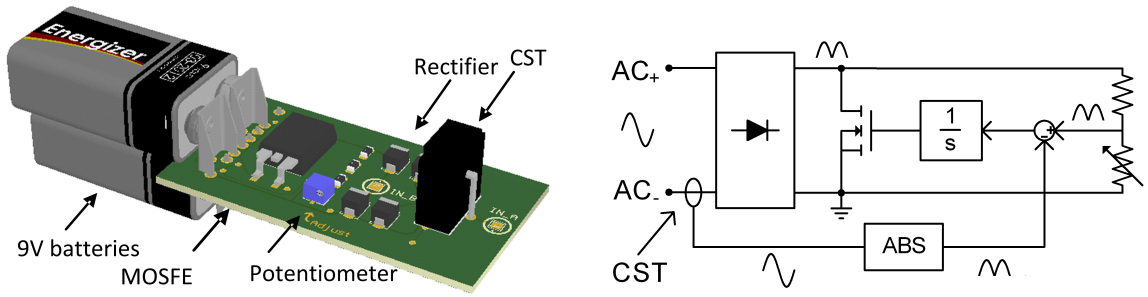

Figure 4.1: The developed active match load (left) and the fundamental electrical circuit (right).

Figure 4.1 illustrates the developed active match load and the fundamental electrical circuit. The circuit relies on a current and voltage measurement, from which a high voltage MOSFET is controlled in the linear region, ensuring that the current is proportional to the voltage, which emulates resistive behavior.

4.2 Soft switching optimized PT's

To date, several soft switching optimized PT's and design guides for soft switching optimization exist, but they primarily deal with the Radial mode PT [36, 38, 39, 40, 71]. But soft switching optimized thickness mode PT's have also been proposed [39, 40, 45, 54]. In [63, 64] a Rosen type PT is utilized, but the soft switching capability is here achieved on the expense of a matched load. In [54] my colleague suggest how to optimize a ring shaped Thickness mod PT, which has led to the patent application [82], which covers soft switching structures, optimized by using the concept of effective coupling factors. This concept is also a part of this study, as it is closely

related to the soft switching capability and the ZVS factor derived in section 3.2.

4.2.1 Effective coupling ZVS factor

The effective coupling factor is a measure of how good an effective electromechanical coupling the structure possess, at a given resonance mode, and includes losses [16, 83]. The expression of the effective coupling factors are refreshed in (4.1) and are calculated from the resonance mode series and parallel resonant frequencies.

$$k^2_{eff\ Pri} = \frac{f^2_{p\ Pri} - f^2_{s\ Pri}}{f^2_{p\ Pri}} \qquad k^2_{eff\ Sec} = \frac{f^2_{p\ Sec} - f^2_{s\ Sec}}{f^2_{p\ Sec}} \tag{4.1}$$

As the model parameters also can be determined from the series and parallel resonant frequencies [25, 53, 54, 55], the ZVS factor (3.4) derived in section 3.2 [D.3], which relies on the input and output capacitors, can be rewritten in terms of effective coupling factors (4.2).

$$\boxed{V'_P = \left(0.304\frac{(1-k^2_{eff\ Sec})/k^2_{eff\ Sec}}{(1-k^2_{eff\ Pri})/k^2_{eff\ Pri}} + 0.538\right)(0.585\eta + 0.414)} \tag{4.2}$$

Instead of stating that the reflected output capacitor have to be larger than the input capacitor, the expression now states that the effective coupling of the primary section have to be larger than the effective coupling of the secondary section. This is advantageous as the effective coupling factors to some extent can be related directly to the mechanical structure and the operational stress, whereas the input and output capacitors are hard to relate to the mechanical structure. This enables a much more intuitive design process and very simplified articulated, the effective coupling is proportional to the electromechanical coupling, of the utilized vibration mode, and the

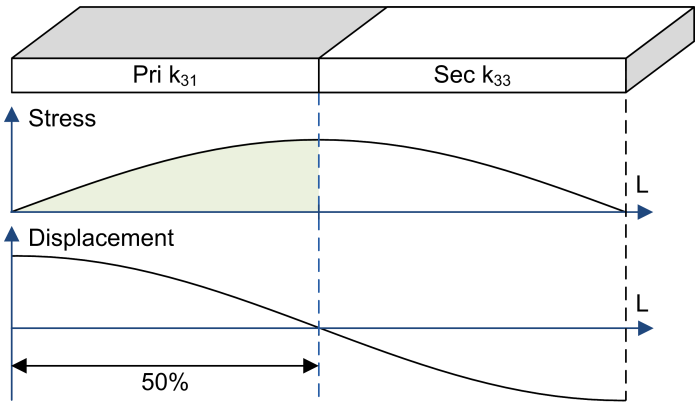

Figure 4.2: Visualization of the displacement and stress across the classical Rosen type PT structure.

area beneath the stress curve covered by the section, as visualized in Figure 4.2. This assumes simple structures, where only a single resonance mode is excited, but is applicable to higher mode shapes than the first mode shape. This leads to the basic rule of thumb: one section should cover more area of the stress curve than the other, in order to achieve a higher effective coupling, if both sections are operated trough the same electromechanical coupling (electromechanical coupling factors). From this statement it can be derived that a classical Rosen type PT cannot soft switch, as the primary section only covers 50 % of the stress curve (both in the first and second mode shape), as well as it has a lower electromechanical coupling k_{31}, than the secondary section k_{33}. Giving the primary section a lower effective coupling than the secondary section.

4.3 Interleaved Rosen type PT

The Interleaved Rosen type PT, which is proposed and developed in [D.2], is essential a classically multilayer Rosen type PT, where the primary section has been interleaved into the secondary section. The interleaved multilayer structure is no breakthrough and is also known as the double sided Rosen type PT [2, 84, 85]. The break through is its native soft switching capabilities, which is achieved by having an optimized primary section size and position. A detailed analysis and description of the research, can be found in [D.2].

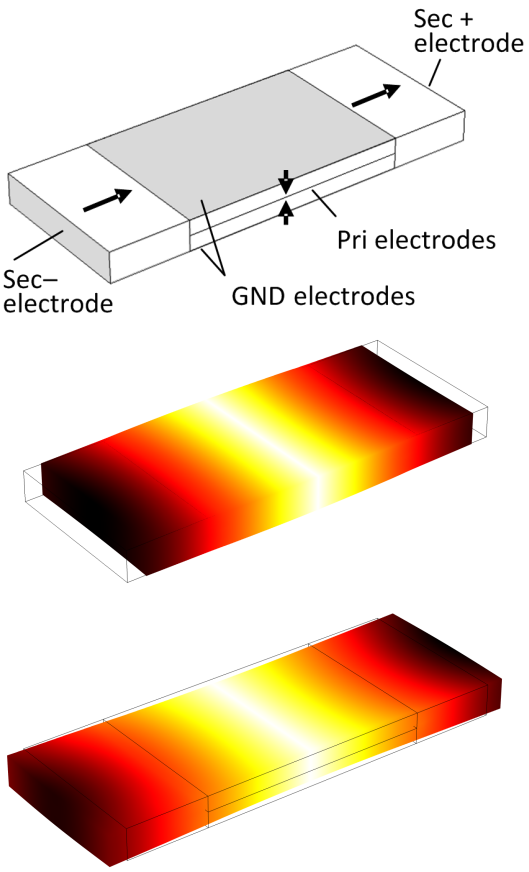

Figure 4.3: The Interleaved Rosen type PT structure (top) and FEM simulated operational mode shape (mid-bottom). For simplicity the PT structure, which has a size of 25 x 10 x 2 mm, only have two primary layers and the arrows indicate the polarization direction. The FEM simulation illustrates operation in the first longitudinal mode shape, at 65.1 kHz, where light colors refer to a low displacement and dark colors to a high displacement.

4.3.1 Structure

Figure 4.3 illustrates the structure of the Interleaved Rosen type PT. The operational vibration resonance is along the longitudinal direction, which also is illustrated in Figure 4.3, and is generated through the electromechanical coupling factors k_{31} and k_{33}, primary and secondary respectively. As it can be seen it has a nodal line in the center of the

structure, which is useful in terms of mounting and fixing it to the power converter. A clear advantage of this structure is the very straight forward and easy manufacturing, when utilizing tape casting technology [17, 18], as the build-up is the same as for a simple multilayer Rosen type PT. Furthermore the design possesses high voltage gain capabilities, which is desirable for this specific application. A drawback of this design (depending on application) is the split secondary, which results in a differential output voltage symmetrical around ground. The main drawback of the Interleaved Rosen type PT is its relative low efficiency, which is a result of the low electromechanical coupling k_{31} of the primary section.

4.3.2 Soft switching optimization

As mentioned, the Interleaved Rosen type PT achieves its native soft switching capabilities through an optimization of the primary section size and position. The PT is operated in its first mode shape, which is where a half-wave sound wave is standing across the structure. The position is key and with the interleaving, the primary section is placed right in the middle of the excitation stress curve, as illustrated in Figure 4.4.

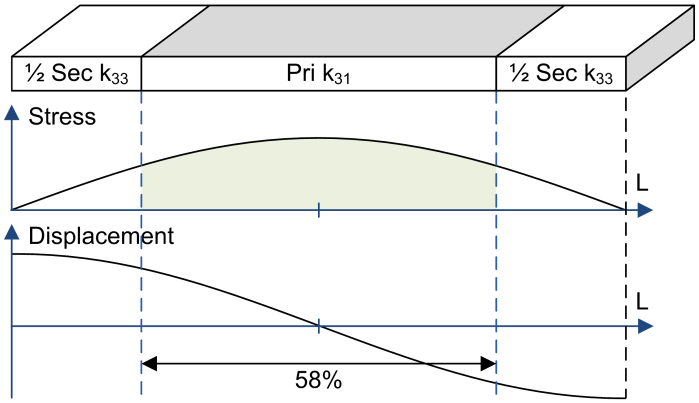

Figure 4.4: Visualization of the displacement and stress across the soft switching optimized Interleaved Rosen type PT.

This gives it a good mechanical coupling to the structure and hence good conditions for a high effective coupling factor. Utilizing a primary section which occupy 50 % of the structure and covers even more of the area below the stress curve, the primary and secondary have approximatly the same effective coupling (Table 4.1), which is not enough in order to achieve soft switching capabilities. This is because the primary section utilize transverse vibrations, which has an electromechanical coupling k_{31} that is lower than for the secondary thickness mode k_{33}.

Table 4.1 illustrates how the effective coupling factors and the ZVS factor are dependent on the size of the primary section. As it can be seen, a sufficiently large ZVS factor is achieved, when increasing the primary section size to 58 % or more.

Primary volume	33%	50%	**58%**	60%	62%	64%	65%
ZVS factor V'_P	61.6%	82.2%	**106.5%**	113.5%	124.1%	138.5%	153.4%
$k_{eff\ Pri}$	24.0%	29.2%	30.7%	31.3%	31.6%	31.8%	31.6%
$k_{eff\ Sec}$	43.8%	30.1%	23.8%	22.9%	21.4%	19.7%	18.1%

Table 4.1: Soft switching optimization of the Interleaved Rosen type PT, achieved by primary section volume optimization and is generated through FEM simulations. The FEM simulation is a 2D simulation of a 30x10x2 mm structure, but the results are general and independent of the size, as long the structure has a reasonable aspect ration ("long" structure). The effective coupling factors are calculated from the FEM simulated primary and secondary impedance, and (4.2) is used to calculate the ZVS factor.

And a size of 58 % is what that have been used for the prototypes in the next section. This is totally independent on the numbers of primary layers and therefore the primary layers can be used to control the voltage gain of the PT. It can be observed that the improved ZVS factor mainly is achieved on the expense of a degraded secondary section effective coupling. As the effective coupling is a measure of the effective electromechanical coupling, which includes losses, it is obvious that as high an effective coupling as possible is desirable. Therefore, it is not desirable to have an unnecessarily high ZVS factor.

4.3.3 Prototype

As described in the previous section, the optimal size of the primary section was found to be 58 % of the center of the structure. From this design constraint, four

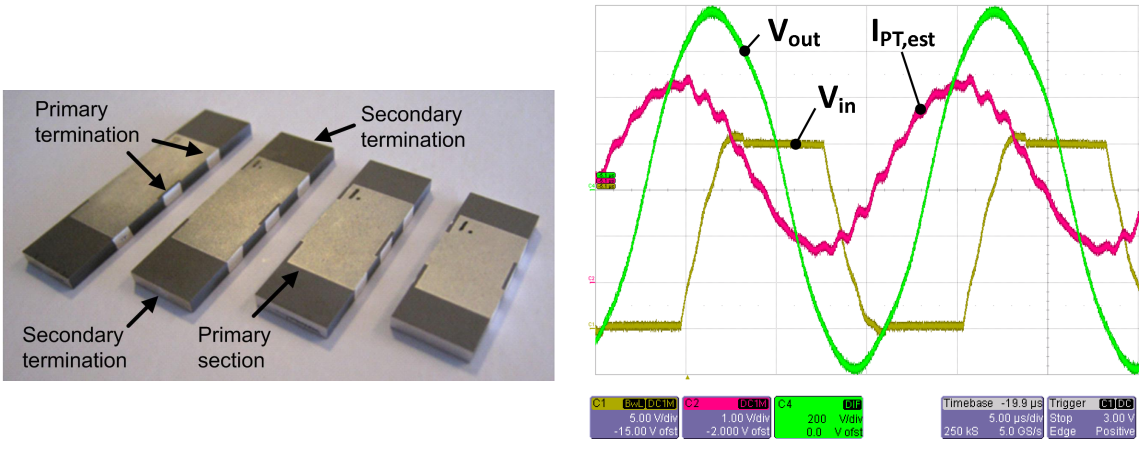

Figure 4.5: Picture of prototype PT's (left) of different sizes (length from left: 40 mm, 35 mm, 30 mm and 25 mm) and operational waveforms of a 25 mm prototype (right), operated at 20 V half-bridge voltage and a matched resistive load (approximately 100 kΩ). The relative slow rising switching flanks and the MOSFET body-diode conduction voltage drop, at supply rails, clearly demonstrates ZVS operation.

sized PT designs were developed and produced, as illustrated in Figure 4.5(left), having a thickness of 2 mm, a width of 10 mm and length ranging from 25 mm to 40 mm. Two numbers of primary layers were manufactured, as the conversion ratio is directly proportional to the secondary and primary layer thickness ratio. As the structure gets smaller, the secondary layer thickness gets smaller and the drop in gain can be compensated by increasing the numbers of primary layers (decreasing primary layer thickness). In Table 4.2 the design specifications of the four sized PT are listed, having voltage gains ranging from 75 to 100.

	Mask 1		Mask 2		
PT length	40	35	30	25	mm
Primary volume	58%	58%	58%	58%	
Primary length	23.2	20.3	17.4	14.5	mm
Primary layers	10	10	12	12	
Pri layer thickness	200.0	200.0	166.7	166.7	μm
Gain	100.5	88.1	90.5	75.3	

Table 4.2: Design specifications of the four developed Interleaved Rosen type PT.

In Figure 4.5(right) the operation of the developed 25 mm PT is illustrated. The waveforms reveals a high voltage conversion ratio, of approximately 68, generating voltages of 565 V rms, from a 20 V half-bridge supply voltage, in to a matched load. The minor drop in voltage conversion ratio is mainly due to the primary layer being 5 % thicker than expected and is further ellaborated in [D.2]. Moreover it clearly demonstrates soft switching capabilities, which has been the main objective. The development furthermore demonstrated a good correlation between the FEM simulated design and the manufactured prototypes.

4.4 Interleaved thickness mode PT

The Interleaved thickness mode PT is based on the classical thickness mode PT concepts [39, 40, 41, 45, 47], where soft switching optimized PT's also have been proposed [39, 40, 45, 54]. Thickness mode PT's have mainly been used for step-down applications and moderate voltages (typically up to rectified AC mains voltages), due to the limited build-up height (typically 2-4 mm). This puts some limits on the voltages in terms of breakdown voltages, which to some extent can be extended by incorporating the electrodes in to the structure. But it is also limiting as the applied electrical field should not exceed a certain level, in order to maintain efficient operation and it should definitely be far below the poling field of the material. The main challenge here is therefore the high voltage, which dictates a high structure. The Interleaved thickness mode PT also possesses native soft switching capabilities, which mainly is achieved by having an interleaved primary section.

4.4.1 Structure

Figure 4.6 illustrates the structure of the Interleaved thickness mode PT, where the operational vibration resonance is along the longitudinal direction and it is operated in its first longitudinal mode shape. As both the primary and secondary section is

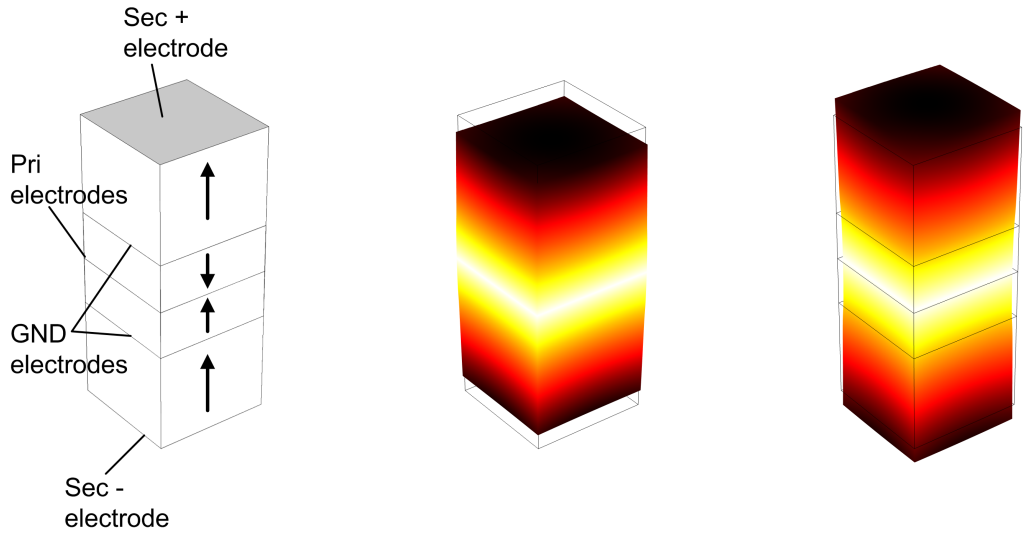

Figure 4.6: The Interleaved thickness mode PT structure (left) and FEM simulation of the operational resonance mode (mid-right). For simplicity the PT structure, which has a size of 8 x 8 x 20 mm, only shows two primary layers and the arrows indicate the polarization direction. The FEM simulation illustrates the operation in the first longitudinal mode shape, at 70.1 kHz, where light colors refer to a low displacement and dark colors to a high displacement.

operated through the thickness mode electromechanical coupling k_{33}, which approximately is twice as large as the transverse mode k_{31}, the thickness mode PT has a much higher potential for high efficiency and high power density. Furthermore the design possesses potentially high soft switching capabilities, which will be shown in the

Primary volume	20%	25%	27%	**30%**	33%
ZVS factor V_P'	75.6%	89.4%	96.5%	**110.0%**	125.9%
$k_{eff\ Pri}$	45.1%	49.7%	51.5%	53.8%	55.9%
$k_{eff\ Sec}$	51.2%	46.8%	45.2%	42.5%	40.1%

Table 4.3: Soft switching optimization of the Interleaved thickness mode PT, achieved by primary section volume optimization and is generated through FEM simulations. The FEM simulation is a 2D simulation of a 8x8x20 mm structure, but the results are general and independent of the size, as long the structure has a reasonable aspect ration ("high" structure). The effective coupling factors are calculated from the FEM simulated primary and secondary impedance, and (4.2) is used to calculate the ZVS factor.

following section, as well as high voltage gain capabilities, which is directly proportional to the secondary and primary layer thickness ratio. Similar to the Interleaved Rosen type PT, it has a split secondary, which results in a differential output voltage symmetrical around ground. The main drawback of the structure is the challenging manufacturing, in relation to the high build-up height, as described in the previous section.

4.4.2 Soft switching optimization

Just as the Interleaved Rosen type PT, the Interleaved thickness mode PT achieves its native soft switching capabilities through the interleaving design and the optimization of the primary section size. Again, the interleaving places the primary section right in the middle of the excitation stress curve, as illustrated in Figure 4.7. But contrary to the primary section of a Rosen type PT, the primary section utilizes the thickness mode electromechanical coupling k_{33}, which gives it a much higher effective coupling. This enables the primary section to be approximately half the size (due to a doubling of the electromechanical coupling), while maintaining soft switching capabilities. Table 4.3 illustrates how the effective coupling factors and the ZVS factor are dependent on the size of the primary section.

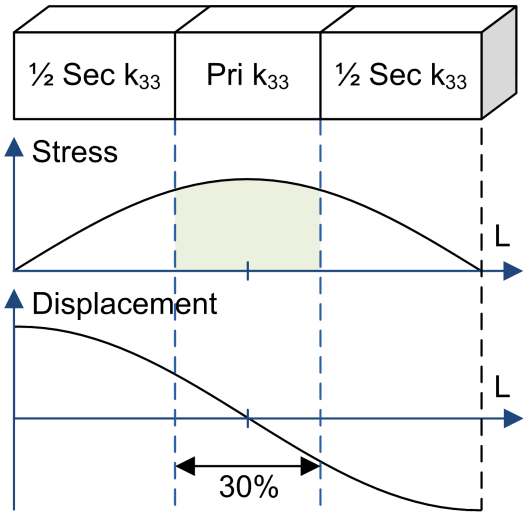

Figure 4.7: Visualization of the displacement and stress across the soft switching optimized Interleaved thickness mode PT.

As it can be seen, a sufficiently large ZVS factor is achieved, with a primary section size of 30 % or more. It can also be observed that the primary and secondary sections have significantly larger effective couplings, which reflects the higher potential of high efficiency and high power density. Again this is independent on the numbers of primary layers, so the results are general and the primary layers can be used to control the voltage gain of the PT.

PT height	20	mm
Primary volume	32.6%	
Primary "length"	6.53	mm
Primary layers	64	
Pri layer thickness	99	μm
Gain	98.8	

Table 4.4: Design specifications of the Interleaved thickness mode PT.

4.4.3 Prototype

Unfortunately no operational prototypes were built, due to the challenge of the very high build-up height. The 20 mm build-up height proved that it was very challenging to maintain consistency trough the build-up of 606 layers of 33 μm thick tape, to maintain consistent inter tape connection and to mill out the high structure. Table 4.4 lists the design specification of a 8 x 8 x 20 mm sized PT, having a voltage gain of 98.8. This design is pushing the limits of the build-up and manufacturing of our suppliers manufacturing capabilities, but not the limits of the thickness mode principle and operation, in terms of voltage and electrical field levels.

4.5 Interleaved interdigitated electrode PT

As it was described in the previous section, a thickness mode PT has a much higher potential for high efficiency and high power density, due to the high electromechanical coupling k_{33} of thickness mode vibrations. But as the build-up proved too challenging to manufactured, the Interleaved thickness mode PT was not the design to proceed with and another solutions was required. The basic principle of the Interleaved interdigitated electrode PT, is that it is a thickness mode PT, with at interleaved primary section, just as the Interleaved thickness mode PT. But instead of having the high build-up height of the Interleaved thickness mode PT, the structure is pushed over, so it is built-up "sideways", giving it a much lower build-up height. In this manner it combines the performance advantages of the thickness mode PT and the manufacturing advantages of the Rosen type PT. A detailed analysis and description of the research, can be found in [D.5].

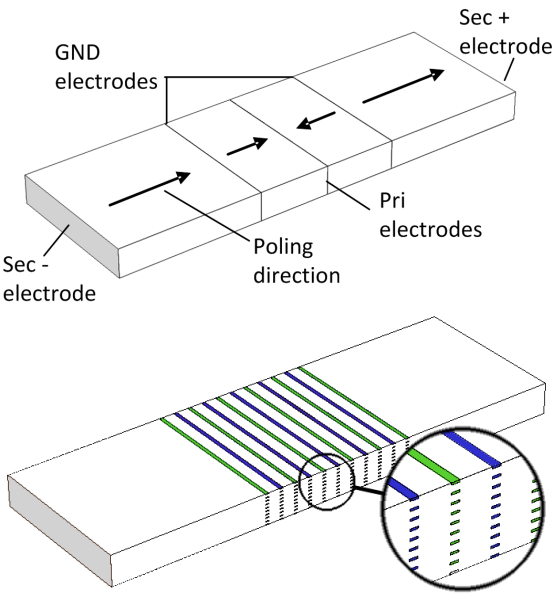

Figure 4.8: The Interleaved IDE PT structure (top) and principle of the IDE structure (bottom). For simplicity the PT structure, which has a size of 30 x 10 x 2 mm, only shows two primary layers and the arrows indicate the polarization direction. The IDE structure consists of a stack of thin horizontal electrode "line" (70 μm), which is printed on every tape layer, forming a vertical electrode.

4.5.1 Structure

Figure 4.8 illustrates the structure of the Interleaved interdigitated electrode PT and the principle of the interdigitated electrodes (IDE). As it can be seen the IDE structure consists of a stack of thin horizontal electrode "lines", instead of a single vertical electrode, as the tape casting technology only permits electrodes to be printed in the same plane as the tape (in-between the tape layers). The lines have a width of 70 μm, which is relatively wide compared to the thickness of 2-3 μm, and is limited by the printing technology. The lines are printed on every tape layer, which complicates the build-up process somewhat. In this manner a vertical electrode is constructed, that permits a low build-up height, which enables the utilization of simple tape casting manufacturing for long thickness mode structures.

The operational vibration resonance is along the longitudinal direction and is operated in its first longitudinal mode shape, as illustrated in Figure 4.9. The Interleaved IDE PT has the same potential of high soft switching and high voltage gain capabilities, as the Interleaved thickness mode PT. The voltage gain is also here directly proportional to the secondary and primary layer thickness ratio.

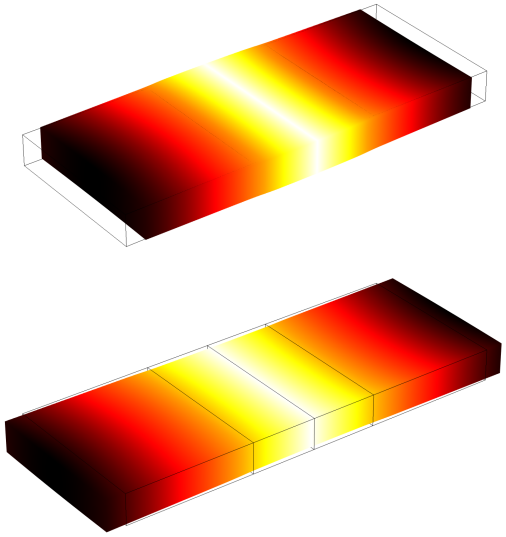

Figure 4.9: FEM simulation illustrating the operation in the first longitudinal mode shape, at 47.5 kHz, where light colors refer to a low displacement and dark colors to a high displacement.

The drawback of utilizing IDE's, when designing for high gain i.e. a high number of primary layers is needed, is that as the electrode lines have a finite width (70 μm) the IDE's occupy a significant part of the primary section. As the piezoelectric material enclosed by the IDE's is inactive[1], the active part of the primary section has been reduced, which degrades the effective coupling and performance. A high gain design is therefore a trade-off between the number of layers and the inactive volume occupied by the electrodes. Furthermore the layer thickness should be significantly thicker, than the spacing between the electrode lines (tape thickness of 33 μm), in order for the IDE structure to appear as a solid vertical electrode and produce a uniform electrical field

[1]No electrical field can be generated across the material by the IDE structure, thus making it impossible to polarize and excite it.

across the layer. Therefor the ratio between the primary layer thickness and the tape thickness, should be kept sufficiently large, preferably lager than 10.

4.5.2 Soft switching optimization

The Interleaved IDE PT achieves its native soft switching capabilities, through the optimization of the primary section size and position, just as the Interleaved Rosen type PT. Here again the interleaving design is key. The primary section is placed right in the middle of the excitation stress curve, as illustrated in Figure 4.10. As the

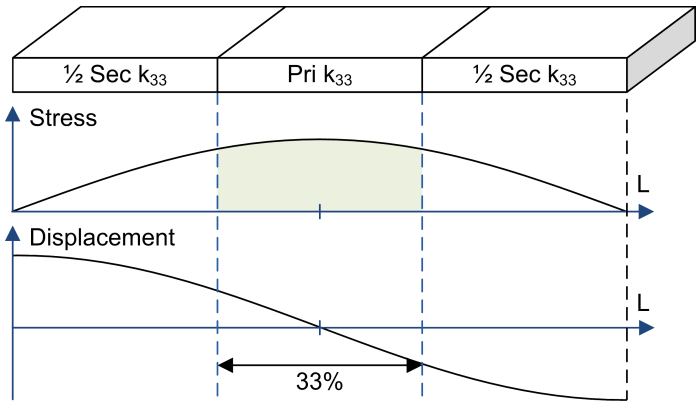

Figure 4.10: Visualization of the displacement and stress across the soft switching optimized Interleaved IDE PT.

IDE's occupy a significant and inactive part of the primary section, the effective coupling and hence soft switching capability is degraded somewhat. Therefor a primary section size of 30 % is not sufficient, as it were for the Interleaved thickness mode PT.

Table 4.5 illustrates how the effective coupling factors and the ZVS factor are dependent on the size of the primary section and the IDE's, of designs with 40 primary layers. As it can be seen a primary section size of 33 % and 36 % is needed, in order to achieve a sufficiently large ZVS factor, for a 30 mm and 20 mm design. The IDE's of the 30 mm design occupies 27.6 % of the primary section, which is high, but for the 20 mm design, the IDE's occupies an astonishing 37.9 % of the primary section, which really is pushing the limits of the concept, but maintains a decent effective coupling. Moreover the primary layer to tape thickness ratio for a 20 mm design is as low as 3.3 and the IDE's cannot be considered as solid electrodes any more, and the results are somewhat optimistic and misleading. The 30 mm design has a primary layer to tape thickness ratio for 5.5, which still is pushing the limits. Here the soft switching capability is not independent on the numbers of primary layers, but the primary layers can still be used to control the conversion ratio and voltage gain of the PT.

	Thickness mode		IDE structure		
PT length	30mm	30mm	30mm	20mm	20mm
Primary volume	30%	33%	**33%**	33%	**36%**
Primary layers	40	40	40	40	40
IDE vol. of Pri			27.6%	41.4%	37.9%
ZVS factor V'_P	110.3%	125.9%	106.2%	96.1%	105.3%
$k_{eff\ Pri}$	53.8%	55.9%	49.5%	45.0%	46.8%
$k_{eff\ Sec}$	42.4%	40.1%	39.8%	39.3%	37.7%
Pri th./Tape th.			5.4	2.9	3.3

Table 4.5: Soft switching optimization of the Interleaved IDE PT, achieved by primary section volume optimization and is generated through FEM simulations. The FEM simulation is a 2D simulation of a 30x10x2 mm structure, with 40 primary layers, where the IDE structure has been simplified to solid vertical electrodes. The results are independent of the size of the structure, but it is clear that it is dependent on the IDE volume (Primary to IDE volume ratio). The effective coupling factors are calculated from the FEM simulated primary and secondary impedance, and (4.2) is used to calculate the ZVS factor.

As it is evident, the high gain and high voltage requirements are really pushing the limits of IDE PT concept and dilutes the obvious advantages and high performance. The advantages of the IDE PT concept may be exploited in other more suited applications, of lower gain and lower numbers of primary layer, such as step-down applications or lower step-up applications[2].

4.5.3 Prototype

The discoveries of the previous section led to the development of three specific designs, which are shown in Figure 4.11(left). They all have a width of 10 mm and a height of 2 mm, which is very suitable for tape casting technology, and lengths of 20 mm, 25 mm and 30 mm.

Table 4.6 lists the specification of the three developed designs, possessing voltage gains from 44 to 47. These lower gains are the result of the limited opportunity of increasing the amount of primary layers. In the hunt of high gain and high voltage, the designs are really pushing the limits of the concept. Both in terms of inactive material in the primary section and the primary layer to tape thickness ratio, as describe in the previous section.

[2]If this DEAP application were to be driven by a higher supply voltage.

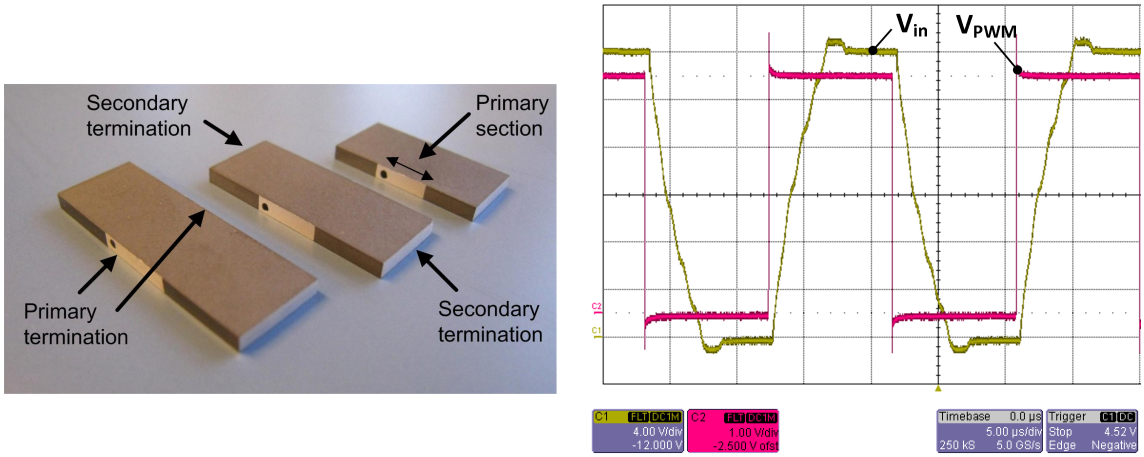

Figure 4.11: Picture of prototype PT's (left) of different sizes (length from left: 30 mm, 25 mm and 20 mm) and operational waveforms of a 25 mm prototype (right), operated at 24 V half-bridge voltage and a matched resistive load. The relative slow rising switching flanks and the MOSFET body-diode conduction voltage drop, at supply rails, clearly demonstrates ZVS operation.

Figure 4.11(right) illustrates the operation of the developed 30 mm IDE PT. As the waveforms reveals the half-bridge is clearly operated under ZVS, demonstrating the PT's soft switching capabilities. Moreover the PT has a moderate voltage gain, of approximately 38, in to a matched load. The drop in gain is due to the shortcomings of some of the IDE approximations and is elaborated further in [D.5]. As demonstrated earlier the FEM simulations formed a good development tool and there were a good correlation between the design and the manufactured prototypes.

PT length	20	25	30	mm
Primary volume	35.7%	33.3%	33.1%	
Primary length	7.13	8.33	9.93	mm
Primary layers	40	40	40	
Primary layer "thickness"	110	140	180	μm
IDE width	70	70	70	μm
IDE vol. of Pri	38.3%	32.8%	27.5%	
Gain	46.9	47.0	44.0	

Table 4.6: Design specifications of the Interleaved IDE PT, where the primary thickness have been rounded off in order to simplify the mechanical layout, which results in the bit odd primary volumes, compared to the ones of Table 4.5.

4.6 Summary

In this chapter several PT designs have been presented, all targeted at achieving high gain voltage and native soft switching capabilities. Furthermore the soft switching factor of section 3.2 is related to the structure of the PT, through the effective electromechanical coupling factors. This is advantageous as the effective coupling factors to some extent can be related directly to the mechanical structure and the excitation stress, enabling a much more intuitive design process and it has been heavily relied on through the research of soft switching optimized PT's.

The Interleaved Rosen type PT distinguish itself by being very straight forward and easy to manufacture, as the build-up structure and process is the same as for a simple multilayer Rosen type PT. The design possesses high voltage gain capabilities, demonstrating a voltage conversion ratio of 68, as well as it demonstrates soft switching capabilities. The main drawback is its low efficiency, due to the low electromechanical coupling k_{31}. A detailed analysis and presentation of the design is found in [D.3].

The Interleaved thickness mode PT has a high potential for higher efficiency, as both the primary and secondary section utilizes thickness mode vibrations, which has the highest electromechanical coupling. The challenging part of utilizing a pure thickness mode structure is the relative high build-up height, which is the result of the targeted high voltage output. A 20 mm high design is proposed, which possesses soft switching capabilities and a high voltage conversion ratio of 98. But the build-up of 606 layers of tape proved too challenging and as a result no operational prototypes were manufactured. The design is pushing the limits of the manufacturing process and improvements and optimizations are necessary, in order to exploit a pure thickness mode high voltage PT.

The Interleaved interdigitated electrode PT distinguish itself by having a higher efficiency, as both the primary and secondary section utilizes thickness mode vibrations, which has the highest electromechanical coupling. The usage of interdigitated electrodes and low build-up height, retain some of the easy manufacturing advantages. The drawback of using interdigitated electrodes and a high number of primary layers is that the electrodes occupy a significant part of the primary section, which degrades its performance. The design only demonstrates a moderate voltage gain of 38, due to the limited amount of primary layers, which is the result of a design trade-off between the number of layers and the inactive volume occupied by the electrodes. But the design does demonstrate soft switching capabilities and the advantages of the design may be exploited in other more suited applications, such as step-down applications. A detailed analysis and presentation of the design is found in [D.5].

Chapter 5

Piezoelectric transformer based power converter control

A big part of the research in this study has been focused on control methods for PT based power converter, in order to overcome some of the control challenges, prompted by the nature of the PT. As described in Overview and State of the art chapter 2 the PT resonance is of very high quality factor and the band of optimal and efficient operation is very narrow. The band of operation is even further reduced when employing inductor-less topologies (chapter 3), that utilizes PT's with native soft switching capabilities (chapter 4). As the resonant frequency is subject to variations, caused by internal or external influences, such as temperature, load variations, aging etc., the main objective is to ensure optimal operation and a tight control of the operating frequency. Even small deviations from the optimal operating frequency can easily totally destroy the operation and efficiency.

Furthermore efforts have been made to develop a bi-directional control method, as this will greatly improve the performance of the overall system, of the highly capacitive DEAP load. But also because no bi-directional PT concepts exist to date and it will have a huge potential in various other applications, such as enabling line and load regulation.

An additional challenge of the DEAP application is the high output voltage (up to 2.5 kV) and high output impedance, as it makes it quite difficult to have an output feedback, without dissipating a significant part of the output power or adding any significant parasitic component to the switching node. A detailed analysis of a high impedance and high voltage measurement (HVM) circuit is presented in [D.1] and is used for output voltage feedback.

5.1 Self-oscillating control

As it was shown in section 3.2, soft switching optimized PT's possess an optimal point of operation, where inductive behavior and resonating energy of the PT is maximized, maximizing soft switching capability. This point of operation was closely linked to the phase and magnitude of the PT voltage gain and resonant current. As the PT resonance is of very high quality factor, the phase will change rapidly just around the resonance. The phase shift is locked to the resonance, as well as the point of maximal

soft switching capability. And as the phase lag at the point of optimal operation stays constant, despite changes in frequency, makes it a very applicable feedback signal. Control methods such as PLL relies on this phase response, but also the phase shift self-oscillating control takes advantages of the phase response, which can be exploited in PT based converters. Self-oscillating control is widely used for class-D amplifiers [86, 87, 88, 89] and has also been used in PT based converters [42, 66], but has never been used in connection with inductor-less topologies and soft switching optimized PT's.

The combination of inductor-less PT based power converters and self-oscillating control has shown to be very advantageous, due to the high requirements of a tight frequency control, and has led to the patent application [D.8]. Furthermore, the concept is fairly simple, as well as it has a very fast response to track and "hit" the resonant frequency at startup, which is beneficial when utilizing burst-mode control (see subsection 2.4.4).

5.1.1 Self-oscillating control with voltage feedback

Figure 5.1 illustrates the basic principle of the self-oscillating control with voltage feedback. The concept is simply to have a phase shift in the closed loop of a multiple of 360^o, making it highly unstable, which induces self-oscillation. As the PT has a output voltage phase lag of 102^o, at the optimal operating point, the remaining parts in the closed loop should be adjusted, so they add up to 360^o. As the output voltage is a sine-wave an additional phase lag can be added by a simple low-pass filter, which is easily adjusted. But also other circuits can be utilized, such as a time delay or

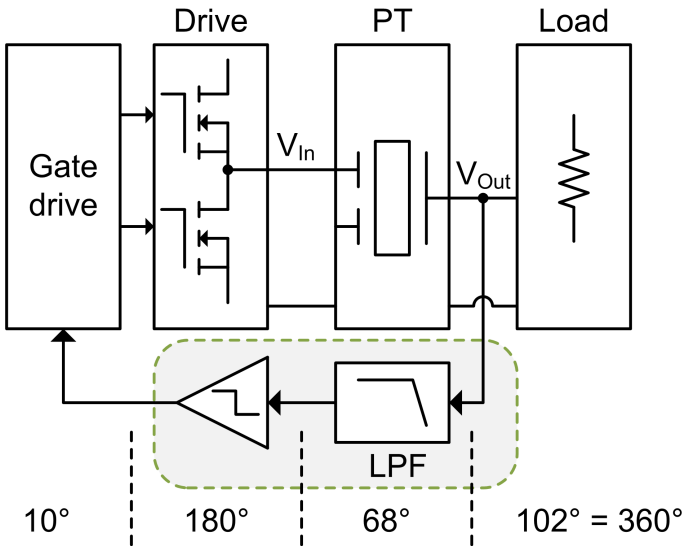

Figure 5.1: Block diagram of the self-oscillating control scheme with voltage feedback, where the PT has a output voltage phase lag of 102^o, at the optimal operating point.

even a high-pass filter, where the total phase lag of the loop should add up to 0^o. Common for them all are that the phase response will occur much slower than for the PT, making the phase lag of the PT the determining factor in the closed loop. Furthermore the inverting comparator, which generates 50 % PWM from the sine-signal, adds a phase lag of 180^o, and some delay in the gate drive is expected, as well as the gate drive handle the dead-time of the switches. Adding everything up, result in a required phase lag of the low-pass filter of 68^o, in order to lock to the optimal operating point.
The method is also applicable for rectified outputs, where the feedback signal will be squarish, but a simple low-pass filter can still be utilized and add phase lag.

5.1.2 Self-oscillating control with current feedback

Due to the challenges of high output voltage (up to 2.5 kV) and high output impedance, the self-oscillating control with voltage feedback might not be the most obvious and straightforward choice. An obvious alternative is to use the PT resonant current as feedback signal instead, as it also was shown that the optimal operating point was linked to a resonant current phase lag of 56^o.

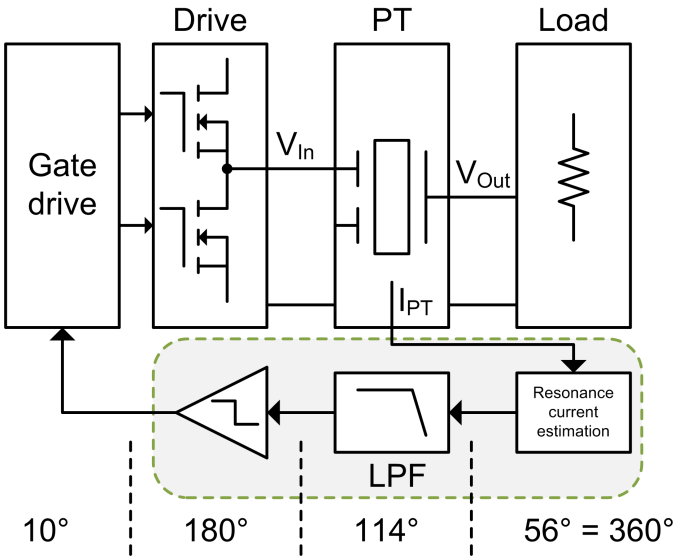

Figure 5.2: Block diagram of the self-oscillating control with resonant current feedback, where the PT has a resonant current phase lag of 56^o, at the optimal operating point.

Figure 5.2 illustrates the basic principle of the self-oscillating control with current feedback, where the phase summation is analogue to voltage feedback, though needing a higher phase lag of the low-pass filter, in order to achieve a total of 360^o. But as the resonant current only is externally available when the switches are conducting, only parts of the resonant current can be measured directly.

5.1.3 Resonant current estimation

The missing parts of the resonant current can be estimated as shown in [63, 64], by differentiating the voltage of the switching flanks, as the input voltage over the input capacitor C_{d1} reflects the resonant current, when it is charged and discharged. This principle can be used to generate the feedback for the self-oscillating control, as illustrated in Figure 5.3.

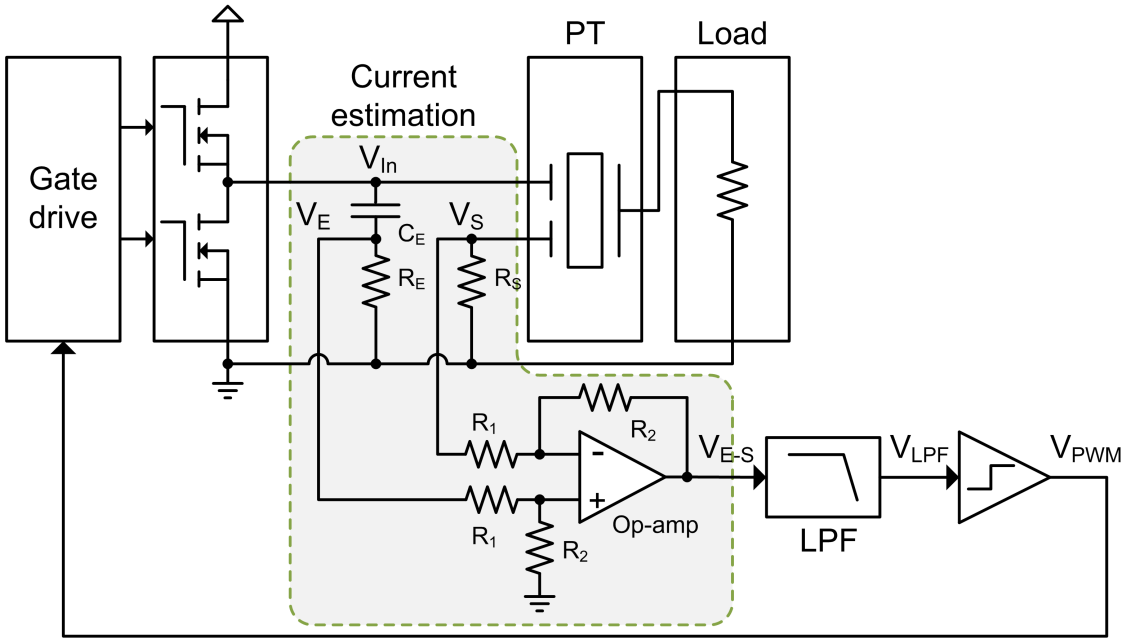

Figure 5.3: Block diagram of the self-oscillating control with resonant current feedback and the implementation of the current estimation.

As it can be seen a differential coupled operational-amplifier is used to subtract the two measurements, instead of a adding configuration. This has the advantage of a bit more straightforward configuration of the measurement resistors R_E and R_S, which retain common ground for the entire circuit. Furthermore the gain of the differential amplifier can be controlled by R_1 and R_2, so that a large and clear signal (V_{E-S}) is passed on to the low-pass filter. R_S is a simple current measurement resistor, which measures the conducted resonant current. R_E and C_E forms a simple high-pass filter, which acts as a differentiator, when configured with a crossover frequency considerably higher than the operating frequency. Through the component values of the high-pass filter, the gain can to some extent be controlled and matched to the gain of R_S. Figure 5.4 illustrates the operational wave-forms of the current estimation and of the remaining components in the closed loop. As it can be seen, the two measurements V_E and V_S resembles the resonant current, as well as the inversion of the differential amplifier and the added phase lag by the low-pass filter, can be observed. Furthermore the slow rising switching flanks of the input voltage V_{In} clearly reveals soft switching operation, which confirm operation at the optimal

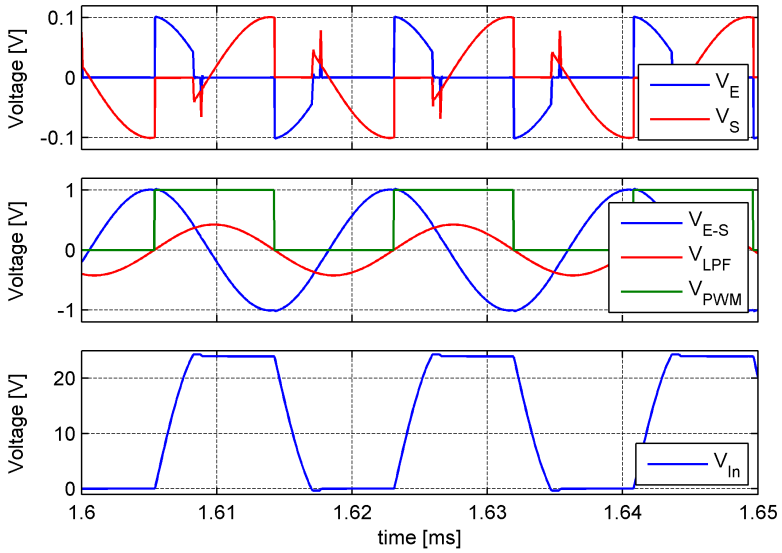

Figure 5.4: Operational wave-forms illustrating the functionality of the current estimation and the self-oscillating control.

point of operation and validates the self-oscillating control.

5.1.4 Experimental verification

The self-oscillating control has been substantially used throughout this study and primarily together with the resonant current estimation, in order to avoid the high

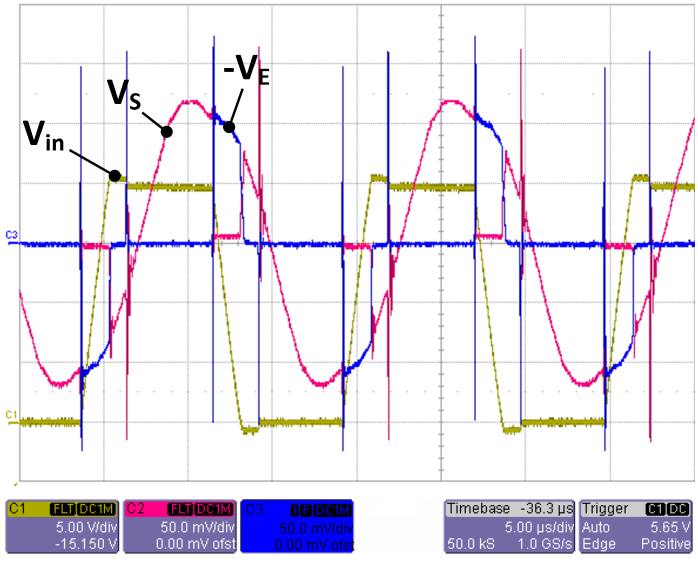

Figure 5.5: Operational wave-forms demonstrating the functionality of the current estimation, as well as demonstrating that the self-oscillating control locks to the point of optimal operation, as the slow rising switching flanks clearly reveals soft switching operation. The utilized PT is a 25x10x2 mm Interleaved Rosen type PT [D.2] (section 4.3).

voltage output. Figure 5.5 demonstrates the functionality of the self-oscillating control with resonant current feedback and resonant current estimation, where it can be seen that the magnitude of the two current estimation measurements are matching each other. Moreover it validates the self-oscillating control, as the slow rising soft switching flanks confirms operation at the optimal point of operation.

The self-oscillating control with resonant current feedback and resonant current estimation has proven to have some obvious advantages, primarily being the tight frequency control, but also the avoidance of the high voltage output. Another obvious advantage is that no signal from the secondary side is required, which is desirable in isolated applications, as it is inconvenient and troublesome to transfer signals across the isolation boundary. A thorough description of the self-oscillating control and resonant current estimation can be found in [D.8].

5.2 Forward conduction mode control

As it was shown in section 3.2 the point of optimal operation was closely linked to the phase and magnitude of the PT resonant current. The forward conduction mode (FCM) control proposed in [D.7], relies on the phase response of the PT resonant current, just as the self-oscillating control, but in a manner that resembles the PLL control. The FCM control method depends on a detection of the forward conduction period of the half-bridge switches, which can be measured with a simple sense resistor. The resonant current phase lag is reflected in the forward conduction period, as the switches forward conduction is getting limited at increasing phase lag, which can be used as a feedback signal. Furthermore the FCM control is very simple and hence low cost, as well as it is purely primary based, avoiding the need of crossing any isolation

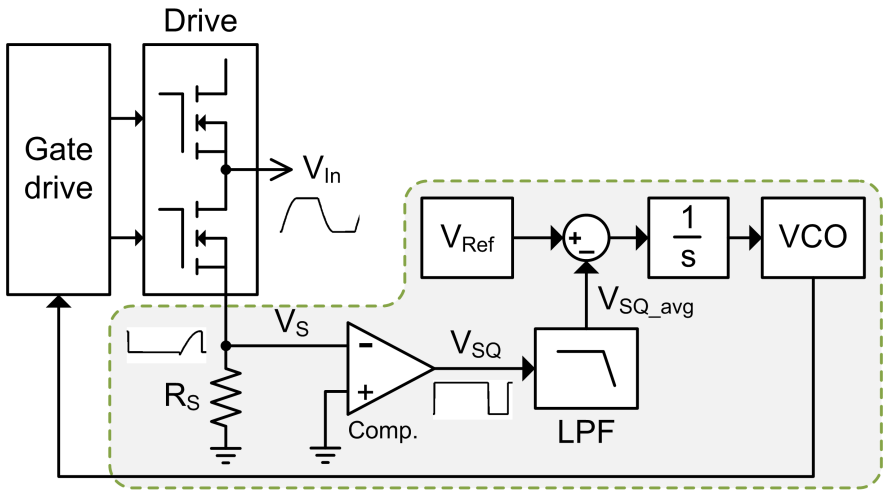

Figure 5.6: Functional block diagram of the FCM control method, composing a forward conduction detector (Comp.), an averaging low-pass filter, an error signal generating subtracter, an integrator and a VCO.

boundary, which is desirable in isolated applications.

5.2.1 Operational principle

Figure 5.6 illustrates the functional block diagram of the FCM control, where the sense resistor R_S and the comparator detects the forward conduction period of the low side switch. The comparator produces a square-wave signal V_{SQ}, which is passed through an averaging low-pass filter, where the average signal is proportional to the forward conduction period and duty cycle (FCD) (5.1).

$$V_{SQ,avg} = V_{CC} \cdot \frac{T_{Forward}}{T} = V_{CC} \cdot FCD \tag{5.1}$$

Together with a reference, the average signal is used to control a VCO, which drives the gate-drive, closing the loop around the half-bridge. In this manner the FCM con-

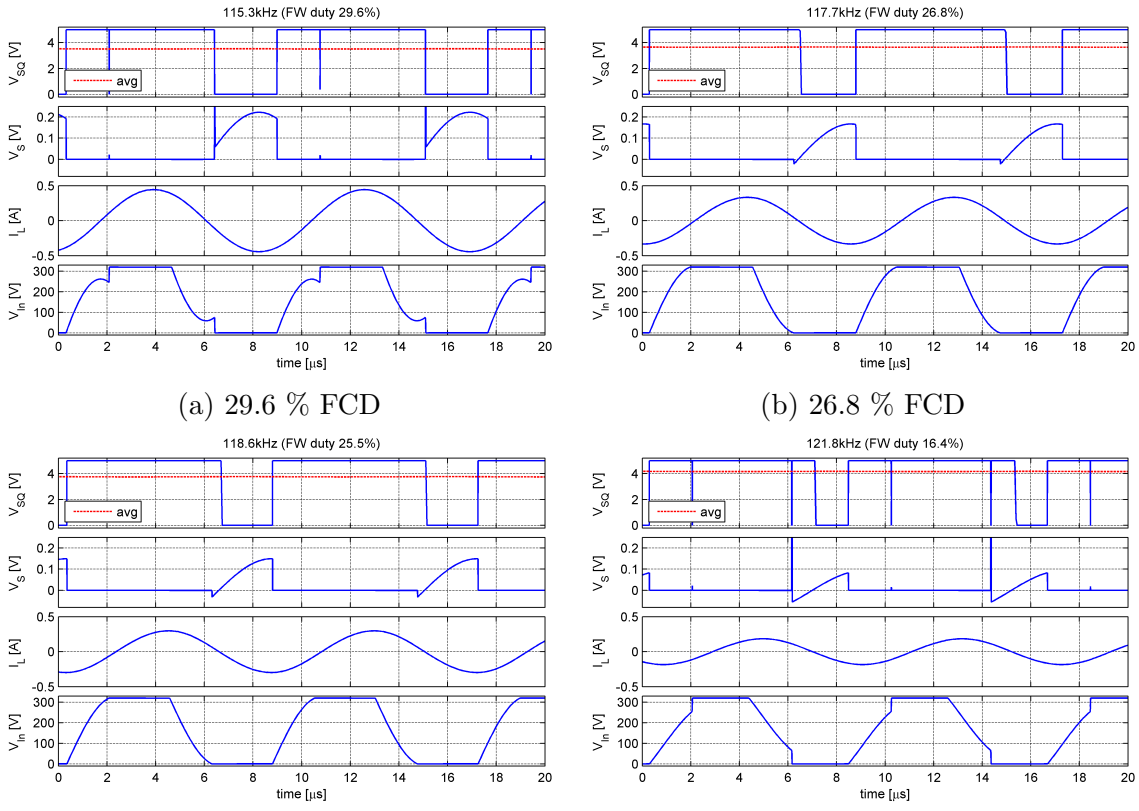

(a) 29.6 % FCD

(b) 26.8 % FCD

(c) 25.5 % FCD

(d) 16.4 % FCD

Figure 5.7: Forward conduction mode control operation waveforms, at different operation frequencies and with constant dead-time, illustrating the forward conduction period and duty cycles (FCD) variation. In (a) and (d) the half-bridge (V_{IN}) is clearly operated under hard switching, whereas (b) and (c) is operation under ZVS. (b) and (c) are furthermore close to the boundary of soft switching operation, where the optimal point of operation is located roughly right in-between (b) and (c).

trol seeks to maintain a constant forward conduction duty cycle, of approximately 26 %, and henche a constant resonant current phase lag, ensuring operation at the optimal operation point. Compared to the self-oscillating control, the FCM control achieves the same objectives of operating at the optimal operating point, but a drawback could be the much slower control loop. Figure 5.7 illustrates the operational wave-forms of the FCM control, at different operation frequencies. As the wave-forms reveals the forward conduction period and the average signal V_{SQ}, are modulated continuously over the frequency range, which makes it a very applicable and reliable feedback signal. In Figure 5.7 (b) and (c) the slow rising switching flanks of the input voltage V_{In} clearly reveals soft switching operation, and in-between these two operating points soft switching operation is maintained and the optimal point of operation is located roughly right in-between (b) and (c).

5.2.2 Experimental verification (PFC LED drive)

A clear advantage of the FCM control is that the feedback signal is independent on the magnitude of the resonant current, as the forward conduction period measurement is independent of the magnitude. And as the FCM control ensures a constant and optimal operating point, the PT is essentially equivalent to a transformer with a constant gain. This has been utilized in a simple passive PFC LED application, where the half-bridge voltage is allowed to vary with the rectified AC mains voltage, resulting in a AC mains current modulation, and is presented in [D.7].

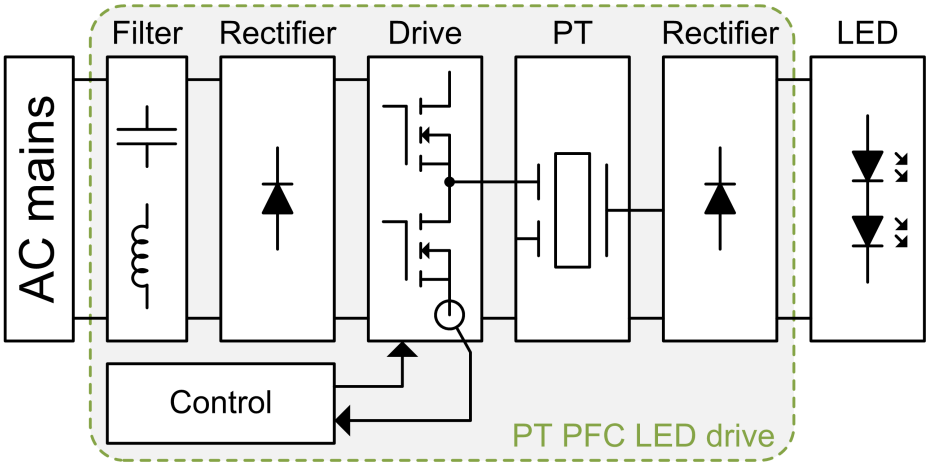

Figure 5.8: Block diagram of the PT LED drive, employing passive PFC and Forward Conduction Mode (FCM) control.

Figure 5.8 illustrates the block diagram of the proposed PT LED drive, with the intention of acting as a simple resistive load, without load and line regulation. The passive PFC is achieved by having a sufficiently small half-bridge supply voltage buffer capacitor, after the input full-bridge rectifier, allowing the voltage to follow the rectified AC mains voltage. As the PT can be assumed to have a constant gain

(assuming a constant operation point and load), the resonant current will be proportional to the rectified AC mains voltage and the resulting current drawn from the AC mains will therefore also be proportional to the AC mains voltage. This is a very simple way of achieving PFC, no additional components or control are needed, on the contrary it minimizes the voltage buffer capacitor, which typically is quite large in order to buffer energy for 10 ms (100 Hz). The drawback of doing it in this way is that the output power will also be modulated by the AC main. This modulation is acceptable for this LED application, but for other DC output applications this PFC method might not be applicable.

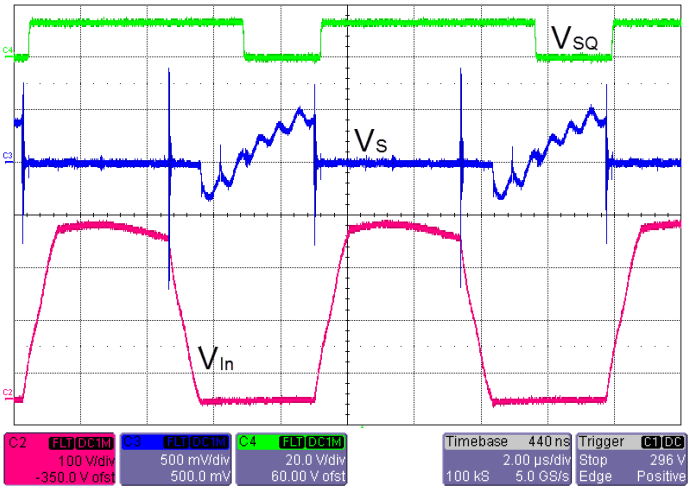

Figure 5.9: Forward conduction mode waveforms, demonstrating the FCM functionality and has a 26.4 % FCD.

Figure 5.9 demonstrates the functionality of the FCM control, near AC mains peak voltage, where the current sense V_S, the comparator square-wave V_{SQ} and input voltage V_{In} are shown. As it can be seen the half-bridge switches are operated under soft switching, which confirms that the PT is operated at the optimal point of operation and validates the FCM control.

Figure 5.10 demonstrates the functionality of the passive PFC, where the input voltage V_{AC} and current I_{AC} are shown. As the figure reveals the voltage and current are in phase, as well as the current somewhat resembles a sinusoidal, although it has some distortion. The main reason for this distortion, is the fact that the LED load does not represent a perfect constant load, as assumed. This results in some variation in the operating point, hence variation in gain, as the very slow control loop (14.2 Hz crossover frequency), of the implemented FCM control, is unable to track this variation. The slow control loop is implemented in order to overcome the challenge of the AC zero voltage crossing[1], as the resonant current also reaches zero,

[1]The AC zero voltage crossing is also a challenge for all other control methods and is typically managed by having a very slow control loop.

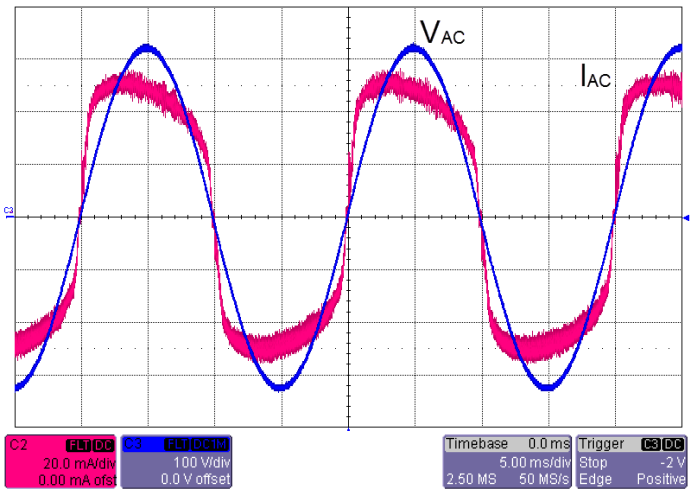

Figure 5.10: AC mains input voltage and current, having an input power of 9.5 W and a power factor of 0.96.

making it impossible to detect the forward conduction period. With a power factor of 0.96, the circuit demonstrates the ability of PFC, but with room for improvements.

This simple PFC LED application demonstrates the functionality of the FCM control, as well as its usage in PFC applications. Further details of the PFC LED application and FCM control can be found in [D.7].

5.3 Bi-directional control

As described in chapter 2 the targeted DEAP load is highly capacitive and the objective is to performing a controlled voltage modulation of the DEAP load, or in other words charge and discharge the capacitive load. So far the discharge of the DEAP has been performed by dissipating the energy in a resistive network, which is inefficient, but very simple. As only a small fraction of the electrical applied energy is converted to mechanical energy (2-5 %) and the remaning energy is stored as electrical energy in the capacitance of the DEAP, a resistive discharge results in a very inefficient overall system. Since the electrical stored energy is recoverable, it is very desirable to develop a bi-directional PT concept, as this will greatly improve the efficiency and performance of the overall system.

Furthermore no bi-directional PT concepts exist to date and it will have a huge potential in various other applications, such as enabling line and load regulation applications. The proposed bi-directional control method of the following section has demonstrated fully bi-directional capabilities, which has led to the patent application [D.9], where a thorough description of the control method can be found.

5.3.1 Active phase shift

The proposed bi-directional control concept is fairly simple, as illustrated in Figure 5.11, but as it will be evident in the following, the implementation becomes a bit more complex, when employing self-oscillating control.

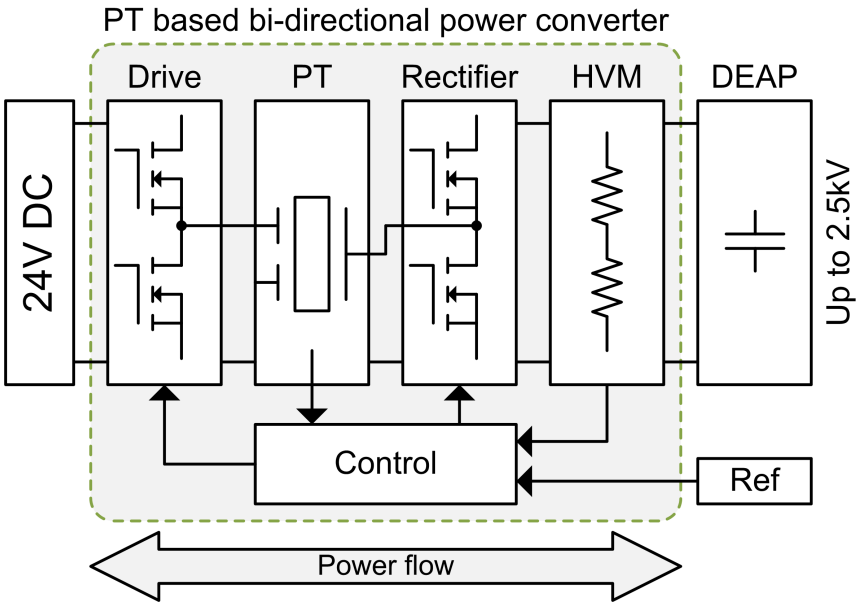

Figure 5.11: Block diagram of the bi-directional control method, with the addition of an active output rectifier.

The fundamental basis of the bi-directional control is the replacement of the simple diode output rectifier, with an active MOSFET half-wave rectifier. Instead of controlling the rectifier switches directly and synchronized with the PWM of the input half-bridge, the rectifier is just acting as a simple active rectifier, for now. Where active diodes simply turn ON when exposed to a forward current. The reason not to use control or gate signals directly derived from the half-bridge PWM, is due to the varying ON-time of the rectifier switches, which is a result of the PT output capacitor C_{d2}. When the PT resonant current is reversed, the currently conducting diode stops to conduct, as it is getting reversed biased. But before the second diode is forward biased and starts to conduct the current, the resonant current need to charge or discharge C_{d2}. And as the rectifier output voltage is variable, hence the charge and discharge voltage of C_{d2} is variable, the charge and discharge time is also variable, making it very difficult to determine the exact turn ON-time.

In this approach the simple active diodes turns ON when exposed to a forward current, but are allowed to conduct a reverse current until it is turned OFF. The turn OFF signal is derived from the half-bridge PWM and this signal can then be phase shifted from the point where only a forward current is conducted, to the point where almost only a reverse current is conducted. In this manner the power can

be continuously modulated from full forward power, to full reverse power, enabling bi-directional power flow and energy recovery.

Figure 5.12 illustrates a functional block diagram of the bi-directional power converter, where the explained blocks can be recognized, being the MOSFET based half-wave output rectifier and the turn OFF control signal, derived from the half-bridge PWM. The signal is passed through time delay circuits, which adds and controls the phase shift. Furthermore the self-oscillating control with current feedback can be recognized (subsection 5.1.2), as well as the remaining power converting blocks. The additional blocks compose a resonant current control and an output voltage control. Moreover, it can be seen that the high-side gate drive of the rectifier is not connected to the driving signal of the low-side gate drive, but it is in fact indirectly controlled by the same signal and a detailed description will follow in subsection 5.3.3.

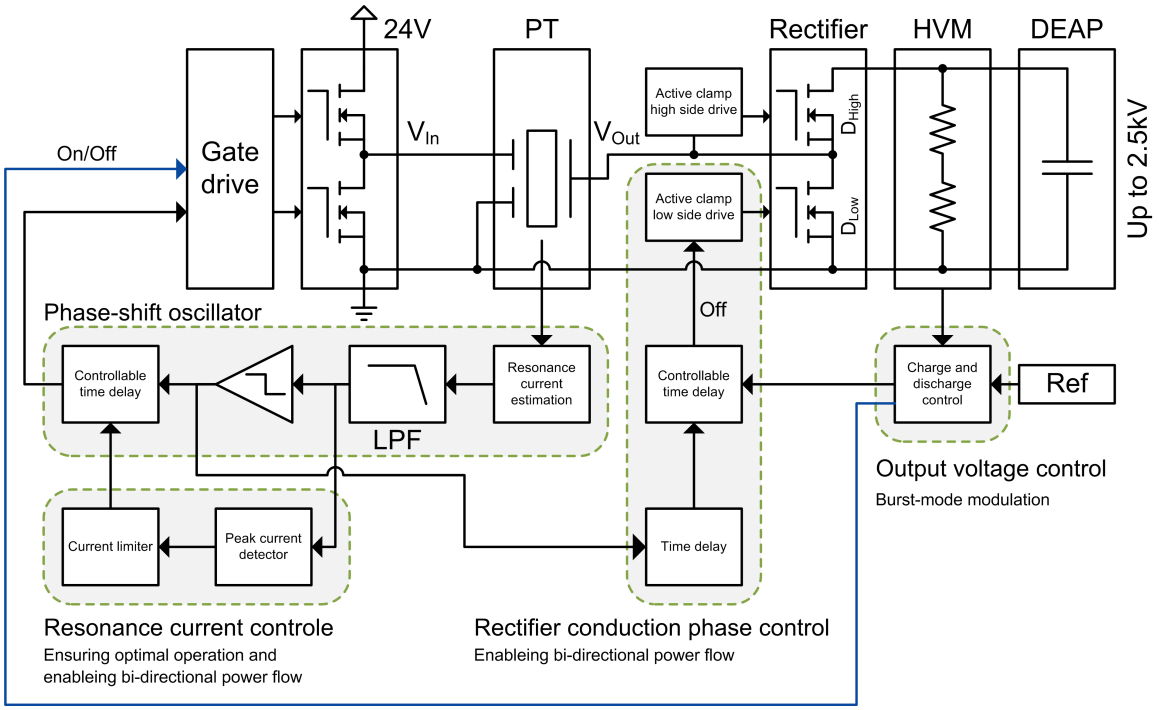

Figure 5.12: Functional block diagram of the bi-directional control method, employing self-oscillating control with current feedback.

The output voltage control simply compares the output voltage with a reference voltage and adjust phase shift accordingly, depending on if a charge or discharge is needed. Moreover, it can totally shut down the converter, if no change is needed, and thereby reduce the idle power consumption, in a burst mode manner (subsection 2.4.4).

The resonant current control ensures a consistent resonant current magnitude, which is required as a result of the change in the PT phase response. The PT phase

response change is caused by the change in impedance of the resonant tank, which is a result of the phase shift of the output rectifier. As the self-oscillating control relies on the PT phase response, the phase shift in the closed loop needs to be adjusted accordingly, in order to maintain operation at the optimal point of operation, this is achieved by the inserted time delay. This complicates the self-oscillating control and the implementations somewhat, which is inconvenient. But this is also a challenge for all other controls that relies on the PT phase response, such as PLL and FCM control, which also need an adjustment of the targeted phase, in order to ensure a constant and optimal operation point.

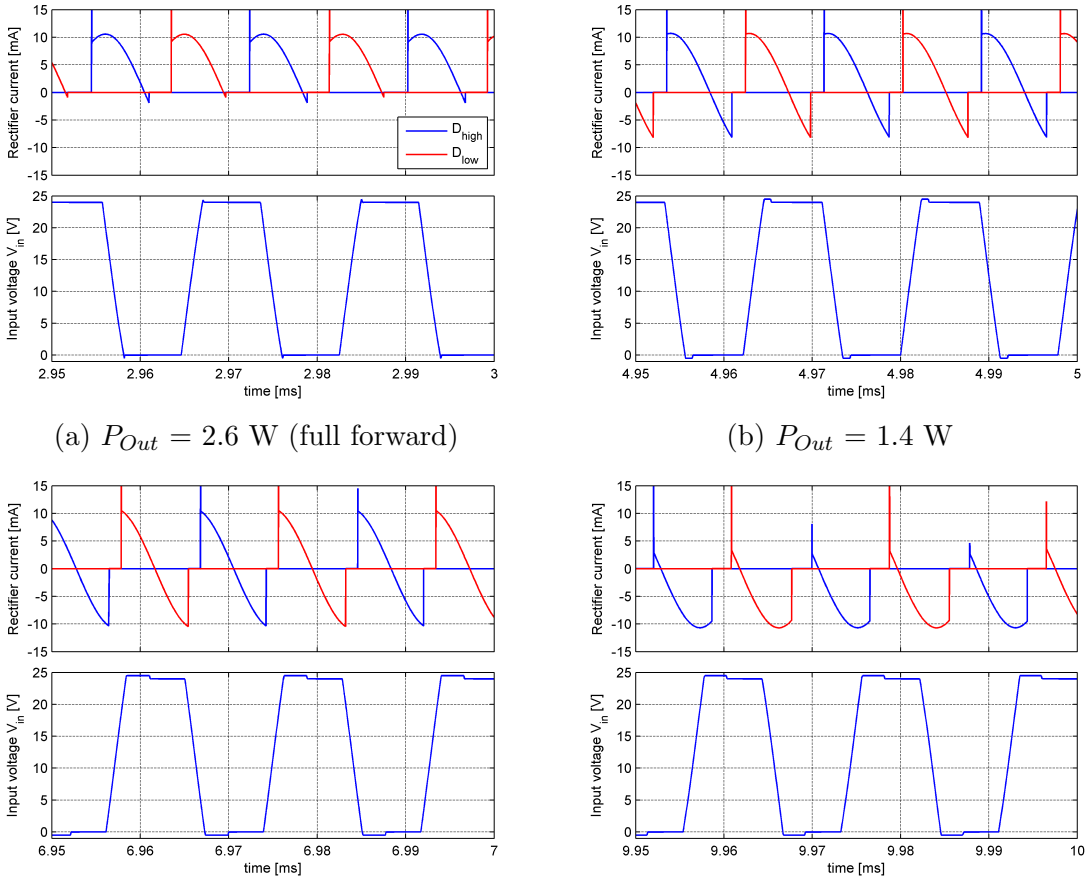

(a) P_{Out} = 2.6 W (full forward)

(b) P_{Out} = 1.4 W

(c) P_{Out} = 0 W

(d) P_{Out} = -2.4 W (full reverse)

Figure 5.13: Operation waveforms of the bi-directional control, at different phase shifts, illustrating the variation in forward and reverse conduction of the output half-bridge.

Figure 5.13 illustrates the operational wave-forms of the bi-directional control, at different phase shifts and power flows. As it can be seen the active diode current can be shifted from full forward to full reverse current, where a 2.6 W forward power flow is sifted to a 2.4 W reverse power flow.

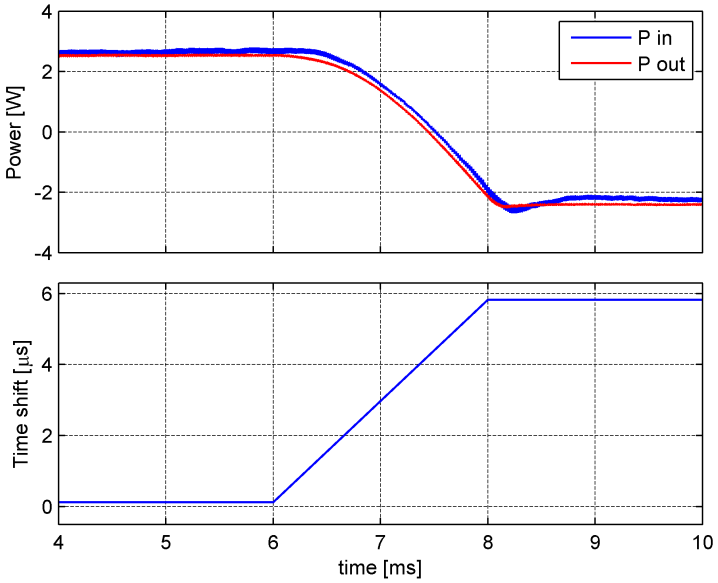

Figure 5.14: Power flow in the bi-directional PT based power converter, showing the shift and reversal in power flow, in relation to the applied time shift.

Figure 5.14 illustrates the power flow change from full forward power to full reverse power flow, in relation to the time delay, which causes the phase shift. As the figure reveals the power flow can be modulated smoothly from full forward power to full reverse power.

5.3.2 Discussion and potential

I this manner bi-directional power flow is achieved in a PT based power converter, which enables energy recovery for this DEAP application and greatly improves the efficiency of the overall system. Furthermore the concept incorporates self-oscillating control, taking advantage of its qualities, but the concept is not limited to self-oscillating control and other PFM control methods can be used. Moreover the proposed bi-directional concept is not limited to this DEAP application and has a huge potential in various other applications, such as applications of line and load regulation. Another huge potential is its enabling of soft switching operation of non-soft switching optimized PT in inductor-less topologies. This can be achieved through the phase shift of the output rectifier and by adding a small phase shift, the retained current will help to charge and discharge C_{d1} and enable soft switching operation. This small phase shift can also be viewed as a change in impedance of the load, so the soft switching operation is achieved by moving away from match load, which increases the soft switching capability.

5.3.3 High voltage high-side gate drive

As mentioned in the previous section, the high-side gate drive of this high voltage DEAP application is a little special. Conventional gate drives are the most obvious choice, but the availability of gate drives rated for more than 2.5 kV are very limited, as well as the high impedance output is very sensitive to any added parasitic components, demanding quite high requirements for low parasitic component in the switching node V_{Out}. Therefore a new type of high-side gate drive has been proposed, which is presented in this section and is included in [D.9] as well.

As a starting point, the most critical part of the switching node V_{Out} is the capacitance, as any parasitic capacitance adds directly to the PT output capacitor C_{d2}, which needs to get charge and discharged and retain some of the resonant current. As the PT designs presented in chapter 4 [D.2,D.5] have a output capacitor C_{d2} in the range of 20 pF, a simple half-wave diode rectifier, with a diode capacitance of 2 pF, is already adding a significant capacitance to the switching node (4 pF). So the main objective has been to minimize the capacitance of the high-side gate drive, as it is directly connected to the switching node V_{Out}. Figure 5.15 illustrates the functional block diagram of the proposed high-side gate drive, which is connected to the high-side switch D_{High} in the rectifier and the output voltage of the PT V_{Out}. As it can be seen it utilizes a traditional bootstrap diode D_{Boot}, which charges the local energy supply V_{Local}, when the switching node V_{Out} is at ground potential, just as for a conventional gate drive. Furthermore the forward current sense can be recognized, which turns ON the switch when a forward current is detected, just as described in the previous section. But instead of using the same turn OFF signal as the low-side gate drive and level shift the signal, a simple timer is in charge of the turn OFF.

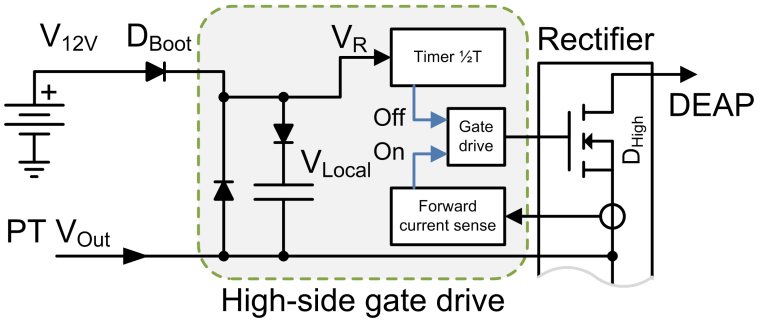

Figure 5.15: Functional block diagram of the high voltage high-side gate drive, utilized in the high voltage bi-directional concept.

The timer is set to half a cycle period and is triggered as the switching node V_{Out} leaves ground potential. In this manner the high-side switch will have the same phase shift as the low-side switch, as the switching node V_{Out} will not leave ground potential before the low-side switch is turned OFF and any added phase shift will be transferred to the high-side switch. Essentially the timer senses when the bootstrap diode D_{Boot}

is reverse biased, where the reverse biasing indirectly will force the voltage V_R to drop from the local supply voltage V_{Local}, to the local ground reference. The principle of the circuit is quite simple and will only adds the parasitic of a single bootstrap diode, as well as the parasitic of the surroundings, to the switching node V_{Out}. But the timer assumes a constant cycle period, which is not true, as the resonant frequency will vary over temperature and aging. But as the variation in frequency is relatively small (up to 1-2 %), a constant and predetermined timer is a durable solution. It should also be remembered that it is only because of the high voltage and low impedance, that a traditional gate-drive is avoided, which would not have this issue. In order to achieve a perfect time delay of the timer, an additional circuit could be implemented, which measures the cycle period time of V_R and adjusts the timer accordingly (half the period time), as V_R has the period time of the operating frequency.

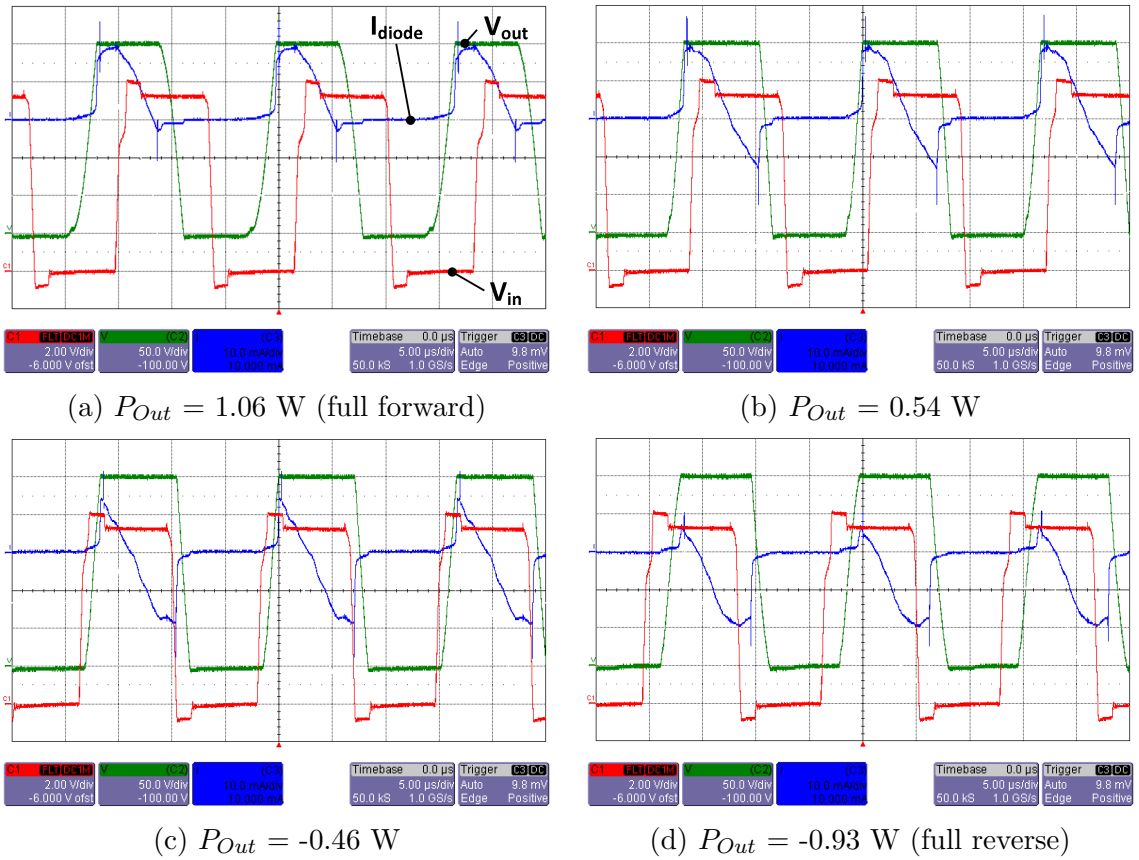

(a) P_{Out} = 1.06 W (full forward)

(b) P_{Out} = 0.54 W

(c) P_{Out} = -0.46 W

(d) P_{Out} = -0.93 W (full reverse)

Figure 5.16: Operational wave-forms for the prototype bi-directional PT based power converter, at different phase shifts, illustrating the variation in forward and reverse conduction of the output rectifier. The converter utilizes the Interleaved IDE PT (section 4.5 [D.5]) and the output is connected to a voltage source, in order to achieve steady state operation. Furthermore the PT output is inverted, giving the output wave-forms a 180^o phase shift, compared to the results of subsection 5.3.1.

5.3.4 Experimental verification

The bi-directional control has been realized in a prototype PT based power converter, in order to demonstrate its functionality and capabilities, and the full schematic of the prototype can be found in Appendix C. The prototype utilizes a 27x10x2 mm Interleaved IDE PT (section 4.5 [D.5]), which has a slightly increased ZVS factor (36% primary volume), compare to the 30 mm version. The interleaved IDE PT puts some limits on the achievable output voltage, due to the moderate voltage gain of this PT type and therefor a full 2.5 kV output voltage were not pursued at this point. On the contrary the output voltage and power level were fixed at a lower level, which eases the setup and measuring somewhat, and the experiment primarily represents a demonstration and validation of the functionality of the bi-directional concept.

Figure 5.16 illustrates the operational wave-forms for the bi-directional prototype, where the phase shift of the high-side rectifier D_{High} can be recognized, which leads to a reduction (Figure 5.16(b)) and reversal (Figure 5.16(c) and (d)) of the power flow. As it can be seen both the input half-bridge V_{In} and output rectifier V_{Out} are operated under ZVS, which clearly validates the functionality of the bi-directional control and concept. It can be observed in Figure 5.16(d) at full reverse power flow, that yet a small forward current is conducted. This is required as the active diode needs to detect a forward current, in order to turn itself ON, or else it will not turn ON, which will led to a unstable situation, where it is conducting every second period and really distort and corrupt the operation of the converter.

	Input			Output			
	V_{in} [V]	I_{in} [mA]	P_{in} [W]	V_{out} [V]	I_{out} [mA]	P_{out} [W]	η
Forward	24.1	85.3	2.05	300	5.67	1.70	83.0%
Reverse	24.1	-42.5	-1.02	300	-4.50	-1.35	75.9%

Table 5.1: Efficiency measurements of the bi-directional prototype. Showing the total converter efficiency, excluding control consumption, in full forward and full reverse operation.

Table 5.1 lists the power and efficiency measurement of the bi-directional prototype, at full forward and full reverse power flow. As it can be seen, the prototype possesses an efficiency of 83.0 % in full forward operation, which is decent. In full reverse operation the prototype possesses an efficiency of 75.9 %, which is an acceptable drop in efficiency. The efficiency is somewhat to the low side and is mainly due to the losses of the PT, as well as the half-wave output rectifier is not a real good match for the PT. Both issues reduce the efficiency. Furthermore the efforts have been focused more on the functionality and demonstration of the concept, than on optimizing the efficiency in particular.

5.4 Summary

In this chapter several control method, suited of PT based power converters, have been proposed, all targeted at achieving optimal and soft switching operation of the PT.

The Self-oscillating control takes advantage of the rapid phase response of the PT right around the resonant frequency, where the self-oscillating control is locked to a predetermined phase shift of the PT. As the optimal point of operation (where soft switching capability is maximized) is closely related to the phase response of the PT, a very tight and precise frequency control is achieved, ensuring optimal operation at all time. The concept is simply to have a phase shift in the closed loop of a multiple of 360^o, making it highly unstable, which induces self-oscillation. Furthermore, it has a very fast response to track and "hit" the resonant frequency at startup, which is beneficial when utilizing burst-mode control.
A configuration with current feedback and resonant current estimation has the advantage of avoiding the high voltage output. Another obvious advantage is that no signal from the secondary side is required, which is desirable in isolated applications, as it is inconvenient and troublesome to transfer signals across the isolation boundary. The combination of inductor-less PT based power converters and self-oscillating control has shown to be very advantageous, and has led to the patent application [D.8].

The Forward conduction mode control relies on a detection of the forward conduction period of the half-bridge switches, in a manner that resembles the PLL control, as the PT resonant current phase lag is reflected in the forward conduction period. As the switches forward conduction is getting limited at increasing phase lag, the forward conduction period can be used as a feedback signal. The FCM control seeks to maintain a constant forward conduction duty cycle, of approximately 26 %, and henche a constant resonant current phase lag, which ensures a constant and optimal point of operation.
As the FCM control ensures a constant operating point, the PT is essentially equivalent to a transformer with a constant gain, which has been utilized and demonstrated in a PFC LED application [D.7]. Furthermore the FCM control is very simple and hence low cost, as well as it is purely primary based, avoiding the need of crossing any isolation boundary, which is desirable in isolated applications.

The Bi-directional control enables bi-directional power flow in a PT based power converter, which is revolutionary for PT based power converters. The fundamental basis of the bi-directional control is the insertion of an active MOSFET half-wave output rectifier, where active diodes simply turns ON when exposed to a forward current. The turn OFF point is then controlled and can be phase shifted from the point where only a forward current is conducted, to the point where almost only a

reverse current is conducted. In this manner the power flow can be continuously modulated, enabling bi-directional power flow and energy recovery, which greatly improves the efficiency of this DEAP application.
The demonstrated concept incorporates self-oscillating control, but is not limited to self-oscillating control and other PFM control methods can be used. The utilization of self-oscillating control showed that a resonant current control were needed, as a result of the change in the PT phase response, caused by the phase shift of the output rectifier. Moreover, the proposed bi-directional concept has a huge potential in various other applications, such as applications of line and load regulation.
Another huge potential is its enabling of soft switching operation of non-soft switching optimized PT in inductor-less topologies, which can be achieved by reducing the forward power slightly.
The research and development of a bi-directional control for PT based power converter, has led to the patent application [D.9].

Furthermore, a high voltage high-side gate drive has been developed, with the qualities of coping with the high voltages, as well as loading the switching node minimally, by only adding the parasitic of a single bootstrap diode. The circuit is simple and relies on a detection of the reverse biasing of the bootstrap diode, which triggers a timer that determines the turn OFF time. As the bootstrap diode will be reverse biased when the low side switch is released, any added phase shift will be transferred to the high-side switch as well.

Chapter 6

Conclusion

This thesis and associated publications are the result of the research into non-magnetic piezoelectric transformer (PT) based power converters, for driving high voltage and highly capacitive dielectric electro active polymer (DEAP) actuators. The PT technology has proven to be an applicable solution for driving DEAP actuators, in terms of generating high step-up ratios and high voltages, non-magnetic, minimize size, operate efficiently and recover the actuator stored energy. Furthermore most of the achieved advancements are general and can be utilized in other applications and contexts.

The thesis gives an overview of the basic PT technology used in general power converters, including the basic piezoelectric nature, converter topologies and control methods. The fundamentals of piezoelectric transformer (PT) based power converters have been investigated. Special attention has been given to the research into the inductor-less half-bridge topology, PT design and optimization for native soft switching capabilities, as well as control methods, which ensure and maintain a optimal and consistent operation of the PT. As a result of this research the following major contributions have been achieved:

- A thorough investigation of the utilized inductor-less half-bridge and its operation has been conducted. The investigation has led to the derivation of a soft switching factor (ZVS factor), which describes the maximal achievable soft switching capability of the PT, which should be fulfilled in order to be employed in inductor-less topologies. The empiric derived expression is simple and transparent, clearly stating the strong dependency of the equivalent model input and output capacitor ratio.

- Furthermore the soft switching factor is related to the structure of the PT through the effective electromechanical coupling factors. The effective coupling factors can to some extent be related directly to the mechanical structure and the excitation stress, which is very advantageous as it enables a much more intuitive design process.

- The investigation of the soft switching capability also revealed a operational point of optimal soft switching capability, where inductive behavior and resonating energy is maximized. This optimal point of operation is closely linked to the transfer functions of the PT and is related to a specific magnitude and phase lag of the PT.

- Design and development methods for PT development utilizing Finite Element Modeling (FEM). Simulation and structure simplifications methods are made, which greatly enhances the FEM tool usefulness and reduce simulation and designe time.

- FEM design strategies for soft switching optimization and high voltage gain PT's have been obtained, which has led to the development of several soft switching optimized PT's, enabling utilization of inductor-less topologies. Especially the interleaved structure has been exploited in three major PT structure, being the Interleaved Rosen type PT, Interleaved thickness mode PT and Interleaved interdigitated electrode (IDE) PT. Where the Rosen type PT has a very straight forward manufacturing structure, the thickness mode PT has the high efficiency of the thickness mode vibrations and the IDE PT retains some of the easy manufacturing advantages, combined with the high efficiency of the thickness mode vibration. All the proposed designs have been simulated, optimized and manufactured, as well as experimental validated, except for the Interleaved thickness mode PT, due to manufacturing challenges.

- Control methods for operating inductor-less PT based power converters under sustained soft switching, ensuring optimal and efficient operation at all time. A self-oscillating control method, which has a very tight and precise frequency control, where the closed-loop takes advantage of the phase response of the PT and accommodate changes in resonant frequency, ensures optimal and soft switching operation. Furthermore a resonant current estimation circuit is designed, which enables self-oscillating control with current feedback, as well as having the advantage of being purely primary side based. A forward conduction mode control method (FCM), resembling PLL control, ensuring a constant and optimal point of operation, which also has the advantage of being purely primary side based.

- A revolutionary bi-directional control method for operating inductor-less PT based power converters with bi-directional power flow. The utilization of active phase shift of the active output rectifier, enables a continuously modulated bi-directional power flow and energy recovery. Soft switching operation is maintained over the full power flow modulation range, ensuring optimal and efficient operation.

- Furthermore a high voltage high-side gate drive has been made, with the qualities of coping with the high voltages, as well as loading the switching node minimally, by only adding the parasitic of a single bootstrap diode.

6.1 Future work

The research conducted in this work has uncovered and clarified the fundamentals of piezoelectric transformer (PT) based power converters, in relation to the inductor-less half-bridge topology, PT design and optimization for native soft switching capabilities, as well as control methods. But several of the advancements made have shown potential for further research and utilization in other applications, as well as further investigation and optimization:

- The continued research in to optimization of PT's, new PT structures and soft switching optimized PT's is needed, in order to obtain high efficiency and increased competitiveness. In terms of high gain high voltage soft switching optimized PT's, the limitations of manufacturing capabilities is to some extend preventing the utilization of thickness mode vibrations. Both new PT structures, PT concepts and manufacturing optimizations can move these limitations and improve the performance of high gain high voltage non-magnetic PT based power converters.

- Further exploration of FEM modeling and increased understanding of the FEM tool is required, in order to further enhance the FEM simulation and structure simplifications, as well as enabling loss and efficiency simulations, which is not yet fully understood and implemented. The introduction of an accurate loss simulation will make it possible to make a realistic evaluation of the efficiency before proceeding with the manufacturing, as well as a useful comparison of different PT designs can be made. Furthermore the introduction of advanced structures, such as IDE structures, prevents some of the simulation and structure simplifications, as the structures produces inhomogeneous electrical fields and polarization. Further investigation is required, in order to determine the impact of the inhomogeneous electrical fields and polarization.

- The bi-directional control method and active phase shift demonstrated that it was possible to achieve a continuously modulated bi-directional power flow and energy recovery. The proposed bi-directional concept is not limited to DEAP application and the continued research can lead to huge advancements in other applications, such as applications of line and load regulation, with a potentially paradigm change as a result.

- Another huge potential of bi-directional control is the possibility of achieving soft switching operation of a non-soft switching optimized PT in inductor-less topologies. This can be achieved through the phase shift of the output rectifier by adding a small phase shift, the retained current will help to charge and discharge C_{d1} and enable soft switching operation. Further research is needed in order to determine if the trade-off of an increase in PT performance is worth the decrease in power flow and power density. The result might lead to new

design approaches of PT's or confirm that soft switching optimized PT's are the optimal solution for inductor-less topologies.

- The bi-directional control method itself could be further optimized, especially the physical implementation. The sub-circuit can definitely be optimized further, as well as major parts of the circuit can be integrated in to a integrated circuit (IC) and increase the possibility of miniaturization and a compact solution.

- Lastly the simple high voltage high-side gate driver might be feasible in other applications and non-PT based power applications as well as the concept can be further optimized.

References

[1] "Electroactive polymers," http://en.wikipedia.org/wiki/Electroactive_polymers, August 2012.

[2] C. Rosen, K. Fish, and H. Rothenberg, "Electromechanical transducer," 1958, US Patent 2,830,274.

[3] C. Rosen, "Ceramic transformers and filters," in *Proceedings of the Electronic Components Symposium*, 1956, pp. 205–211.

[4] M. Day and B. Lee, "Understanding piezoelectric transformers in CCFL backlight applications," *Analog Applications Journal, Texas Instruments Incorporated*, 2002.

[5] C. Lin, Y. Lu, H. Chiu, and C. Ou, "Eliminating the temperature effect of piezoelectric transformer in backlight electronic ballast by applying the digital phase-locked-loop technique," *Industrial Electronics, IEEE Transactions on*, vol. 54, no. 2, pp. 1024–1031, 2007.

[6] G. Kweon, Y. Lim, and S. Yang, "An analysis of the backlight inverter by topologies," in *Industrial Electronics, 2001. Proceedings. ISIE 2001. IEEE International Symposium on*, vol. 2. IEEE, 2001, pp. 896–900.

[7] F. Carpi, D. De Rossi, and R. Kornbluh, *Dielectric elastomers as electromechanical transducers: Fundamentals, materials, devices, models and applications of an emerging electroactive polymer technology.* Elsevier Science, 2008.

[8] Y. Bar-Cohen, "Electroactive polymers as artificial muscles-capabilities, potentials and challenges," *Handbook on biomimetics*, vol. 11, pp. 1–13, 2000.

[9] Y. Bar-Cohen, "Electro-active polymers: current capabilities and challenges," in *Proceedings of SPIE*, vol. 4695, 2002, pp. 1–7.

[10] M. Benslimane and P. Gravesen, "Dielectric composite and a method of manufacturing a dielectric composite," Apr. 14 2009, US Patent 7,518,284.

[11] M. Benslimane and P. Gravesen, "Multilayer composite and a method of making such," Nov. 3 2006, US Patent App. 11/592,675.

[12] M. Hansen, B. Thomsen, M. Tryson, M. Benslimane, Y. Iskandarani, and C. Mose, "Power actuated valve," Apr. 30 2009, US Patent App. 12/990,333.

[13] M. Tryson, H. Kiil, and M. Benslimane, "Powerful tubular core free dielectric electro activate polymer (DEAP) push actuator," in *Proceedings of SPIE*, vol. 7287, 2009, p. 72871F.

[14] M. Benslimane, H. Kiil, and M. Tryson, "Dielectric electro-active polymer push actuators: performance and challenges," *Polymer International*, vol. 59, no. 3, pp. 415–421, 2010.

[15] "Piezoelectricity," http://en.wikipedia.org/wiki/Piezoelectricity, August 2012.

[16] "IEEE standard on piezoelectricity," 1988.

[17] F. Barlow, *Ceramic interconnect technology handbook*. CRC, 2007.

[18] K. Uchino, *Ferroelectric devices*, 2nd ed. CRC, 2000.

[19] "Noliac A/S piezoelectric ceramics datasheet," http://www.noliac.com/Files/Billeder/02%20Standard/Ceramics/Noliac_CEramics_NCE_datasheet.pdf.

[20] "Ferroperm Piezoceramics A/S piezoelectric ceramics datasheet," http://app04.swwwing.net/files/files/Ferroperm%20Catalogue.pdf.

[21] A. Mezheritsky, "Elastic, dielectric, and piezoelectric losses in piezoceramics: how it works all together," *Ultrasonics, Ferroelectrics and Frequency Control, IEEE Transactions on*, vol. 51, no. 6, pp. 695–707, 2004.

[22] E. Horsley, M. Foster, and D. Stone, "State-of-the-art piezoelectric transformer technology," in *Power Electronics and Applications, 2007 European Conference on*. IEEE, 2007, pp. 1–10.

[23] A. Carazo, "50 years of piezoelectric transformers: Trends in the technology," in *MATERIALS RESEARCH SOCIETY SYMPOSIUM PROCEEDINGS*, vol. 785. Cambridge Univ Press, 2004, pp. 33–46.

[24] C. Lin, "Design and analysis of piezoelectric transformer converters," Ph.D. dissertation, Virginia Polytechnic Institute and State University, 1997.

[25] C. Lin and F. Lee, "Design of a piezoelectric transformer converter and its matching networks," in *Power Electronics Specialists Conference, PESC'94 Record., 25th Annual IEEE*. IEEE, 1994, pp. 607–612.

[26] R. Lin, "Piezoelectric transformer characterization and application of electronic ballast," Ph.D. dissertation, Virginia Polytechnic Institute and State University, 2001.

[27] G. Ivensky, I. Zafrany, and S. Ben-Yaakov, "Generic operational characteristics of piezoelectric transformers," *Power Electronics, IEEE Transactions on*, vol. 17, no. 6, pp. 1049–1057, 2002.

[28] S. Bronstein, "Piezoelectric transformers in power electronics," Ph.D. dissertation, Ben-Gurion University of the Negev, 2005.

[29] A. Flynn and S. Sanders, "Fundamental limits on energy transfer and circuit considerations for piezoelectric transformers," *Power Electronics, IEEE Transactions on*, vol. 17, no. 1, pp. 8–14, 2002.

[30] S. Ho, "Design of the longitudinal mode piezoelectric transformer," in *Power Electronics and Drive Systems, 2007. PEDS'07. 7th International Conference on*. IEEE, 2007, pp. 1639–1644.

[31] Y. Hsu, C. Lee, and W. Hsiao, "Electrical and mechanical fully coupled theory and experimental verification of rosen-type piezoelectric transformers," *Ultrasonics, Ferroelectrics and Frequency Control, IEEE Transactions on*, vol. 52, no. 10, pp. 1829–1839, 2005.

[32] H. Fukunaga, H. Kakehashi, H. Ogasawara, and Y. Ohta, "Effect of dimension on characteristics of rosen-type piezoelectric transformer," in *Power Electronics Specialists Conference, 1998. PESC 98 Record. 29th Annual IEEE*, vol. 2. IEEE, 1998, pp. 1504–1510.

[33] E. Horsley, A. Carazo, M. Foster, and D. Stone, "A lumped equivalent circuit model for the radial mode piezoelectric transformer," in *Applied Power Electronics Conference and Exposition, 2009. APEC 2009. Twenty-Fourth Annual IEEE.* IEEE, 2009, pp. 1747–1753.

[34] R. Bishop, "Multi-layer piezoelectric transformer," November 1998, US Patent 5,834,882.

[35] R. Bishop and C. Boyd, "DC-AC converter circuit using resonating multi-layer piezoelectric transformer," April 2000, US Patent 6,052,300.

[36] E. Baker, W. Huang, D. Chen, and F. Lee, "Radial mode piezoelectric transformer design for fluorescent lamp ballast applications," *Power Electronics, IEEE Transactions on*, vol. 20, no. 5, pp. 1213–1220, 2005.

[37] D. Nielsen, M. Andersen, and K. Meyer, "Preliminary investigations of piezoelectric based LED luminary," in *Power Electronics and Applications (EPE 2011), Proceedings of the 2011-14th European Conference on.* IEEE, 2011, pp. 1–9.

[38] K. Meyer and M. Andersen, "One-shot design of radial mode piezoelectric transformer for magneticless power conversion," in *26. Annual IEEE Applied Power Electronics Conference and Exposition 26*, 2011, pp. 498–504.

[39] M. Sanz, A. Sanchez, P. Alou, R. Prieto, J. Cobos, and J. Uceda, "Step by step multi-layer piezoelectric transformer design procedure," in *Power Electronics Specialists Conference, 2004. PESC 04. 2004 IEEE 35th Annual*, vol. 6. IEEE, 2004, pp. 4669–4675.

[40] A. Sánchez, M. Sanz, R. Prieto, J. Oliver, P. Alou, and J. Cobos, "Design of piezoelectric transformers for power converters by means of analytical and numerical methods," *Industrial Electronics, IEEE Transactions on*, vol. 55, no. 1, pp. 79–88, 2008.

[41] T. Zaitsu, T. Inoue, O. Ohnishi, and A. Iwamoto, "2 mhz power converter with piezoelectric ceramic transformer," in *Telecommunications Energy Conference, 1992. INTELEC'92., 14th International.* IEEE, 1992, pp. 430–437.

[42] J. Diaz, J. Martin-Ramos, M. Prieto, and F. Nuno, "A double-closed loop DC/DC converter based on a piezoelectric transformer," in *Applied Power Electronics Conference and Exposition, 2004. APEC'04. Nineteenth Annual IEEE*, vol. 3. IEEE, 2004, pp. 1423–1428.

[43] J. Navas, T. Bove, J. Cobos, F. Nuno, and K. Brebol, "Miniaturised battery charger using piezoelectric transformers," in *Applied Power Electronics Conference and Exposition, 2001. APEC 2001. Sixteenth Annual IEEE*, vol. 1. IEEE, 2001, pp. 492–496.

[44] M. Prieto, J. Diaz, J. Martin, and F. Nuno, "A very simple DC/DC converter using piezoelectric transformer," in *Power Electronics Specialists Conference, 2001. PESC. 2001 IEEE 32nd Annual*, vol. 4. IEEE, 2001, pp. 1755–1760.

[45] C. M. S. Garcia, "Metodologia de diseno de los transformadores piezoelectricos para su aplicacion en fuentes de alimentacion conmutadas CA/CC y CC/CC de baja potencia y baja tension de salida," Ph.D. dissertation, Universidad Politecnica de Madrid, 2003.

[46] T. Bove, W. Wolny, E. Ringgaard, and K. Breboel, "New type of piezoelectric transformer with very high power density," in *Applications of Ferroelectrics, 2000. ISAF 2000. Proceedings of the 2000 12th IEEE International Symposium on*, vol. 1. IEEE, 2000, pp. 321–324.

[47] O. Ohnishi, H. Kishie, A. Iwamoto, Y. Sasaki, T. Zaitsu, and T. Inoue, "Piezoelectric ceramic transformer operating in thickness extensional vibration mode for power supply," in *Ultrasonics Symposium, 1992. Proceedings., IEEE 1992.* IEEE, 1992, pp. 483–488.

[48] W. Mason, *Electromechanical transducers and wave filters.* Van Nostrand Reinhold, 1946.

[49] R. Erickson and D. Maksimović, *Fundamentals of power electronics.* Springer, 2001.

[50] E. Horsley, N. Nguyen-Quang, M. Foster, and D. Stone, "Achieving zvs in inductor-less half-bridge piezoelectric transformer based resonant converters," in *Power Electronics and Drive Systems, 2009. PEDS 2009. International Conference on.* IEEE, 2009, pp. 446–451.

[51] E. Horsley, A. Vazquez Carazo, N. Nguyen-Quang, M. Foster, and D. Stone, "Analysis of inductor-less zero-voltage-switching piezoelectric transformer based converters," *Power Electronics, IEEE Transactions on*, no. 99, pp. 1–1, 2011.

[52] W. Huang, "Design of a radial mode piezoelectric transformer for a charge pump electronic ballast with high power factor and zero voltage switching," Master's thesis, Virginia Polytechnic Institute and State University, 2003.

[53] K. Meyer, "Modeling of Piezoelectric Transformers and Generic Circuit Analysis for Miniaturization of Piezoelectric Power Converters," Master's thesis, Technical University of Denmark, October 2008.

[54] K. Meyer, M. Andersen, and F. Jensen, "Parameterized analysis of zero voltage switching in resonant converters for optimal electrode layout of piezoelectric transformers," in *Power Electronics Specialists Conference, 2008. PESC 2008. IEEE.* IEEE, 2008, pp. 2543–2548.

[55] G. Zerong, J. Lingling, L. Huabo, and W. Ting, "Measurement of PT equivalent circuit model parameters based on admittance circle," in *Mechatronic Science, Electric Engineering and Computer (MEC), 2011 International Conference on.* IEEE, 2011, pp. 20–23.

[56] S. Choi, K. Lee, and B. Cho, "Design of fluorescent lamp ballast with PFC using a power piezoelectric transformer," *Industrial Electronics, IEEE Transactions on*, vol. 52, no. 6, pp. 1573–1581, 2005.

[57] G. Seo, J. Shin, and B. Cho, "A magnetic component-less series resonant converter using a piezoelectric transducer for low profile application," in *Power Electronics Conference (IPEC), 2010 International.* IEEE, 2010, pp. 2810–2814.

[58] F. Bisogno, S. Nittayarumphong, M. Radecker, A. Carazo, and R. do Prado, "A line power-supply for LED lighting using piezoelectric transformers in class-e topology," in *Power Electronics and Motion Control Conference, 2006. IPEMC 2006. CES/IEEE 5th International*, vol. 2, aug. 2006, pp. 1 –5.

[59] T. Zaitsu, T. Shigehisa, T. Inoue, M. Shoyama, and T. Ninomiya, "Piezoelectric transformer converter with frequency control," in *Telecommunications Energy Conference, 1995. INTELEC'95., 17th International.* IEEE, 1995, pp. 175–180.

[60] S. Nittayarumphong, F. Bisogno, M. Radecker, A. Knoll, A. Carazo, and A. Riedlhammer, "Dynamic behaviour of PI controlled class-e resonant converter for step-down applications using piezoelectric transformers," in *Power Electronics and Applications, 2005 European Conference on.* IEEE, 2005, pp. 10–pp.

[61] S. Ben-Yaakov and S. Lineykin, "Maximum power tracking of piezoelectric transformer HV converters under load variations," *Power Electronics, IEEE Transactions on*, vol. 21, no. 1, pp. 73–78, 2006.

[62] C. Lin, Y. Chen, J. Chen, and F. Wen, "The elimination of the temperature effect on a piezoelectric transformer in a backlight inverter based on the phase-locked loop technique," in *Mechatronics, 2005. ICM'05. IEEE International Conference on.* IEEE, 2005, pp. 828–833.

[63] J. Alonso, C. Ordiz, and M. Dalla Costa, "A novel control method for piezoelectric-transformer based power supplies assuring zero-voltage-switching operation," *Industrial Electronics, IEEE Transactions on*, vol. 55, no. 3, pp. 1085–1089, 2008.

[64] J. Alonso, C. Ordiz, M. Dalla Costa, J. Ribas, and J. Cardesin, "High-voltage power supply for ozone generation based on piezoelectric transformer," *Industry Applications, IEEE Transactions on*, vol. 45, no. 4, pp. 1513–1523, 2009.

[65] S. Nakashima, T. Ninomiya, H. Ogasawara, and H. Kakehashi, "Piezoelectric-transformer inverter with maximum-efficiency tracking and dimming control," in *Applied Power Electronics Conference and Exposition, 2002. APEC 2002. Seventeenth Annual IEEE*, vol. 2. IEEE, 2002, pp. 918–923.

[66] J. Díaz, F. Nuño, M. Prieto, J. Martin-Ramos, and P. Villegas Saiz, "Closing a second feedback loop in a DC-DC converter based on a piezoelectric transformer," *Power Electronics, IEEE Transactions on*, vol. 22, no. 6, pp. 2195–2201, 2007.

[67] J. Díaz, F. Nuño, J. Lopera, and J. Martín-Ramos, "A new control strategy for an AC/DC converter based on a piezoelectric transformer," *Industrial Electronics, IEEE Transactions on*, vol. 51, no. 4, pp. 850–856, 2004.

[68] C. Bai, S. Li, Q. Shen, and D. Cui, "A converter of high voltage capacitor charging power supply using piezoelectric transformer," in *Power and Energy Engineering Conference, 2009. APPEEC 2009. Asia-Pacific.* IEEE, 2009, pp. 1–4.

[69] A. Mezheritsky, "Quality factor concept in piezoceramic transformer performance description," *Ultrasonics, Ferroelectrics and Frequency Control, IEEE Transactions on*, vol. 53, no. 2, pp. 429–442, 2006.

[70] K. Uchino and S. Hirose, "Loss mechanisms in piezoelectrics: how to measure different losses separately," *Ultrasonics, Ferroelectrics and Frequency Control, IEEE Transactions on*, vol. 48, no. 1, pp. 307–321, 2001.

[71] W. Huang, D. Chen, E. Baker, J. Zhou, H. Hsieh, and F. Lee, "Design of a power piezoelectric transformer for a PFC electronic ballast," *Industrial Electronics, IEEE Transactions on*, vol. 54, no. 6, pp. 3197–3204, 2007.

[72] M. Shoyama, K. Horikoshi, T. Ninomiya, T. Zaitsu, and Y. Sasaki, "Steady-state characteristics of the push-pull piezoelectric inverter," *IEICE transactions on communications*, vol. 82, no. 8, pp. 1318–1325, 1999.

[73] S. Hamamura, T. Ninomiya, M. Yamamoto, and M. Katsuno, "Combined PWM and PFM control for universal line voltage of a piezoelectric transformer off-line converter," *Power Electronics, IEEE Transactions on*, vol. 18, no. 1, pp. 270–277, 2003.

[74] M. Sanz, P. Alou, R. Prieto, J. Cobos, and J. Uceda, "Comparison of different alternatives to drive piezoelectric transformers," in *Applied Power Electronics Conference and Exposition, 2002. APEC 2002. Seventeenth Annual IEEE*, vol. 1. IEEE, 2002, pp. 358–364.

[75] R. Lin, F. Lee, E. Baker, and D. Chen, "Inductor-less piezoelectric transformer electronic ballast for linear fluorescent lamp," in *Applied Power Electronics Conference and Exposition, 2001. APEC 2001. Sixteenth Annual IEEE*, vol. 2. IEEE, 2001, pp. 664–669.

[76] M. Sanz, P. Alou, A. Soto, R. Prieto, J. Cobos, and J. Uceda, "Magnetic-less converter based on piezoelectric transformers for step-down DC/DC and low power application," in *Applied Power Electronics Conference and Exposition, 2003. APEC'03. Eighteenth Annual IEEE*, vol. 2. IEEE, 2003, pp. 615–621.

[77] F. Bisogno, M. Radecker, A. Knoll, A. Carazo, A. Riedlhammer, G. Deboy, N. Norvez, and J. Pacas, "Comparison of resonant topologies for step-down applications using piezoelectric transformers," in *Power Electronics Specialists Conference, 2004. PESC 04. 2004 IEEE 35th Annual*, vol. 4. IEEE, 2004, pp. 2662–2667.

[78] J. Zhou, F. Tao, and F. Lee, "Inductor-less charge pump PFC electronic ballast," in *Industry Applications Conference, 2001. Thirty-Sixth IAS Annual Meeting. Conference Record of the 2001 IEEE*, vol. 1. IEEE, 2001, pp. 524–529.

[79] J. Qian, F. Lee, and T. Yamauchi, "A single-stage electronic ballast with power factor correction and low crest factor for fluorescent lamps," in *Industry Applications Conference, 1997. Thirty-Second IAS Annual Meeting, IAS'97., Conference Record of the 1997 IEEE*, vol. 3. IEEE, 1997, pp. 2307–2312.

[80] R. Lin and H. Shih, "Piezoelectric transformer based current-source charge-pump power-factor-correction electronic ballast," *Power Electronics, IEEE Transactions on*, vol. 23, no. 3, pp. 1391–1400, 2008.

[81] R. Lin, H. Shih, C. Liu, and K. Liu, "A Family of Piezoelectric Transformer-Based Bridgeless Continuous-Conduction-Mode Charge-Pump Power-Factor Correction Electronic Ballasts," *Industry Applications, IEEE Transactions on*, no. 99, pp. 1–1, 2011.

[82] K. Meyer, "Piezoelectric transformer with high effective electro-mechanical coupling factors," 2011, US Patent 61/521,635 (pending).

[83] R. Woollett, "Effective coupling factor of single-degree-of-freedom transducers," *The Journal of the Acoustical Society of America*, vol. 40, p. 1112, 1966.

[84] Z. Yang, L. Yang, X. Chao, R. Zhang, and Y. Chen, "Electrical characteristics of central driving type piezoelectric transformers with different electrode distributing," *Sensors and Actuators A: Physical*, vol. 136, no. 1, pp. 341–346, 2007.

[85] X. Chu, J. Wu, Z. Xu, and L. Li, "Experiment research on multilayer piezoelectric transformer," in *Piezoelectricity, Acoustic Waves, and Device Applications, 2008. SPAWDA 2008. Symposium on.* IEEE, 2008, pp. 524–527.

[86] M. Andersen, "Efficient audio power amplification-challenges," in *Proceedings of AES International Conference*, 2005, pp. 1–10.

[87] M. Høyerby and M. Andersen, "Carrier distortion in hysteretic self-oscillating class-d audio power amplifiers: Analysis and optimization," *Power Electronics, IEEE Transactions on*, vol. 24, no. 3, pp. 714–729, 2009.

[88] M. Høyerby, "High-performance control in radio frequency power amplification systems," Ph.D. dissertation, Technical University of Denmark (DTU), 2010.

[89] B. Putzeys, "Simple self-oscillating class d amplifier with full output filter control," in *118th AES Convention, Barcelona, Spain*, 2005.

Reference guide

The following table lists the relevant reference by subject, with the intentions of helping the reader to quickly find literature on the subjects. Some references might be relevant in several subjects and hence are listed several times.

Subject	**References**
Electro Active Polymer	[1, 7, 8, 9]
Dielectric Electro Active Polymer	[7, 8, 9]
Danfoss PolyPower DEAP actuator	[10, 11, 12, 13, 14]
The piezoelectric transformer (PT)	[4, 16, 21, 22, 23, 27]
Piezoelectricity	[15, 16, 17, 18, 19, 20, 21]
Modeling of piezoelectric transformers	[22, 24, 26, 27, 28, 48, 50, 51]
Model parameter determination	[24, 26, 30, 32, 36, 38, 45, 52, 53]
Piezoelectric loss and PT loss	[16, 17, 18, 21, 29, 69, 70]
Piezoelectric transformer design	[26, 53]
Rosen type PT	[2, 3, 30, 31, 32]
Radial mode PT	[26, 33, 34, 35, 36, 37, 38]
Thickness mode PT	[39, 40, 41, 42, 43, 44, 45, 46, 47]
Soft switching optimized PT's	[36, 38, 39, 40, 71],[D.2,D.5]
The PT based power converter	[23, 50]
Topologies	[23]
Push-pull	[4, 72]
Class-E	[58, 60, 68]
Half-bridge	[5, 66, 67, 73, 74]
The inductor-less half-bridge	[40, 50, 51, 54, 63, 64, 74, 75, 76],[D.7]
Soft switching factor	[26, 36, 50, 51, 54],[D.3]
Control methods	[23]
Controlled oscillator	[23, 44, 56, 57, 58, 59, 60]
Phase lock loop (PLL)	[5, 23, 61, 62, 63, 64, 65],[D.7]
Self-oscillating control	[42, 66],[D.8]
Burst-mode modulation	[42, 66, 67, 68],[D.1,D.6]
Bi-directional control	[D.9]

Appendix A

ZVS capability simulation circuit

ZVS capability *OrCad PSpice* simulation circuit, where the ZVS capability is measured as the peak voltage of the V_Cd1 node. The circuit has adaptive dead-time, which ensures an optimal dead-time for any given operation point, and the measurement is performed after steady state operation is achieved.

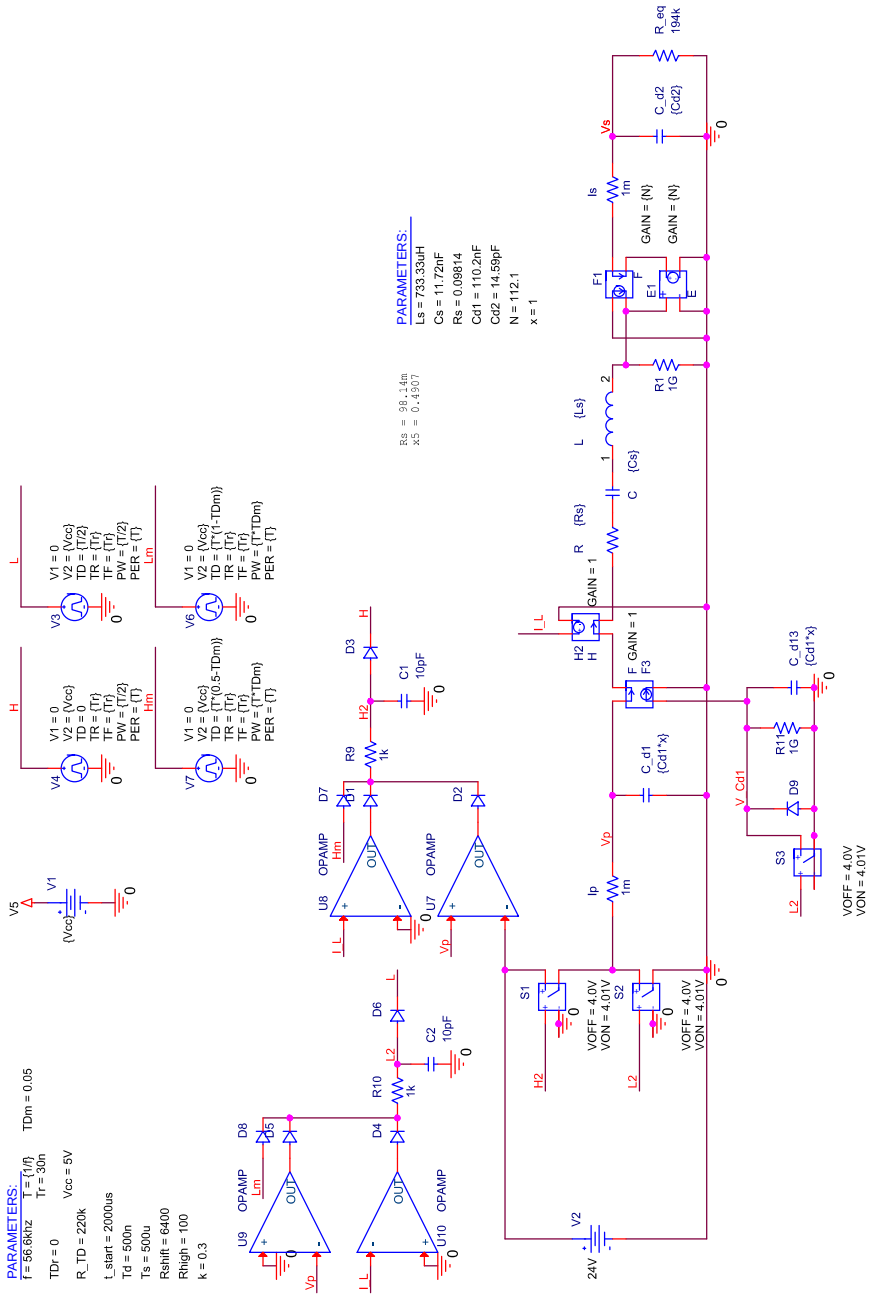

Appendix B

Schematic: Uni-directional PT based DEAP driver

In the following section the schematic of the developed uni-directional PT based DEAP driver can be found. The developed driver is small enough to be integrated into the core of a 110x32 mm DEAP actuator, forming a low voltage (24V) interfaced DEAP actuator. The driver can be configured with a half-bridge or full-bridge, but is targeted for half-bridge operation, utilizing the Interleaved Rosen type PT (section 4.3 [D.2]). The component values is optimized for a 30x10x2 mm Interleaved Rosen type PT and the functionality and operation of the circuits are described in detail in this thesis and associated publications.

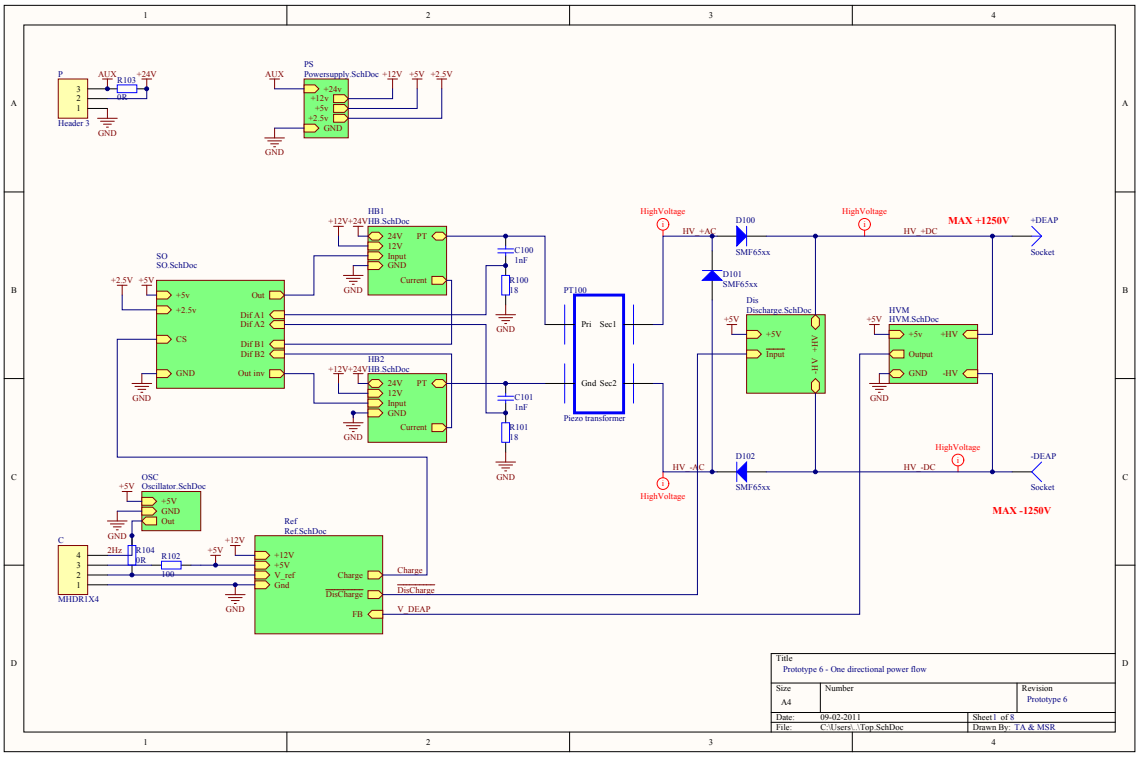

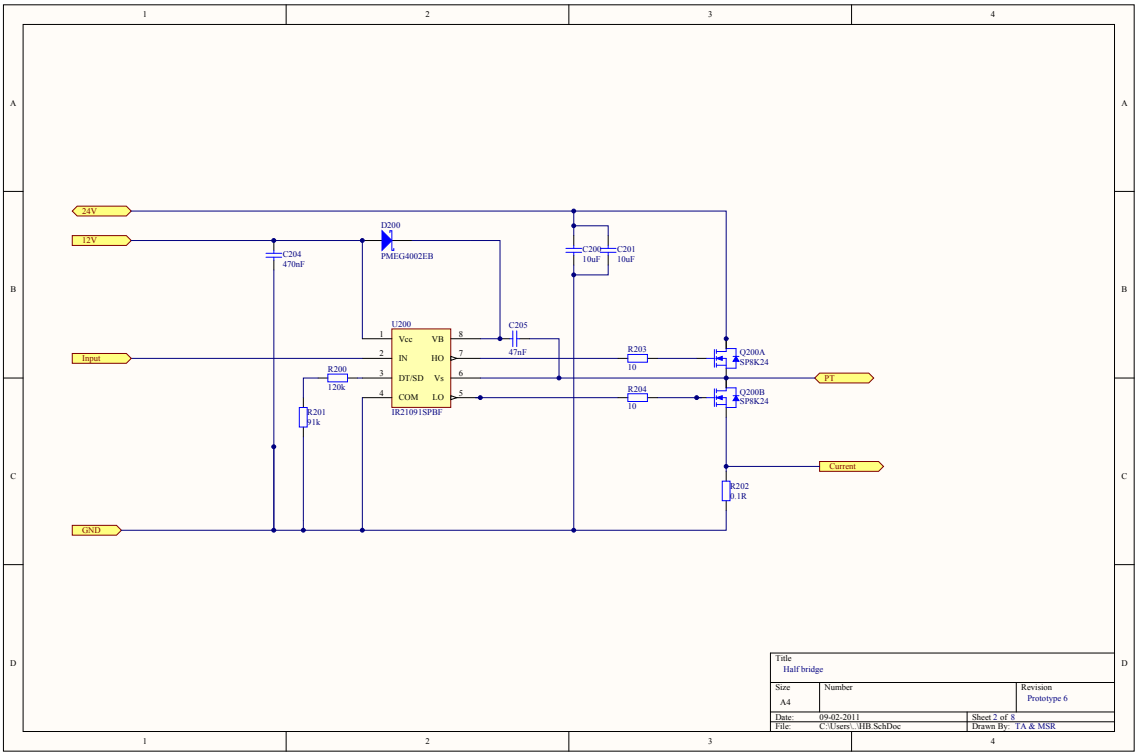
24V
12V
C204
470nF
D200
PMEG4002EB
C200
10uF
C201
10uF
U200
Vcc
VB
IN
HO
DT/SD
Vs
COM
LO
IR21091SPBF
C205
47nF
Input
R200
120k
R201
91k
R203
10
R204
10
Q200A
SP8K24
Q200B
SP8K24
PT
Current
R202
0.1R
GND
Title
Half bridge
Size
A4
Number
Revision
Prototype 6
Date:
09-02-2011
File:
C:\Users\...HB.SchDoc
Sheet 2 of 8
Drawn By:
TA & MSR

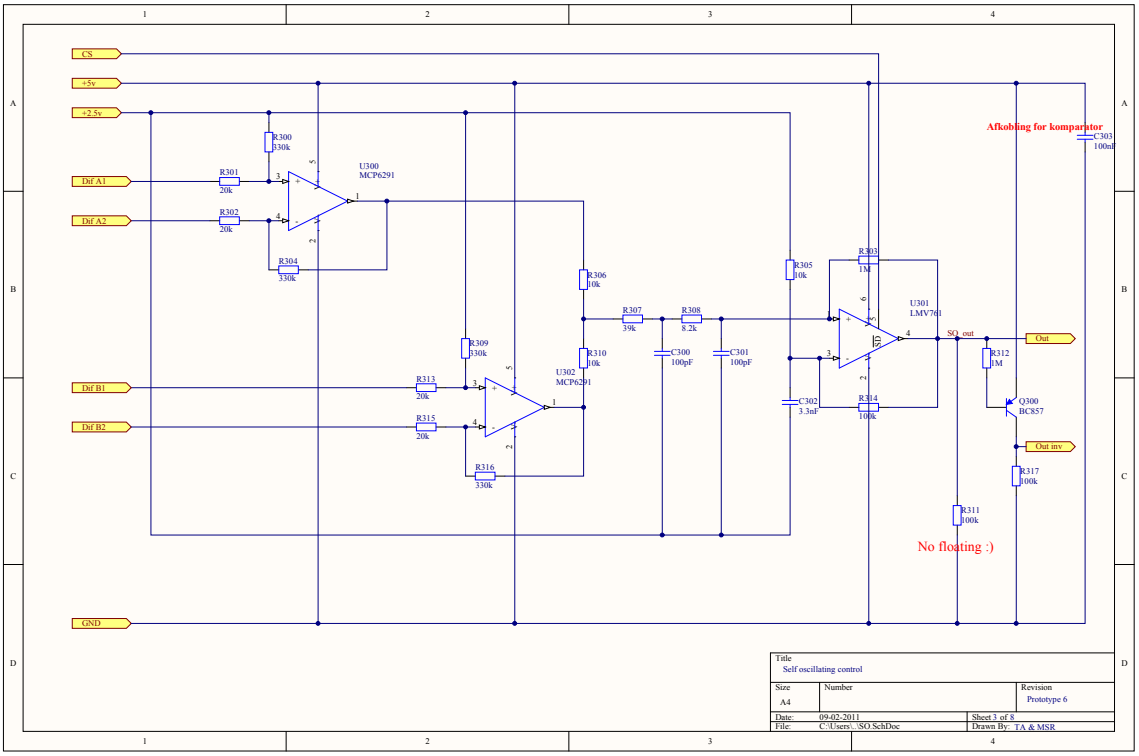
CS
+5v
+2.5v
Dif A1
Dif A2
Dif B1
Dif B2
GND
R300
330k
R301
20k
R302
20k
R304
330k
U300
MCP6291
R306
10k
R307
39k
R308
8.2k
R309
330k
R310
10k
R313
20k
R315
20k
R316
330k
U302
MCP6291
C300
100pF
C301
100pF
R305
10k
R303
1M
U301
LMV761
R314
100k
C302
3.3nF
SO_out
Out
R312
1M
Q300
BC857
Out inv
R317
100k
R311
100k
Afkobling for komparator
C303
100nF
No floating :)
Title
Self oscillating control
Size
A4
Number
Revision
Prototype 6
Date:
09-02-2011
File:
C:\Users\...SO.SchDoc
Sheet 3 of 8
Drawn By:
TA & MSR

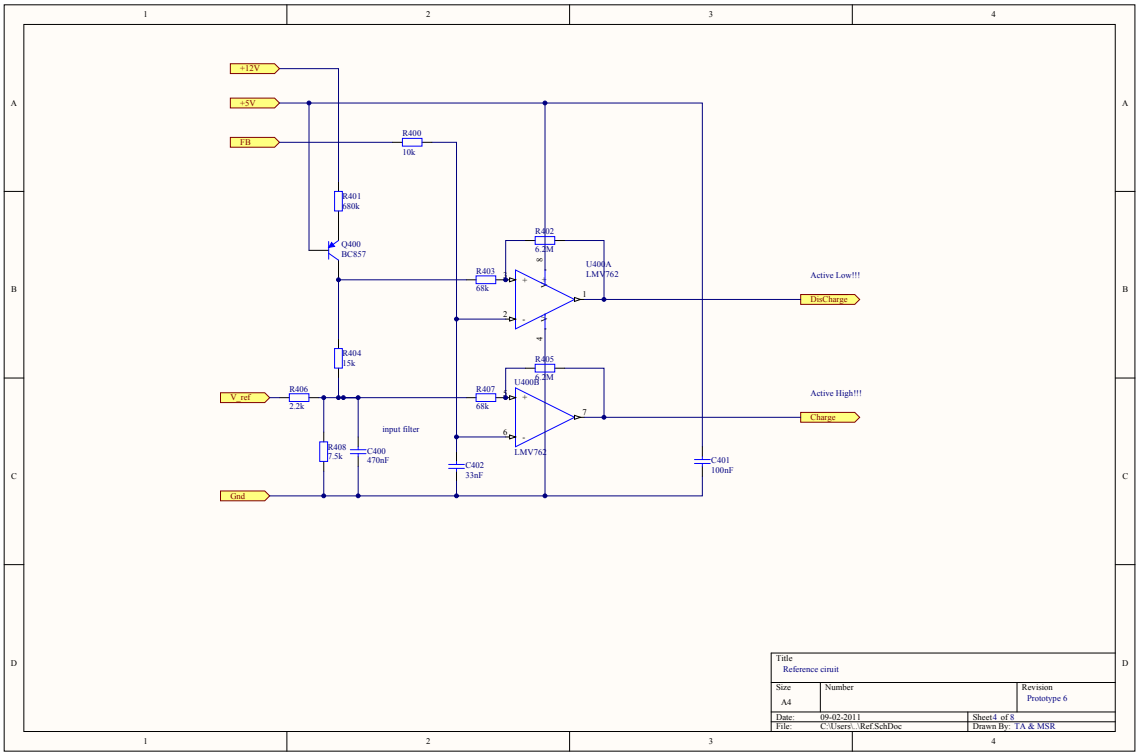
+12V
+5V
FB
R400
10k
R401
680k
Q400
BC857
R402
6.2M
R403
68k
U400A
LMV762
Active Low!!!
DisCharge
R404
8.5k
R405
6.2M
V_ref
R406
2.2k
R407
68k
U400B
Active High!!!
Charge
input filter
R408
7.5k
C400
470nF
C402
33nF
LMV762
C401
100nF
Gnd
Title
Reference ciruit
Size
A4
Number
Revision
Prototype 6
Date:
09-02-2011
Sheet 4 of 8
File:
C:\Users\...\Ref.SchDoc
Drawn By:
TA & MSR

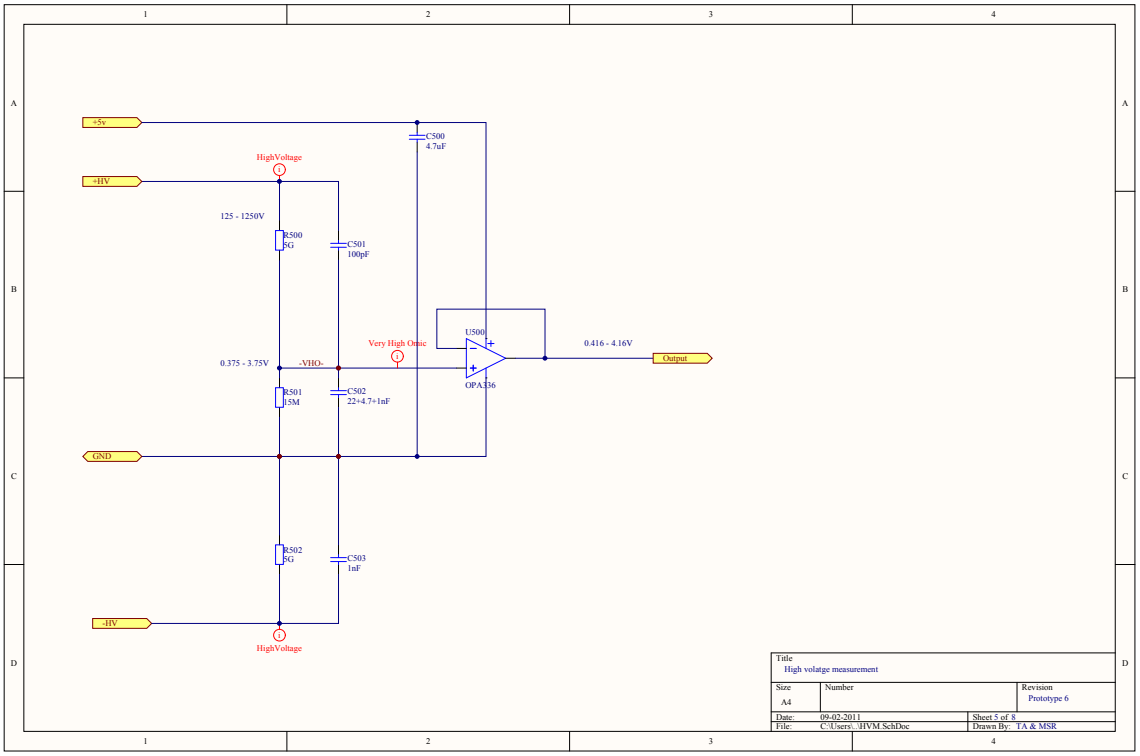
+5v
C500
4.7uF
HighVoltage
+HV
125 - 1250V
R500
5G
C501
100pF
U500
Very High Ohmic
0.375 - 3.75V
-VHO-
0.416 - 4.16V
Output
OPA336
R501
15M
C502
22+4.7+1nF
GND
R502
5G
C503
1nF
-HV
HighVoltage
Title
High volatge measurement
Size
A4
Number
Revision
Prototype 6
Date:
09-02-2011
Sheet 5 of 8
File:
C:\Users\...\HVM.SchDoc
Drawn By:
TA & MSR

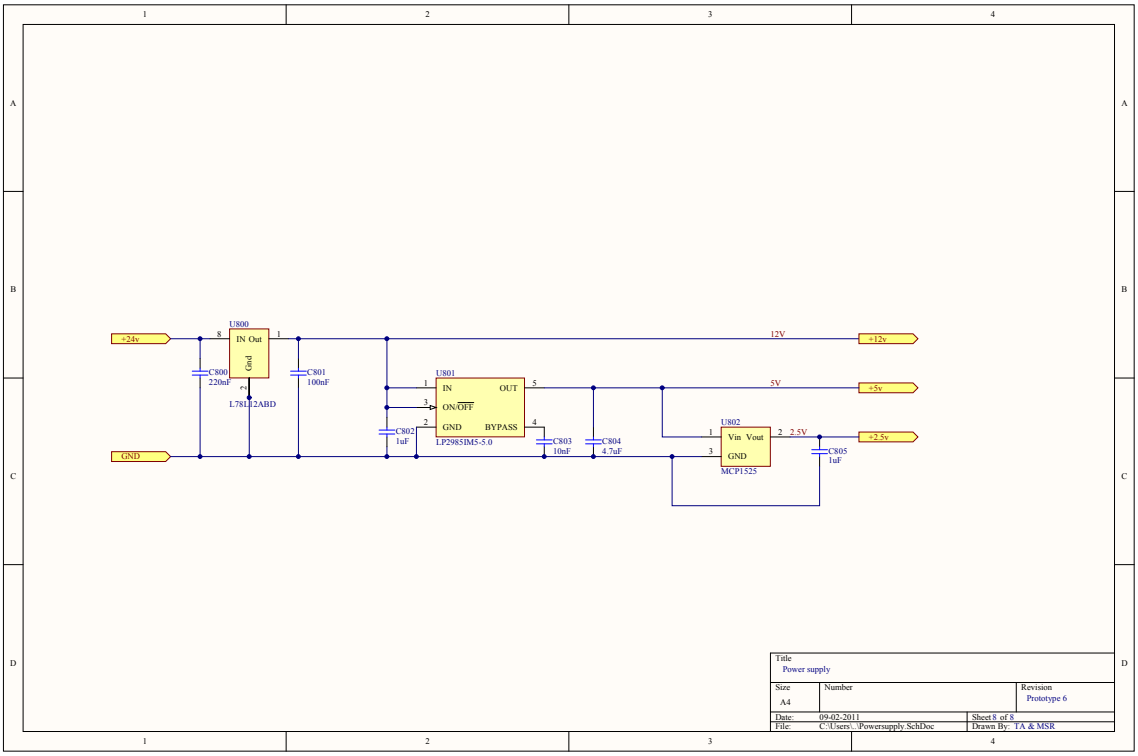
+24v
GND
U800
IN Out
Gnd
L78L12ABD
C800
220nF
C801
100nF
12V
+12v
U801
IN
OUT
ON/OFF
GND
BYPASS
LP2985IM5-5.0
C802
1uF
C803
10nF
C804
4.7uF
5V
+5v
U802
Vin Vout
GND
MCP1525
2.5V
+2.5v
C805
1uF
Title
Power supply
Size
A4
Number
Revision
Prototype 6
Date:
09-02-2011
Sheet 8 of 8
File:
C:\Users\...\Powersupply.SchDoc
Drawn By:
TA & MSR

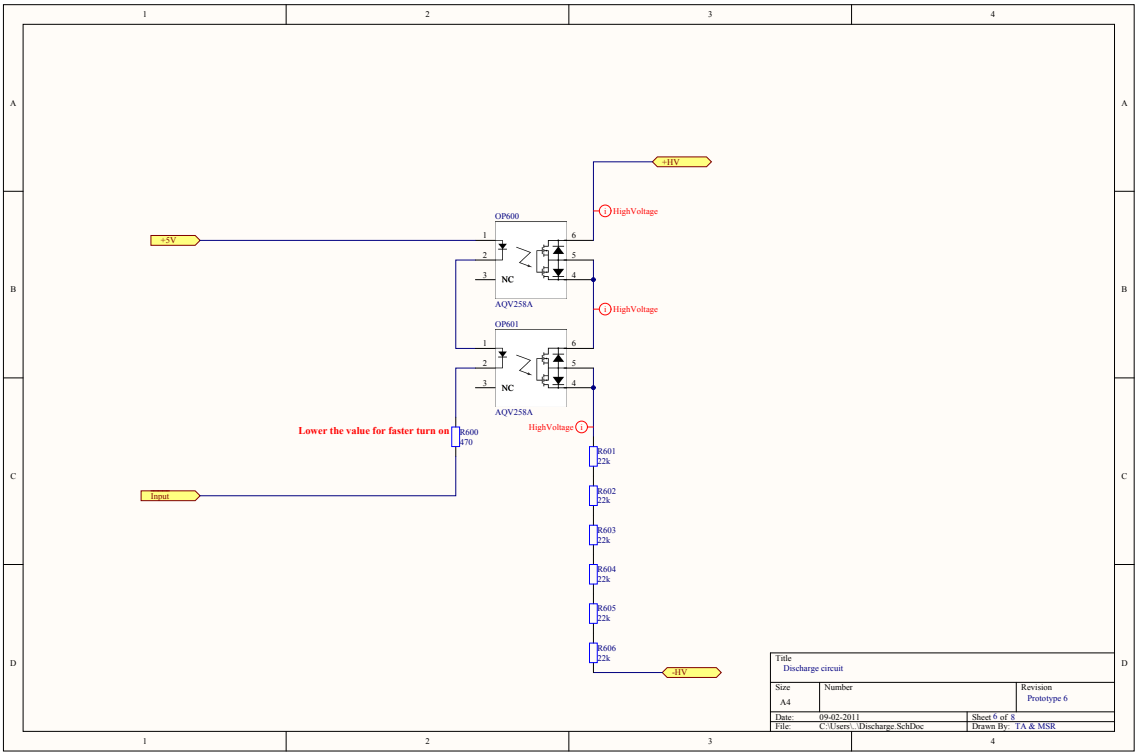
+HV
HighVoltage
+5V
OP600
NC
AQV258A
OP601
Lower the value for faster turn on
R600
470
Input
R601
22k
R602
22k
R603
22k
R604
22k
R605
22k
R606
22k
-HV
Title
Discharge circuit
Size
A4
Number
Revision
Prototype 6
Date:
09-02-2011
Sheet 6 of 8
File:
C:\Users\...\Discharge.SchDoc
Drawn By:
TA & MSR

PCB layout: 95x13 mm

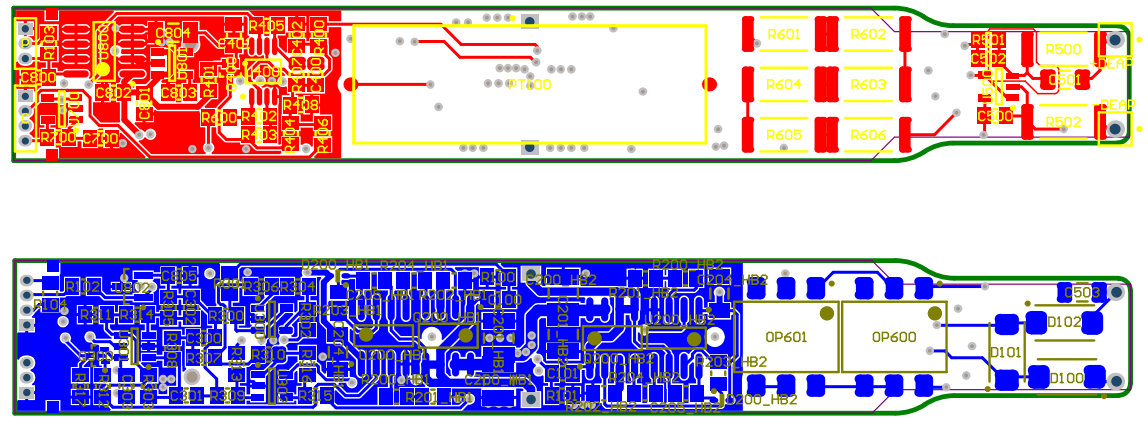

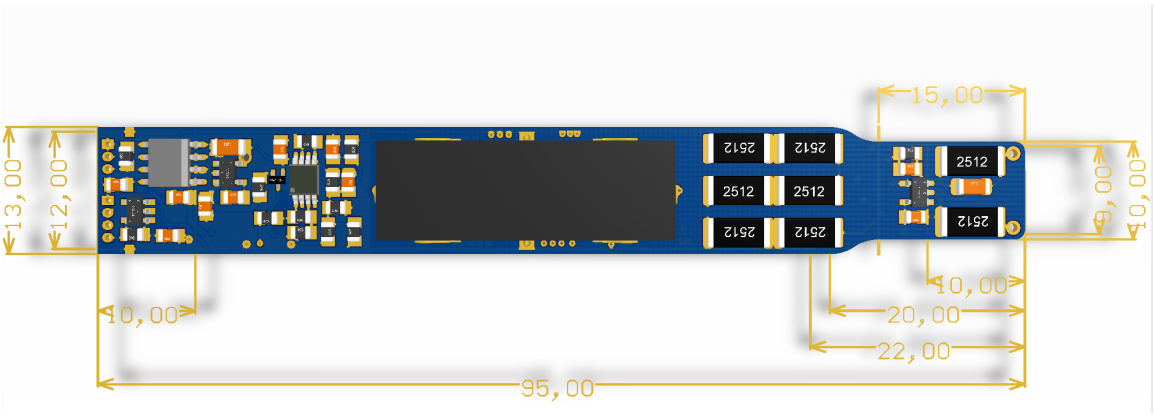

Appendix C

Schematic: Bi-directional PT based DEAP driver

In the following section the schematic of the developed bi-directional PT based DEAP driver can be found. The developed driver is not small enough to be integrated into the core of a DEAP actuator and the prototype is developed to demonstrate and validation of the functionality of the bi-directional concept. The driver can be configured with a half-bridge or full-bridge, but is targeted for full-bridge operation, utilizing the Interleaved interdigitated electrode PT (section 4.5 [D.5]). The component values is optimized for a 27x10x2 mm Interleaved interdigitated electrode PT and the functionality and operation of the circuits are described in detail in this thesis and associated publications.

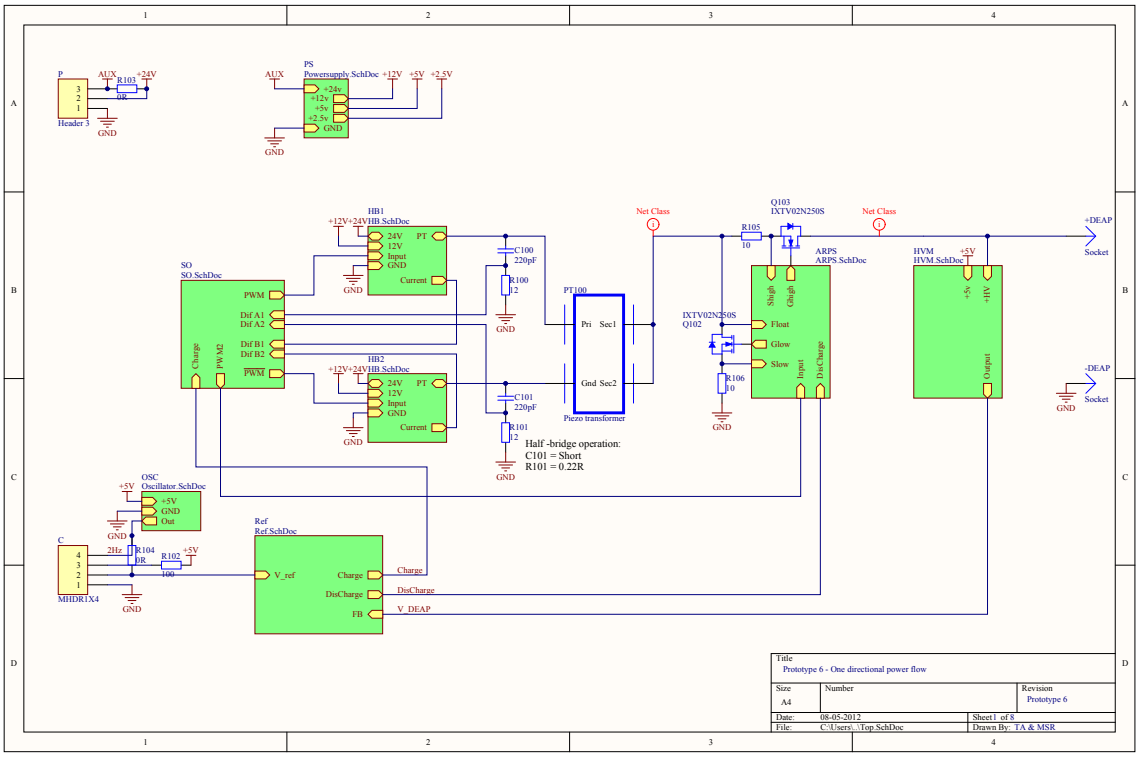

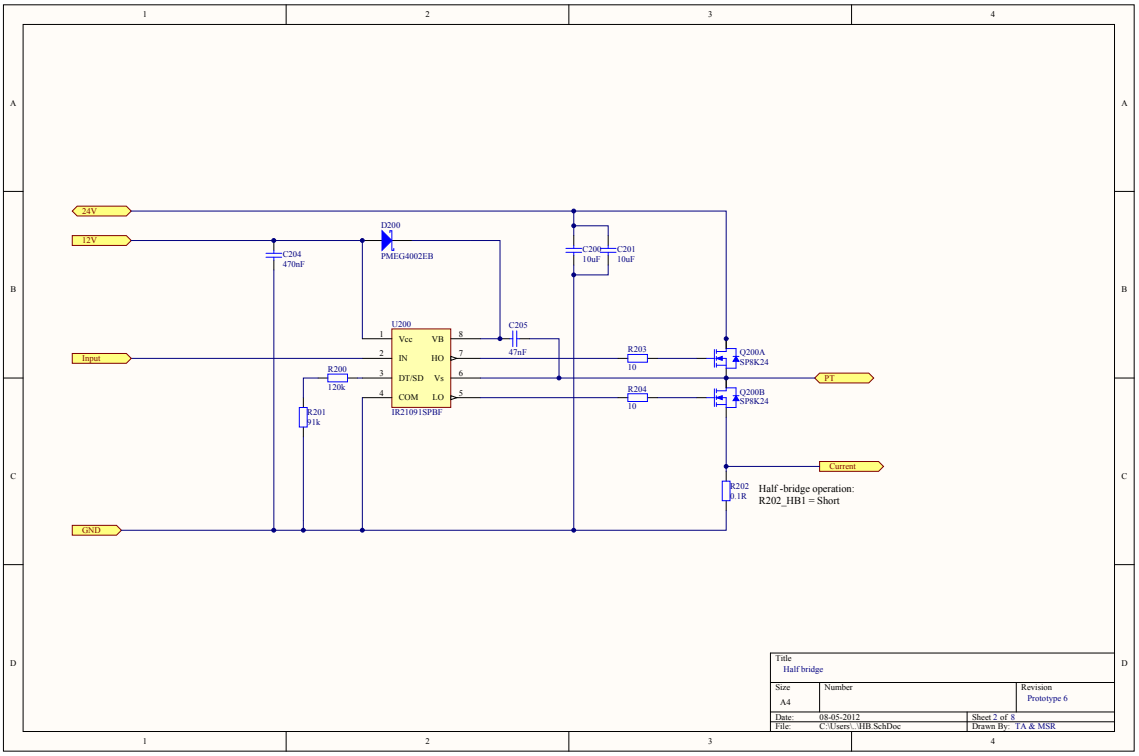
24V
12V
Input
GND
C204
470nF
D200
PMEG4002EB
C200
10uF
C201
10uF
U200
Vcc
VB
IN
HO
DT/SD
Vs
COM
LO
IR21091SPBF
C205
47nF
R200
120k
R201
91k
R203
10
R204
10
Q200A
SP8K24
Q200B
SP8K24
PT
Current
R202
0.1R
Half -bridge operation:
R202_HB1 = Short
Title
Half bridge
Size
A4
Number
Revision
Prototype 6
Date:
08-05-2012
File:
C:\Users\...HB.SchDoc
Sheet 2 of 8
Drawn By:
TA & MSR

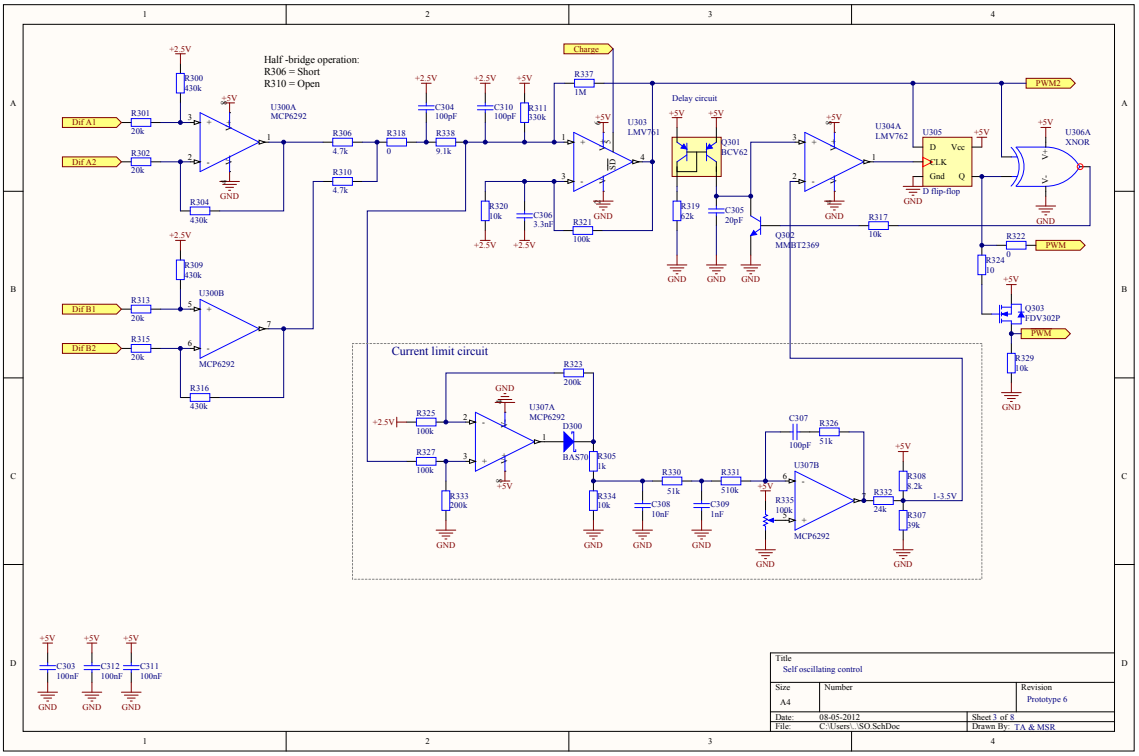
Half -bridge operation:
R306 = Short
R310 = Open
Charge
PWM2
PWM
Dif A1
Dif A2
Dif B1
Dif B2
U300A
MCP6292
U300B
MCP6292
U303
LMV761
Delay circuit
Q301
BCV62
Q302
MMBT2369
U304A
LMV762
U305
D flip-flop
U306A
XNOR
Q303
FDV302P
Current limit circuit
U307A
MCP6292
U307B
MCP6292
D300
BAS70
1-3.5V
Title
Self oscillating control
Size
A4
Number
Revision
Prototype 6
Date:
08-05-2012
File:
C:\Users\...SO.SchDoc
Sheet 3 of 8
Drawn By:
TA & MSR

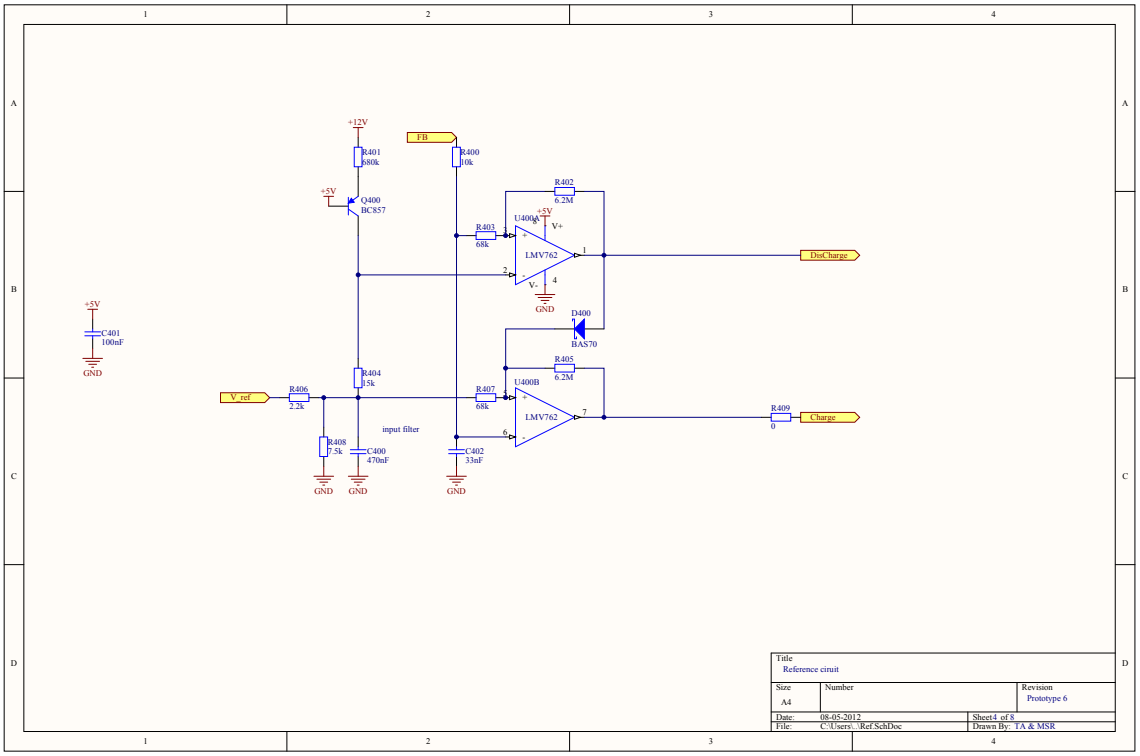
+12V
FB
R401
680k
R400
10k
R402
6.2M
+5V
Q400
BC857
U400A
+5V
V+
R403
68k
LMV762
DisCharge
V-
GND
+5V
C401
100nF
GND
D400
BAS70
R404
15k
R405
6.2M
V_ref
R406
2.2k
R407
68k
U400B
LMV762
R409
0
Charge
input filter
R408
7.5k
C400
470nF
C402
33nF
GND
GND
GND
Title
Reference ciruit
Size
A4
Number
Revision
Prototype 6
Date:
08-05-2012
Sheet 4 of 8
File:
C:\Users\...\Ref.SchDoc
Drawn By:
TA & MSR

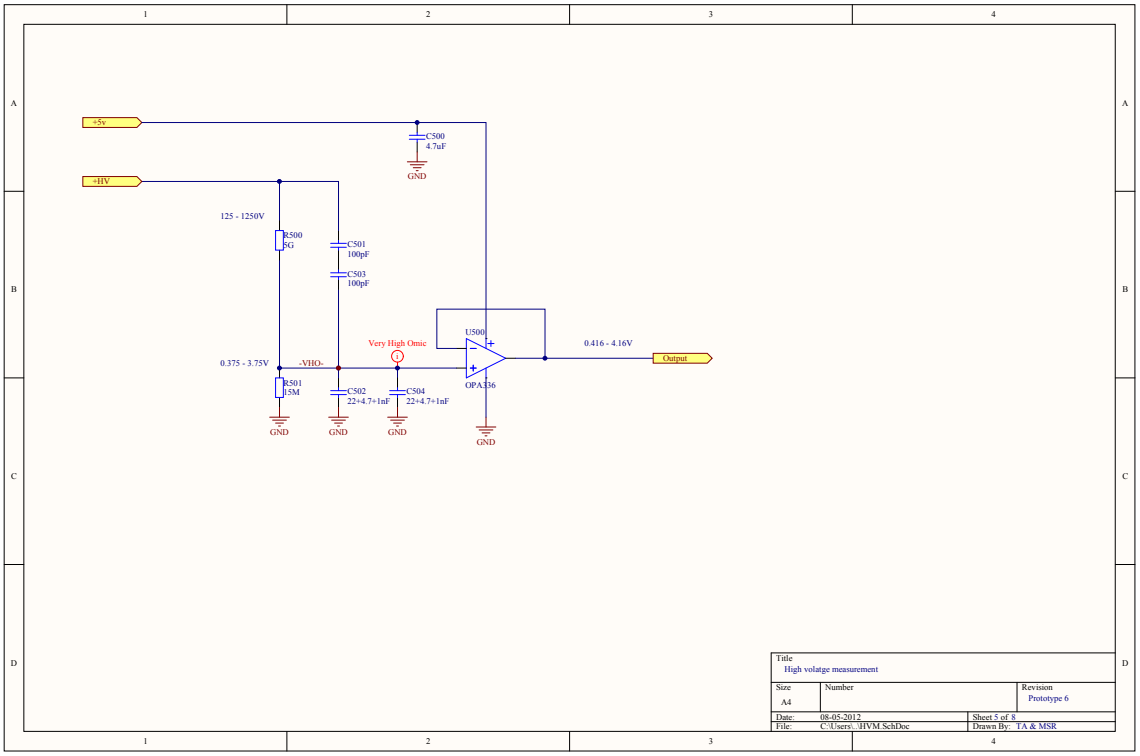
+5v
C500
4.7uF
GND
+HV
125 - 1250V
R500
5G
C501
100pF
C503
100pF
U500
Very High Omic
0.416 - 4.16V
Output
0.375 - 3.75V
-VHO-
R501
15M
C502
22+4.7+1nF
C504
22+4.7+1nF
OPA336
GND
GND
GND
GND
Title
High volatge measurement
Size
A4
Number
Revision
Prototype 6
Date:
08-05-2012
Sheet 5 of 8
File:
C:\Users\...\HVM.SchDoc
Drawn By:
TA & MSR

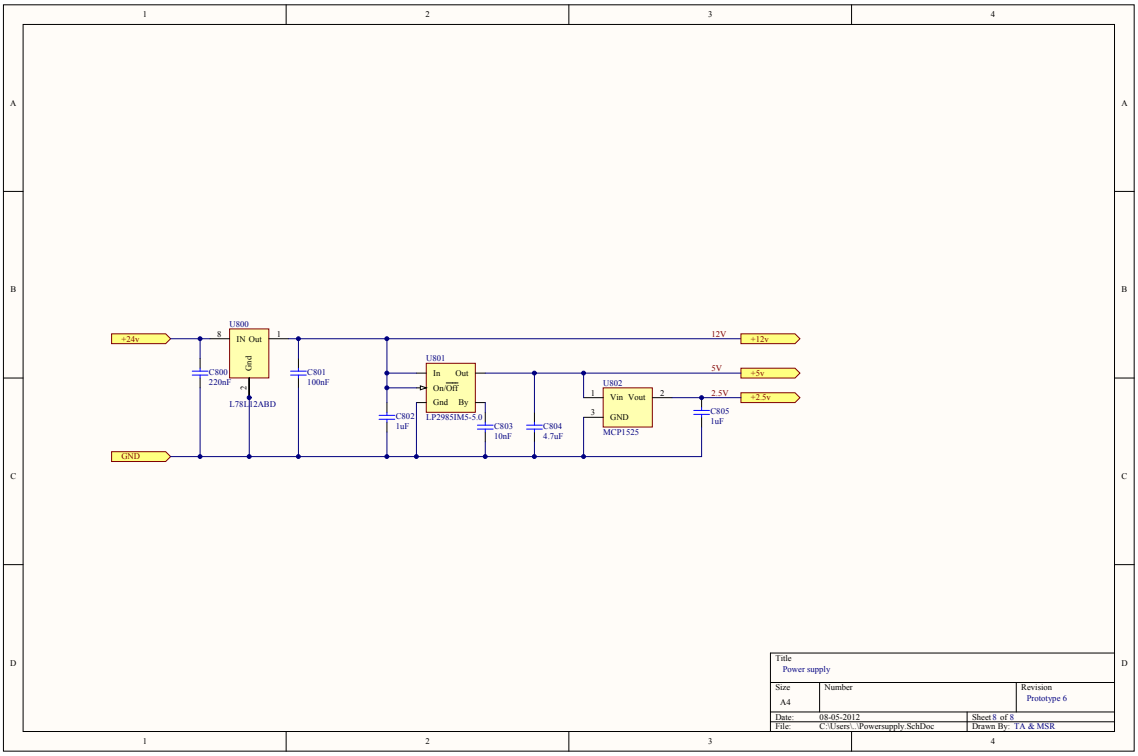
+24v
GND
U800
IN Out
Gnd
L78L12ABD
C800
220nF
C801
100nF
U801
In Out
On/Off
Gnd By
LP2985IM5-5.0
C802
1uF
C803
10nF
C804
4.7uF
U802
Vin Vout
GND
MCP1525
C805
1uF
12V
+12v
5V
+5v
2.5V
+2.5v
Title
Power supply
Size
A4
Number
Revision
Prototype 6
Date:
08-05-2012
Sheet 8 of 8
File:
C:\Users\..\Powersupply.SchDoc
Drawn By:
TA & MSR

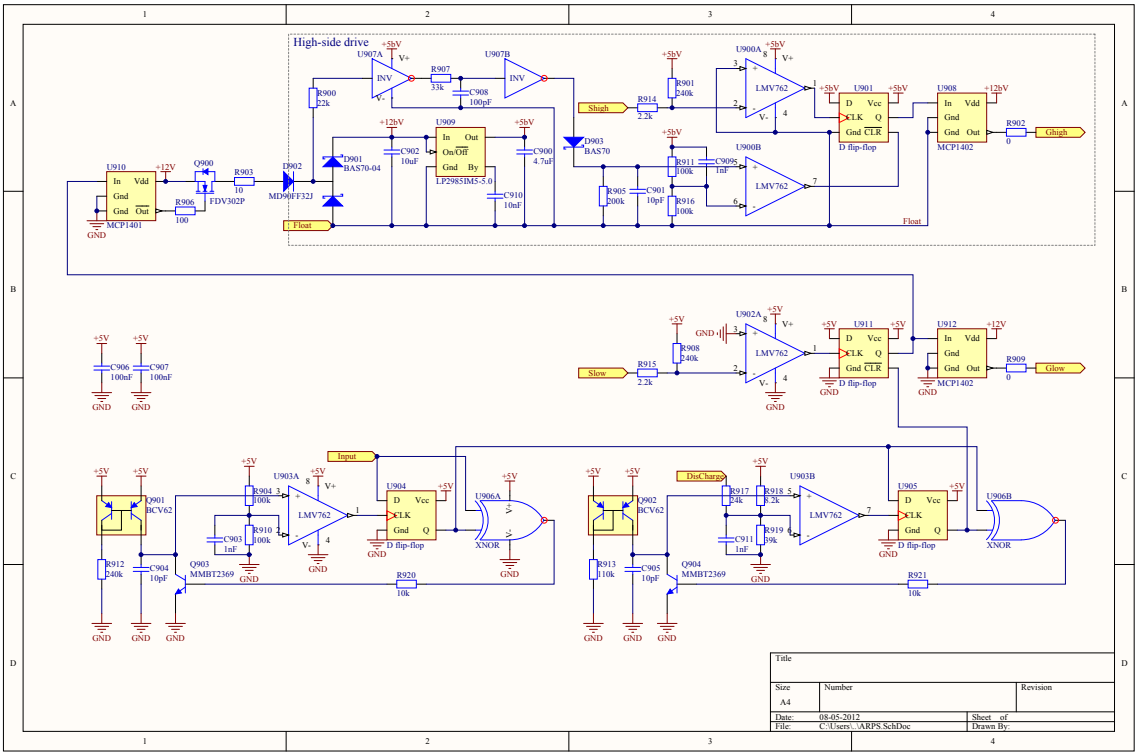
High-side drive
U907A
U907B
R907
33k
C908
100pF
R900
22k
U909
C902
10uF
C900
4.7uF
C910
10nF
D901
BAS70-04
D902
MD90FF32J
D903
BAS70
Float
Shigh
R914
2.2k
R901
240k
U900A
U900B
LMV762
R911
100k
C909
1nF
R905
200k
C901
10pF
R916
100k
U901
D flip-flop
U908
MCP1402
R902
0
Ghigh
U910
MCP1401
Q900
FDV302P
R903
10
R906
100
Slow
R915
2.2k
R908
240k
U902A
U911
U912
R909
Glow
C906
100nF
C907
100nF
Input
U903A
U903B
R904
100k
R910
100k
C903
1nF
R912
240k
C904
10pF
Q901
BCV62
Q903
MMBT2369
U904
R920
10k
U906A
XNOR
DisCharge
R917
24k
R918
2.2k
R919
19k
C911
1nF
R913
110k
C905
10pF
Q902
BCV62
Q904
MMBT2369
U905
R921
10k
U906B
Title
Size
A4
Number
Revision
Date:
08-05-2012
File:
C:\Users\..\ARPS.SchDoc
Drawn By:

PCB layout: 89x60 mm

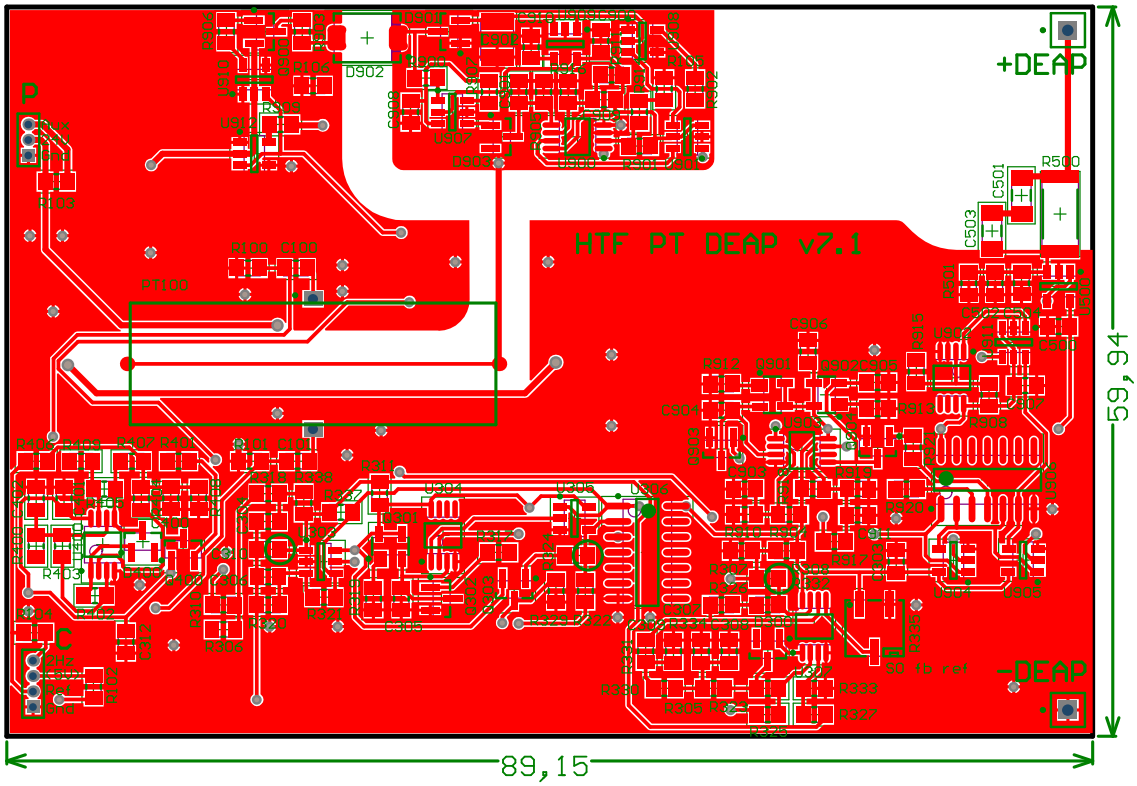

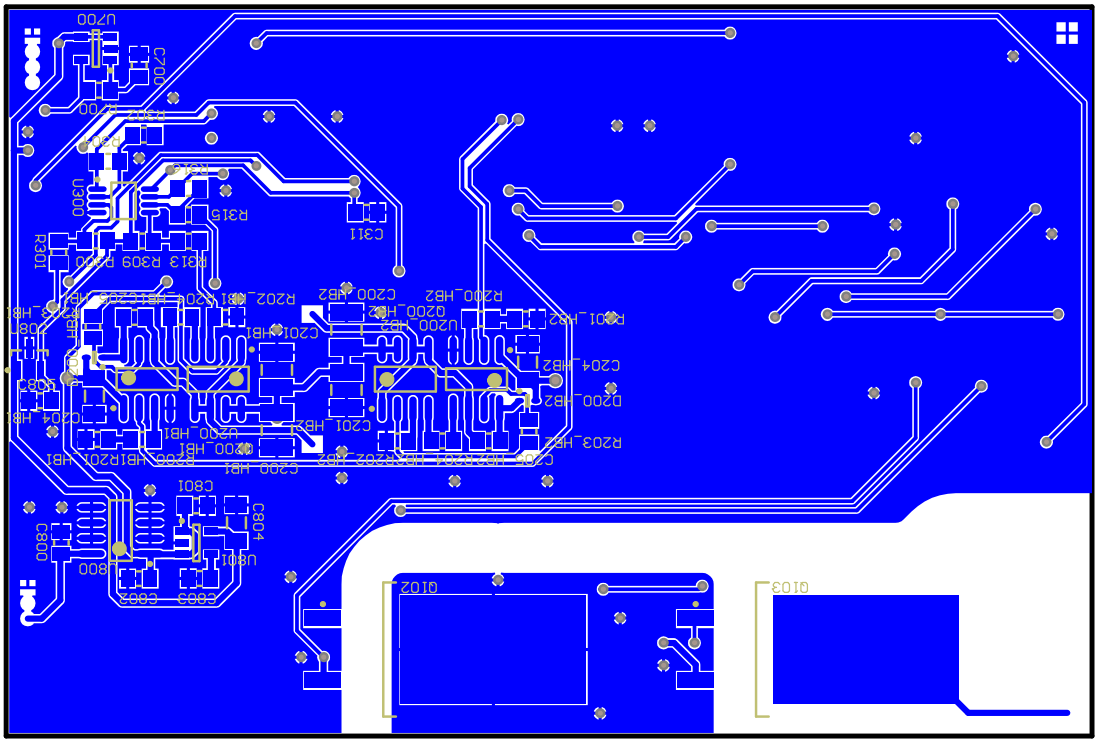

Appendix D

Publications

The following appendix contains the publications made during this PhD study and made as part of this thesis.

D.1 T. Andersen, M. Rødgaard, O. Thomsen, and M. Andersen, "Low voltage driven dielectric electro active polymer actuator with integrated piezoelectric transformer based driver," in *Proceedings of SPIE*, vol. 7976. SPIE Smart Structures/NDE, 2011, pp. 7976–95.

D.2 M. Rødgaard, T. Andersen, K. Meyer, and M. Andersen, "Design of interleaved multi layer rosen type piezoelectric transformer for high voltage DC/DC applications," in *Power Electronics, Machines and Drives (PEMD 2012), 6th International Conference on.* IET, 2012.

D.3 M. Rødgaard, T. Andersen, and M. Andersen, "Empiric analysis of zero voltage switching in piezoelectric transformer based resonant converters," in *Power Electronics, Machines and Drives (PEMD 2012), 6th International Conference on.* IET, 2012.

D.4 T. Andersen, M. Rødgaard, and M. Andersen, "Active match load circuit intended for testing piezoelectric transformers," in *Power Electronics, Machines and Drives (PEMD 2012), 6th International Conference on.* IET, 2012.

D.5 M. Rødgaard, T. Andersen, K. Meyer, and M. Andersen, "Design of interleaved interdigitated electrode multilayer piezoelectric transformer utilizing longitudinal and thickness mode vibrations," in *PECON 2012 - IEEE International Conference on Power and Energy.* IEEE, 2012.

D.6 T. Andersen, M. Rødgaard, O. Thomsen, M. Andersen, K. P. Lorenzen, C. Mangeot, and A. R. Steenstrup, "Integrated high voltage power supply utilizing burst mode control and its performance impact on dielectric electro active polymer actuators," in *ACTUATOR 12 - International Conference and Exhibition on New Actuators and Drive Systems*, 2012.

D.7 M. Rødgaard, M. Weirich, and M. Andersen, "Piezoelectric transformer based PFC LED drive, utilizing forward conduction mode control," *Power Electronics, IEEE Transactions on*, 2012.

D.8 K. Meyer, M. Rødgaard, and T. Andersen, "Self-oscillating loop based piezoelectric power converter," 2011, US Patent 61/638,883 (pending).

D.9 M. Andersen, K. Meyer, M. Rødgaard, and T. Andersen, "Piezoelectric power converter with bi-directional power transfer," 2011, US Patent 61/567,924 (pending).

D.1 Low voltage driven dielectric electro active polymer actuator with integrated piezoelectric transformer based driver

Conference paper

SPIE Smart Structures and Materials + Nondestructive Evaluation and Health Monitoring 2011
6 - 10 March 2011
San Diego, California USA
http://spie.org/x12228.xml

Low voltage driven dielectric electro active polymer actuator with integrated piezoelectric transformer based driver

T. Andersen, M. S. Rødgaard, O. C. Thomsen, M. A. E. Andersen
Technical University of Denmark, DTU Elektro,
Ørsteds Plads, bygning 349, DK-2800 Kgs. Lyngby, Denmark
ta@elektro.dtu.dk, +45 45 25 34 71
msr@elektro.dtu.dk, +45 45 25 34 82

ABSTRACT

Today's Dielectric Electro Active Polymer (DEAP) actuators utilize high voltage (HV) in the range of kilo volts to fully stress the actuator. The requirement of HV is a drawback for the general use in the industry due to safety concerns and HV regulations.
In order to avoid the HV interface to DEAP actuators, a low voltage solution is developed by integrating the driver electronic into a 110 mm tall cylindrical coreless Push InLastor actuator. To decrease the size of the driver, a piezoelectric transformer (PT) based solution is utilized. The PT is essentially an improved Rosen type PT with interleaved sections. Furthermore, the PT is optimized for an input voltage of 24 V with a gain high enough to achieve a DEAP voltage of 2.5 kV. The PT is simulated and verified through measurements on a working prototype. With the adapted hysteretic based control system; output voltage wave forms of both impulse response and sinusoidal shapes up to 2.5 kV are demonstrated. The control system, together with a carefully designed HV output stage, contributes to low power consumption at a static DEAP force. The HV stage consists of a HV measurement circuit and a triple diode voltage doubler optimized for low leakage current drawn from the DEAP.
As a result, a 95 mm x 13 mm x 7 mm driver is integrated in a 110 mm x 32 mm actuator, forming a low voltage interfaced DEAP actuator.

Keywords: Piezoelectric Transformer, high voltage, Dielectric Electro Active Polymer, PolyPower, hysteretic control, integrate, actuator, converter

1. INTRODUCTION

DEAP devices are based on polymer materials and change shape as a result of the electrostatic forces, generated by an applied voltage. The DEAP technology has a wide potential in applications such as surgical tools, grippers for material handling and valve actuators for example. The DEAP material can be modulated as a high voltage capacitor with a very low leakage current, where the force from the DEAP is related to the applied voltage. The DEAP technology available today requires a high voltage (HV) to fully utilize it as an actuator. The voltage is dependent among other by the thickness of the DEAP film. The film thickness is around 80 µm [2][13] and has a maximum working voltage of 2.5 kV. One of the barriers for using these actuators commercial is the need of a HV source. The HV interface is undesirable for practical and safety reasons. The approach in this paper is to construct a DEAP actuator with a low voltage interface, by integrating a HV driver inside the actuator. This has some requirements for the DEAP actuator and the driver itself. The actuator need to be hollow to make space for the driver inside. For that purpose a coreless Push InLastor actuator [2][13] is used for prototyping the concept. As for the driver its primary goal is to be small enough to fit inside the actuator and to deliver adequate power.
The driver typically consists of a step-up switch mode power converter and trough out this paper, the driver is also referred to as a converter. To date, conventional converters utilize electromagnetic components for converting the energy and are the only available HV sources for driven DEAP actuators. However these HV converters have poor efficiency, are bulky and provide limited opportunities for miniaturization. Piezoelectric Transformer (PT) based converters, however, is compact and offers high efficiency, especially in high step up applications. The PT based converter is a perfect match for DEAP technology and offers the miniaturization possibilities needed to integrate it in to a core less DEAP actuator. PTs were originally developed by Rosen in 1957 [1] and uses piezoelectric ceramics to convert electrical

energy trough mechanical vibrations and are already commonly used for backlighting LCD displays, but are still limited to these simple applications (with constant high frequency AC load). In the last decade a lot of research in to the area of PTs has improved Rosen's fist transformer and new types of transformers has been designed [4][15][17][18][20].

2. PIEZOELECTRIC TRANSFORMER

A piezoelectric material is a material that has an electromechanical coupling. This coupling generates a charge displacement, which is proportional to the deformation of the material. A PT is basically two piezoelectric elements which is joined together to form a transformer. The primary side element is then exited by an electrical voltage, which induces a deformation of the two joined elements, that generates a voltage on the secondary side element. With a proper design of the PT, a desired voltage conversion can be obtained from the primary to the secondary side. In order to convert power at a high efficiency, the PT is operated in one of its resonance modes [14][16][17][20]. PT resonates each time it is possible to generate a standing wave in the element. However the design is usually optimized for one specific resonance mode in order to gain the highest efficiency [14][17].
The PT resembles a distributed network, but for simplicity and mathematical representation, only the resonance mode of interest is modeled [14][16][17]. One of the most used PT models is the lumped parameter model, which was first derived by Mason in 1942 [3] and is show in figure 1.

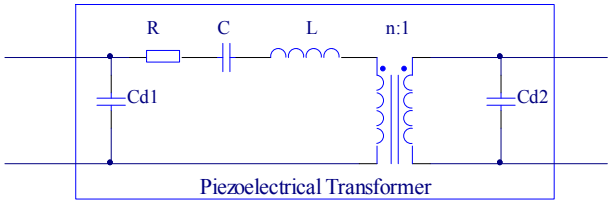

Figure 1: Lumped parameter model, which describes the behavior of the PT in narrow band around the resonance mode.

The circuit is basically a LCC resonance tank and the behavior of the PT based converter is also quit similar to a traditional resonance converter.

2.1 PT design

The Piezoelectric Transformer (PT) developed for this application is essential an interleaved multi layer Rosen-type, as the one presented in [4].
To the left in figure 2 the structure of the PT is shown, which consists of a primary section with 12 layers and one split secondary layer.

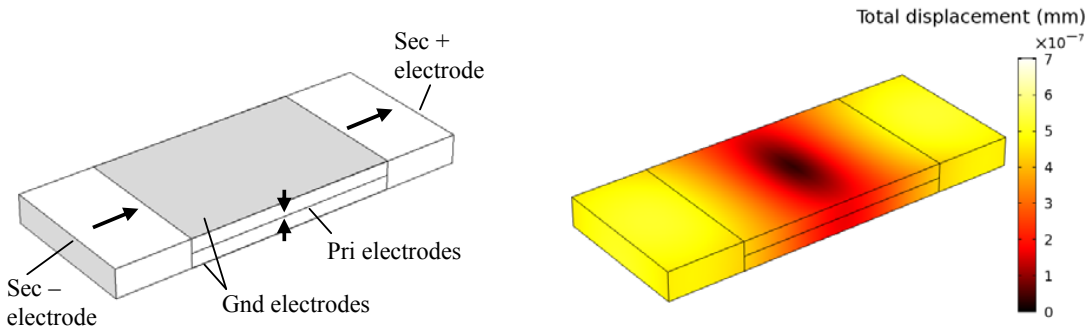

Figure 2: Left: PT structure, where the arrows indicate the polarization direction. Right: COMSOL finite element method simulation of the PT, operating in the first longitudinal mode shape, at 65.1 kHz. The coloring illustrates the total displacement, where dark colors refer to a low displacement and light colors to at high displacement, as the color bar indicates.

The figure only illustrates two primary layers, for simplicity, and the arrows indicate the polarization direction. The PT is build using tape casting technology. The piezoelectric material used is the NCE46 [19] and the PT has the following dimensions 25 mm x 10 mm x 2 mm.
The PT design is quite similar to one presented in [4], with the exception of the secondary polarization. The operational vibration resonance is along the longitudinal direction and is generated trough the electromechanical coupling factors k31 and k33, primary and secondary respectively. To the right in figure 2 a finite element method (FEM) simulation of the operational vibration resonance is shown. The PT operates in its first mode shape and it can be seen that it has a nodal line in the center of the structure.
One of the drawbacks of this design, for this application, is the split secondary. This results in a differential output voltage symmetrical around ground, which complicates the electronics somewhat, which is addressed in section 0. One could have polarized the two half secondary layers in opposite directions, which results in a two layer secondary structure, with a common voltage potential with reference to ground, as in [4]. But this approach would also half the gain of the PT, because of two secondary layers instead of one. For this application we need a high gain, so the extra effort in the electronic is rewarded with a doubling in gain.

In order to evaluate the electrical characteristics of the PT, the lumped equivalent parameters are found trough the method described in [5]. Trough a FEM simulation of the PT impedance the following equivalent parameters are found.

R	C	L	C_{d1}	C_{d2}	1/n
114 mΩ	9.8 nF	609 µH	91.7 nF	17.5 pF	93.5

Table 1: PT lumped equivalent parameter obtained trough FEM simulations.

From these equivalent parameters some more general performance properties of the PT can be calculated, as the matched load (1), efficiency (2) and gain (3).

When the load is matched to the PT output, the PT operates at its highest efficiency [5]. Match load condition (1) is depended on the terminal capacitance on the secondary side and the operating frequency.

The total loss mechanisms of piezoelectric materials are not fully implemented in the FEM simulation. The efficiency (2) is only a non stressed efficiency (derived in [5]), because the simulation is performed with small signals. Therefore this efficiency is generally a measure between different designs.

$$R_{match} = \frac{1}{C_{d2}\omega_r} \tag{1}$$

$$\eta_{match} = 1 - \frac{2RC_{d2}}{n^2\sqrt{LC}} \tag{2}$$

The gain (3) is the maximal obtainable gain, from the input of the PT to the split output. The maximum gain occurs at resonance.

$$A_{\max} = \frac{\sqrt{2}}{n}\eta \tag{3}$$

The following table contains the found PT properties.

A_{max}	R_{match}	η_{match}
130	138 kΩ	98.6 %

Table 2: PT performance properties calculated from FEM simulated equivalent parameters.

Evaluating these properties it can be seen that it has a high efficiency and a high gain, which results in a 1258 V_{rms} output voltage, in to a matched load, with a PT modulation of 9.67 V_{rms}. The PT modulation voltage is the first harmonic, of the 24 V input voltage, as derived in [5].

2.2 Prototype verification

After receiving the prototype PTs, the functionality and properties were verified. The following equivalent parameters and performance properties are found.

R	C	L	C_{d1}	C_{d2}	1/n
461 mΩ	6.74 nF	922.7 µH	111.7 nF	24.8 pF	88.6

Table 3: PT lumped equivalent parameter obtained trough prototype measurements.

A_{max}	R_{match}	η_{match}
116	100 kΩ	93.3 %

Table 4: PT performance properties calculated from prototype measured equivalent parameters.

Comparing these numbers, it can be seen that the gain are 10 % lower than expected. This is partly because the prototype buildup were 2.1 mm high, instead of the intended 2 mm, and therefore the primary layers are 5 % higher, which results in a 5 % decrease in gain. Furthermore there is some inactive piezoelectric material in the primary section, due to the termination of the primary electrodes on the side of the PT. This is not included in the FEM simulation and accounts for some of the remaining 5 % deviation. Hence there is a very good correlation between the FEM model and the prototype concerning the gain.
Looking at the capacitances C_{d1}, C_{d2} and the efficiency, the correlation is not very good. This is expected to be caused by a bad correlation between the NCE46 material parameters in the FEM model and what they in fact are in real life, as well as an incomplete loss model in the simulation. This problem will be addressed in a future paper. Nevertheless the FEM simulation makes it possible to design PTs with a desired gain, as well as the possibility to compare the efficiency between different designs. For this specific case there is not a well defined resistive load and therefore the matching inaccuracy is not a problem.

3. CONVERTER STRUCTURE

The converter structure contains several parts: control circuit, a power stage, the PT, a voltage doubler rectifier, discharge circuit and a high voltage measurement circuit. A block diagram is shown in figure 3 including a capacitor for modeling the DEAP. The PT based converter is essentially just a resonance converter, with some unique PT characteristics [12][14][16][17][18]. One of the characteristic of the PT is that the resonance network is of a high quality factor, hence giving it a very narrow bandwidth of operation. Therefore a good and precise control of the operating frequency is important, in order to maximize efficiency and ensure proper operation. The power stage of the converter is a typical half-bridge solution. The discharge of the DEAP is performed trough a resistive load controlled by the controller. The power stage and discharge circuit will not be addressed in this paper [14][21].

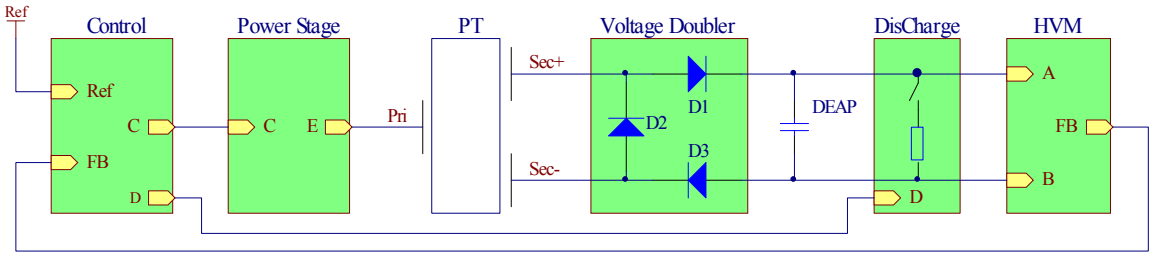

Figure 3: Block diagram of the PT based converter including the DEAP model.

4. VOLTAGE DOUBLER RECTIFIER

The sinusoidal output of the PT is rectified in a voltage doubler rectifier [8], which in this case consists of three diodes (D1, D2, D3) unlike the normal two (D1, D2). The extra diode (D3) is added to support the PTs split output, which produces a differential voltage symmetrical around ground. Without D3 one of the DEAP terminals would be connected directly to the PTs output, resulting in the DEAP bouncing up and down, with the potential of the PT output. Furthermore this would load the output of the PT with the DEAP's parasitic capacitance and lead to an increase in the common mode EMC. Beside a lower EMC, the third diode allows for the DEAP voltage to be steady around ground. This also has the advantage of lowering the current consumption in the high voltage measuring circuit, which is addressed in section 6.

5. CONTROL

As mentioned in section 3, the PT based converter is very sensitive to its operating frequency, thus a good and precise tracking of the resonance frequency is important, in order to compensate variations, caused by operating conditions and external influences. To insure this, a closed phase-loop is made, which is very similar to the one presented in [9]. This closed loop will tune itself to tracks the resonance frequency, ensuring optimal operation.
A second loop is closed around the output voltage, in order to control the output voltage. The measurement of the output voltage is not trivial and is described in detail in the section 6. Figure 4 illustrates the implementation of the charge and discharge control, which controls the output voltage.
The feedback signal (FB) is a 0 - 4 V feedback, which is proportional to the 0 - 2.5 kV variation of the output voltage and is compared to the reference voltage (Ref). R5 and C2 form a low-pass filter that limits the feedback bandwidth (BW) to 500 Hz, as well as it suppresses high frequency noise. The reference voltage is passed through a voltage divider (R3 and R4), that makes a 0 - 5 V reference voltage swing correspond to the 0 - 2.5 kV output voltage swing. Together with C1 they form a low-pass filter, which limits the reference voltage BW to 170 Hz. This is done to ensure an upper limit of operation, which should be at least 20 Hz.

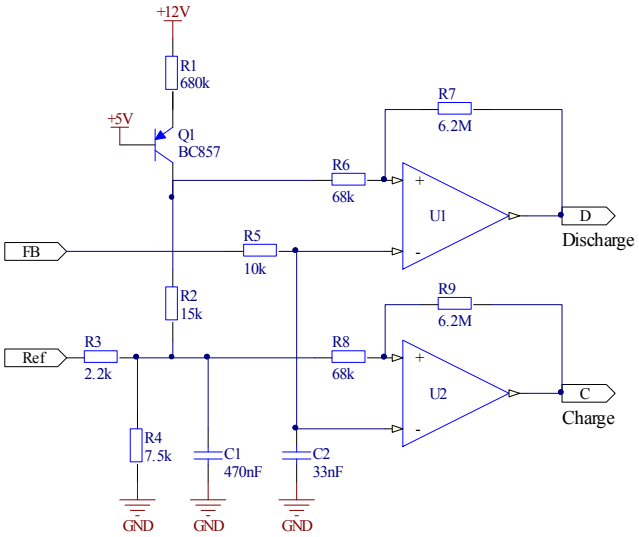

Figure 4: Hysteresis based control circuit, for the control of charge and discharge of the DEAP/output voltage, based on the HV measurement feedback.

The two comparators (U1 and U2) and their two associated resistors (R6, R7 and R8, R9) form two hysteresis windows of 55 mV, which corresponds to approximately 34 V on the output voltage. The lower comparator (U2) controls the charge cycle and when the feedback signal (FB) drops below the lower boundary of the hysteresis, the converter is turned on and charges the DEAP. The converter is then charging until the feedback hits the upper boundary, which would be a 34 V charge, if the reference voltage was kept constant. The same applies for the upper comparator (U1),

with the difference that it discharges the DEAP when the feedback hits the upper hysteresis boundary, until it reaches the lower boundary. The DEAP is simply discharge trough a resistive load, until it hits the lower boundary.
In order to separate these two hysteresis windows, R1, Q1 and R2 are added to the circuit. R1 and Q1 form a small current source, which generates a constant current. This current is passed through R2, resulting in a constant voltage across it, which separates the hysteresis windows with a constant voltage of approximately 150 mV, corresponding to 94 V on the output voltage.
Trough small bursts of charging and discharging, dependent on the reference voltage, the output voltage is kept within a limited range of the reference voltage. The separation voltage and hysteresis windows can be optimized further, in order to make the output voltage follow the reference even tighter.

6. HIGH VOLTAGE MEASUREMENT

The control circuit uses a feedback signal from a high voltage measurement circuit to regulate the output voltage. The high voltage measurement circuit has to handle voltages of at least 2.5 kV at frequencies below 20 Hz. The impendence of the measurement circuit becomes important in static operations, when a static force from the DEAP has to be maintained. In static operation the output voltage is maintained by the DEAP's capacitance, however the impedance of the measurement circuit together with the DEAP's leakage current will discharges the DEAP over time. The converter has to supply the current drawn from the DEAP to keep a constant output voltage. The overall power consumption in static operation depends on the current drawn from the DEAP. It is not in the scope of this paper to change the leakage current of the DEAP, it is therefore the objective to make the leakages current dominant compared to the current drawn by the measurement circuit. The leakage current of six DEAP samples is measured and spans from 14 nA to 959 nA, measured at 2 kV. For the DEAP leakages current to be dominant the total impedance of the measurement circuit has to be higher than: 143 GΩ - 2 GΩ (depending on the DEAP sample). For practical reasons it is not possible to work with physical small sized HV impedances in the 100 GΩ range, for comparison the volume resistivity of normal PCB is 1 - 1000 GΩ·cm depending on humidity, temperature, etc. [10].

6.1 Circuit analysis and design

The output of the PT is equivalent with two ground connected AC current sources each in parallel with a capacitor and then rectified to form a positive rail (A) and a negative rail (B). The two output rails are ideally symmetrical around ground and together forms the output voltage (A - B = V_{out}).The converters output stage equivalent is shown to the left of figure 5.

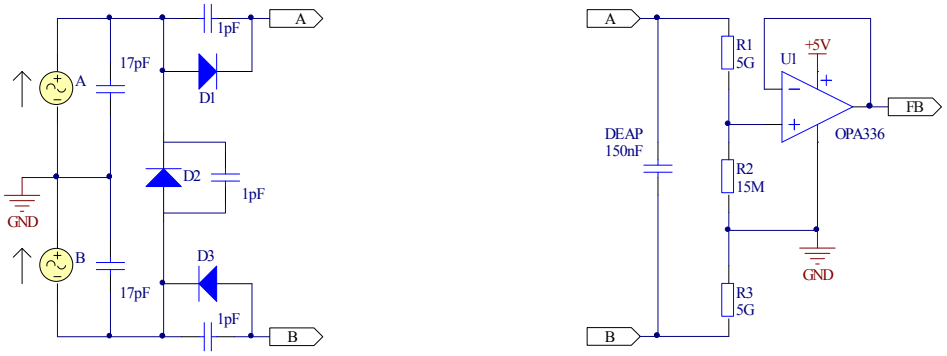

Figure 5: Left: Converter output stage equivalent circuit, with symmetric output voltage around ground. Right: High voltage measurement circuit, with resistive voltage divider, for low voltage ground referenced feedback signal.

To the right hand side of figure 5 a resistive high voltage measurement circuit together with the DEAP equivalent is shown. A resistive voltage divider from the positive to the negative rail (R1 & R2 & R3) gives a low voltage signal, referenced to ground, which is proportional to the output voltage. This signal is buffered by an operational amplifier with a very high input impedance (>10 TΩ) and is used as the feedback signal (FB) for the converters controller circuit. To keep the output voltage symmetric around ground, the resistance from the two rails to ground must be equal.

The low frequency relationship between the output voltage and the feedback signal for the circuit in figure 5 is given by the transfer function (4).

$$\frac{FB}{V_{out}} = \frac{R_2}{R_1 + R_2 + R_3} \tag{4}$$

For the circuit to handle dynamic measurements the parasitic capacitors in the circuit cannot be ignored. For this application the resistor values need to be comparable with the DEAP's leakage current, in order to minimize discharge of the DEAP. These high value resistors together with a highly compact circuit layout increase the impact from the parasitic capacitors on the transfer function, resulting in a frequency depended feedback signal. Furthermore the parasitic capacitance from the DEAP to the surroundings introduces significant noise on top of the high voltage rails from the 50 Hz mains. A model with the parasitic capacitors is seen to the left of figure 6. To eliminate the impact of the parasitic capacitors, without increasing the static discharge of the DEAP, a capacitive voltage divider is added. By using relatively large capacitors in the divider the impact from the parasitic capacitors is neglected. The transfer function for the combined resistive and capacitive voltage divider is given in (5) and is now frequency depended. By using the relation in (6) the transfer function becomes independent of frequency (7).

$$\frac{FB}{V_{out}} = \frac{\dfrac{R_2}{1 + j\omega R_2 C_2}}{\dfrac{R_1}{1 + j\omega R_1 C_1} + \dfrac{R_2}{1 + j\omega R_2 C_2} + \dfrac{R_3}{1 + j\omega R_3 C_3}} \tag{5}$$

$$R_1 C_1 = R_2 C_2 = R_3 C_3 \tag{6}$$

$$\frac{FB}{V_{out}} = \frac{R_2}{R_1 + R_2 + R_3} = \frac{\dfrac{1}{C_2}}{\dfrac{1}{C_1} + \dfrac{1}{C_2} + \dfrac{1}{C_3}} \tag{7}$$

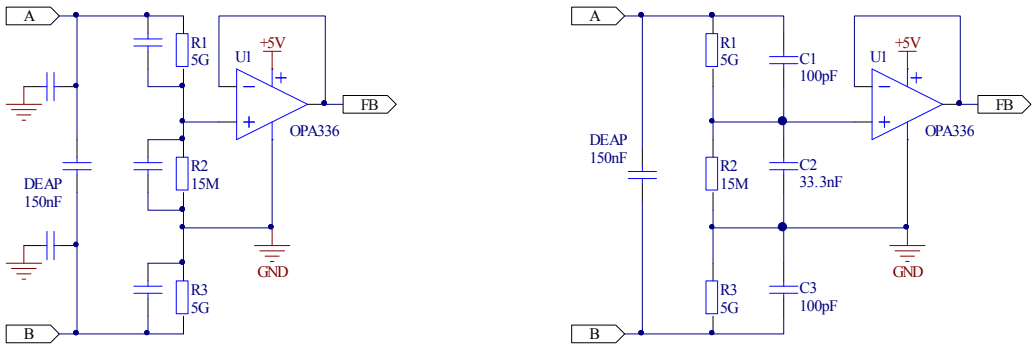

Figure 6: Left: High voltage measurement circuit including unknown parasitics. Right: High voltage measurement circuit with resistive and capacitive voltage divider to avoid the impact from parasitic components.

7. INTEGRATION

The integration of the electronics into the DEAP actuator has been a main concern right from the start. Therefore the physical size and shape of the driver has also been a significant part of the development, as well as the mechanical interface and incorporation of the driver in the actuator.
The actuator has a winding-insert in each end to support the coreless DEAP actuator. The cross-section area of the prototype converter is 12.8mm x 7.5mm and fits into the elliptical cross-section area of the winding-inserts, as seen to the left in figure .

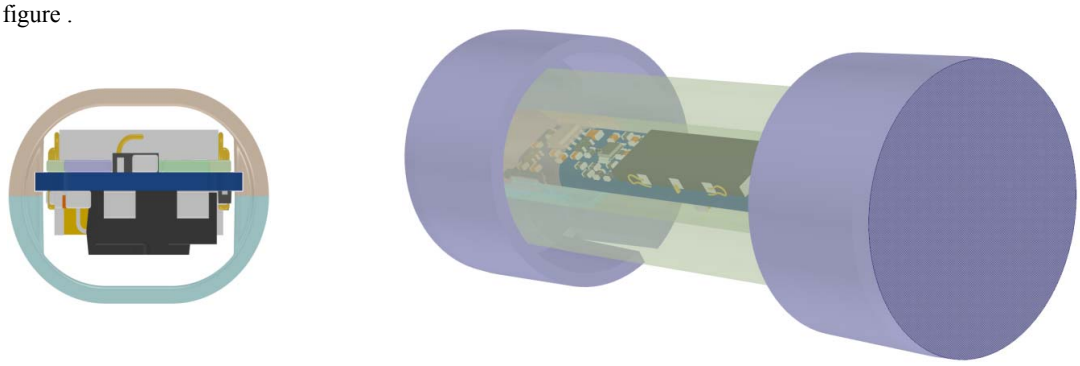

Figure 7: Left: Cross-section view of the converter surrounded by a winding-insert. Right: 3D view of the actuator with transparent DEAP material to illustrate how the converter is placed inside the actuator.

In one of the winding-inserts a set of grooves in each side provide two functions. The first function is to guide the converter straight into the actuator, when sliding in the PCB. The second function is to fix the driver in only one end of the actuator. In the opposite end the PCB is narrowed to avoid friction with the winding-insert, this ensures that the rest of the actuator can move freely. Each end of the actuator is encapsulated with an end fitting, made of plastic. A 3D view of the actuator with end-fittings is seen to the right in figure , were the DEAP material is transparent to illustrate how the converter is placed inside.

The physical size of the prototype driver is only 95 mm x 12.8 mm x 7.5 mm (L x W x H) and a photo of the prototype is seen in figure 8.

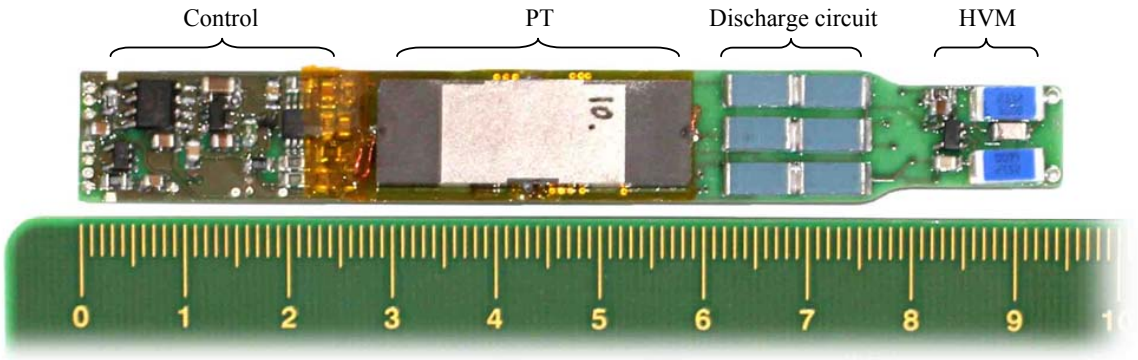

Figure 8: Prototype driver showing the control circuit, a 30 mm PT, resistive discharge array and the high voltage measurement circuit. The voltage doubler rectifier is placed on the opposite side, underneath the high voltage measurement circuit. The power stage is also placed on the opposite side of the PCB and is located underneath the PT.

The external size of the actuator is 110x32 mm and a picture of the final DEAP actuator with the integrated driver is seen in figure 9.

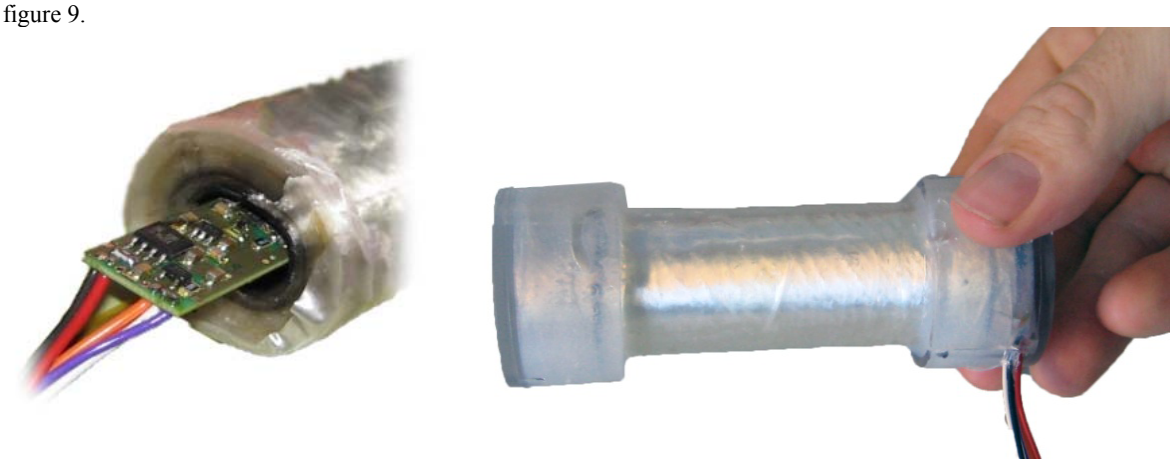

Figure 9: Left: Picture of the driver sliding into the DEAP actuator. Right: Picture of the final “low voltage” DEAP actuator.

8. EXPERIMENTAL RESULTS

8.1 High Voltage measurement

Practical experience revealed that care should be taken when selecting the high voltage capacitors (C1 & C3) referred to figure 6. Voltage dependent capacitance (DC-bias) destroys the relation in (6) and splits the transfer function for the feedback signal into a static and a dynamic gain (8). For this application ceramic multilayer capacitors are preferred because of their high volumetric capacitance, which allows small package size. The widely used ceramic for high volumetric capacitors are ferroelectric and therefore inhere strong voltage dependent capacitance. Increased capacity per volume for these capacitor types increases the voltage dependency. To avoid the voltage dependency of ceramic capacitors the ceramic type to use is paraelectricity. The main component of temperature compensation type (C0G, NP0, U2J, etc.) is paraelectricity and therefore the capacity does not vary with voltage [11].

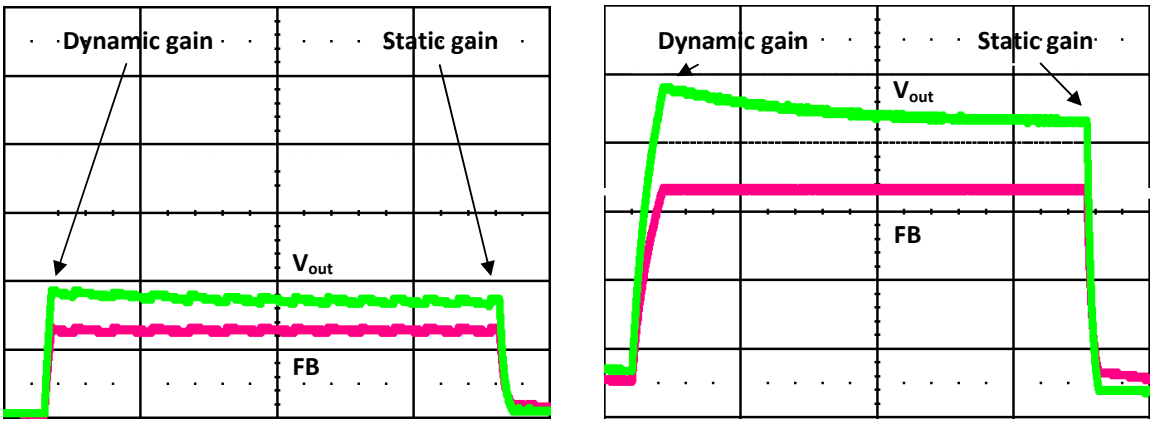

Figure 10: Measured illustration of the erroneous dynamic gain caused by non liner dielectric in HV capacitors C1, C3. Output voltage (V_{out}: 500 V/div & 500 ms/div) and the feedback signal (FB: 1 V/div & 500 ms/div) in closed loop at two different reference signals. Left: low voltage case. Right: high voltage case.

In figure 10 are the output voltage and the feedback signal measured with two different amplitude of a square wave reference input to the controller. The output voltage is adjusted by the converter so the feedback signal matched the square wave reference. C1 & C3 are both ceramic capacitors (100 pF– 2 kV) in category X7R. Table 5 compares the dynamic and static gain from the two measurements in figure 10. The dynamic gain is dominated by the capacitive voltage divider where as the static gain is dominated by the resistive divider. As the voltage increase the dynamic gain decreases because the capacitance of C1 & C3 decreases with applied voltage. This result agrees with the equation stated in (8).

$$\frac{FB}{V_{out}} = \begin{cases} \dfrac{R2}{R1+R2+R3} & \omega \to 0 \quad \text{Static} \\ \dfrac{\dfrac{1}{C2}}{\dfrac{1}{C1}+\dfrac{1}{C2}+\dfrac{1}{C3}} & \omega \to \infty \quad \text{Dynamic} \end{cases} \tag{8}$$

			Voltage	Gain	Deviation	Delta deviation
Low voltage case	Dynamic gain	V_{out}	940 V	1.43 mV/V	-4.8 %	Δ4.9
		FB	1.34 V			
	Static gain	V_{out}	860 V	1.50 mV/V	0.1 %	
		FB	1.29 V			
High voltage case	Dynamic gain	V_{out}	2405 V	1.39 mV/V	-7.1 %	Δ9.7
		FB	3.35 V			
	Static gain	V_{out}	2165 V	1.54 mV/V	2.6 %	
		FB	3.33 V			

Table 5: Comparison of dynamic and static gain in both a low and high voltage case, with voltage dependent capacities.

8.2 Control and operation

The fully functionality of the converter is demonstrated in figure 11. The left plot illustrates how the converter is capable of charging the DEAP, to a desired voltage and the keep the output voltage steady at this voltage, trough small bursts of operation.

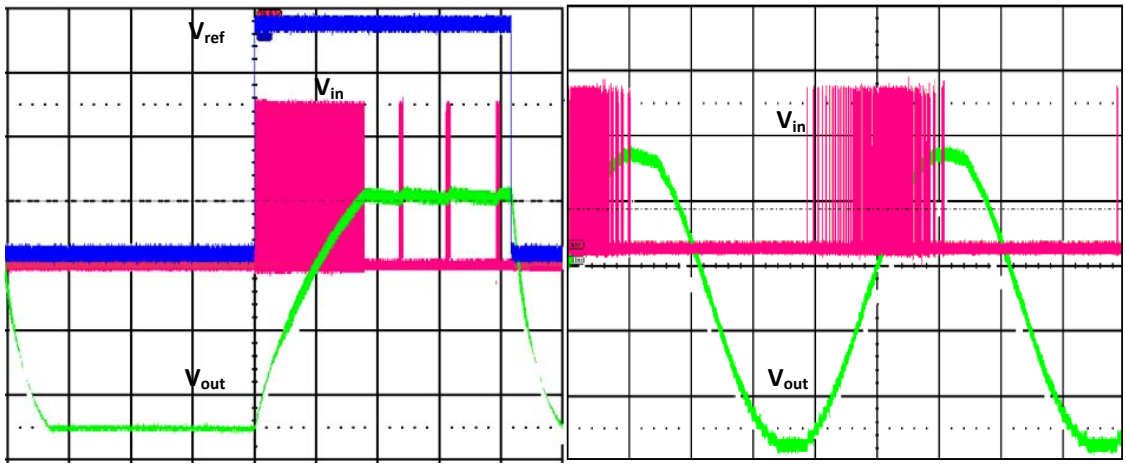

Figure 11: Measurement of the output voltage across the DEAP (green –500 V/div), reference voltage (blue – 1 V/div) and input voltage (red –10 V/div). Left: Square-wave reference signal. Time base 50 ms/div. Right: Sinusoidal reference signal. Time base 100 ms/div.

The first stage, where the DEAP is charged, the output voltage has a certain rise time, this is essential the impulse response of the converter. This is due to the limited power available from the converter, it will take some time to deliver the needed energy. In the second stage, the converter is operated in a burst mode manner. The bursts have a separation of less than 50 ms, which indicates a rapid discharge of the DEAP. This discharge is in fact caused by the oscilloscope's HV probe itself and is not a sign of a bad DEAP or HVM circuit. This is because of the impedance of the HV differential probes used, which has an impedance of 10 MΩ and accounts for a 162 mW discharge of the DEAP at 1.8 kV. Without the oscilloscope probes the only discharge of the DEAP, is caused by its own leakage, the leakage in the diodes and the HVM circuit. Without oscilloscope probes a burst-rate of 30 seconds separation has been observed. The third stage is the discharge of the DEAP and this is done trough a resistive load.
The right plot in figure 11 demonstrates how the converter is capable of following a sinusoidal reference voltage, with a frequency of approximately 2 Hz. It can be seen how the burst periods becomes denser as the slope of the output voltage increases. Furthermore the energy needed to charge the DEAP is dependent on the voltage squared, resulting in the largest burst periods at a point where the voltage and slope is high.

9. CONCLUSION

The world first low voltage DEAP solution is presented. By utilizing a piezoelectric transformer, it is succeeded to design and produce a driver small enough to be integrated into a coreless DEAP actuator. Piezoelectric transformer simulations is verified by measurements to ensure a gain, high enough to produce the needed output voltage of 2.5kV from input voltage of 24 V to fully stress the DEAP actuator.
There is a good correlation between the piezoelectric transformer prototype and finite element method simulations, concerning the gain. The correlation between the equivalent lumped parameters in general, could be improved. The presented control system only turns on the driver when necessary, in a burst-mode manner. That together with a careful design of the output stage, which minimizes the discharge current of the DEAP, the power consumption, at a static DEAP force is kept as low as possible.

REFERENCES

[1] C. A. Rosen, "Ceramic transformers and filters", Proc. Electron. Comp. Symp. 205-211, (1957).
[2] Tryson M, Kiil HE, Benslimane M, "Powerful tubular core free dielectric electro activate polymer (DEAP) 'PUSH' actuator", SPIE Vol. 7287, (2009)
[3] Mason W. P., "Electromechanical Transducers and Wave Filters", D. Van Nostrand Co , (1942)
[4] Xiang-cheng CHU, Jun-fei WU, Zhi-han XU, Long-tu LI, "EXPERIMENT RESEARCH ON MULTILAYER PIEZOELECTRIC TRANSFORMER", IEEE 978-1-4244-2891-5, 524-527 (2008)
[5] Meyer K. S., Andersen M. A. E. ," Parameterized Analysis of Zero Voltage Switching in Resonant Converters for Optimal Electrode Layout of Piezoelectric Transformers", PESC IEEE 978-1-4244-1668-4, 2543-2548 (2008)
[6] Horsley, E.L., Nguyen-Quang, N., Foster, M.P., Stone, D.A., "Achieving ZVS in inductor-less half-bridge piezoelectric transformer based resonant converters", PEDS2009, 446-451 (2009)
[7] Alonso J. M., Ordiz C., Costa M. A. D., Ribas J., Cardesín J., " High-Voltage Power Supply for Ozone Generation Based on Piezoelectric Transformer", IEEE TRANSACTIONS ON INDUSTRY APPLICATIONS, VOL. 45 NO. 4, 1513-1523 (2009)
[8] Ivensky G., Shvartsas M., Ben-Yaakov S.,"Analysis and modeling of a voltage doubler rectifier fed by a piezoelectric transformer", IEEE Transactions on Power Electronics, Vol.19 Issue.2, 542-549 (2004)
[9] Díaz J., Martín-Ramos J.A., Prieto M.J., Nuño F.,"A Double-Closed Loop DC/DC Converter Based On A Piezoelectric Transformer", APEC 2004 Vol.3, 1423-1428 (2004)
[10] [Low Level Measurements Handbook 6th edition], Keithley, Cleveland Ohio, (2004)
[11] Waugh M. D., "Design solutions for DC bias in multilayer ceramic capacitors", Electronic Engineering Times Europe, August (2010)
[12] Bai C., Li S., Shen Q., Cui D., "A Converter of High Voltage Capacitor Charging Power Supply Using Piezoelectric Transformer", APPEEC, (2009)

[13] Benslimane M. Y., Kiil HE, Tryson M. J., “Dielectric electro-active polymer push actuators: performance and challenges”, Society of Chemical Industry, Wiley Interscience, 415-421 (2010)
[14] LinC. Y., “Design and analysis of piezoelectric transformer converters,” PhD dissertation, Blacksburg Virginia (1997), http://scholar.lib.vt.edu/theses/available/etd-82097-163753/unrestricted/diss0917.pdf
[15] Navas J. C. J., Bove T., Breboel K., “Miniaturised battery charger using piezoelectric transformers,” Applied Power Electronics Conference and Exposition, APEC 2001 Sixteenth Annual IEEE, vol.1, 492–496 (2001)
[16] F. L. CY Lin, “Design of a piezoelectric transformer converter and its matchingnetworks”, Power Electronics Specialists Conference, PESC’ 94 Record, (1994)
[17] Lin R. L.,“Piezoelectric Transformer Characterization and Application of Electronic Ballast”, PhD dissertation, Blacksburg Virginia (2002)
[18] Baker E. M.,“Design of Radial Mode Piezoelectric Transformers for Lamp Ballast Applications”, PhD thesis, Blacksburg Virginia (2002)
[19] Noliac A/S Piezo ceramics datasheet, http://www.noliac.com/Files/Billeder/02%20Standard/Ceramics/Noliac_CEramics_NCE_datasheet.pdf
[20] Horsley E.L., Foster M.P., Stone D.A.,“State-of-the-art Piezoelectric Transformer Technology”, European Conference on Power Electronics and Applications, 1-10 (2007)
[21] Erikson W. R., Maksimović D., [Fundamentals of Power Electronics], Springer Science+Business Media inc., (2001)

D.2 Design of interleaved multilayer Rosen type piezoelectric transformer for high voltage DC/DC applications

Conference paper

PEMD 2012 - Power Electronics, Machines and Drives Conference
27 - 29 March 2012
University of Bristol, United Kingdom
http://conferences.theiet.org/pemd/

DESIGN OF INTERLEAVED MULTILAYER ROSEN TYPE PIEZOELECTRIC TRANSFORMER FOR HIGH VOLTAGE DC/DC APPLICATIONS

M. S. Rødgaard*, T. Andersen*, K. S. Meyer †, M. A. E. Andersen*

**Technical University of Denmark, DTU Elektro, Ørsteds Plads, building 349, DK-2800 Kgs. Lyngby, Denmark,*
msr@elektro.dtu.dk
†Noliac A/S, Hejreskovvej 18, 3490 Kvistgaard, Denmark

Keywords: Piezoelectric transformer, step-up, converter, soft switching

Abstract

Research and development within piezoelectric transformer (PT) based converters are rapidly increasing as the technology is maturing and starts to prove its capabilities. Especially for high voltage and high step-up applications, PT based converters have demonstrated good performance and DC/AC converters are widely used commercially. The availability of PT based converters for DC/DC applications are very limited and are not that developed yet. I this paper an interleaved multi layer Rosen-type PT for high step-up and high output voltage is developed, for driving a 2.5kV dielectric electro active polymer actuator [17]. The targeted application utilises an inductor-less half-bridge driving topology, where the reward of eliminating the series inductor is a reduction in component count, size and price. The absence of a series inductance calls for other means to avoid large hard switching losses and obtain soft switching capabilities. This can be achieved by utilising an advantageous PT structure, which is the main advantage of the interleaved Rosen-type PT. Furthermore the design should be further optimised, in order to achieve soft switching capability. The goal of this paper is to develop a soft switching optimised PT, capable of generating output voltages higher than 2kV from a 24V supply voltage. Furthermore finite element method (FEM) has been the main tool through the PT development.

1 Introduction

The piezoelectric transformer (PT) was originally developed by Rosen in 1957 [16] and utilises piezoelectric ceramics to convert electrical energy through mechanical vibrations. PT based converters have demonstrated good performance and DC/AC converters are widely used commercially, especially for high step-up and high voltage (HV) applications, like LCD backlighting. But they are still limited to these simple applications (with a constant and high frequency AC load) and the availability of PT based converters for DC/DC applications are very limited and are not that developed yet. However new applications, like electro active polymer (EAP) actuators [5][17], require a high and adjustable DC voltage and calls for DC/DC converters of high step-up and high output voltage.
EAP devices are based on polymer materials and change shape as a result of the electrostatic forces, generated by an applied voltage. The EAP technology has a wide potential in applications such as surgical tools, grippers for material handling and valve actuators for example. The EAP material is essentially just a thin film of polymer with an electrode on each side. It can be modulated as a HV capacitor with a very low leakage current and the force generated by the EAP is related to the applied voltage. The voltage required is dependent among others by the thickness of the EAP film. The EAP technology available today has a film thickness of around 80 µm [5][17], it has a maximum working voltage of 2.5 kV and requires a voltage above 2kV to fully utilise it as an actuator.

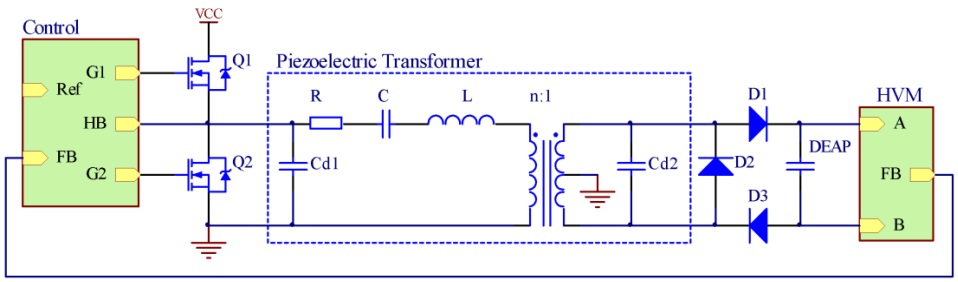

Figure 1: Schematical diagram of the inductor-less half-bridge topology and the PT equivalent lumped parameter model.

To date, conventional converters utilize electromagnetic components and are the only available HV sources for driven EAP actuators. However these HV converters have poor efficiency, are bulky and provide limited opportunities for miniaturization. PT based converters, on the other hand, are compact and offers high efficiency, especially for high step-up applications. This makes the PT based converter the perfect match for the EAP technology.
In the last decade a lot of research in to the area of PT's has improved Rosen's fist PT and new types of PT's have been developed [4][8][11][14][18]. I this paper an interleaved multi layer Rosen-type PT for high step-up and high output voltage is developed, for driving a 2.5kV EAP actuator [17]. The specific EAP actuator application is described in more detail in [1] and is similar to the one in [3]. Figure 1 illustrates a schematical diagram of the converter, which utilises an inductor-less half-bridge topology [2][13]. An inductor in series with the PT is usually necessary, in order to achieve soft switching and efficient operation. The absence of a series inductance calls for other means to avoid large hard switching losses and obtain soft switching capabilities. By utilising an advantageous PT structure, soft switching capability can be obtained, which is the main advantage of the interleaved Rosen-type PT. Furthermore the design should be optimised further, in order to obtain soft switching capability. This optimisation has been performed through iterative FEM simulations, as well as the optimisation of the gain and the PT properties in general. Due to the increasing complexity of PT structures and the complexity of the electromechanical behaviour in general, a pure mathematical solution of PT design problems is very challenging, as well as a high degree of knowledge of the electromechanical domain is needed. With today's multi physics FEM simulators, one can fine-tune PT structures, without having to rewrite the math every time.
As a result an interleaved Rosen-type PT, with a soft switching factor [13] of 1.43 and a gain of 68 has been developed.

2 Piezoelectric transformer

PT's are based on a piezoelectric material. This material has an electromechanical coupling and through this coupling a charge displacement is generated, which is proportional to the deformation of the material. A PT is basically two piezoelectric elements which is joined together to form a transformer. The primary side element is then exited by an electrical AC voltage, which induces a deformation of the two joined elements. This deformation generates an output voltage on the secondary side element and with a proper design of the PT, a desired voltage conversion can be obtained from the primary to the secondary side.
In order to convert power at a high efficiency, the PT is operated in one of its resonance modes [8][9][10][11]. The PT resonates each time it is possible to generate a standing wave in the element. But the design is usually optimised for one specific resonance mode, in order to obtain the highest efficiency [9][11].

The PT resembles a distributed network, but for simplicity and mathematical representation, only the resonance mode of interest is modelled [9][10][11]. One of the most used PT models is the lumped parameter model, which was derived by Mason in 1942 [12] and is illustrated in Figure 2.

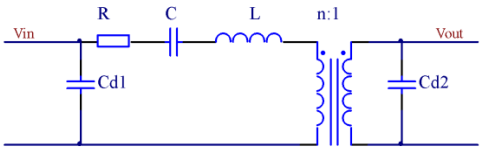

Figure 2: Lumped parameter model, which describes the behaviour of the PT in a narrow band around the opperating resonance mode.

The model is basically a LCC resonance tank and the behaviour of a PT based converter is also quite similar to a traditional resonance converter [6].

2.1 Piezoelectric transformer design

The PT developed for this application is essential an interleaved multi layer Rosen-type, meaning that the primary section of the PT has been interleaved into the secondary section. Figure 3 illustrates the structure of the PT, which consists of a primary section with 12 layers, of 166µm in thickness and one split secondary layer. For simplicity the figure only shows two primary layers and the arrows indicate the polarization direction. The PT is build using tape casting technology and the NCE46 piezoelectric material [15]. The PT has the dimensions of 25mm x 10mm x 2mm, but PT's of 20mm, 30mm and 35mm in length were also designed and produced in the same process.

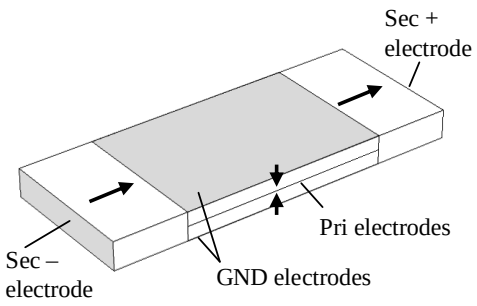

Figure 3: The interleaved multi layer Rosen-type PT structure, where the arrows indicate the polarization direction.

The PT design is quite similar to the one presented in [18], but differs with the polarization of the secondary being in the same direction, as well as it has been optimised for soft switching. Meaning that it is capable of operating the half-bridge under zero voltage switching (ZVS), without any added inductance in series with the PT. The operational vibration resonance is along the longitudinal direction and is generated through the electromechanical coupling factors k_{31} and k_{33}, primary and secondary respectively. In Figure 4 a

FEM simulation of the operational vibration resonance is shown. The PT operates in its first longitudinal mode shape and it can be seen it has a nodal line in the center of the structure.

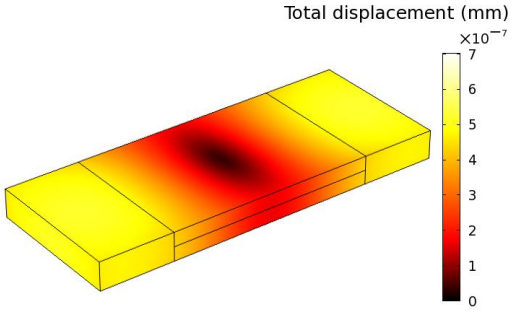

Figure 4: FEM simulation of the PT, operating in the first longitudinal mode shape, at 65.1 kHz. The colouring illustrates the total displacement, where dark colours refer to a low displacement and light colours to at high displacement, as the colour bar indicates.

One of the drawbacks of this design, for this application, is the split secondary. This results in a differential output voltage symmetrical around ground, which complicates the electronics somewhat. One could polarise the two half secondary layers in opposite directions, which results in a two layer secondary structure, obtaining a common voltage potential with reference to ground, as in [18]. But this approach would also divide the gain by two, because of two secondary layers, of half the thickness, instead of one full thickness secondary. For this application we need a very high gain, so the extra effort in the electronic is rewarded with a doubling in gain.

2.2 Piezoelectric transformer development

The major part of the development has been performed through iterative FEM simulations, where the two main design criteria have been a high gain and the capability of inductor-less operation. In order to utilise an inductor-less topology, the PT should poses soft switching capabilities. This is achieved through the relative location and size of the primary section. Furthermore the PT is operated slightly above the resonance frequency, where the series resonance network becomes inductive and contains enough resonating energy, to charge and discharge the input capacitance C_{d1}. The interleaving of the primary section is the main advantage of this design, as this increases the soft switching capability. This is due to the placement right in the middle of the stress curve, which is a half-wave sine wave for the first resonance mode. Furthermore the primary section size has been optimised in order obtain soft switching capability.
Rosen-type PT's has a native high gain, which is good for this application. The gain is mainly determined by the thickness of the primary layers, but of course the primary section size also affects the gain.

Figure 5 shows a frequency sweep of the primary and secondary impedance, around the operating resonance mode. In order to evaluate the electrical characteristics of the PT, the lumped parameter model should be created.

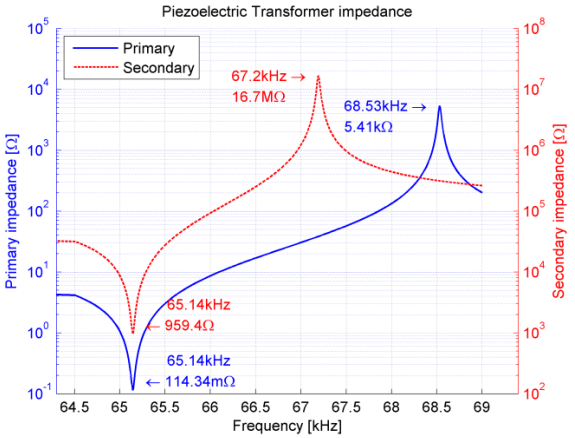

Figure 5: FEM simulation of the PT primary and secondary impedance magnitude, with the opposite side shorted.

The lumped parameters are calculated from the primary and secondary impedance resonance and anti-resonance, plus a DC impedance measurement, as described in detail in [13]. Trough the FEM simulation of the PT impedance Figure 5, the equivalent parameters of Table 1 are found.

R	C	L	C_{d1}	C_{d2}	1/n
114mΩ	9.8nF	609µH	91.7nF	17.5pF	93.5

Table 1: PT equivalent lumped parameters obtained through FEM simulations.

From the lumped parameters some more general performance properties of the PT can be calculated, as the soft switching factor, matched load, power in matched load, gain and efficiency.
The load is usually matched to the output capacitance C_{d2} of the PT, Equation (1), or the other way around, because this maximises the power transfer of the resonance network to the load. Furthermore all the following performance properties assume a matched load.

$$R_{match} = \frac{1}{C_{d2}\omega_r} \qquad (1)$$

Equation (2) expresses the soft switching factor or ZVS factor, which is derived in [13] and is a measure of the PT's soft switching capabilities. If the ZVS factor is more than 1, the PT is capable of performing ZVS at the half-bridge, operated with a matched load.

$$V_P' = \frac{1}{n^2}\frac{C_{d2}}{C_{d1}}\frac{32\sqrt{6}}{9\pi^2}\eta \qquad (2)$$

Through our own experience, this equation has its short comings, properly because of some of the assumption in the derivation, which is demonstrated in detail in [7]. But it has shown to predict soft switching when working with factors above approximately 1.4 and it is very simple and straight forward to use, compared to the one derived in [7].
Equation (2) is the maximal obtainable soft switching capability, which is located slightly above the resonance frequency, where the series resonance network becomes inductive and contains enough resonating energy, to charge and discharge C_{d1}, if the soft switching factor is above 1.4.
The efficiency Equation (3) is a small signal efficiency, because the FEM simulation is only a small signal simulation of the impedance. Furthermore the loss mechanisms of piezoelectric materials are not fully implemented in the FEM simulation, therefore the efficiency is mostly just a measure to compare between different designs.

$$\eta_{match} = 1 - \frac{2RC_{d2}}{n^2\sqrt{LC}} \qquad (3)$$

The following PT properties of Table 2 are found from the equivalent parameters of Table 1 and the index "ZVS" is referring to that the PT is operating at its maximum ZVS point.

V'_P	A_{ZVS}	P_{ZVS}	R_{match}	η	$V_{out,rms}$
1.45	75.3	3.79W	138kΩ	0.986	728V

Table 2: PT equivalent lumped parameter model performance properties.

Evaluating these properties it can be seen that it has a sufficient high ZVS factor of 1.45, which enables the inductor-less operation, a high efficiency and a high gain. The high gain results in a 728 V_{rms} output voltage, into a matched load, with a PT modulation voltage of 9.67V_{rms}. The PT modulation voltage is the first harmonic, of the 24V input voltage, as derived in [13].

3 Experimental results

In the following section the functionality and properties of the received prototype PT's are verified.

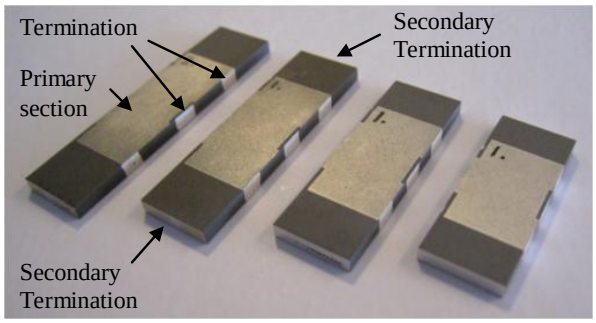

Figure 6: Picture of prototype PT's of different sizes (length from left: 35mm, 30mm, 25mm and 20mm).

Figure 7 shows an impedance measurement of one of the prototype PT's and from these measurements the equivalent lumped parameters of Table 3 and the performance properties of Table 4 are calculated.

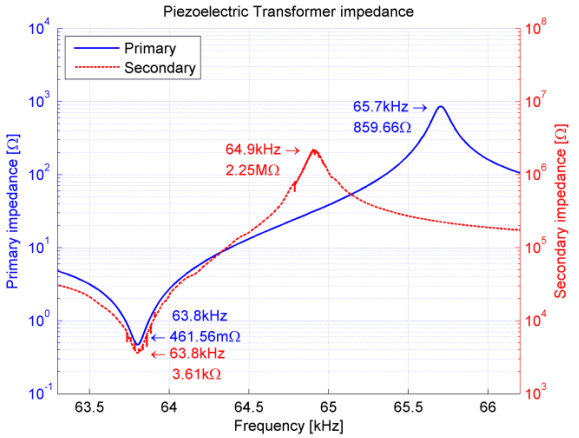

Figure 7: Measurement of prototype PT primary and secondary impedance magnitude, performed with a HP4194A impedance/gain-phase analyzer.

R	C	L	C_{d1}	C_{d2}	1/n
462mΩ	6.74nF	923µH	112nF	24.8pF	88.6

Table 3: Prototype PT equivalent lumped parameters obtained through impedance measurements.

V'_P	A_{ZVS}	P_{ZVS}	R_{match}	η	$V_{out,rms}$
1.43	67.5	4.23W	100kΩ	0.933	653V

Table 4: Prototype PT equivalent lumped parameter model performance properties.

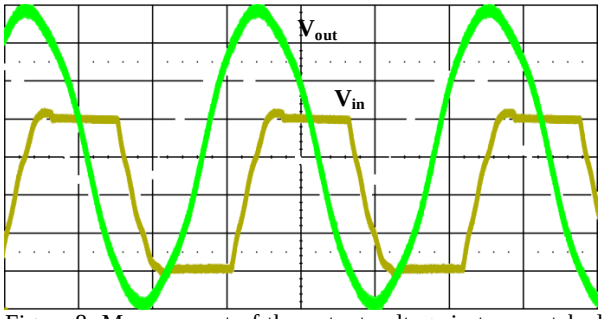

Figure 8: Measurement of the output voltage in to a matched load (green) and input half-bridge voltage (yellow), which clearly is operating under ZVS. Time base [5µs/div], output voltage [200V/div] and input half-bridge voltage [5V/div].

Figure 8 shows the PT operating with a half-bridge voltage of 20V and with a matched resistive load. From the input voltage waveform, it can clearly be seen that the half-bridge is operating under ZVS, which verifies the designs soft switching capability. Looking at the output voltage it resembles a nice sine wave, with a peak voltage of

approximately 780V, from which the gain of Equation (4) can be calculated.

$$A_{ZVS} = \frac{|V_{out}|}{|V_{in}|} = \frac{780V}{0.57 \cdot 20V} = 68.2 \qquad (4)$$

Where 0.57 is the approximate amplitude of the first harmonic of a trapezoidal waveform, as derived in [13]. When employing a rectifying voltage doubler instead of a matched load, voltages over 2kV can be achieved for DC/DC applications.

4 Discussion

Comparing measured figures (Table 3 and Table 4) with the FEM simulation obtained figures (Table 1 and Table 2), it can be seen that the gain (A_{ZVS}) is 10% lower than expected. This is partly because the prototype build-up were 2.1mm high, which is 0.1mm higher than expected, making the primary layers 5% higher and this results in a 5% decrease in gain. Furthermore there is some inactive piezoelectric material in the primary section, due to the termination of the primary electrodes on the side of the PT, as shown in Figure 6. For simplicity the termination is not included in the FEM simulation, which accounts for some of the remaining 5 % deviation. Hence there is a very good correlation between the FEM model and the prototype concerning the gain. Comparing the gain of Equation (4) with the calculated from the lumped parameters (Table 4), it can be seen that there is a very good correlation between a fully stressed PT and the small signal impedance measurement.
The correlation between the soft switching factors (V'_P) is also very good.
Looking at the capacitances C_{d1}, C_{d2} and the efficiency, the correlation is not that good. This is expected to be because of a bad correlation between the NCE46 material parameters in the FEM model and what they are in real life, as well as an incomplete loss model in the FEM simulation. Nevertheless the FEM simulation makes it possible to design soft switching optimised PT's for inductor-less operation, having a desired soft switching factor, a desired gain, as well as the possibility to compare the performance between different designs. For this specific case there is not a well defined resistive load and the load matching inaccuracy is therefore not a problem.

5 Conclusion

In this paper a new interleaved multi layer Rosen-type piezoelectric transformer (PT), optimised for soft switching, inductor-less operation and high output voltage has been developed. The development has been performed through iterative finite element method simulations, which has proven its capabilities as a good design tool for PT development. The measurements of the prototype PT showed a good correlation between the design and the prototype. The prototype PT has demonstrated to have a sufficiently high soft switching factor of 1.43 to operate in an inductor-less topology, as well as having a high gain of 68, enabling the generation of high output voltages.

Acknowledgements

Finally we would like to thanks Noliac A/S for the production of prototype PT's, as well as general PT design support. We would also like to thanks Danfoss PolyPower A/S for supplying the application and EAP actuators.

References

[1] T. Andersen, M. S. Rødgaard, O. C. Thomsen, M. A. E. Andersen, "Low voltage driven dielectric electro active polymer actuator with integrated piezoelectric transformer based driver", *SPIE Electroactive Polymer Actuators and Devices (EAPAD)*, Volume 7976, pp. 79762N, (2011)

[2] J. M. Alonso, C. Ordiz, M. A. D. Costa, J. Ribas, J. Cardesín, " High-Voltage Power Supply for Ozone Generation Based on Piezoelectric Transformer", *IEEE TRANSACTIONS ON INDUSTRY APPLICATIONS*, VOL. 45 NO. 4, 1513-1523 (2009)

[3] C. Bai, S. Li, Shen Q., D. Cui, "A Converter of High Voltage Capacitor Charging Power Supply Using Piezoelectric Transformer", *APPEEC*, 2009

[4] E. M. Baker,"Design of Radial Mode Piezoelectric Transformers for Lamp Ballast Applications", *PhD thesis*, Blacksburg Virginia (2002)

[5] M. Y. Benslimane, HE. Kiil, M. J. Tryson, "Dielectric electro-active polymer push actuators: performance and challenges", *Society of Chemical Industry, Wiley Interscience*, 415-421 (2010)

[6] W. R. Erikson, D. Maksimović, [Fundamentals of Power Electronics], Springer Science+Business Media inc., (2001)

[7] E. L. Horsley, N. Nguyen-Quang, M.P. Foster, D. A. Stone, "Achieving ZVS in inductor-less half-bridge piezoelectric transformer based resonant converters", *PEDS*, 2009, 446-451

[8] E. L. Horsley, M. P. Foster, D. A. Stone, "State-of-the-art Piezoelectric Transformer Technology", *European Conference on Power Electronics and Applications*, 1-10 (2007)

[9] C. Y. Lin, "Design and analysis of piezoelectric transformer converters," *PhD dissertation*, Blacksburg Virginia, (1997)

[10] F. L. CY. Lin, "Design of a piezoelectric transformer converter and its matching networks*", Power Electronics Specialists Conference*, PESC' 94 Record, (1994)

[11] R. L. Lin, "Piezoelectric Transformer Characterization and Application of Electronic Ballast", *PhD dissertation*, Blacksburg Virginia (2001)

[12] W. P. Mason, "Electromechanical Transducers and Wave Filters", D. Van Nostrand Co, (1942)

[13] K. S. Meyer, M. A. E. Andersen," Parameterized Analysis of Zero Voltage Switching in Resonant Converters for Optimal Electrode Layout of

Piezoelectric Transformers*", PESC IEEE*, 978-1-4244-1668-4, 2543-2548 (2008)
[14] J. C. J. Navas, T. Bove, K. Breboel, "Miniaturised battery charger using piezoelectric transformers", *Applied Power Electronics Conference and Exposition*, APEC 2001 Sixteenth Annual IEEE, vol.1, 492–496 (2001)
[15] Noliac A/S Piezoelectric ceramics datasheet, http://www.noliac.com/Files/Billeder/02%20Standard/Ceramics/Noliac_CEramics_NCE_datasheet.pdf
[16] C. A. Rosen, "Ceramic transformers and filters", *Proc. Electron. Comp. Symp.* 205-211, (1957).
[17] M. Tryson, HE. Kiil, M. Benslimane, "Powerful tubular core free dielectric electro activate polymer (DEAP) 'PUSH' actuator", *SPIE*, Vol. 7287, (2009)
[18] CHU Xiang-cheng, WU Jun-fei, XU Zhi-han, LI Long-tu, "EXPERIMENT RESEARCH ON MULTILAYER PIEZOELECTRIC TRANSFORMER", *IEEE* 978-1-4244-2891-5, 524-527 (2008)

D.3 Empiric analysis of zero voltage switching in piezoelectric transformer based resonant converters

Conference paper

PEMD 2012 - Power Electronics, Machines and Drives Conference
27 - 29 March 2012
University of Bristol, United Kingdom
http://conferences.theiet.org/pemd/

EMPIRIC ANALYSIS OF ZERO VOLTAGE SWITCHING IN PIEZOELECTRIC TRANSFORMER BASED RESONANT CONVERTERS

M. S. Rødgaard *, T. Andersen*, M. A. E. Andersen*

**Technical University of Denmark, DTU Elektro, Ørsteds Plads, building 349, DK-2800 Kgs. Lyngby, Denmark,*
msr@elektro.dtu.dk

Keywords: Piezoelectric Transformer, inductor-less, converter, soft switching, ZVS factor

Abstract

Research and development within piezoelectric transformer (PT) based converters are rapidly increasing, as the technology is maturing and starts to prove its capabilities. High power density and high efficiencies are reported and recently several inductor-less converters have emerged [1][2][7][10][13], which demonstrates soft switching capabilities. The elimination of a bulky inductor, reduces size and price of the converter, but demands a soft switching optimised PT. Several attempts of expressing the soft switching capability have been made [5][12], with some shortcomings. The goal of this paper is to derive a simple expression of the maximal obtainable soft switching capability (ZVS factor), for a specific PT design, assuming a matched load. The expression has been derived through series of parametric sweep simulations of the inductor-less half-bridge topology, which revealed that a linearization of the maximal soft switching capability can be performed, in the area of interest. This expression is intended to form a basic tool for development of soft switching optimised PT's, which enables the utilisation of inductor-less topologies.

1 Introduction

Piezoelectric transformer (PT) based converters have been around for some time now, but within resent years PT based converters have emerged, that exploit an inductor-less topology [1][2][7][10][13]. The elimination of the bulky inductor reduces size and price of the converter. But the parasitic input capacitance of the PT usually prevents the utilisation of an inductor-less power stage and an external series inductance is typically inserted in order to achieve soft switching capabilities. In a simple half-bridge power stage the input capacitance can lead to hard switching losses in the same range as the output power, resulting in a very poor efficiency. This calls for other means in order to avoid large hard switching losses, obtain soft switching capabilities and efficient operation. This can be achieved by utilising an advantageous PT structure and optimised design. But in order to evaluate the properties of the PT, a better understanding of the PT and what factors influences the soft switching capability is required. Several attempts of deriving a mathematical expression of the soft switching capability, directly from the lumped parameter model Figure 1 [11], have been made [3][5][10][12]. Great progress has been achieved, but they still have some shortcomings.

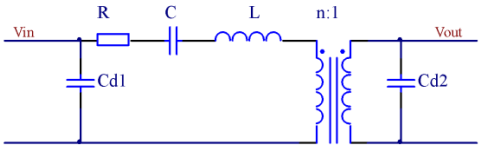

Figure 1: Lumped parameter model, which describes the behaviour of the PT in a narrow band around the operating resonance mode.

The approach in [5] has been to derive the full mathematical problem of the lumped parameter model, with respect to the input voltage, which should reach at least the half-bridge rail voltages, in order to soft switch. The result is a very precise expression of the soft switching capability. Its advantages are that it takes all the lumped parameters and the load resistance in to account, meaning that the soft switching capability can be calculated for any given PT and load, as well as the result is very accurate. The drawback of taking all the parameters and the load resistance in to account are a very complex expressing, making it quit computational heavy, as well as the expression still is a function of dead time and frequency. Furthermore there are no transparent relation between the parameters and the soft switching capability.
The approach in [12] has been to derive the expression in the frequency domain, as the lumped parameter model is of frequency domain nature. The derivation assuming matched load and has been accomplished by making a couple of assumptions. Equation 1 expresses the derived ZVS (zero voltage switching) factor, which is the maximal obtainable soft switching capability.

$$V_P' = \frac{1}{n^2}\frac{C_{d2}}{C_{d1}}\frac{32\sqrt{6}}{9\pi^2}\eta \qquad (1)$$

It has the advantages of being very short and handy, as well as being transparent, providing a very good relation between the parameters and the ZVS factor. And as it can be seen, it is only a few parameter of the model that affects the ZVS factor.

The drawback is that it is too optimistic. Through employment of the expression, within PT development and experimental work, it is found that a ZVS factor of at least 1.4 is needed in order to achieve soft switching.
The approach of this paper has been to perform a series of parametric sweep simulations of the lumped parameter model, searching for linearization opportunities in respect to the soft switching capability. The ZVS factor Equation (1) has been the starting point for the simulations and search, as it has demonstrated to relate to the soft switching capability, although it is optimistic. And as this paper will demonstrate, linearization opportunities were found in the area of interest. As a result a simple expression of the ZVS factor is derived, which demonstrates good accuracy and is only a function of the input and output capacitor ratio and the efficiency, just as Equation (1).

1.1 Piezoelectric transformer

PT's are based on piezoelectric materials, which usually is a ceramic material. This material has an electromechanical coupling and through this coupling a charge displacement is generated, that is proportional to the deformation of the material. A PT is basically two piezoelectric elements joined together to form a transformer. The primary side element is then exited by an electrical AC voltage, which induces a deformation of the two joined elements. This deformation generates an output voltage on the secondary side element and through a proper design of the PT, a desired voltage conversion can be achieved from the primary to the secondary side.
The PT is operated in one of its resonance modes, in order to convert energy at a high efficiency [6][8][9][10]. The PT resonates each time it is possible to generate a standing wave in the element, but the design is usually optimised for one specific resonance mode, in order to achieve the highest efficiency [8][10].
The PT resembles a distributed network, but for simplicity and mathematical representation, only the resonance mode of interest is modelled [8][9][10]. The lumped parameter model is one of the most frequently used PT models and was derived by Mason in 1942 [11]. The model is illustrated in Figure 1 and is basically a LCC resonance tank, as well as the behaviour of a PT based converter is quite similar to a traditional resonance converter [4].

2 Inductor-less half-bridge

Figure 2 illustrates the inductor-less half-bridge topology, where the absence of a series inductance and the parasitic input capacitor C_{d1}, calls for a soft switching optimised PT. The topology is quite simple, making it easy to understand the subject of soft switching. But the soft switching requirements of the PT for a bit more advance topologies, like the full-bridge, are the same. However for the more advanced topologies, like the PFC charge pump topologies [7], the requirements to the soft switching capability of the PT are higher, as the apparent parasitic input capacitance is increased.

The PT is loaded with a matched load as this maximises the power transfer of the resonance network, as well as this is the worst case condition for the soft switching capability [12].

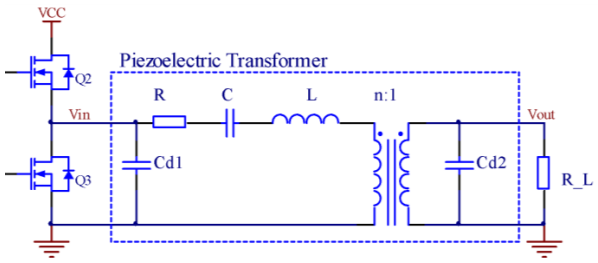

Figure 2: Schematical diagram of the inductor-less half-bridge topology and the PT equivalent lumped parameter model.

The target of soft switching is to achieve ZVS of the switches in the half-bridge. This can be achieved by operating the PT slightly above its resonance frequency, where the series resonance network becomes inductive and contains enough resonating energy to charge and discharge C_{d1}. And as it will be shown in the following section, there is an optimum where the resonance networks inductivity and energy is maximised, to make the largest energy transfer to C_{d1}. Furthermore there should be a certain dead time in between the two switches, in order to let the charge and discharge occur.

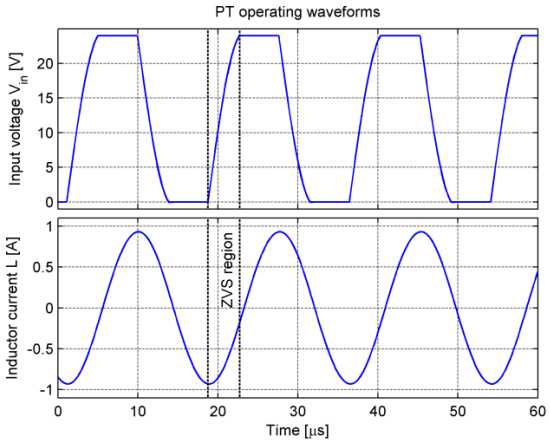

Figure 3: Input voltage and resonance current waveforms of the inductor-less half-bridge topology. From the input voltage it can clearly be seen that the half-bridge is operating under ZVS.

Figure 3 illustrates the operation of the inductor-less half-bride and as it can be seen the resonance current possesses sufficient phase shift and magnitude, to achieve ZVS. There is also sufficient dead time (ZVS region) in between the switches and it can clearly be seen that C_{d1} is charged and discharged, obtaining ZVS.

3 Soft switching factor

In the following section an expression of the maximal obtainable soft switching capability, also referred to as the soft switching factor or ZVS factor, is derived. The derivation is based on a series of parametric sweep time domain PSpice simulations of the inductor-less half-bridge, where the figures of Table 1 are the used lumped parameters. The figures origins from the interleaved multi layer Rosen-type PT design presented in [14], but as the lumped parameter mode is independent of PT design, the results should be general. The simulations have been preformed with at least 100 cycles before any measurements were made, in order to insure steady-state operation. Furthermore the simulated circuit utilises idealised switches and body diodes.

R	C	L	C_{d1}	C_{d2}	1/n
98mΩ	11.7nF	733µH	112nF	14.6pF	112

Table 1: FEM simulated PT equivalent lumped parameters obtained through impedance measurements.

From Equation (1) the ZVS factor of [12] can be calculated, as well as the match load and efficiency [12][14], as well as the resonance frequency. And as it can be seen from Table 2, the design possesses a ZVS factor which is sufficient to achieve soft switching.

$V'_{P\text{-}Old}$	R_{match}	η	f_R
1.43	198kΩ	0.987	55.2kHz

Table 2: FEM simulated PT equivalent lumped parameter model performance properties.

Equation (1) revealed that the soft switching capability is strongly dependent of the input and output capacitance. Figure 4 illustrates a frequency swept series of simulations, with the parameter of the input capacitance C_{d1} being swept as well.

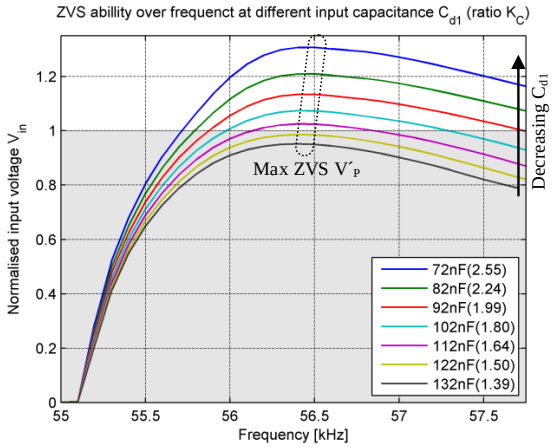

Figure 4: Simulated PT soft switching capability over frequency, with different input capacities Cd1 (capacitor ratio K_C).

As it can be seen the soft switching capability is strongly dependent of the input capacitance C_{d1} and the frequency. As for the shape of the curves there are a very good correlation to what were discovered in [5][12]. From the curves the maximal obtainable soft switching capability can be extracted, which is the parameter of interest. This ZVS factor can then be plotted in relation to the input capacitance C_{d1} or more interesting, in relations to the input and output capacitor ratio K_C Equation (2), which is illustrated in Figure 5.

$$K_C = \frac{1}{n^2}\frac{C_{d2}}{C_{d1}} \qquad (2)$$

The ZVS factors extracted from Figure 4 resemble the second topmost line in Figure 5. Moreover the series resistance R has been swept, creating several curves relating the ZVS factor to the PT efficiency.

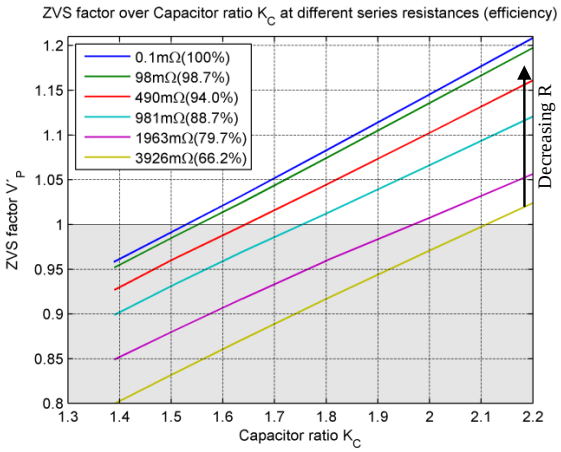

Figure 5: Simulated PT maximal soft switching capability (ZVS factor) in relation to the capacitor ratio K_C, at different efficiencies.

As Figure 5 reveals, there is a fine linear relation between the capacitor ratio K_C and the ZVS factor. By making a linear regression of the topmost line (η ≈ 100%), the most simplified expression of the ZVS factor is found Equation (3).

$$V'_{P\_100\%} = \left(0.304\frac{1}{n^2}\frac{C_{d2}}{C_{d1}} + 0.538\right) \qquad (3)$$

This expression is as simple as it gets, it is very handy and holds for high efficient PT's, which in the end is the ultimate goal of PT development.
But when working with less efficient PT's (< 97%), the efficiency should be taken in to account as well, in order to get a reliable result. Taking a look at Figure 5 it can be seen that the curves, which are lines of different efficiency, are nearly parallel. By taking a closer look at the curves it is found that they intersect the x-axis in roughly the same point, which indicates that the ZVS factor Equation (3) can be adjusted with an efficiency dependent factor.

Figure 6 illustrates how the ZVS factor is dependent on the efficiency at different capacitor ratios K_C and here as well the figure reveals a clear dependency of the efficiency. Although the dependency is not perfectly linear and differentiates a bit over the capacitor ratio K_C, a linear regression is made.

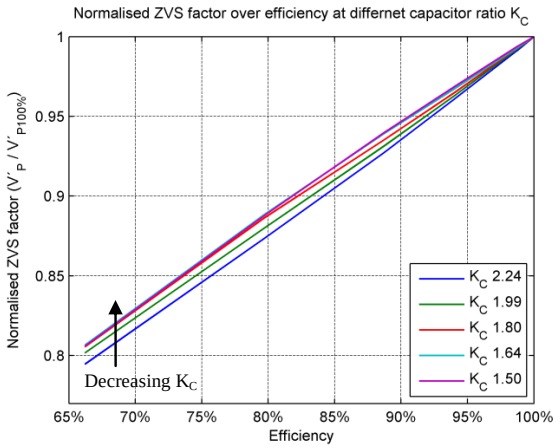

Figure 6: Simulated PT normalised maximal soft switching capability in relation to the efficiency.

The result is the correction factor Equation (4), which joined together with Equation (3) forms the final ZVS factor Equation (5).

$$K_\eta = (0.585\eta + 0.414) \qquad (4)$$

$$V_P' = \left(0.304\frac{1}{n^2}\frac{C_{d2}}{C_{d1}} + 0.538\right)(0.585\eta + 0.414) \qquad (5)$$

The expression is verified through comparison with the already simulated data of Figure 5 and as can be seen in Table 3 there are a very good correlation.

4 Experimental results

In order to fully validate the developed ZVS factor, the ZVS factor of a prototype PT has been measured.
The prototype PT is of the same design as the one simulated [14], with the exception of a bit different polarisation, which divides the turn's ratio (n) by two. Its properties are listed in Table 4 and Table 5, and as it can be seen it possesses a quit high ZVS factor.

η = 100%			**η = 94%**			**η = 80%**		
Sim	V'_P	**Δ**	Sim	V'_P	**Δ**	Sim	V'_P	**Δ**
0,96	0,96	**0,1%**	0,93	0,93	**-0,1%**	0,85	0,85	**-0,5%**
0,99	0,99	**0,2%**	0,96	0,96	**-0,2%**	0,88	0,88	**-0,6%**
1,03	1,03	**0,2%**	1,00	1,00	**0,0%**	0,92	0,91	**-0,6%**
1,08	1,08	**0,1%**	1,04	1,05	**0,1%**	0,96	0,95	**-0,5%**
1,14	1,14	**0,0%**	1,10	1,10	**0,2%**	1,01	1,01	**0,1%**
1,22	1,22	**-0,3%**	1,17	1,17	**0,1%**	1,07	1,07	**0,6%**

Table 3: Comparison between some of the simulated and calculated ZVS factors.

R	C	L	C_{d1}	C_{d2}	1/n
361mΩ	8.33nF	1052µH	129nF	93.2pF	55

Table 4: Prototype PT equivalent lumped parameters obtained through impedance measurements. The measurements have been performed with the PT mounted in the test circuit, including the additional parasitic.

$V'_{P\text{-}Old}$	V'_P	R_{match}	η	f_R
1.67	1.15	33.7kΩ	0.936	54.2kHz

Table 5: Prototype PT equivalent lumped parameter model performance properties.

By employing the inductor-less half-bridge, it is not directly possible to measure ZVS factors above 1, because of the clamping body diodes in the MOSFET's. Only ZVS factor below 1 is measurable, as the measurement shown in Figure 8.

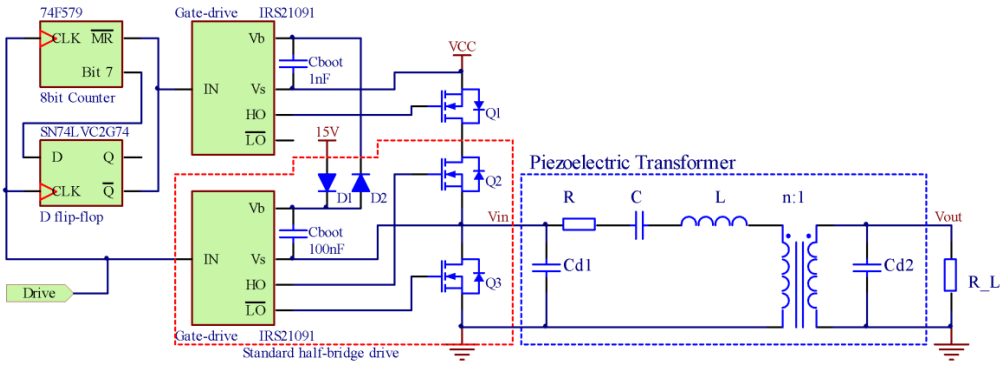

Figure 7: Schematical diagram of the inductor-less half-bridge, half-bridge driving circuit and the implemtatin of the soft switching capabability measurement circuit.

A diode could be placed in series with the top MOSFET and the input voltage (V_{in}) is thereby allowed to rise above supply voltage. This will enable a ZVS factor measurement, but it will also change the shape of the input voltage somewhat, changing the operation point. However by utilising a MOSFET instead of a diode, as in Figure 7 Q1, the input voltage is only allowed to rise above supply voltage once in a while. This is implemented as shown in Figure 7, with an N-channel MOSFET, a D flip-flop and a 8bit counter. The idea is to turn on Q1 and as Q2 and Q3 operates normally as a half-bridge, the counter counts the driving signal cycles. And when the counter reaches 256 cycles, the D flip-flop turns off Q1 for one cycle and resets the counter. In this manner the input voltage (V_{in}) is "released" and a ZVS factor higher than 1 can be measured, just as shown in Figure 9.

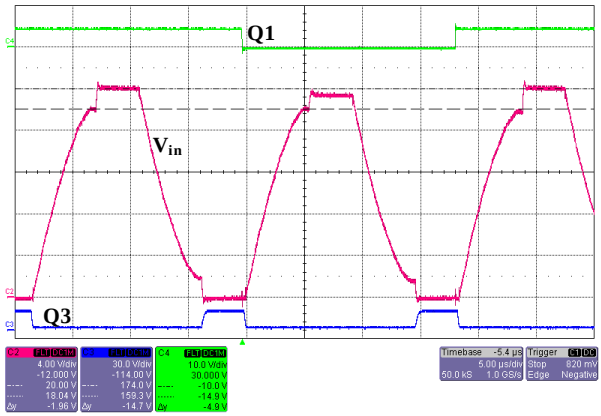

Figure 8: ZVS factor measurement of the prototype PT, with at capacitor ratio K_C of 1.38 (C_{d1} = 189nF). C3 and C4 shows gate signals, and C2 is the input voltage [4V/div].

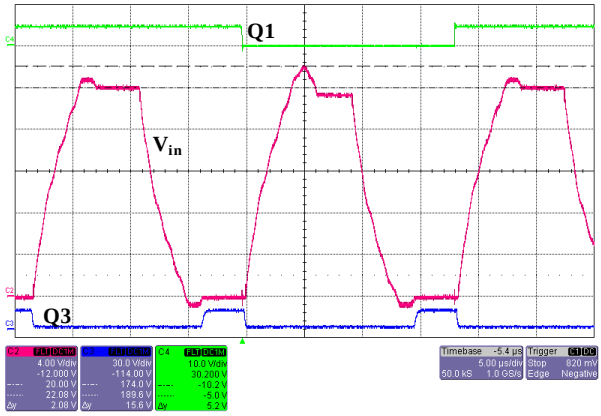

Figure 9: ZVS factor measurement of the prototype PT, with at capacitor ratio K_C of 2.16 (C_{d1} = 129nF). C3 and C4 shows gate signals, and C2 is the input voltage [4V/div].

Two sets of ZVS factor measurements have been collected through the experimental work. The approach in the experimental work has been to make a stepwise increment of the input capacitor C_{d1} and measure the drop in ZVS factor, just as the parametric sweep performed in the simulations. The tests have been performed with two different half-bridge supply voltages, 10V and 20V, as the increase in voltage should reflect a decrees in efficiency. This is due to the nonlinear nature of the piezoelectric loss.
Figure 10 illustrates the test results and it can be observed that the measurements are not as linear as anticipated, but the test setup also involved a certain measurement inaccuracy. But just as expected the ZVS factor drops when employing a higher half-bridge supply voltage.

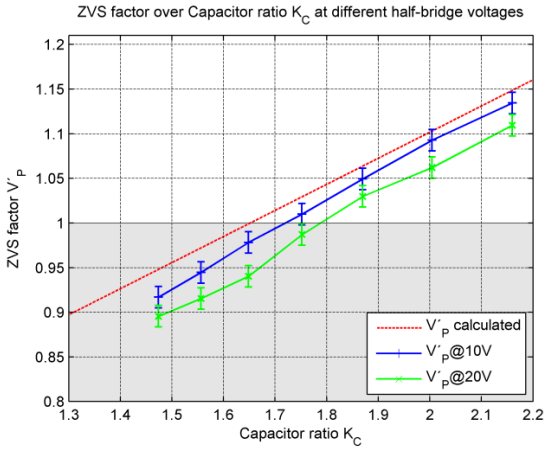

Figure 10: ZVS factor measurement of prototype PT in relation to the capacitor ratio K_C, compared with the ZVS factor equation.

5 Discussion

Comparing the predictions of the developed ZVS factor Equation (5) with the results extracted from the simulations, there is a very good correlation as illustrated in Table 3, where an accuracy below 1% is demonstrated. As for the results obtained through the experimental work Figure 10, it reveals that the ZVS factor is a bit more optimistic than the results. This is mainly due to the fact that the PT efficiency drops when the half-bridge voltage is increased. And as the lumped parameters of Table 4 are extracted from small-signal impedance measurements, the efficiency is also a measure of efficiency at small signals. The ZVS factor predictions of Figure 10 are based on this efficiency, so it is obvious that it will be a bit optimistic. Basically the efficiency used for the prediction should be modified as the working point changes to 10V and 20V. This is quite difficult though, because of the lack of a good and reliable efficiency measurement method. This is due to the high frequency AC load and standard power analysers are typically optimised for DC or low frequency 50/60Hz AC mains. Taking a closer look at Figure 10 it can be seen that the results are not as linear as expected, nor parallel to the predicted ZVS factor. However just looking at the result with a ZVS factor above 1, they are quite linear and parallel to the predicted ZVS factor. Some of the deviation could defiantly be due to measurement inaccuracy, as the measurements are extracted by hand, from oscilloscope plots as Figure 8 and Figure 9. Nonetheless the deviations could

also origin from elements in the circuit, which is not include in the idealised simulation, such as the highly nonlinearities of semiconductor parasitic capacitances. Although not taking the efficiency drop in to account, the developed ZVS factor manages to do a prediction within 3% of the 10V test results and within 6% of the 20V test results. As a final note it can be noted that a capacitor ration K_C of at least 1.55 is needed in order to achieve soft switching capability and a ZVS factor above 1.

6 Conclusion

Through a series of parametric sweep PSpice simulations an expression describing the maximal obtainable soft switching capability has been derived, also known as the ZVS factor. The expression is very simple and transparent, clearly stating the strong dependency of the input and output capacitor ratio, as well as the dependency of the efficiency. As a result the soft switching capability of a specific PT design can be evaluated easily and directly from the lumped parameter model. The ZVS factor forms a basic soft switching capability measuring tool, to assist through the development of ZVS optimised PT's. The developed ZVS factor has been evaluated up against the simulations as well as against a developed prototype DC/AC inductor-less half-bridge converter. It demonstrated below 1% accuracy compared to the simulations, validating its functionality. And a 3-6% accuracy compared to the prototype, bearing in mind that a too optimistic efficiency for calculating the ZVS factor were used.

Acknowledgements

Finally we would like to thanks Noliac A/S for supplying prototype PT's, as well as general PT design support.

References

[1] J. M. Alonso, C. Ordiz, M. A. D. Costa, J. Ribas, J. Cardesín, " High-Voltage Power Supply for Ozone Generation Based on Piezoelectric Transformer", *IEEE TRANSACTIONS ON INDUSTRY APPLICATIONS*, VOL. 45 NO. 4, 1513-1523 (2009)

[2] E. M. Baker,"Design of Radial Mode Piezoelectric Transformers for Lamp Ballast Applications", *PhD thesis*, Blacksburg Virginia (2002)

[3] S. Bronstein, S. Ben-Yaakov, "Design considerations for achieving zvs in a half bridge inverter that drives a piezoelectric transformer with no series inductor", *Power Electronics Specialists Conference, PESC 02*, vol. 2, pp. 585-590 (2002)

[4] W. R. Erikson, D. Maksimović, [Fundamentals of Power Electronics], Springer Science+Business Media inc., (2001)

[5] E. L. Horsley, N. Nguyen-Quang, M.P. Foster, D. A. Stone, "Achieving ZVS in inductor-less half-bridge piezoelectric transformer based resonant converters", *PEDS*, 2009, 446-451

[6] E. L. Horsley, M. P. Foster, D. A. Stone, "State-of-the-art Piezoelectric Transformer Technology", *European Conference on Power Electronics and Applications*, 1-10 (2007)

[7] W. Huang, D. Chen, E. M. Baker, J. Zhou, H-I. Hsieh, F. C. Lee, "Design of a Power Piezoelectric Transformer for a PFC Electronic Ballast", *IEEE TRANSACTIONS ON INDUSTRIAL ELECTRONICS*, VOL. 54, NO. 6 (2007)

[8] C. Y. Lin, "Design and analysis of piezoelectric transformer converters," *PhD dissertation*, Blacksburg Virginia, (1997)

[9] F. L. CY. Lin, "Design of a piezoelectric transformer converter and its matching networks*", Power Electronics Specialists Conference*, PESC' 94 Record, (1994)

[10] R. L. Lin, "Piezoelectric Transformer Characterization and Application of Electronic Ballast", *PhD dissertation*, Blacksburg Virginia (2001)

[11] W. P. Mason, "Electromechanical Transducers and Wave Filters", D. Van Nostrand Co, (1942)

[12] K. S. Meyer, M. A. E. Andersen," Parameterized Analysis of Zero Voltage Switching in Resonant Converters for Optimal Electrode Layout of Piezoelectric Transformers*", PESC IEEE,* 978-1-4244-1668-4, 2543-2548 (2008)

[13] R. L. Lin, F. C. Lee, E. M. Baker, D. Y. Chen, "Inductor-less piezoelectric transformer electronic ballast for linear fluorescent lamp", *Applied Power Electronics Conference and Exposition*, vol.2, 664-669 (2001)

[14] M. S. Rødgaard, T. Andersen, K. S. Meyer, M. A. E. Andersen, "DESIGN OF INTERLEAVED MULTILAYER ROSEN TYPE PIEZOELECTRIC TRANSFORMER FOR HIGH VOLTAGE DC/DC APPLICATIONS", *Power Electronics, Machines and Drives Conference*, (2012)

D.4 Active Match Load Circuit Intended for Testing Piezoelectric Transformers

Conference paper

PEMD 2012 - Power Electronics, Machines and Drives Conference
27 - 29 March 2012
University of Bristol, United Kingdom
http://conferences.theiet.org/pemd/

Active Match Load Circuit Intended for Testing Piezoelectric Transformers

T. Andersen*, M. S. Rødgaard**, M. A. E. Andersen †

Technical University of Denmark, DTU Elektro, Ørsteds Plads, building 349, DK-2800 Kgs. Lyngby, Denmark

* ta@elektro.dtu.dk, ** msr@elektro.dtu.dk, † ma@elektro.dtu.dk

Keywords: Piezoelectric transformer, Match load.

Abstract

An adjustable high voltage active load circuit for voltage amplitudes above 100 volts, especially intended for resistive matching the output impedance of a piezoelectric transformer (PT) is proposed in this paper. PTs have been around for over 50 years, were C. A. Rosen is common known for his famous Rosen type design back in the 1950s [1]. After the discovered of new piezoelectric materials and new PT designs have been invented, the PT based power converters are in the area where they can outperform tradition electromagnetic based converters in certain applications [2]. The performance of PTs can be measured and compared on its zero voltage switching (ZVS) factor [3-5], power density, and efficiency. Common for these three parameters are that they need to be measured with a match load connected at the output of the PT.

1 Introduction

A PT is a highly resonant electromechanical component where energy is transferred by acoustical waves. In order to transfer energy through the PT it is operated close to one of its resonant frequencies. For each resonance frequency there is a corresponding acoustical standing wave in the PT. The resonance frequencies are determined by the material, geometrical shape, temperature and its load conditions. Due to the relatively high quality factor of a PT (Q > 1000) the electrical behaviour around one of its resonance frequency can be described by the Mason model [6].

From the Mason equivalent model, figure 1, the efficiency of the transformer can be calculated for a given load [3, 7]. For a resistive load, the maximum efficiency is obtained if the load satisfied the match load condition as equation (1) and is

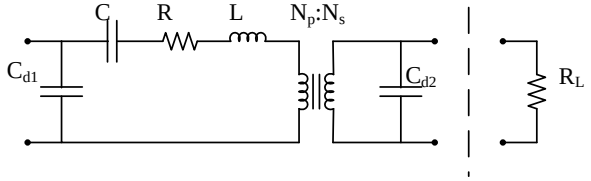

Figure 1: Mason model of a piezoelectric transformer valid only around the resonance frequency.

dependent on the operating frequency and the output capacitance C_{d2} [7].

$$R_{L,match} = \frac{1}{2\pi f \cdot C_{d2}} \approx \frac{1}{2\pi f_r \cdot C_{d2}} \qquad (1)$$

It can also be shown that the ZVS factor, the PTs ability to soft switch, has a global minimum at match load [3]. If the PT is capable of soft switching at mach load, it can soft switch for any resistive load. Measuring the power density of PTs is done where the efficiency is highest. Therefore a match load is connected at the output to obtain maximum efficiency.

Prior art within resistive match loading, has been to solder off-the-shelf ¼ watt leaded resistors together in a manner to obtain the correct resistive value as well as handle the power dissipation (< 20 watt) and voltage stress (< 1.2kV). Potentiometers that can handle the power and the voltages suffers from high parasitic inductions and can therefore not be used. Figure 2 show a typical example of a match load construction. A standard ¼ watt resistor has a voltage rating of 250V. It is a time consuming process of solder a match load, especially for high voltage and high power.

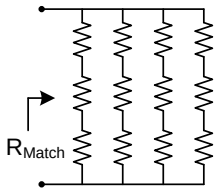

Figure 2: 4 by 3 matrixes of leaded ¼ watt resistors.

Each PT design usually requires a new match load design. It is also time consuming to adapt one match load matrix to another value.

2 Active match load

There is a need for an adjustable resistive load with low parasitic capacitance and parasitic inductance. The proposal in this paper is to control a MOSFET in its linear region to act as a resistor. In figure 3 the principle is illustrated. By measuring the voltage across the MOSFET as a reference signal and subtracting the current through the MOSFET an error signal is generated.

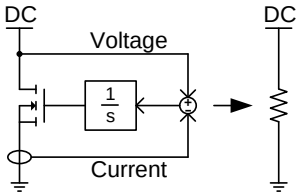

Figure 3: Simulated resistor by a MOSFET with feedback. Only valid for positive voltages.

The error signal is then integrating and the result is a current proportional with the voltage; a resistor. The principle in figure 3 only works for positive voltages. At negative voltages the body diode of the MOSFET becomes forward biased and the voltage across the MOSFET is clamped to the forward voltage drop of the body diode. At negative voltages the circuit acts as a diode and not as a resistor.

For the circuit to act as a resistor for both positive and negative voltages a full wave bridge rectifier is used. The voltage drop of the rectifier contributes to a non-resistor characteristic, especially at voltages comparable with the voltage drop of the rectifier. As the circuit is indented for sinus waveforms at amplitudes above 100 volts, it is of less concern. The output of the rectifier is a positive voltage with twice the frequency of the input. The principle circuit from figure 3 combined with a full wave bridge rectifier is illustrated in figure 4.

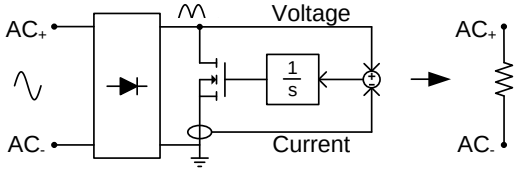

Figure 4: Simulated resistor for positive and negative voltages.

2.1 Voltage measurement

The voltage feedback signal is used as a reference signal for the current feedback. Ideally the voltage should be measured at the input terminals to the rectifier to avoid the voltage drop from the rectifier. Measuring the voltage on the input at the rectifier, require high common mode rejection to operate successfully, which complicates the voltage measuring circuit. As the circuit is indented for voltage amplitudes above 100 volts the induced error by measuring the voltage after the rectifier is of little concern. However sacrificing the precision of the measurement by measure the voltage after the rectifier greatly reduces the complexity of the circuit. A resistive voltage divider can then be used. Changing the ratio of the divider is an easy way of adjusting the value of the active load. A potentiometer is used for the adjusting.

2.2 Current measurement

The current can be measured in different ways. One method is to the sense the voltage across a resistor placed in series with the source pin of the MOSFET, see figure 5.

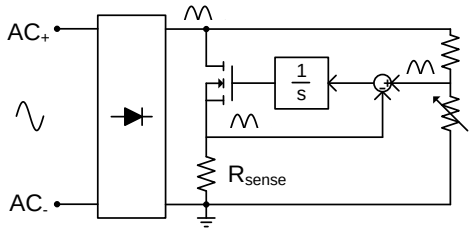

Figure 5: Simulated resistor using a sense-resistor (R_{sense}) in the MOSFETs source path to obtain the current feedback signal.

The benefit of a sense-resistor (R_{sense}) in the source path of the MOSFET is clear from a measuring point of view. It is a low impedance and low voltage measurement directly related to ground potential of the circuit. However from a control point of view the resistor is not only measuring the current running into drain of the MOSFET but also the current running through the parasitic gate-source capacitance. In application where a high ohmic load is preferred in combination with high frequency, the drain current becomes comparable with the current running through the gate-source capacitance. The sense resistor sums both currents and feed them back, resulting in an error estimation of the real current (drain current). To compensate for the contribution from the gate-source current an independent measurement of the gate-source current is needed and will complicated the overall current measurement circuit.

Another approach to measure the current is to use a current sense transformer (CST). With a CST the current in the drain path of the MOSFET can be measured even at high voltages. Measuring of the current at the input to the bridge rectifier can be done event at the high common mode voltages due to the low capacitive coupling between primary and secondary of a CST. Placing the CST at the input to the bridge rectifier ensures that non-linearity from the rectifier is measured. A block diagram is shown in figure 6. Measuring the current at the input has the drawback of complicating the measurement circuit compared to a drain current measurement. The input current is sinusoidal and therefore the output of the CST is also sinusoidal and cannot be used directly as a feedback signal before it has been rectified. A full wave bridge rectifier consisting of diodes cannot be used here, as the output voltages from the CST is lower or in best case comparable with the forward voltage drop of the rectifier itself. Instead an active rectification (ABS) circuit is used to rectifier the sinusoidal signal from the CST. Thereby the signal is rectified without any voltage drop.

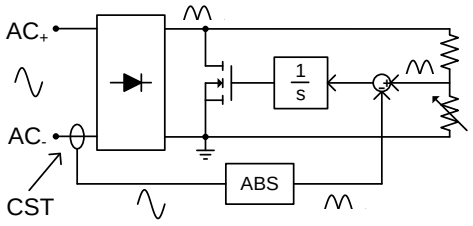

Figure 6: Simulated resistor using a current sense transformer (CST) together with an active rectifier (ABS).

3 Results

In this section the results from simulations as well as measurements will be conducted. Simulations are made in PSpice. Measurements are performed with a Rohde & Schwarz 2GHz RTO oscilloscope. A prototype is developed as illustrated in figure 7. Control together with ABS circuit is placed on the back of the PCB. Size of the PCB: 70mm x 40mm.

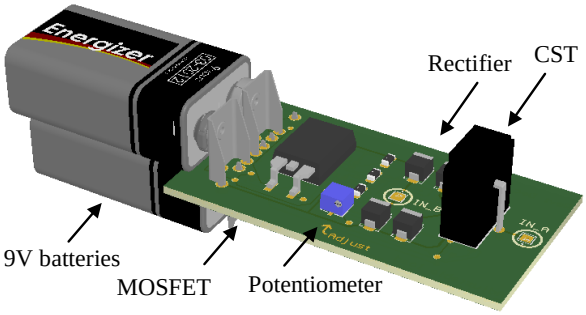

Figure 7: 3D model of the active load circuit. Control circuit is placed on the back of the PCB.

3.1 Measurement setup

For comparing the simulation and the measurement the setup illustrated in figure 8 is used. A tone-generator connected to an amplifier delivers a signal with maximum amplitude of 200 volt at a frequency of 50 kHz. The active load circuit is connected through a 100 ohms resistor. The resistor is used to measure the current through the active load. In this way a voltage across the sense resistor of 100 mV equals 1.0 mA. The rectifier diodes are rated to 50 mA, at that current the voltage across the sense resistor reached 5 volt.

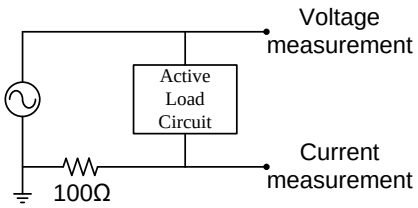

Figure 8: Setup used for measuring input voltage [1V/V] and input current [0.01A/V]

3.2 Simulations

The active load circuit has been simulated in PSpice. The result of the simulation is shown at figure 9. The sinus wave (blue) is the voltage across the active load and is perfectly sinusoidal with an amplitude of 200 volts as expected. The square-like graph (red) is a plot of the current.

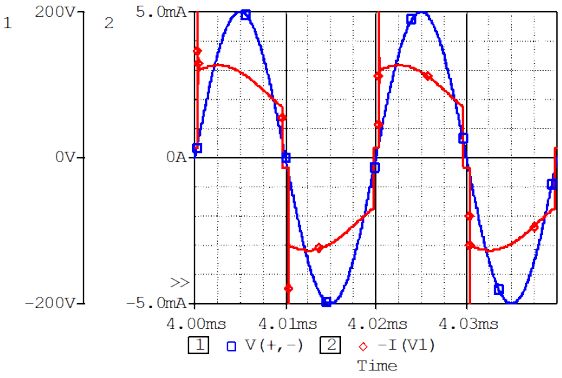

Figure 9: PSpice simulation of input voltage (blue) and input current (red) an active load. Input: ±200V@50kHz

3.3 Measurements

Measurements on the active load circuit are performed accordant to the measurement setup in figure 8. The result is shown in figure 10 as a plot from the oscilloscope (note: colours are changed and enhanced for better visibility). The blue graph is the input voltage across the active load with an amplitude close to 200 volts and a frequency of 50 kHz. The red graph is the voltage measured across a 100 ohms resistor and equivalent to the input current.

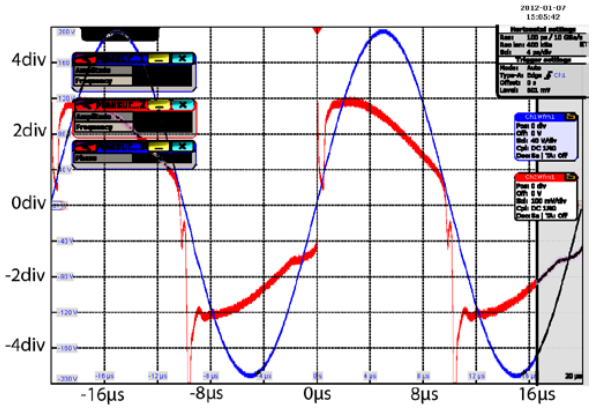

Figure 10: Oscilloscope plot (colours are changed) measurement on the prototype. Input voltage: 40V/div (blue). Input current: 1mA/div (red)

3.4 Discussion

The correlation between simulation and measurement is good. The current is in phase with the voltage indicating low parasitic capacitance and inductance. The asymmetry in the measured current is due to unmatched parasitic capacitance between the rectifier diodes as well as uneven influence from parasitic capacity from the surroundings to the circuit. Each time the voltage crosses zero a current peak is observed, this peak is caused by the parasitic capacitance in the diodes of the bridged rectifier.

Conclusion

A proposal for an active load circuit intended for resistive matching the output impedance of a PT is given. The correlation between simulation and measurement is good, however a more sinusoidal current shaped would have been preferred. The benefit compared with prior art is the ability to change the load simply by adjusting a potentiometer and thereby saving the time consuming process of construct a new resistor matrix.

References

[1] C. A. Rosen, "Electromechanical Transducer," Patent 2,830,274, 1958.

[2] E. Horsley, *et al.*, "State-of-the-art piezoelectric transformer technology," 2007, pp. 1-10.

[3] K. S. Meyer, *et al.*, "Parameterized analysis of Zero Voltage Switching in resonant converters for optimal electrode layout of Piezoelectric Transformers," pp. 2543-2548.

[4] E. Horsley, *et al.*, "Achieving ZVS in inductor-less half-bridge piezoelectric transformer based resonant converters," pp. 446-451.

[5] S. Bronstein and S. Ben-Yaakov, "Design considerations for achieving ZVS in a half bridge inverter that drives a piezoelectric transformer with no series inductor," 2002, pp. 585-590 vol. 2.

[6] W. P. Mason, *Electromechanical transducers and wave filters*: D. Van Nostrand company, inc., 1942.

[7] R. L. Lin, "Piezoelectric Transformer Characterization and Application of Electronic Ballast," Blacksburg, Virginia, Nov. 26, 2001.

D.5 Design of Interleaved Interdigitated Electrode Multilayer Piezoelectric Transformer utilizing Longitudinal and Thickness Mode Vibrations

Conference paper

PECON 2012 - 2012 IEEE International Conference on Power and Energy
2 - 5 December 2012
Universiti Teknologi MARA, Shah Alam, Malaysia
http://www.ieeepecon.org/2012/

2012 IEEE International Conference on Power and Energy (PECon), 2-5 December 2012, Kota Kinabalu Sabah, Malaysia

Design of Interleaved Interdigitated Electrode Multilayer Piezoelectric Transformer utilizing Longitudinal and Thickness Mode Vibrations

M. S. Rødgaard, T. Andersen, M. A. E. Andersen
DTU Elektro, Department of Electrical Engineering
Technical University of Denmark
Kgs. Lyngby, Denmark
msr@elektro.dtu.dk; ta@elektro.dtu.dk; ma@elektro.dtu.dk

K. S. Meyer
Noliac A/S
Kvistgaard, Denmark
www.noliac.com

***Abstract*— In applications of high voltage and low power capacitor charging, conventional magnetic based power converters often suffer from bulky components and poor efficiency. Piezoelectric transformer (PT) based converters however, are compact and efficient, especially at high step-up applications. In this paper an interleaved interdigitated electrode (IDE) multilayer PT utilizing longitude and thickness mode vibration for high step-up and high output voltage is developed, for driving capacitive loads of up to 2.5kV. The PT possesses native soft switching capabilities, enabling the utilization of inductor-less topologies. One of the main advantages of the IDE's is that it enables the PT to operate in longitudinal vibration and thickness mode through the electromechanical coupling coefficient k_{33}. This also permits the realization of the PT through a low build-up height (below 2-4mm), making the manufacturing much easier and cheaper. As a result an interleaved IDE PT, with a soft switching factor of 1.00 and a gain of 38 has been developed.**

Keywords-component; Piezoelectric transformer, step-up, converter, soft switching, Interdigitated Electrode (IDE)

I. INTRODUCTION

The piezoelectric transformer (PT) developed in this work, is targeted for high voltage and low power capacitor charging applications. The application is of high step-up conversion and for this specific application [1] stepping-up from a 48V supply voltage, to voltages of up to 2.5kV, giving a step-up ration of around 50. Conventional power converters are built of magnetic transformers and inductors, but in high step-up and low power applications, as this one, they often suffer from bulky components and poor efficiency. PT based converters however, are compact and efficient, especially for high step-up applications. The PT was originally developed by Rosen in 1957 [2] and utilizes piezoelectric ceramics to convert electrical energy through mechanical vibrations. PT based converters have demonstrated good performance and DC/AC converters are widely used commercially, such as for LCD backlighting. But PT based converters for DC/DC applications are still very limited and are not fully developed. Fig. 1 illustrates the PT based DC/DC converter, which utilizes an inductor-less half-bridge topology [3-5] and the specific application is described in more detail in [1] and is similar to the one of [6]. Usually an inductor in series with the PT is necessary, in order to achieve zero voltage switching (ZVS) and avoid large hard switching losses, achieving efficient operation. The absence of a series inductor calls for other means to obtain soft switching capabilities, which can be achieved by utilizing an advantageous and soft switching optimized PT structure.

In this paper an interleaved interdigitated electrode (IDE) multilayer PT utilizing longitude vibration for high step-up and high output voltage is developed, for driving a 2.5kV EAP actuator [7]. The main advantage of this interleaved PT structure is its native good soft switching capabilities. Another big advantage is the build-up with IDE's, which enables the PT to operate in longitudinal vibration and thickness mode through the electromechanical coupling coefficient k_{33}, where the direction of polarization and vibration are the same. The IDE

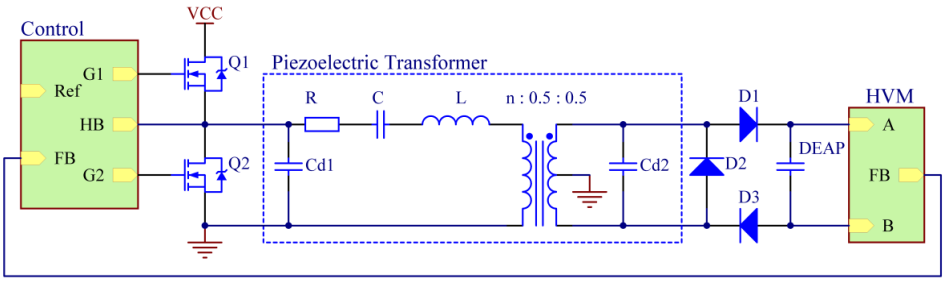

Figure 1. Schematically diagram of the inductor-less half-bridge topology and the PT equivalent lumped parameter model.

Danish National Advanced Technology Foundation grant no. HTF-008-2008-3

978-1-4673-5019-8/12/$31.00 ©2012 IEEE

structure essential permits the realization through a low build-up height (below 2-4mm), resulting in a much easier and cheaper manufacturing. The PT structure and section size are optimized further, in order to obtain a sufficient soft switching capability, similar to the optimisation of [8]. As the complexity of PT structures increases, as well as the complexity of the electromechanical domain in general, the PT design optimization has been performed through iterative finite element method (FEM) simulations. It is very challenging to derive a pure mathematical solution of PT design problems and with today's multi physics FEM simulators, one can fine-tune PT structures, without having to rewrite the mathematical problem. The main objective of this work has been to achieve a soft switching optimized PT design, where gain and load matching have been secondary, and hence is not treated in detail.

A. The piezoelectric transformer

PT's are based on a piezoelectric material. This material has an electromechanical coupling and through this coupling a charge displacement is generated, which is proportional to the deformation of the material. A PT is basically two piezoelectric elements joined together to form a transformer. The primary side element is then exited by an electrical AC voltage, which induces a deformation of the two joined elements. This deformation generates an output voltage on the secondary side element and with a proper design of the PT, a desired voltage conversion can be obtained from the primary to the secondary side.

In order to convert power at a high efficiency, the PT is operated in one of its resonance modes [9-12]. The PT resonates each time it is possible to generate a standing acoustical sound wave in the element. But the design is usually optimized for one specific resonance mode, in order to obtain the highest efficiency [10, 12].

The PT resembles a distributed network, but for simplicity and mathematical representation, only the resonance mode of interest is modeled [10-12] . One of the most used PT models is the lumped parameter model, which was derived by Mason in 1942 [13] and is illustrated in Fig. 2. The model is basically a LCC resonance tank and the behavior of a PT based converter is also quite similar to a traditional resonance converter.

II. PIEZOELECTRIC TRANSFORMER DESIGN

The PT developed is an interleaved IDE thickness mode PT, meaning that the primary section of the PT has been interleaved into the secondary section. Fig. 3 illustrates the structure of the PT, which consists of a primary section with 40

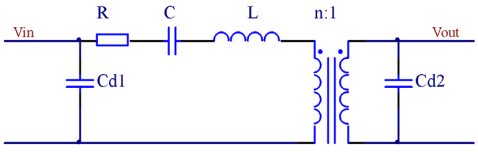

Figure 2. Lumped parameter model, which describes the behavior of the PT in a narrow band around the operating resonance mode

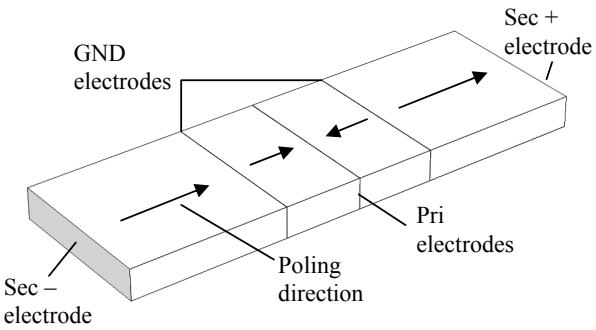

Figure 3. The interleaved multilayer PT structure, where the arrows indicate the polarization direction.

layers, having a layer thickness of 180µm and one split secondary layer. For simplicity the figure only shows two primary layers and the arrows indicate the polarization direction. The PT dimensions is 30x10x2mm, but PT's of 20x10x2mm, and 25x10x2mm were also designed and produced in the same process.

Both sections is operated through the thickness mode electromechanical coupling coefficient k_{33}, which is the most efficient mode [10, 12, 14], giving it a high potential for high efficiency, contrary to the classical Rosen type PT where only the secondary section is operating in thickness mode. Fig. 4 illustrate a FEM simulation of the operational vibration resonance of the PT operating in its first longitudinal mode shape, where it also can be noticed that it has a nodal line in the center of the structure.

One of the drawbacks of this design is the split secondary, which results in a differential output voltage symmetrical around ground. This complicates the electronics somewhat, compared to a ground referenced output. But for this application we need a very high gain, so the extra effort in the electronic is rewarded with a high gain.

The PT is build using tape casting technology, using the NCE46 piezoelectric material [15] and platinum electrode prints. Furthermore the design utilizes IDE's, where thin platinum lines (70µm) are printed on every tape layer, resulting in a stack of lines placed on top on each other, as illustrated in Fig. 5. The electrode lines are shorted through a termination on the side of the PT and thereby forms a vertical electrode. Tape

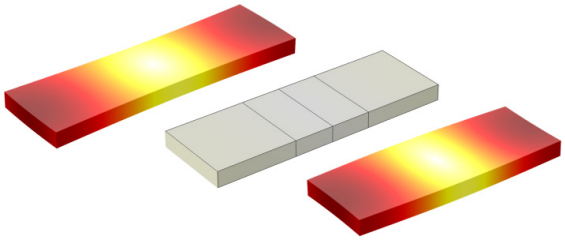

Figure 4. FEM simulation of the PT, operating in the first longitudinal mode shape, at 47.53 kHz. The coloring illustrates the total displacement, where light colors refer to a low displacement and dark colors to at high displacement.

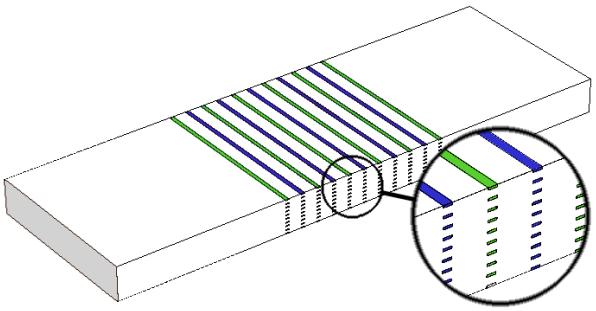

Figure 5. The interleaved multilayer PT structure, illustrating the IDE structure, with 10 primary layers and exaggerated electrode prints.

casting does not allow implementation of vertical electrodes, meaning that this design should have a build-up height of 30mm, when using traditional electrodes, making it almost impossible to produce. The IDE structure enables the utilization of thickness mode operation, while retaining some of the easy manufacturing advantages, of the low build-up height.

The drawback of using IDE's is that the electrodes have a finite thickness of 70µm (line print width), compare to the negligible 2µm thickness of traditional electrodes. As there are production limits to how thin the IDE layers can be made, a certain part of the primary section is going to consist of the electrodes and hence inactive material. The percentage of inactive material is determined by the IDE thickness and the primary layer thickness. The percentage of inactive material is desired to be as low as possible, as it only contribute to higher losses, and will degrade the performance of the primary section. Furthermore the tape thickness should be small compared to the primary layer thickness, so that the IDE appears as a consistent vertical electrode. With a tape thickness of 33µm and a primary layer thickness of 180µm, the tape thickness is only 5.5 times smaller, but has shown to be sufficient.

III. PIEZOELECTRIC TRANSFORMER DEVELOPMENT

In order to utilizes inductor-less topologies and utilize ZVS operation, the PT should possess soft switching capabilities. Furthermore the PT is operated slightly above the resonance frequency, where the series resonance network becomes inductive and contains enough resonating energy, to charge and discharge the input capacitance C_{d1}. The main design optimization criterion has been the soft switching capability, as well as a reasonable high ratio of active and inactive material is desired.

The main advantage of the interleaved primary section is its native good soft switching capabilities. This is due to the placement right in the middle of the excitation stress curve, which is a half-wave sine wave for the first resonance mode, as illustrated in Fig. 6. The primary section size has been optimized in order to obtain sufficient soft switching capability. The gain is mainly determined by the primary and secondary layer thickness ratio, but it is also affected by the primary section size. And as a small primary layer thickness is desired, hence a high gain, the percentage of inactive material is pushed

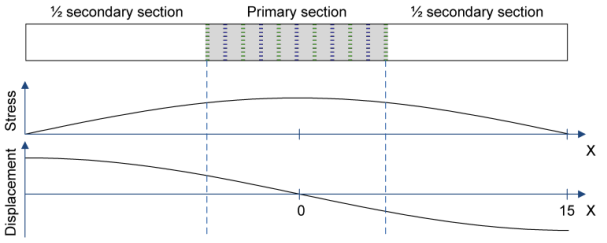

Figure 6. The interleaved multilayer PT structure, illustrating the stress and displacement in its first mode shape.

to its limits. So in the end this percentage has also been optimized, as well as it affects the soft switching capability and gain. In order to simplify the PT structure for the FEM simulation, the IDE's have been approximated by solid vertical electrodes, of inactive piezoelectric material with an electrode thickness of 70µm, as well as only a 2D simulation has been performed.

Fig. 7 shows a frequency sweep of the primary and secondary impedance of the resulting design, in the vicinity of the operating resonance mode. In order to evaluate the electrical characteristics of the PT, the lumped parameter has been calculated from the impedance measurements. From the primary and secondary impedances resonance and anti-resonance, plus a DC impedance measurement, the lumped parameters has be calculated, as described in detail in [4, 11, 16]. Through the FEM simulation of the PT impedances Fig. 7, the equivalent parameters of table I are found. The lumped parameters does not tell much about the performance of the PT, but some more general performance properties can be calculated, such as the soft switching factor, matched load, power in matched load, gain and efficiency.

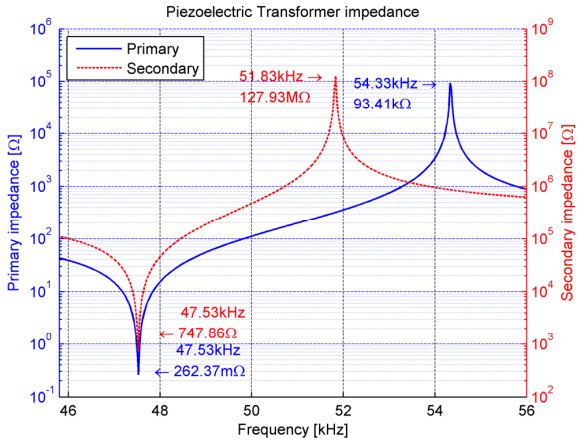

Figure 7. FEM simulation of the PT primary and secondary impedance magnitude, with the opposite side shorted.

TABLE I. PT EQUIVALENT LUMPED PARAMETERS OBTAINED THROUGH FEM SIMULATIONS.

R	C	L	C_{d1}	C_{d2}	1/n
262mΩ	4.56nF	2.46mH	14.85nF	8.23pF	54.1

Usually the load is matched to the output capacitance C_{d2} of the PT, Equation (1), or the other way around, as the load matching maximizes the power transfer of the resonance network to the load. Where ω_r is the operating frequency and can be approximated as the resonance frequency. Furthermore all the following performance properties assume a matched load.

$$R_{match} = \frac{1}{C_{d2}\omega_r} \quad (1)$$

Equation (2) expresses the soft switching factor or ZVS factor [5] which is a measure of the PT's soft switching capabilities. If the ZVS factor is greater than 1, the PT is capable of performing ZVS operation of the half-bridge, where the matched load is the worst case condition [4].

$$V'_P = \left(0.304\frac{1}{n^2}\frac{C_{d2}}{C_{d1}} + 0.538\right)(0.585\eta + 0.414) \quad (2)$$

The soft switching factor is an expression of maximum obtainable soft switching capability. This point of maximum soft switching capability is located slightly above the resonance frequency and if the soft switching factor is greater than 1, the resonance network contains sufficient resonating energy, to charge and discharge C_{d1}.

Equation (3) expresses the efficiency of the PT, in to a matched load, with the simplified loss resistor R [4]. The loss resistor extracted from the FEM simulation is only a small signal simulation of the impedance and hence only results in a small signal efficiency. Furthermore the loss mechanisms of piezoelectric materials are not fully implemented in the FEM simulation, therefore this efficiency is more a relative measure to compare between different FEM designs.

$$\eta_{match} = 1 - \frac{2RC_{d2}}{n^2\sqrt{LC}} \quad (3)$$

The performance properties for the interleaved IDE PT design are calculated in table II. The gain A_{ZVS} from the first harmonic input to the output, output power P_{ZVS} and output voltage $V_{out,rms}$ [17], is the respective gain, power and voltage, at a 48V half-bridge voltage, when operating at the maximum ZVS point.

With a soft switching factor of 1.03 the PT possesses soft switching capabilities, which enables the inductor-less operation. It has a high efficiency and a high gain, that results in a $851V_{rms}$ output voltage, into a matched load, with a PT modulation voltage of $19.3V_{rms}$, which is the first harmonic, of the 48V half-bridge voltage [4]

TABLE II. PT EQUIVALENT LUMPED PARAMETER MODEL PERFORMANCE PROPERTIES.

V'_P	A_{ZVS}	P_{ZVS}	R_{match}	η_{match}	$V_{out,rms}$
1.03	44	1.78W	389kΩ	0.996	851V

A. Volume optimization

With 40 primary layers of 180µm and IDE thickness of 70µm, the primary section occupies 33% of the PT structure, where the IDE's occupies 27.7% of the primary section. In table III it can be seen that the primary section size has to be approximately 5% larger than a normal thickness mode structure (no inactive material). As the 27.7% of inactive material degrades the performance of the primary section and hence degrades the soft switching capability. Furthermore the ratio of the primary layer thickness and the tape thickness is shown and for a 20mm IDE PT design, this ratio is as low as 3.3 and the IDE's cannot be considered as solid electrodes any more. Furthermore the primary section size has to be increased from 33% to 36%, in order to achieve soft switching, where as 38% of the primary section is inactive material and this 20mm design is pushing the IDE PT structure beyond its limits.

B. Power density

Power density is a figure of merit with in power electronic to compare different topologies, designs and components [18]. By definition power density is the ratio between output power and volume (4). However the output power of the PT depends on a lot of external factors: Input amplitude, input wave shape (e.g. sinus or square), frequency, temperature and cooling, load condition and mechanical fixture, are all factors that have influence on the output power of the PT [4, 10, 12, 19-21].

$$\rho = \frac{P_o}{Vol} \quad (4)$$

For the volume parameter it is normal to only include the actual volume of the PT itself. The limiting factor of the power density is the ability to dissipate the power loss of the component. A temperature rise of 40ºC is at typical allowable temperature rise [17].

IV. EXPERIMENTAL RESULTS

Several prototypes were produced, as shown in Fig. 8, and in the following section the functionality and properties of the 30x10x2mm prototype PT is investigated.

A. PT impedance and performance

Fig. 9 illustrate the impedance measurement of the prototype PT, showing a clear resonance and anti-resonance of the operational resonance mode. From the impedance measurements the equivalent lumped parameters of table IV and the performance properties of table V are calculated.

TABLE III. PT PRIMARY VOLUME AND SOFT SWITCHING CAPABILITY OPTIMIZATION.

	Thickness mode		**IDE structure**		
PT size	***30mm***	***30mm***	***30mm***	***20mm***	***20mm***
Pri vol.	30%	33%	33%	33%	36%
IDE vol. of Pri			**27.7%**	**41.6%**	**38.2%**
Pri th./Tape th.			5.5	2.9	3.3
V'_P	1.096	1.255	**1.028**	**0.955**	**1.039**

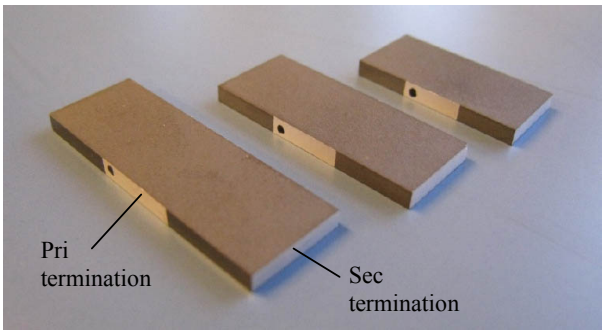

Figure 8. Picture of prototype PT's of different sizes (length from left: 30mm, 25mm and 20mm).

As it can be seen that the prototype PT is right on the boundary of soft switching capability, having a ZVS factor of 1.028 and has shown to be insufficient to operate under ZVS with a matched load, as the half-bridge does add some parasitic capacitance. But when utilizing an output rectifying circuit, the matched load condition is not fulfilled and ZVS operation is possible, as illustrated in Fig. 10.

B. Power density measurements

The power density of the prototype PT have been measured and compared with the Interleaved Rosen type PT [22], and as they have the exact same dimensions, giving them the same volume, surface and ability to dissipate power, they can be

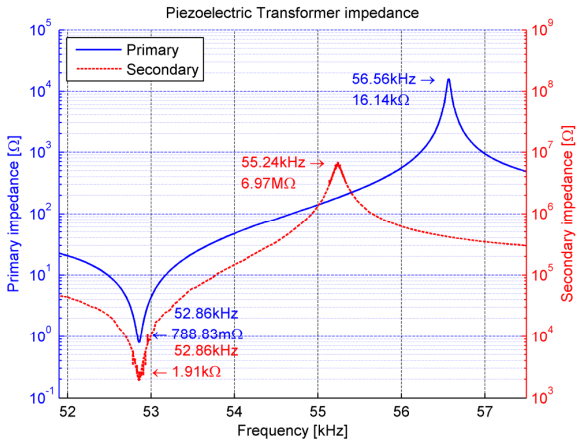

Figure 9. Measurement of the 30x10x2mm prototype PT primary and secondary impedance magnitude, performed with a HP4194A impedance/gain-phase analyzer.

TABLE IV. PROTOTYPE PT EQUIVALENT LUMPED PARAMETERS OBTAINED THROUGH IMPEDANCE MEASUREMENTS.

R	C	L	C_{d1}	C_{d2}	1/n
789mΩ	3.91nF	2.32mH	27nF	18.62pF	47.8

TABLE V. TABLE 1: PROTOTYPE PT EQUIVALENT LUMPED PARAMETER MODEL PERFORMANCE PROPERTIES.

V'_P	A_{ZVS}	P_{ZVS}	R_{match}	η_{match}	$V_{out,rms}$
1.00	38	3.37W	158kΩ	0.978	738V

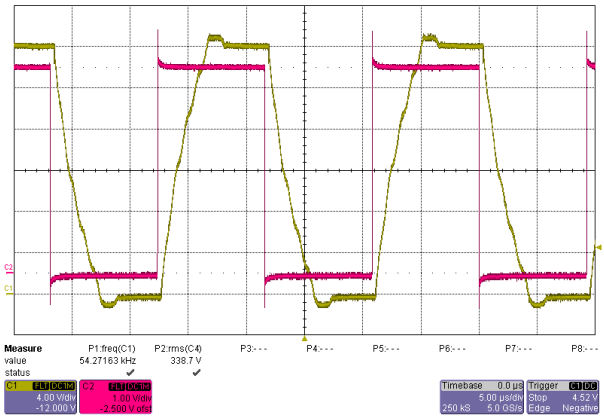

Figure 10. Measured driving PWM (red) and input half-bridge voltage (yellow), where the relative slow rising switching flanks (resonance current charges C_{d1}) and body-diode conduction voltage drop, when reaching the supply rails, clearly reveals ZVS operation. Time base [5µs/div], driving PWM [1V/div] and input half-bridge voltage [4V/div].

compared directly. The measurements have been performed with an applied AC excitation voltage and a matched load. The excitation voltage has been stepwise increased, increasing the output power, and the settling temperature rise has been measured. Furthermore the PT is excited at the frequency of maximal soft switching capability, in order to reflect the performance of the actual operation. The power density measurements of Fig. 11 show that a power density of 11W/cm^3, of the interleaved IDE PT, can be expected, with a temperature rise of 40ºC. The interleaved IDE PT also demonstrates close to 5 times better power density compared to the Interleaved Rosen type PT.

V. DISCUSSION

In order to evaluate the design the measured figures of table IV and V, is compared with the FEM simulation obtained figures of table I and II. As it can be seen the correlation between the soft switching factors (V'_P) is very good, despite it

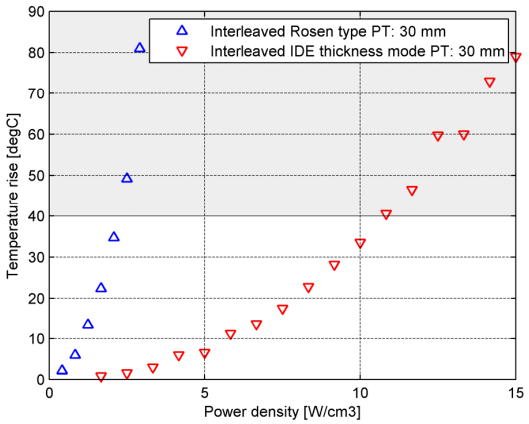

Figure 11. Power density measurement of the Interleaved IDE PT, compared with the Interleaved Rosen type PT [22], operated at the maximum soft switching frequency.

being too low to operate under ZVS at matched load condition. But it has shown to be sufficient when operating with an output rectifier. Looking at the lumped parameters C_{d1}, C_{d2} and the efficiency, the correlation is not that good. This is expected to be caused by a bad correlation between the NCE46 material parameters in the FEM simulation and what they are in real life, as well as the FEM simulation has an incomplete loss model for piezoelectric materials. Looking at the gain (A_{ZVS}) it is also 15% lower than expected. All in all the correlation between the FEM simulation and the prototype are not that good, except for the soft switching factor, but we did also face inconsistence results, when reproducing the prototypes. The two most likely reasons for this, is the FEM simulation simplification of consistent vertical electrodes, instead of the real IDE structure, and with a primary layer thickness to tape thickness ratio as low as 5.5, this simplification does simply not reflect reality. The second reason is the physical consequences of such a low ratio, as the electrical fields of the IDE's do not produce a relative homogeneous field across the primary layers, which can result in an inefficient polarization, leading to even more inactive or inefficient material [23]. Nevertheless the interleaved IDE PT does demonstrate soft switching capabilities, as well as it demonstrates its potential in power density Fig. 11. If the IDE PT structure is to exploit its potential, a less aggressive design than the one presented here, should be used. The main concern is to have a higher primary layer to tape thickness ratio, preferably higher than 10, which can simply be achieved by decreasing the tape thickness for this design. It can obviously also be achieve by increasing the primary layer thickness, which could be accomplished by doubling the driving voltage, demanding half the PT gain, resulting in a doubling of the primary layer thickness. Furthermore the inactive material should be minimized, where the IDE thickness is primarily determined by production limitations. In the end the IDE PT structure might be better suited for other applications, with higher input voltage and lower gain requirements.

VI. Conclusion

In this paper an interleaved interdigitated electrode (IDE) multilayer piezoelectric transformer (PT) utilizing longitude and thickness mode vibrations has been developed. The PT is optimized for soft switching, inductor-less operation, high step-up and high output voltage, for driving a 2.5kV EAP actuator. The development has been performed through iterative FEM simulations. With a primary layer thickness to tape thickness ratio as low as 5.5, the simplified FEM model did have some shortcomings, resulting in a degrade correlation. Furthermore this low ratio is pushing the physical limits of the IDE PT structure, resulting in inconsistent prototypes, as well as a further degradation of the correlation. Nevertheless the developed 30x10x2mm prototype PT has demonstrated to possess soft switching capabilities, with a soft switching factor of 1.00, which enables the utilization of inductor-less topologies, as well as having a high gain of 38. Furthermore it demonstrates its high efficiency potential, having a power density of 11W/cm^3.

Acknowledgements

Finally we would like to thanks Noliac A/S for the production of prototype PT's, as well as general PT design support. We would also like to thanks The Danish National Advanced Technology Foundation for their financial support.

References

[1] T. Andersen, M. S. Rødgaard, O. C. Thomsen, and M. A. E. Andersen, "Low voltage driven dielectric electro active polymer actuator with integrated piezoelectric transformer based driver," in *SPIE Smart Structures*, 2011, p. 79762N.
[2] C. A. Rosen, "Electromechanical Transducer," US Patent 2,830,274, 1958.
[3] J. M. Alonso, C. Ordiz, M. A. Dalla Costa, J. Ribas, and J. Cardesín, "High-voltage power supply for ozone generation based on piezoelectric transformer," *IEEE Transactions on Industry Applications,* vol. 45, pp. 1513-1523, 2009.
[4] K. S. Meyer, M. A. E. Andersen, and F. Jensen, "Parameterized analysis of Zero Voltage Switching in resonant converters for optimal electrode layout of Piezoelectric Transformers," 2008, pp. 2543-2548.
[5] M. S. Rødgaard, T. Andersen, and M. A. E. Andersen, "Empiric analysis of zero voltage switching in piezoelectric transformer based resonant converters," in *PEMD*, England, 2012.
[6] C. Bai, S. Li, Q. Shen, and D. Cui, "A Converter of High Voltage Capacitor Charging Power Supply Using Piezoelectric Transformer," 2009, pp. 1-4.
[7] M. Tryson, H. E. Kiil, and M. Benslimane, "Powerful tubular core free dielectric electro activate polymer (DEAP) push actuator," in *SPIE*, 2009, p. 72871F.
[8] K. S. Meyer, "Piezoelectric transformer with high effective electromechanical coupling factors," US Patent 61/521,635, Pending.
[9] E. Horsley, M. Foster, and D. Stone, "State-of-the-art piezoelectric transformer technology," in *EPE*, 2007, pp. 1-10.
[10] C. Lin, "Design and analysis of piezoelectric transformer converters," PhD Dissertation, 1997.
[11] C. Lin and F. Lee, "Design of a piezoelectric transformer converter and its matching networks," 1994, pp. 607-612 vol. 1.
[12] R. L. Lin, "Piezoelectric transformer characterization and application of electronic ballast," PhD Dissertation, Virginia Polytechnic Institute and State University, 2001.
[13] W. P. Mason, *Electromechanical transducers and wave filters*: Van Nostrand Reinhold, 1946.
[14] A. Meitzler, "IEEE standard on piezoelectricity," *Society,* 1988.
[15] Noliac. *Piezoelectric ceramics datasheet*. Available: http://www.noliac.com/Files/Billeder/02%20Standard/Ceramics/Noliac_CEramics_NCE_datasheet.pdf
[16] G. Zerong, J. Lingling, L. Huabo, and W. Ting, "Measurement of PT equivalent circuit model parameters based on admittance circle," 2011, pp. 20-23.
[17] K. S. Meyer and M. A. E. Andersen, "One-shot Design of Radial Mode Piezoelectric Transformer for Magneticless Power Conversion," 2011, pp. 498-504.
[18] J. W. Kolar, U. Drofenik, J. Biela, M. Heldwein, H. Ertl, T. Friedli, ... "PWM converter power density barriers," 2007, pp. P-9-P-29.
[19] X. Chu, J. Wu, Z. Xu, and L. Li, "Experiment research on multilayer piezoelectric transformer," 2008, pp. 524-527.
[20] A. M. Flynn and S. R. Sanders, "Fundamental limits on energy transfer and circuit considerations for piezoelectric transformers," *IEEE Transactions on Power Electronics,* vol. 17, pp. 8-14, 2002.
[21] D. Guyomar, C. Magnet, E. Lefeuvre, and C. Richard, "Nonlinear processing of the output voltage a piezoelectric transformer," *IEEE Transactions on Ultrasonics, Ferroelectrics and Frequency Control,* vol. 53, pp. 1362-1375, 2006.
[22] M. S. Rødgaard, T. Andersen, K. S. Meyer, and M. A. E. Andersen, "Design of interleaved multilayer rosen type piezoelectric transformer for high voltage DC/DC applications," in *PEMD*, 2012.
[23] T. Andersen, M. A. E. Andersen, and O. C. Thomsen, "Simulation of Piezoelectric Transformers with COMSOL," in *COMSOL conference, unpublished*, 2012.

D.6 Integrated high voltage power supply utilizing burst mode control and its performance impact on dielectric electro active polymer actuators

Conference paper

ACTUATOR 12 - International Conference and Exhibition on New Actuators and Drive Systems
18 - 20 June 2012
Bremen, Germany
http://www.actuator.de/templ_act_en_12.php

Integrated high voltage power supply utilizing burst mode control and its performance impact on dielectric electro active polymer actuators

T. Andersen, M.S. Rødgaard*, M.A.E. Andersen*, O.C. Thomsen*, K. P. Lorenzen†, C. Mangeot‡, A. R. Steenstrup‡*
**Technical University of Denmark, DTU Elektro, Kgs. Lyngby, Denmark*
†Danfoss PolyPower A/S, Nordborg, Denmark
‡Noliac A/S, Noliac Motion, Kvistgaard, Denmark

Abstract:
Through resent years new high performing Dielectric Electro Active Polymers (DEAP) have emerged. To fully utilize the potential of DEAPs a driver with high voltage output is needed. In this paper a piezoelectric transformer based power supply for driving DEAP actuators is developed, utilizing a burst mode control technique. Controlling and driving a DEAP actuator between 250V to 2.5kV is demonstrated, where discrete like voltage change and voltage ripple is observed, which is introduced by the burst mode control. Measurements of the actuator strain-force reveal that the voltage ripples translates to small strain-force ripples. Nevertheless the driver demonstrates good capabilities of following an input reference signal, as well as having the size to fit inside a 110 mm x 32 mm cylindrical InLastor Push actuator, forming a "low voltage" DEAP actuator.

Keywords: Dielectric Electro Active Polymers, Driver, Power supply, Piezoelectric transformer

Introduction

The resent years emergence of new high performing DEAP materials, calls for higher performing drivers in order to fully utilize its potential. Figure 1 top illustrates the state of the art driver for driving the cylindrical InLastor Push actuator. The driver is electromagnetic transformer (EMT) based and converts the input DC voltage of 24 volt to an output voltage between 250V and 2.5kV depending on a control signal.

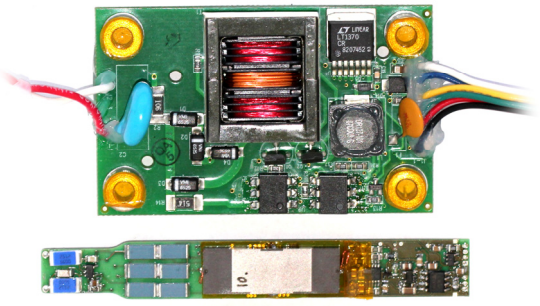

Figure 1: *Converters for driven DEAP actuators. Top: The state of the art electromagnetic (EMT) based driver. Bottom: Novel piezoelectric transformer (PT) based driver*

At the bottom of figure 1 the novel piezoelectric transformer (PT) based driver is illustrated. It utilizes an inductor less topology which enables operation in high external magnetic fields, as well as the elimination of bulky inductors reduces overall volume. The decrease in volume of the PT based driver allows the driver to be integrated into a cylindrical DEAP actuator, which is illustrated in figure 2. The benefits of integrating the driver into the DEAP are to avoid the high voltage interface. Issues regarding high voltage safety are avoided. The availability of low voltage power supplies is far greater than for high voltage.

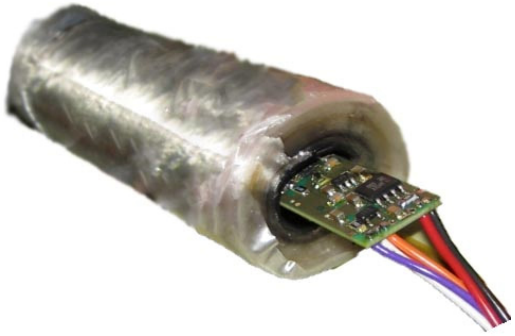

Figure 2: *Cylindrical DEAP actuator with integrated driver. The driver is pulled a bit out of the actuator for the purpose of illustration*

In this work the performance of the novel PT based driver is compared with the state of the art EMT based driver. The general design will be presented, as well as the basic operation and functionality. The efficiency and EMI performance will be compared and evaluated. Furthermore the performance of the resulting integrated cylindrical DEAP actuator is presented and evaluated.

Inductor-less PT based driver

The principle of an inductor-less PT based driver relies on a half-bridge driven PT topology [1]. The electrical equivalent of a PT, valid in the vicinity of a single resonance mode, can be modeled with the Mason lump parameter equivalent [2-4]. The Mason equivalent connected with a half-bridge is illustrated in figure 3. The capacitance C_{d1} is large, easily 100 times greater than the output capacitance of the two MOSFETs. The high capacity load on the half-bridge is a disadvantage. Each time the half-bridge voltage (V_1) is hard switched the stored energy in C_{d1} is dissipated in the MOSFETs.

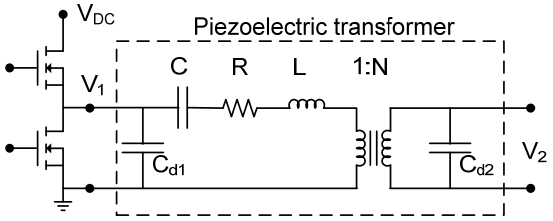

Figure 3: *Inductor-less PT topology. Half-bridge connected with the Mason equivalent model of a piezoelectric transformer*

To improve efficiency of the converter the half-bridge must be soft switched instead of hard switched. Soft switching is in this case referred to as zero voltage switching (ZVS) and occurs when the voltage across the MOSFET is zero when it turns on. ZVS can be obtained by the PT, however the PT and the control must be optimized for ZVS operation [1, 5-7].

The driver utilizes an interleaved multilayer Rosen type transformer [8], which is ZVS optimized. Figure 4 sketches the structure of the PT and the polarization directions and for simplification only two primary layers are shown.

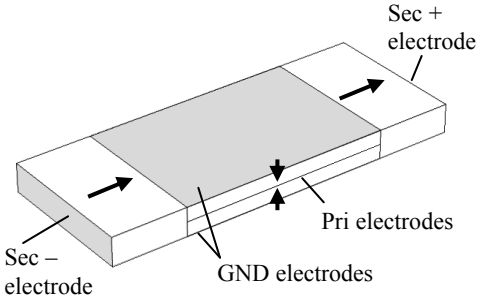

Figure 4: *The interleaved multi layer Rosen-type PT structure, where the arrows indicate the polarization direction. Size: 30mm x 10mm x 2mm*

The secondary sections of the transformer are polarized in the same direction. Thereby the output voltage of the two secondary electrodes is 180 degrees out of phase, which increase the gain of the transformer. The equivalent model of the PT is illustrated in figure 5. To further increase the overall step-up ratio of the converter a voltage doubler rectifier circuit is utilized at the output of the PT [9, 10]. However a three diode version is used instead of the standard two diode solution. This is necessary for the ground referred output voltage feedback circuit to work correctly, as well as avoiding a large common mode voltage signal over the actuator.

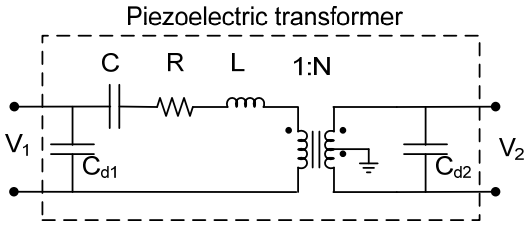

Figure 5: *Electrical equivalent of the interleaved Rosen type transformer, with both secondary sections polarized in the same direction*

To ensure high efficiency of the converter a inner closed-loop control circuit similar to [11] is used to maintain ZVS operation of the PT. An outer closed-loop is controlling the output voltage in a bust mode (quantum-mode) manner [11-13]. Feedback from the output voltage across the DEAP actuator closes the outer loop. Decrease of the output voltage is done by discharging the DEAP actuator through a resistive network. Figure 6 illustrates the driver with the DEAP connected.

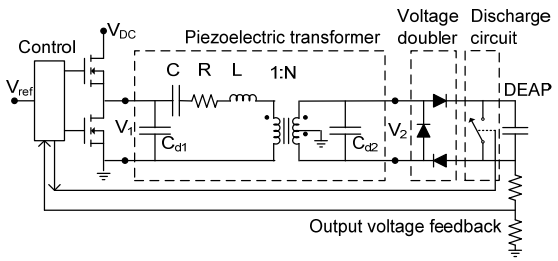

Figure 6: *Block diagram of inductor-less PT converter with voltage doubler rectifier, discharging circuit and DEAP actuator connected*

A reference signal (V_{ref}) is controlling the voltage across the DEAP actuator. When the output voltage feedback is below the reference signal the driver is turned on. When the output voltage feedback is above the reference signal the driver is turned off and the discharging circuit is turned on.
With a constant reference signal, the driver will charge the DEAP to the output voltage corresponding to the reference signal and then turn off the driver. The DEAP will retain the output voltage, however leakage current within the DEAP and the diodes together with the current drawn by

the output voltage feedback circuit is slowly discharging the DEAP. When the DEAP is discharge below a certain lower threshold of the reference signal, the driver is turned on again to charge the DEAP until a certain upper threshold of the reference signal. This control method is referred to as burst mode control. Figure 7 shows an oscilloscope plot of the PT driver in action. Notice that the voltage of the DEAP is attenuated by 1000 times. The time between each burst is determined by the discharge rate of the DEAP and the hysteretic window around the reference signal. The time length of each burst is controlled by adjusting the hysteretic window around the reference signal. The size of the hysteretic window is a trade-off between efficiency and output voltage ripple. As the hysteretic window goes towards zero the burst frequency and burst time length goes towards zero, decreasing the output voltage ripple. However efficiency will drop as the time length of each burst decreases. The explanation is that it takes time to build up the necessary resonance current within the PT for ZVS operation. Every start-up of the PT is therefore very inefficient compared to ZVS operation.

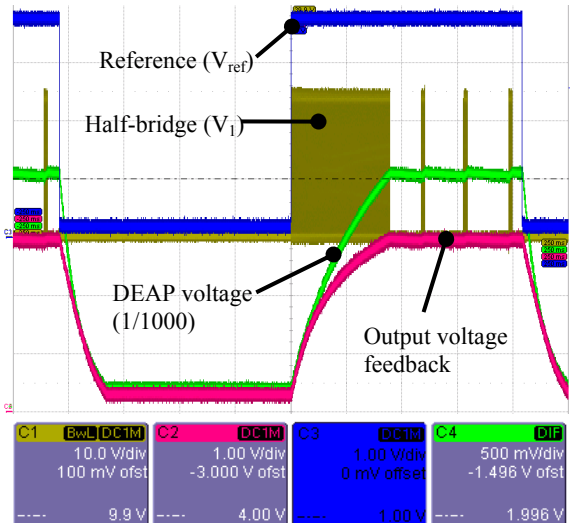

Figure 7: *Oscilloscope plot of the PT based driver with a square wave reference signal. Burst mode control of the half-bridge is observed. DEAP voltage is attenuated by x1000*

Driver performance

In this section the electrical properties of the PT based driver is compared to the state of the art EMT based driver.

Efficiency

The efficiency of the driver is defined as the ratio between energy stored in the DEAP and energy delivered to the driver (1). Figure 8 shows the used setup for measure the efficiency of the two drivers. Prior to the measurement output is discharged to zero volt. The input voltage is 24 volt and the DEAP is substituted with a fixed capacitance of 47nF. The input current is measured as the output capacity is charged from zero to 1.9kV.

$$\eta = \frac{E_{DEAP}}{E_{input}} = \frac{0.5 \cdot C_{DEAP} \cdot V_{DEAP}^2}{\int V_{DC} \cdot I_{in} \cdot dt} \quad (1)$$

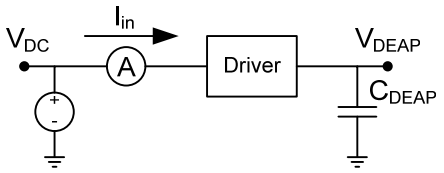

Figure 8: *Setup for measure efficiency of the driver*

The measured input current for the PT based and EMT based driver is plotted in figure 9. When the output voltage reached 1.9kV the control circuit turns off the half-bridge stage and the input current drops sudden and only auxiliary current consumption is left.

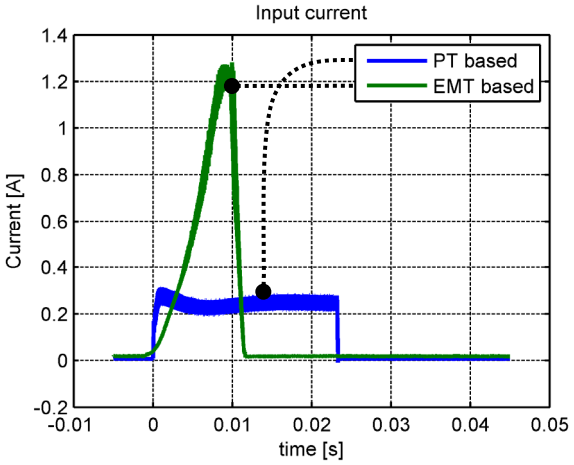

Figure 9: *Measurement of input current while charging the output voltage from 0V to 1.9kV*

From the measured input current and the definition (1) is the efficiency calculated for both drivers, see table 1.

Driver type:	E_{input} (24V)	E_{DEAP} (47nF)	Efficiency
PT based	138mJ	81.2mJ	58.8%
EMT based	182mJ	82.4mJ	45.3%

Table 1: *Efficiency of PT based and EMT based driver*

$$PT_{loss\,reduction} = \frac{E_{loss,EMT} - E_{loss,PT}}{E_{loss,EMT}} = 41\% \quad (2)$$

The energy loss for PT based driver is reduced by 41% compared to the EMT based driver (2).

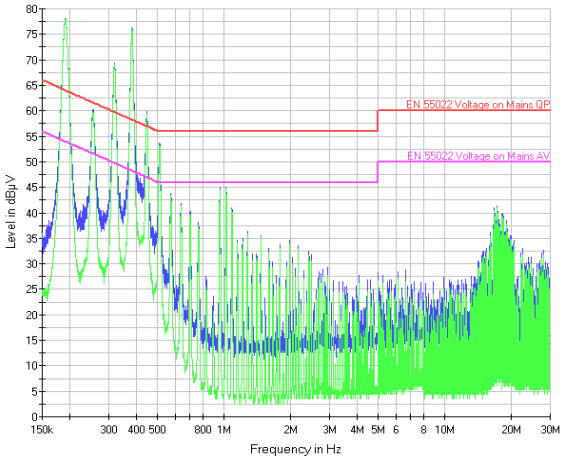

Figure 10: *EMI measurement of PT based driver at 4 watts output power*

EMI

As the PT based driver does not contain any magnetic components, the emitted magnetic fields are expected to be low. But this also means that the driver has no input filter to suppress the fundamental switching frequency. As the PT based driver is a soft switched resonance converter, the general EMI performance is expected to be good.

The setup used for the measurement the conducted EMI is illustrated in figure 11. The LISN network is connected to an EMC receiver. The utilized EMC receiver requires a steady state operation of the device under test in order to measure the EMI correct. The driver is therefore loaded with a resistive load (R_L) instead of a capacitive load.

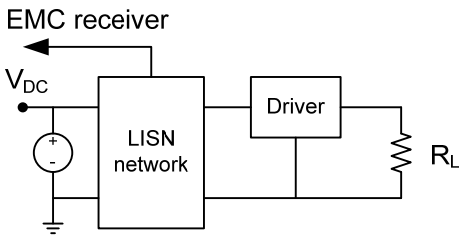

Figure 11: *Setup for measure conducted EMI*

The result of the EMC receiver is shown in figure 10 and figure 12 for the PT based and the EMT based driver respectively. Both measurements are performed with an output power of 4 watts. None of the drivers have any dedicated EMI filtering. As expected both drivers lacks the ability to suppress fundamental frequencies with a peak of around 80dBµV. However the PT based driver performs well in the high frequency region (above 1MHz) with a ≈25dBµV decrease between the peak values compared with the EMT based driver.

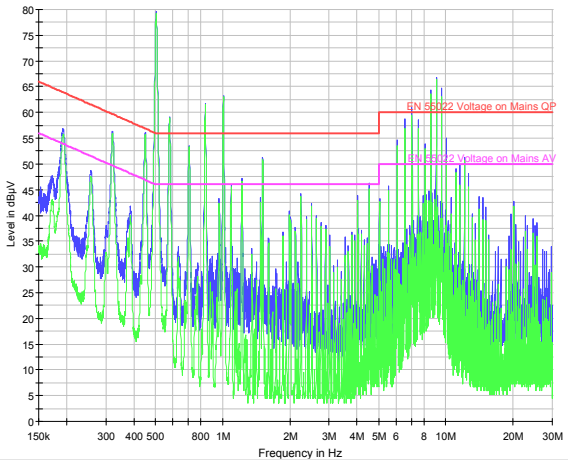

Figure 12: *EMI measurement of EMT based driver at 4 watts output power*

DEAP performance with integrated driver

The mechanical performance of the integrated DEAP actuator is evaluated trough a Stroke-Force measurement. The measurement is performed by prevent the movement of the actuator, when applying the voltage. The actuator is then slowly released, while the force and stroke is measured. Stroke-Force measurements of the DEAP actuator, with and without driver integration, are shown in figure 13.

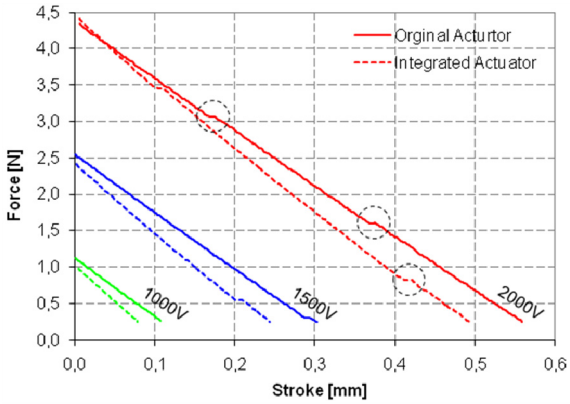

Figure 13: *Stroke-Force measurement of the DEAP actuator, with and without driver integration, at different DEAP voltages*

It can be seen that the integration do decrease the stroke performance somewhat. Approximately 12% decrease in stroke. This is due to increased tension and friction, as the PCB is attached in one end of the actuator and is sliding in a slot in the other end. Furthermore small jumps can be observed on the measurements. This is small burst from the driver, as the voltage drops due to the increase in capacitance, as the film is getting thinner. The driver will counteract this drop as it will maintain a constant output voltage.

Conclusion

The basic structure and operational functionality of the novel PT based DEAP actuator driver are presented in this work. Furthermore the performance is compared with the state of the art EMT based driver, as well as the performance of the resulting integrated DEAP actuator is evaluated. The PT based driver demonstrated a 14% point increase in efficiency, compared to the EMT based driver, resulting in a 41% loss reduction. The EMI performance of the PT based driver showed a good improvement of 25dBµV in the high frequency region (above 1MHz). Finally the resulting integrated cylindrical DEAP actuator demonstrated full functionality, with approximately 12% decrease in stroke performance, compared to the original actuator.

References

[1] J. M. Alonso, C. Ordiz, and M. A. Dalla Costa, "A novel control method for piezoelectric-transformer based power supplies assuring zero-voltage-switching operation," *Industrial Electronics, IEEE Transactions on,* vol. 55, pp. 1085-1089, 2008.

[2] C. Lin and F. Lee, "Design of a piezoelectric transformer converter and its matching networks," 1994, pp. 607-612 vol. 1, ISBN: 0780318595.

[3] G. Zerong, J. Lingling, L. Huabo, and W. Ting, "Measurement of PT equivalent circuit model parameters based on admittance circle," 2011, pp. 20-23, ISBN: 1612847196.

[4] C. Lin, "Design and analysis of piezoelectric transformer converters," PhD Dissertation, 1997.

[5] E. Horsley, N. Nguyen-Quang, M. Foster, and D. Stone, "Achieving ZVS in inductor-less half-bridge piezoelectric transformer based resonant converters," 2009, pp. 446-451, ISBN: 1424441668.

[6] S. Bronstein and S. Ben-Yaakov, "Design considerations for achieving ZVS in a half bridge inverter that drives a piezoelectric transformer with no series inductor," 2002, pp. 585-590 vol. 2, ISBN: 078037262X.

[7] K. S. Meyer, M. A. E. Andersen, and F. Jensen, "Parameterized analysis of Zero Voltage Switching in resonant converters for optimal electrode layout of Piezoelectric Transformers," 2008, pp. 2543-2548, ISBN: 1424416671.

[8] M. S. Rødgaard, T. Andersen, K. S. Meyer, and M. A. E. Andersen, "Design of interleaved multilayer rosen type piezoelectric transformer for high voltage DC/DC applications," in *PEMD*, 2012.

[9] G. Ivensky, M. Shvartsas, and S. Ben-Yaakov, "Analysis and modeling of a voltage doubler rectifier fed by a piezoelectric transformer," *Power Electronics, IEEE Transactions on,* vol. 19, pp. 542-549, 2004.

[10] G. Ivensky, S. Bronstein, and S. Ben-Yaakov, "A comparison of piezoelectric transformer AC/DC converters with current doubler and voltage doubler rectifiers," *Power Electronics, IEEE Transactions on,* vol. 19, pp. 1446-1453, 2004.

[11] J. Diaz, J. Martin-Ramos, M. Prieto, and F. Nuno, "A double-closed loop DC/DC converter based on a piezoelectric transformer," 2004, pp. 1423-1428 Vol. 3, ISBN: 0780382692.

[12] J. A. Martin-Ramos, M. A. J. Prieto, F. N. García, J. D. González, and F. M. F. Linera, "A new full-protected control mode to drive piezoelectric transformers in DC-DC converters," *Power Electronics, IEEE Transactions on,* vol. 17, pp. 1096-1103, 2002.

[13] J. Díaz, F. Nuño, J. M. Lopera, and J. A. Martín-Ramos, "A new control strategy for an AC/DC converter based on a piezoelectric transformer," *Industrial Electronics, IEEE Transactions on,* vol. 51, pp. 850-856, 2004.

D.7 Forward Conduction Mode Controlled Piezoelectric Transformer based PFC LED Drive

Journal paper

IEEE Transactions on Power Electronics
2012

This article has been accepted for publication in a future issue of this journal, but has not been fully edited. Content may change prior to final publication.

Forward Conduction Mode Controlled Piezoelectric Transformer based PFC LED Drive

Martin S. Roedgaard*, Michael Weirich†, *Member, IEEE,* Michael A. E. Andersen*, *Member, IEEE,*

***Abstract*—Light Emitting Diode (LED) illumination is getting more and more common, as LED's performance is rising, the price is falling and is getting competitive. Some of the challenges of AC mains supplied illumination is the requirement of Power Factor Correction (PFC) and the competitiveness of a low priced marked. In this paper a new Forward Conduction Mode (FCM) control method for Piezoelectric Transformer (PT) based power converters is proposed. A PT based LED drive facilitating passive PFC is developed, utilizing and validating the FCM control method. The drive utilizes a inductor-less half-bridge topology and for circuit minimization and simplicity it has no load regulation and has a 100 Hz output modulation. The proposed FCM control method ensures that the PT is operated at it's optimal operation frequency, which ensures soft switching operation and a constant gain. As a result a 6.5 W PT based PFC LED drive has been developed, supplied from 230 V 50 Hz AC mains, achieving a power factor of 0.96.**

***Index Terms*—Piezoelectric Transformer, LED, PFC, Forward Conduction Mode control.**

I. Introduction

FOR low power applications, such as LED illumination [1], [2], the Piezoelectric Transformer (PT) offers minimization of component count and overall size [3]–[7], as well as potential high efficiency [4]–[7] and low production cost. The market of AC mains supplied illumination is very competitive, demanding low product prices, making it challenging to enter the market. But as LED's performance is rising and the price is falling, LED illumination is getting more and more popular as an more environmentally friendly alternative to traditional illumination [2], [8]–[13]. One of the challenges of AC mains supplied illumination is the EN61000-3-2 requirement of Power Factor Correction (PFC).

In this paper a new Forward Conduction Mode (FCM) control method for PT based power converters is proposed, as well as a PT based LED drive facilitating passive PFC is developed. Fig. 1 illustrates a functional block diagram of the proposed PT LED drive, which consist of an input filter, a full-bridge rectifier, an inductor-less half-bridge drive, with FCM control and the PT, followed by an output rectifier and the LED load. In order to achieve consistent and efficient operation, the inductor-less half-bridge topology requires a zero voltage switching (ZVS) optimized PT [3], [14]–[16]. This application utilizes a 20 mm radial mode ZVS optimized PT [7], [17]–[19]. Usually a series inductor is necessary, in order to achieve ZVS operation and avoid large hard switching losses. But with the elimination of a bulky series inductor, the size and cost of the driver is minimized.

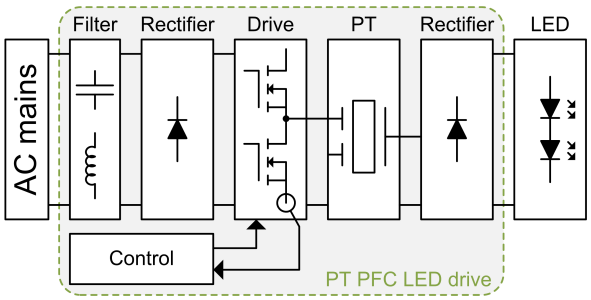

Fig. 1: Functional block diagram of the PT LED drive, employing passive PFC and Forward Conduction Mode (FCM) control

The operation frequency is one of the most critical parts, when utilizing PT based converters, as the PT resonance frequency is very narrow [3], [5]–[7], [14]–[16], [20]–[22]. Some of the most common control methods are Phase Lock Loop's (PLL) [23]–[27] and resonance current control [28], but self-tuned control has also been proposed [29]. In this work a new FCM control method is proposed and relies on a detection of the forward conduction period of the half-bridge switches, which reflects the resonance current phase-lag. The control method is fairly simple and ensures a controlled and optimal operation frequency, which ensures soft switching operation and a constant gain.

PFC can be obtained in various ways and for higher power and high quality converters, this is typically obtained in the first of two stages, but for low power and low price converters only a single stage is feasible. In PT based converters several single stage charge-pump topologies offers PFC [28], [30]–[33], but has demanding requirements for the PT. In this approach PFC is obtained simply by having a sufficiently small input buffer capacitor, allowing the half-bridge supply voltage to be modulated by the 100 Hz rectified AC mains voltage. As a result the output power has 100 Hz modulation as well, however this is acceptable for this LED application. Furthermore this design has no load regulation, as the LED's resembles a fairly constant load and the implementation of load regulation will just increase complexity and price.

In the following subsection a basic introduction to PT's is

Danish National Advanced Technology Foundation grant no. HTF-008-2008-3

*Department of Electrical Engineering, Technical University of Denmark, Kongens, Lyngby DK-2800, Denmark (e-mail: msr@elektro.dtu.dk; ma@elektro.dtu.dk)

†Fairchild Semiconductor GmbH, D-82256 Fuerstenfeldbruck, Germany (e-mail: michael.weirich@fairchildsemi.com)

This article has been accepted for publication in a future issue of this journal, but has not been fully edited. Content may change prior to final publication.

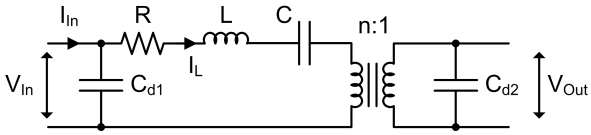

Fig. 2: Lumped parameter model, which describes the behavior of the PT in a narrow band around the operating resonance mode [35].

TABLE I: Lumped parameter model parameters of the utilized 20 mm radial mode PT.

R	L	C	C_{d1}	C_{d2}	n
12.4 Ω	9.46 mH	219 pF	1.19 nF	131 nF	8.15

given. Section II describes the utilized inductor-less half-bridge topology, its operation and how passive PFC is obtained. Section III presents and explains the proposed FCM control. And finally section IV presents a developed prototype PT LED drive, which is verified trough experimental results, followed by a conclusion in section V.

A. The Piezoelectric Transformer

PT's are based on piezoelectric ceramic materials, which has an electromechanical coupling. A PT is basically two piezoelectric elements joined together to form a transformer. The primary side element is then exited by an electrical AC voltage, which induces a deformation of the joined PT structure. The deformation of the secondary element generates an output voltage and through proper PT design, a desired primary to secondary voltage conversion can be obtained. In order to convert energy at a high efficiency, the PT is operated in one of its resonance modes [6], [7], [34]. The PT resonates each time it is possible to generate a standing sound wave in the structure. But in order to obtain the highest efficiency, the PT design is usually optimized for one specific resonance mode [6], [7], [34].

The electromechanical structure resembles a distributed network, but for simplicity and mathematical representation, normally only the resonance mode of interest is modeled [6], [7]. One of the most used PT models is the lumped parameter model [6], [7], [21], [22], [35], which is illustrated in Fig. 2. The model is basically an electrical LCC resonance tank and the behavior of a PT based converter is also quite similar to a traditional resonance converter.

The PT used for this application is a 20 mm radial mode PT [7], [17]–[19] and its primary resonance frequency is approximately 114 kHz. The PT is not designed for this particular application, which results in a degradation in efficiency. The PT has the model parameters of table I and is not treated in further detail in this paper.

II. Inductor-less half-bridge topology

The proposed PT LED drive utilizes an inductor-less half-bridge topology [3], [14]–[16], [22], [26], which eliminates the bulky series inductor and only converts energy through

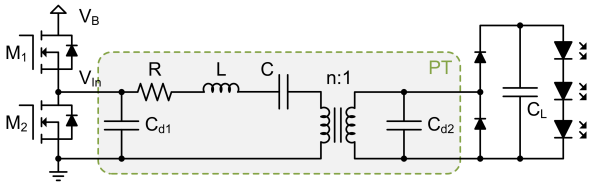

Fig. 3: Schematic diagram of the inductor-less half-bridge topology.

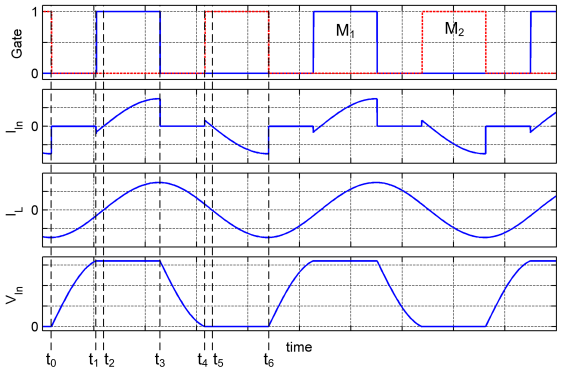

Fig. 4: Operational waveforms of the inductor-less half-bridge topology.

the electromechanical PT resonance tank. Fig. 3 illustrates the inductor-less half-bridge, consisting of a MOSFET based half-bridge, the lumped parameter mode, a half-bridge output rectifier and a output voltage buffer capacitor, followed by the LED load. Usually a series inductor is required in the PT based half-bridge topology [5], [29], in order to achieve ZVS operation of the half-bridge switches and avoid large hard switching losses, in connection to the PT input capacitor C_{d1}. But through a ZVS optimized PT design, soft switching can be obtained without auxiliary components [3], [14]–[16], [19]. However ZVS operation of a ZVS optimized PT is only obtainable in a narrow frequency band, located just above the operating resonance frequency, where the series resonance (L and C of the lumped parameter model) becomes inductive and possesses enough resonating energy to charge and discharge C_{d1}. Hence the excitation frequency is key, in order to achieve ZVS, consistent and efficient operation.

A. Operational principle

Fig. 4 illustrates the steady-state operation of the inductor-less half-bridge PT topology, which is operated slightly above its resonance frequency, where inductivity and resonating energy are maximized. The circuit (Fig 3) has 6 modes of operation, divided into the following periods:

$\mathbf{t_0 - t_1}$: Both switches are turned of in this period and the reverse resonance current I_L charges the input capacitor C_{d1}.

$\mathbf{t_1 - t_2}$: When the input capacitor C_{d1} is charged to the supply voltage the body diode of M_1 conducts the reverse resonance current I_L and it is in this period M_1 is switched

This article has been accepted for publication in a future issue of this journal, but has not been fully edited. Content may change prior to final publication.

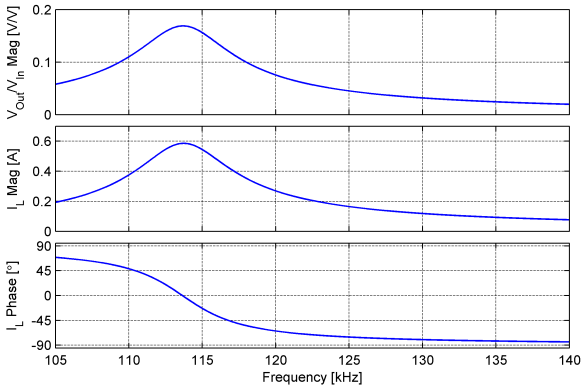

Fig. 5: Magnitude and phase plot of the resonance current I_L (2), at a 152V rms AC input voltage V_{In} (first harmonic of the half-bridge applied V_{In}), as well as a magnitude plot of the voltage conversion. It can clearly be seen that the resonance current phase-lag increases as the frequency increases above the resonance frequency, as well as the resonance current and voltage conversion magnitude decreases.

on, achieving ZVS.
$\mathbf{t_2 - t_3}$: At t_2 the resonance current I_L is inverted, switch M_1 conducts the resonance current I_L and transfers energy to the resonance tank.
$\mathbf{t_3 - t_4}$: At t_3 switch M_1 is turned off and the resonance current I_L discharges the input capacitor C_{d1}.
$\mathbf{t_4 - t_5}$: When the input capacitor C_{d1} is totally discharged the body diode of M_2 conducts the resonance current I_L and it is in this period M_2 is switched on, achieving ZVS.
$\mathbf{t_5 - t_6}$: At t_5 the resonance current I_L is reversed and the resonance current I_L is freewheeling through switch M_2. The period ends at t_6, where M_2 is switched off and a new cycle begins.

As mentioned the switches should be turned on in between the time periods $t_1 - t_2$ and $t_4 - t_5$, so sufficient dead-time should be supplied to the gate signals, in order to utilize the ZVS capability.

B. Power factor correction

The PT LED drive utilizes passive PFC, which is achieved by having a sufficiently small supply voltage buffer capacitor C_B, after the input full-bridge rectifier. In this way the half-bridge supply voltage V_B will follow the rectified AC mains voltage and the resonance current will be proportional to the excitation voltage, as shown in (2) (assuming a consistent operation point and load). The transfer function (1) describes the voltage conversion of the lumped parameter model (Fig. 2) and (2) describes the resonance current, where an AC input voltage V_{In} is applied, Z_{In} is the PT input impedance (excluding C_{d1}) and R_L is the load resistance.

$$\frac{V_{Out}}{V_{In}} = \frac{\frac{1}{j\omega C_{d2}} \| R_L}{(R + j\omega L + \frac{1}{j\omega C})/n^2 + (\frac{1}{j\omega C_{d2}} \| R_L)} \frac{1}{n} \quad (1)$$

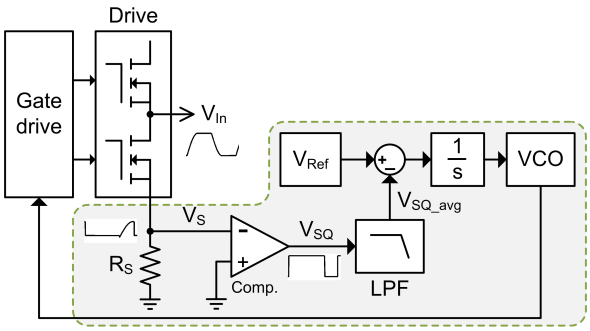

Fig. 6: Block diagram of the FCM control scheme, composing a forward conduction detector (Comp.), an averaging low-pass filter, an error signal generating subtracter, an integrator and a VCO.

$$I_L = \frac{V_{In}}{Z_{In}} = \frac{V_{In}}{R + j\omega L + \frac{1}{j\omega C} + (\frac{1}{j\omega C_{d2}} \| R_L) n^2} \quad (2)$$

Fig. 5 illustrates the resonance current magnitude and phase in relation to the frequency, as well as the voltage conversion. As it can be seen from (2) the resonance current is directly proportional to the input voltage V_{In}, at a constant operating frequency, which leads to the current drawn from the AC mains is proportional to the AC mains voltage.
This is a very simple way of achieving PFC, no additional components or control are required and in fact it minimizes the components, as the buffer capacitor C_B typically is quiet large, in order to buffer energy for 10 ms (100 Hz). The drawback of doing it this way is that the converted power is modulated by the 100 Hz of the rectified AC mains, hence the output power will also have this modulation. This 100 Hz output power modulation is acceptable for this LED application, but for other DC output applications this PFC method might not be applicable. Furthermore this PFC method has no line and load regulation, resulting in output power variations in connection to AC mains voltage variations. This is again acceptable for this application, but line and load regulation can be achieved and implemented in the control to some extend, by modulating the operation point.

III. Proposed Forward Conduction Mode Control Method

As described in the previous section, a precise and controlled excitation frequency is crucial, in order to achieve sustained ZVS operation of the half-bridge switches, but also to ensure a constant operation point. The resonance frequency of the PT varies somewhat with temperature and aging, which also should be tracked and compensated.
The proposed control method accommodate these challenges and as the name implies, the control method relies on a detection of the forward conduction period of half-bridge switches, essentially measuring the periods $t_2 - t_3$ and $t_5 - t_6$ (Fig. 4). Besides having the advantage of sustaining a optimal operation frequency, the FCM control is also very simple and hence low cost, as well as it is purely primary based,

This article has been accepted for publication in a future issue of this journal, but has not been fully edited. Content may change prior to final publication.

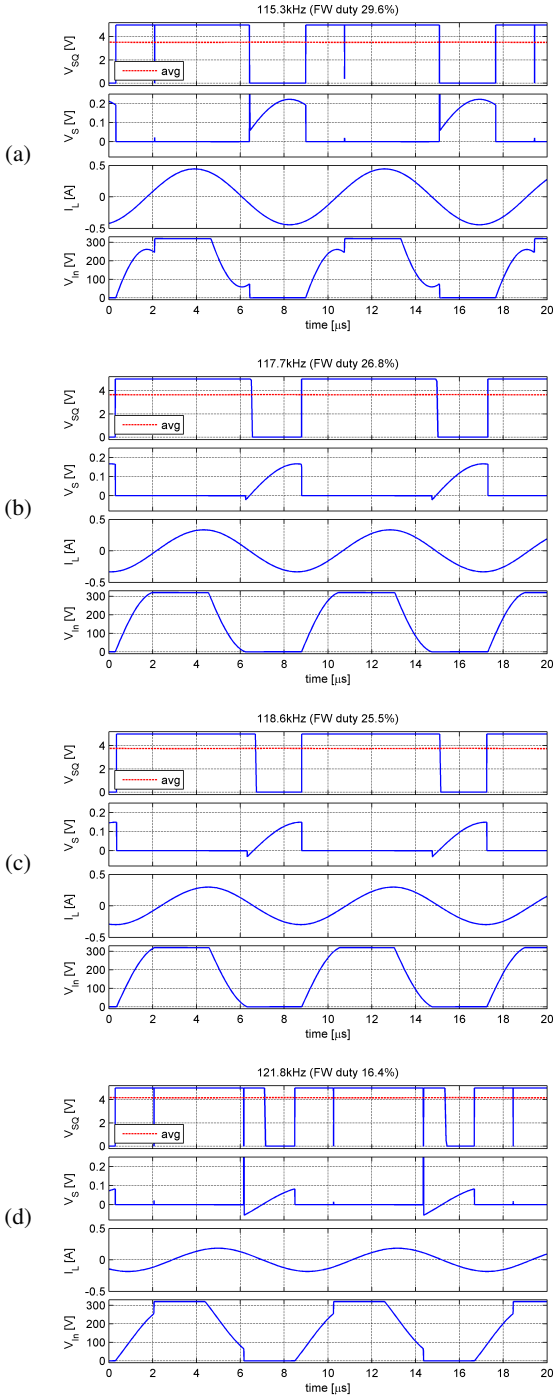

Fig. 7: Forward conduction mode control operation waveforms, at different operation frequencies and with constant dead-time, illustrating the forward conduction period variation. a and d is clearly operated under hard switching, whereas b and c is soft switching.

not needing signals to cross the primary secondary isolation barrier.

The resonance current I_L (2) has a phase-lag in relation to the input voltage V_{In}, due to the operation above the resonance frequency, in order to achieve ZVS operation. This phase-lag is illustrated in Fig. 5 and is reflected in the forward conduction period, as the switches forward conduction is getting limited at increasing phase-lag and this can be used as a feedback signal. At a specific phase-lag, hence a specific forward conduction period, the inductivity and resonating energy are maximized and ZVS capability is maximized.

Fig. 6 illustrates a functional block diagram of the proposed FCM control method. The essential parts are the sense resistor R_S and the comparator, which detects the forward conduction period of the low side switch. Only a low side current measurement is performed, since this is very simple with a sensing resistor, and using both low and high sensing only increases sensitivity, on the expense of circuit complexity. The comparator produces a square-wave signal V_{SQ} from the current measurement V_S, containing the forward conduction period information, and in this configuration the signal is inverted, assuming a high output when the sensing signal V_S is zero. This signal is passed through an averaging low-pass filter, where the average signal value is proportional to the forward conduction period (3).

$$V_{SQ\_avg} = V_{CC} \cdot \frac{T - T_{FW}}{T} = V_{CC}(1 - D_{FW}) \quad (3)$$

The average signal is compared with a reference and the error signal is passed to an integrator, that controls a voltage controlled oscillator (VCO). The VCO drives the gate-drive, which closes the loop around the half-bridge.

The FCM control operation is illustrated in Fig. 7, at different operation frequencies. It can be seen how the forward conduction period increases, as the frequency is decreased towards the resonance frequency, as well as the resonance current I_L increases and the average V_{SQ} signal decreases. When the frequency is increased away from the resonance frequency the resonance current I_L decreases, the forward conduction period decreases and the average V_{SQ} signal increases. The two operating points at 117.7 kHz and 118.6 kHz (Fig. 7 b and c) are located close to the boundary of ZVS operation and in between these boundaries ZVS operation is sustained, which also can be observed on the switching flanks of the input signal V_{In}. Beyond these boundaries ZVS operation is not possible and this is also clear at 115.3 kHz and 121.8 kHz (Fig. 7 a and d), where hard switching of the input signal V_{In} is observed. But most importantly the forward conduction period and the average signal V_{SQ_avg}, are modulated continuously over the frequency range, making it a very applicable feedback signal. As the point of maximal soft switching capability and optimal operation is located at a specific resonance current phase lag of approximately 56^o [3], [6], [7], [14]–[16], [20], this point of operation is also linked to a specific forward conduction duty cycle of approximately 26%.

The reference signal should be selected to match the average signal V_{SQ_avg} (3) at this forward conduction duty cycle and with a local supply voltage V_{CC} of 15 V, a 11.1 V reference

This article has been accepted for publication in a future issue of this journal, but has not been fully edited. Content may change prior to final publication.

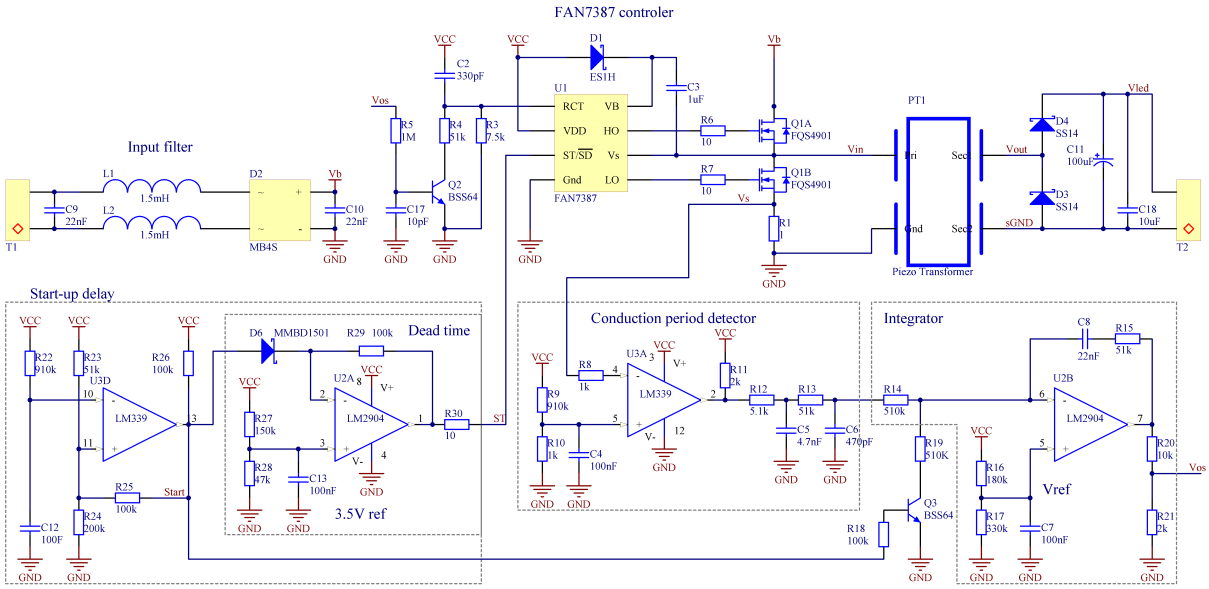

Fig. 8: Schematic of prototype PT LED drive, resembling the fundamental blocks of the converter and the FCM control, with the addition of a start-up delay and dead time reference circuit.

signal is selected (4).

$$V_{Ref} = V_{SQ\_avg} = V_{CC}(1-D_{FW}) = 15\,V(1-0.26) = 11.1\,V \quad (4)$$

In this manner the FCM control seeks to maintain a constant forward conduction duty cycle of 26%, and hence a constant resonance current phase lag of 56^o, ensuring operation at the optimal point of operation.

A clear advantage of this control method is that the feedback signal is not dependent on signal magnitude, such as the resonance current, as the magnitude is modulated by the AC mains for this passive PFC application. Although the zero voltage crossing remains a challenge, as the resonance current also reaches zero, making it impossible to detect a forward conduction period. But this is also a challenge for all other control methods and is typically managed by having a very slow control loop. Furthermore the control method is applicable for variable load and output power, as the optimal point of operation still is linked to the resonance current phase lag and forward conduction period. Although the gain and soft switching capability are load dependent and are changing with load variations.

IV. Experimental results

The presented designs were implemented and validated in a developed prototype PT LED drive and the results is presented and disused in the following section. Pictures of the prototype PT LED drive is shown in Fig. 10 and Fig. 8 shows the circuit schematic of the implementation. The prototype is developed as a PT based solution of a Fairchild $FL6961$ Single-Stage Flyback 8.4 W LED design proposal. The prototype is designed for 230 V 50 Hz AC mains supply and 6.5 W output power, it has an input filter and a full-bridge rectifier. It utilizes a 20 mm radial mode PT and is operated at approximately 117 kHz. Furthermore 3 series coupled $OSLON\ SSL$ 80 LED's forms the LED load, where the LED load has a nominal voltage of 9.6 V and current of 350 mA. In Fig. 9 the operational waveforms of the LED load is shown, where the 100 Hz modulation is obvious.

The converter uses the $FAN7387$ controller, as it comes with a build-in relaxation oscillator and a gate-drive, with a programmable dead-time. The control loop is build around $U3A$ and $U2B$, where the comparator $U3A$ detects the forward conduction period and produces the square-wave signal. The averaging low-pass filter is implemented with two first order RC low-pass filters, with a corner frequency of 6.6 kHz.

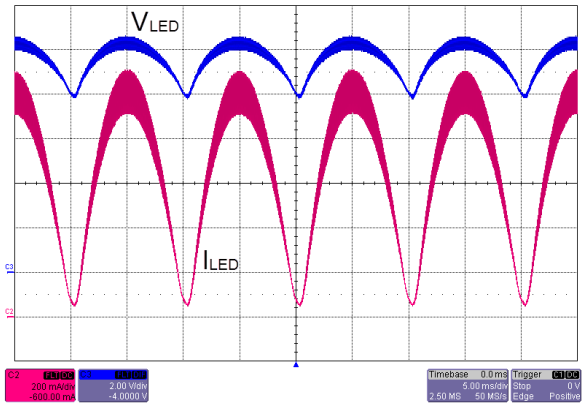

Fig. 9: LED load waveforms, with a 100 Hz output modulation and an 6.5 W average output power. V_{LED} [Ch3: 2 V/div], I_{LED} [Ch2: 200 mA/div], time base [5 ms/div].

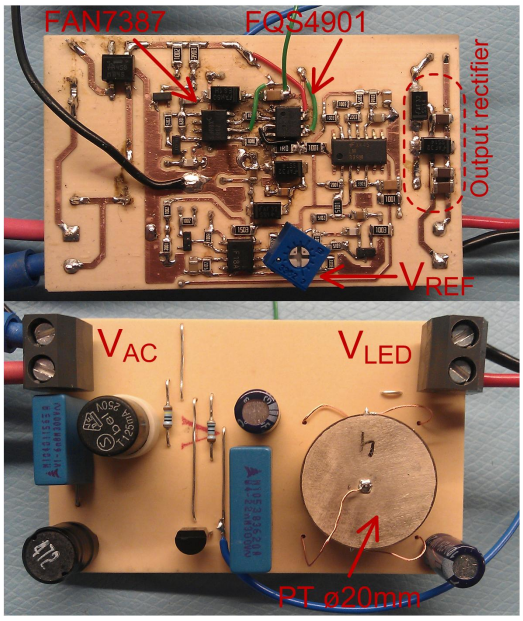

Fig. 10: Developed prototype LED PT drive, showing the top and bottom side of the PCB. It utilizes the $FAN7387$ controller and a 20 mm ZVS optimized radial mode PT, operated at approximately 117 kHz. The PCB has a size of 39.5 x 65 mm.

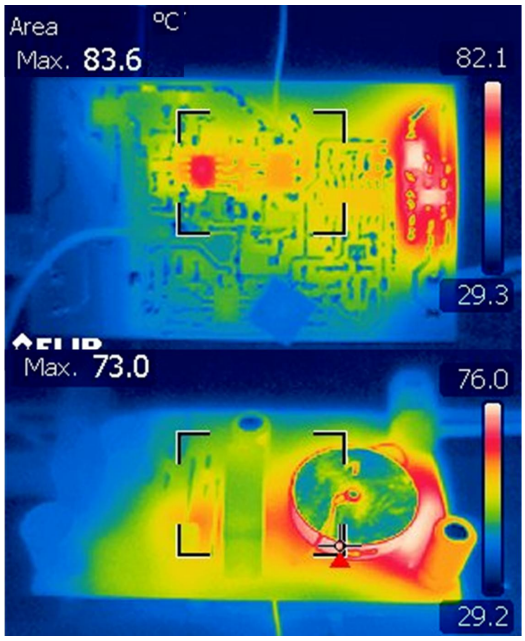

Fig. 11: Thermal IR images of the developed prototype LED PT drive, showing the top and bottom side of the PCB. The colors indicate the temperature, with light colors being hot and dark colors less hot. The temperature of the PT is misleading, as the PT has a silver electrode on the top, which prevents IR radiation. But a PT temperature of 73° C can be seen, as well as the heat from the output rectifier can be observed through the PCB.

The integrator is implemented around the operational amplifier $U2B$ and it controls the resistance of the relaxation oscillator, closing the control loop. For this PFC application the crossover frequency of the integrator is 14.2 Hz, in order to suppress the influence of the zero voltage crossing.
The relative high dead-time required resulted in an abnormal startup of the controller, as the programmable dead-time pin ($ST/\overline{DT}$) also functions as a shutdown input. In order to work around this the operational amplifier $U2A$ supplies the pin with a low impedance voltage, instead of the traditional way of setting the voltage with a resistor. Furthermore comparator $U3B$ ensures a certain startup delay, as well as it initializes the integrator trough $Q3$, ensuring a smooth startup and initialization of a high operation frequency.
The utilized radial mode PT occupies a relative large PCB area, but offers a very low profile (4 mm PT thickness) and small overall size of the prototype. The size can be minimized even further by replacing the electrolytic capacitors with ceramic capacitors, as well as the input filter and circuit can be further compressed, by using smaller packaging and a denser layout. Furthermore the control circuits could be integrated into a controller IC, which both minimizes cost and size. In the design process the prototype size has not been targeted in particular, but the prototype still offers a reasonable small size, which is compared to the Fairchild $FL6961$ LED design proposal in table II.

TABLE II: Size comparison of the prototype PT LED drive and the Fairchild $FL6961$ LED design proposal.

	Prototype	Fairchild	
Output power	6.5	8.4	W
Height	15.0	25.5	mm
Width	39.5	38.1	mm
Length	65.0	49.5	mm
Volume	38.5	48.1	cm^3

A. Power factor correction

The AC mains input current of Fig. 12 is both in phase with the input voltage and it somewhat resembles a sinusoidal, although it has some distortion. And with a measured power factor of 0.96, the circuit demonstrates the ability of PFC. In Fig. 13 it shown how the prototype complies with the EN61000-3-2 standard for current harmonics of Class C devices and as it can be seen the prototype fails to comply. But it only slightly exceeds the limits for the second and fifth harmonic and it is expected that the harmonics can be improved through further optimization of the circuit and control, which is discussed further in the following section.

This article has been accepted for publication in a future issue of this journal, but has not been fully edited. Content may change prior to final publication.

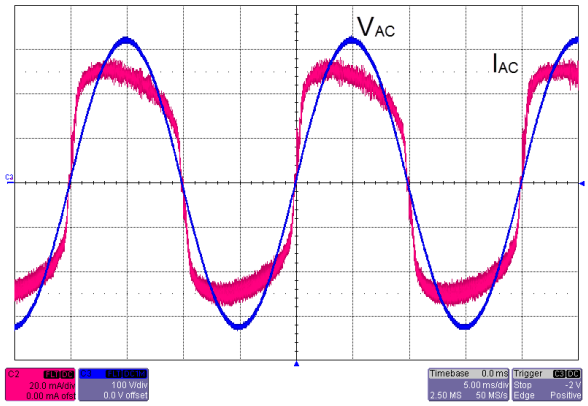

Fig. 12: AC mains input voltage and current, having an input power of 9.5 W and a power factor of 0.96. V_{AC} [Ch3: 100 V/div], I_{AC} [Ch2: 20 mA/div], time base [5 ms/div].

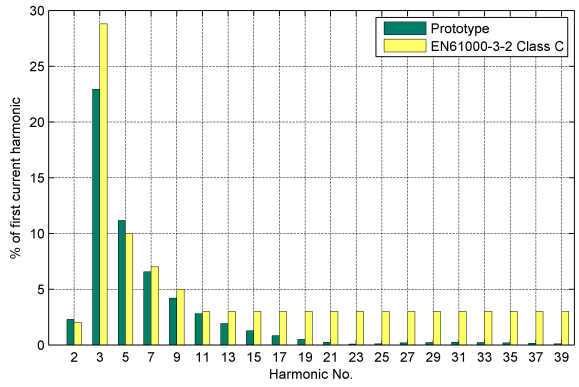

Fig. 13: Comparison of prototype measurements and the EN61000-3-2 standard for current harmonics of Class C devices.

B. Forward conduction mode

As described earlier the FCM control method is based on a forward conduction period detection, which is realized with a current sense resistor and a comparator. The operational waveforms of the current sense (V_S) and comparator square-wave (V_{SQ}) are shown in Fig. 14, near AC mains peak voltage, as well as the PT input voltage (V_{In}). The figure demonstrates and validates the functionality of the proposed FCM control method, as well as ZVS operation of the half-bridge can be observed. On top of the sensed resonance current a high frequency signal can be seen. This is one of the higher frequency mode shapes of the PT, which is exited somewhat, but does not affect the functionality of the FCM control. Taking a closer look at the PT input voltage (V_{In}), it can be observed that the half-bridge supply voltage has some variance and is not constant as compared to Fig. 4. This is because of the relative low buffer capacitor C_{10} of 22 nF, which allows the resonance current to charge the voltage a little bit and then discharge it, as the resonance tank is charged.

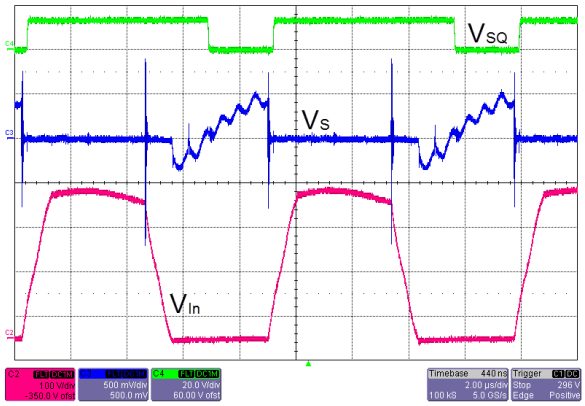

Fig. 14: Forward conduction mode waveforms, demonstrating the FCM functionality and has a 26.4 % forward duty. V_{In} [Ch2: 100 V/div], V_S [Ch3: 500 mV/div], V_{SQ} [Ch4: 20 V/div], time base [2 μs/div].

In Fig. 15 the average square-wave feedback signal ($V_{SQ,avg}$) is shown in relation to the AC mains voltage (V_{AC}). As it can be seen, the feedback signal is fairly constant, with the exception near zero voltage crossing. This is due to the fact that the resonance current also reaches zero, making it impossible to detect a forward conduction period. This issue were expected and in order to have a minimal influence, it is suppressed by having a integrator crossover frequency of only 14.2 Hz.

By taking a closer look at the average feedback signal ($V_{SQ,avg}$), it can be seen that the "constant" part of the signal in fact has a periodic modulation. Due to the very slow control loop, this is not caused by a variation in operation frequency. This is reflecting a change in operation condition and operation point of the PT, as the LED load does not resemble a resistive load. Therefore the load impedance seen by the PT also has a

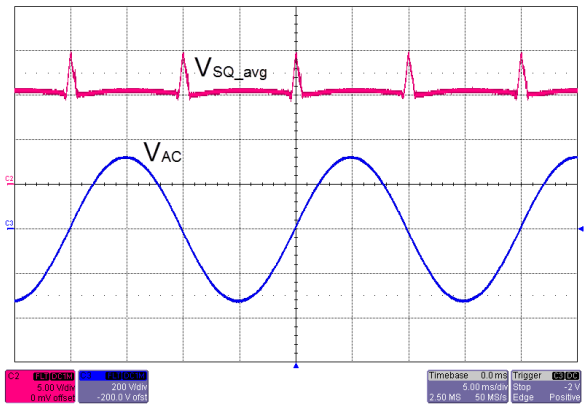

Fig. 15: Forward conduction mode feedback signal in relation to the AC mains voltage, revealing dropouts in the feedback signal near the zero voltage crossing. V_{SQ_avg} [Ch2: 5 V/div], V_{AC} [Ch3: 200 V/div], time base [5 ms/div].

This article has been accepted for publication in a future issue of this journal, but has not been fully edited. Content may change prior to final publication.

100 Hz modulation, which results in a change in operation condition and resonance frequency. This might suggest to have a faster reacting control loop, which can compensate this change in operation condition, and then take care of the zero voltage crossing in another way. A solution could be to freeze or pause the integrator near the zero voltage crossing and thereby ignoring the dropout in the feedback.
The change in operation point has a negative influence on the PFC and results in a distortion of the input current, which was observed in the previous section. The passive PFC requires a constant operation point, in order to achieve a resonance current proportional to the AC mains voltage. As the operation point changes the resonance current is in fact not proportional to the AC mains voltage, which degrades the fundamental operational principle of the passive PFC. This results in a little too large resonance current at low voltages and a little too small resonance current at high voltages and explains the somewhat "pressed down" and degraded sinusoidal input current of Fig. 12, which degrades the PFC performance. A faster reacting control loop will improve the PFC performance, as the control will be able to track and compensate these changes in operation condition. Again the zero voltage crossing needs to be taken care of in another way. The main advantage of the implemented slow control loop is that it copes with the zero voltage crossing, as well as no additional support circuits is needed.

C. Efficiency

The efficiency has not been the main focus point in this research, as well as the utilized PT is not optimized for this particular application, which results in a moderate efficiency. By calculation the efficiency of AC mains input power of Fig. 12 and the output power of Fig. 9, it results in a very moderate efficiency of 68 % (5).

$$\eta = \frac{P_{Out}}{P_{In}} = \frac{P_{LED}}{P_{AC}} = \frac{6.5[W]}{9.5[W]} = 68\ \% \tag{5}$$

As the thermal images of Fig. 11 reveals, the PT and the half-bridge output rectifier are the biggest sources of heat. And it is also within these components the biggest improvements of the overall efficiency can be obtained. In table III a loss breakdown is conducted, where it is obvious that the PT is the most inefficient component, which is a result of the utilized "off the shelf" non-application optimized PT. The PT is the main efficiency limiting factor for this prototype and by utilizing an application optimized PT, efficiencies above 90 % are achievable. A optimized redial mode PT can be achieved through the design process presented in [19] or [17], where the PT is designed to match the applied load, have a desired gain, which matches the input and output voltages, as well as matching the desired load power, and finally the PT is designed to possess soft switching capabilities. Other step-down PT structures can also be utilized, such as thickness mode PT's [4], [36]–[38], using the same optimization criteria. Furthermore by utilizing an active full-bridge output rectifier, efficiency improvements of 2-5 % points can be expected.

TABLE III: Loss breakdown of the prototype LED PT drive.

Output power	6.51 W	
MOSFET drive	0.26 W	2.7 %
PT	1.88 W	19.7 %
Output rectifier	0.60 W	6.3 %
Efficiency		68.3 %

V. Conclusion

A new Forward Conduction Mode (FCM) control method has been proposed and investigated in this paper. The FCM control method relies on the phase information of the PT resonance current running in the half-bridge switches, which is reflected in the forward conduction period of the switches. The proposed FCM control has been investigated in detail and has demonstrated to operate the PT at it's optimal operation frequency, which ensures soft switching operation and a constant gain.
Furthermore a PT based PFC LED drive has been proposed and developed. The devolved prototype is supplied from 230 V 50 Hz AC mains and produces a low voltage 6.5 W output, for three series coupled LED's. The background and functionality of the utilized inductor-less half-bridge topology has been investigated and explained in detail.
A very simple passive PFC method has been proposed, which has demonstrated good PFC capabilities, demonstrating a power factor of 0.96 and is on the boundary of comply with the EN61000-3-2 standard. The resulting PFC capability has been evaluated and suggestions for improvements have been put forward, in order to improve the PFC capability and comply with the EN61000-3-2 standard.
Moreover the developed prototype shows good opportunity for minimization and the circuit can be compressed even further. The control circuits can be greatly compressed or even integrated, leaving the PT and the input filter as the only large components.

Acknowledgment

The authors would like to thank Noliac A/S for supplying prototype PT's, as well as general PT design support. We would like to tank Fairchild Semiconductors for making this collaboration possible. We would also like to thank the Advanced Technology Foundation for their financial support.

References

[1] Z. Ye, F. Greenfeld, and Z. Liang, "A topology study of single-phase offline AC/DC converters for high brightness white LED lighting with power factor pre-regulation and brightness dimmable," in *Industrial Electronics, 2008. IECON 2008. 34th Annual Conference of IEEE*. IEEE, 2008, pp. 1961–1967.
[2] F. Yam and Z. Hassan, "Innovative advances in LED technology," *Microelectronics Journal*, vol. 36, no. 2, pp. 129–137, 2005.
[3] K. Meyer, M. Andersen, and F. Jensen, "Parameterized analysis of zero voltage switching in resonant converters for optimal electrode layout of piezoelectric transformers," in *Power Electronics Specialists Conference, 2008. PESC 2008. IEEE*. IEEE, 2008, pp. 2543–2548.
[4] T. Bove, W. Wolny, E. Ringgaard, and K. Breboel, "New type of piezoelectric transformer with very high power density," in *Applications of Ferroelectrics, 2000. ISAF 2000. Proceedings of the 2000 12th IEEE International Symposium on*, vol. 1. IEEE, 2000, pp. 321–324.

[5] E. Horsley, M. Foster, and D. Stone, "State-of-the-art piezoelectric transformer technology," in *Power Electronics and Applications, 2007 European Conference on*. IEEE, 2007, pp. 1–10.

[6] C. Lin, "Design and analysis of piezoelectric transformer converters," Ph.D. dissertation, Virginia Polytechnic Institute and State University, 1997.

[7] R. Lin, "Piezoelectric transformer characterization and application of electronic ballast," Ph.D. dissertation, Virginia Polytechnic Institute and State University, 2001.

[8] H. Chiu, Y. Lo, J. Chen, S. Cheng, C. Lin, and S. Mou, "A high-efficiency dimmable LED driver for low-power lighting applications," *Industrial Electronics, IEEE Transactions on*, vol. 57, no. 2, pp. 735–743, 2010.

[9] H. Chiu, H. Huang, H. Yang, and S. Cheng, "An improved single-stage flyback PFC converter for high-luminance lighting LED lamps," *International Journal of Circuit Theory and Applications*, vol. 36, no. 2, pp. 205–210, 2008.

[10] W. Yu, J. Lai, H. Ma, and C. Zheng, "High-efficiency DC–DC converter with twin bus for dimmable LED lighting," *Power Electronics, IEEE Transactions on*, vol. 26, no. 8, pp. 2095–2100, 2011.

[11] J. Zhang, H. Zeng, and T. Jiang, "A primary-side control scheme for high-power-factor LED driver with TRIAC dimming capability," *Power Electronics, IEEE Transactions on*, vol. 27, no. 11, pp. 4619–4629, 2012.

[12] Y. Hu, L. Huber, and M. Jovanovic, "Single-stage, universal-input AC/DC LED driver with current-controlled variable PFC boost inductor," *Power Electronics, IEEE Transactions on*, vol. 27, no. 3, pp. 1579–1588, 2012.

[13] J. Garcia, A. Calleja, D. Gacio Vaquero, L. Campa *et al.*, "Interleaved buck converter for fast PWM dimming of high-brightness LEDs," *Power Electronics, IEEE Transactions on*, vol. 26, no. 9, pp. 2627–2636, 2011.

[14] M. Rødgaard, T. Andersen, and M. Andersen, "Empiric analysis of zero voltage switching in piezoelectric transformer based resonant converters," in *PEMD 2012*. Institution of Engineering and Technology, 2012.

[15] E. Horsley, N. Nguyen-Quang, M. Foster, and D. Stone, "Achieving zvs in inductor-less half-bridge piezoelectric transformer based resonant converters," in *Power Electronics and Drive Systems, 2009. PEDS 2009. International Conference on*. IEEE, 2009, pp. 446–451.

[16] E. Horsley, A. Carazo, N. Nguyen-Quang, M. Foster, and D. Stone, "Analysis of inductorless zero-voltage-switching piezoelectric transformer-based converters," *Power Electronics, IEEE Transactions on*, vol. 27, no. 5, pp. 2471 –2483, may 2012.

[17] E. Baker, W. Huang, D. Chen, and F. Lee, "Radial mode piezoelectric transformer design for fluorescent lamp ballast applications," *Power Electronics, IEEE Transactions on*, vol. 20, no. 5, pp. 1213–1220, 2005.

[18] D. Nielsen, M. Andersen, and K. Meyer, "Preliminary investigations of piezoelectric based LED luminary," in *Power Electronics and Applications (EPE 2011), Proceedings of the 2011-14th European Conference on*. IEEE, 2011, pp. 1–9.

[19] K. Meyer and M. Andersen, "One-shot design of radial mode piezoelectric transformer for magneticless power conversion," in *26. Annual IEEE Applied Power Electronics Conference and Exposition 26*, 2011, pp. 498–504.

[20] K. S. Meyer, "Modeling of Piezoelectric Transformers and Generic Circuit Analysis for Miniaturization of Piezoelectric Power Converters," *Master thesis*, October 2008.

[21] S. Bronshtein, A. Abramovitz, A. Bronshtein, and I. Katz, "A method for parameter extraction of piezoelectric transformers," *Power Electronics, IEEE Transactions on*, vol. 26, no. 11, pp. 3395–3401, 2011.

[22] Y. Yuanmao, K. Cheng, and K. Ding, "A novel method for connecting multiple piezoelectric transformer converters and its circuit application," *Power Electronics, IEEE Transactions on*, vol. 27, no. 4, pp. 1926–1935, 2012.

[23] S. Ben-Yaakov and S. Lineykin, "Maximum power tracking of piezoelectric transformer HV converters under load variations," *Power Electronics, IEEE Transactions on*, vol. 21, no. 1, pp. 73–78, 2006.

[24] C. Lin, Y. Chen, J. Chen, and F. Wen, "The elimination of the temperature effect on a piezoelectric transformer in a backlight inverter based on the phase-locked loop technique," in *Mechatronics, 2005. ICM'05. IEEE International Conference on*. IEEE, 2005, pp. 828–833.

[25] J. Alonso, C. Ordiz, and M. Dalla Costa, "A novel control method for piezoelectric-transformer based power supplies assuring zero-voltage-switching operation," *Industrial Electronics, IEEE Transactions on*, vol. 55, no. 3, pp. 1085–1089, 2008.

[26] J. Alonso, C. Ordiz, M. Dalla Costa, J. Ribas, and J. Cardesin, "High-voltage power supply for ozone generation based on piezoelectric transformer," *Industry Applications, IEEE Transactions on*, vol. 45, no. 4, pp. 1513–1523, 2009.

[27] S. Nakashima, T. Ninomiya, H. Ogasawara, and H. Kakehashi, "Piezoelectric-transformer inverter with maximum-efficiency tracking and dimming control," in *Applied Power Electronics Conference and Exposition, 2002. APEC 2002. Seventeenth Annual IEEE*, vol. 2. IEEE, 2002, pp. 918–923.

[28] S. Choi, K. Lee, and B. Cho, "Design of fluorescent lamp ballast with PFC using a power piezoelectric transformer," *Industrial Electronics, IEEE Transactions on*, vol. 52, no. 6, pp. 1573–1581, 2005.

[29] J. Díaz, F. Nuño, M. Prieto, J. Martin-Ramos, and P. Villegas Saiz, "Closing a second feedback loop in a DC–DC converter based on a piezoelectric transformer," *Power Electronics, IEEE Transactions on*, vol. 22, no. 6, pp. 2195–2201, 2007.

[30] J. Zhou, F. Tao, and F. Lee, "Inductor-less charge pump PFC electronic ballast," in *Industry Applications Conference, 2001. Thirty-Sixth IAS Annual Meeting. Conference Record of the 2001 IEEE*, vol. 1. IEEE, 2001, pp. 524–529.

[31] J. Qian, F. Lee, and T. Yamauchi, "A single-stage electronic ballast with power factor correction and low crest factor for fluorescent lamps," in *Industry Applications Conference, 1997. Thirty-Second IAS Annual Meeting, IAS'97., Conference Record of the 1997 IEEE*, vol. 3. IEEE, 1997, pp. 2307–2312.

[32] R. Lin and H. Shih, "Piezoelectric transformer based current-source charge-pump power-factor-correction electronic ballast," *Power Electronics, IEEE Transactions on*, vol. 23, no. 3, pp. 1391–1400, 2008.

[33] R. Lin, H. Shih, C. Liu, and K. Liu, "A Family of Piezoelectric Transformer-Based Bridgeless Continuous-Conduction-Mode Charge-Pump Power-Factor Correction Electronic Ballasts," *Industry Applications, IEEE Transactions on*, no. 99, pp. 1–1, 2011.

[34] G. Ivensky, I. Zafrany, and S. Ben-Yaakov, "Generic operational characteristics of piezoelectric transformers," *Power Electronics, IEEE Transactions on*, vol. 17, no. 6, pp. 1049–1057, 2002.

[35] W. Mason, *Electromechanical transducers and wave filters*. Van Nostrand Reinhold, 1946.

[36] A. Sánchez, M. Sanz, R. Prieto, J. Oliver, P. Alou, and J. Cobos, "Design of piezoelectric transformers for power converters by means of analytical and numerical methods," *Industrial Electronics, IEEE Transactions on*, vol. 55, no. 1, pp. 79–88, 2008.

[37] M. Sanz, A. Sanchez, P. Alou, R. Prieto, J. Cobos, and J. Uceda, "Step by step multi-layer piezoelectric transformer design procedure," in *Power Electronics Specialists Conference, 2004. PESC 04. 2004 IEEE 35th Annual*, vol. 6. IEEE, 2004, pp. 4669–4675.

[38] O. Ohnishi, H. Kishie, A. Iwamoto, Y. Sasaki, T. Zaitsu, and T. Inoue, "Piezoelectric ceramic transformer operating in thickness extensional vibration mode for power supply," in *Ultrasonics Symposium, 1992. Proceedings., IEEE 1992*. IEEE, 1992, pp. 483–488.

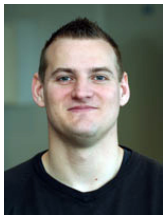

Martin S. Rødgaard received the M.Sc.E.E. in power electronics from the Technical University of Denmark, Kongens Lyngby, Denmark, in 2009. He is currently employed at Noliac A/S and is awaiting his Ph.D defense and degree at the Technical University of Denmark. His research interests include switch-mode power supplies, piezoelectric transformers and piezoelectric transformer based power converters, satellite power systems and power factor correction.

Michael A. E. Andersen (M'88) received the M.Sc.E.E. and Ph.D. degrees in power electronics from the Technical University of Denmark, Kongens Lyngby, Denmark, in 1987 and 1990, respectively. He is currently a Professor of power electronics at the Technical University of Denmark. Since 2009, he has been Deputy Director in the Department of Electrical Engineering. He is the author or coauthor of more than 100 papers. His research interests include switch-mode power supplies, piezoelectric transformers, power factor correction, and switch-mode audio power amplifiers.

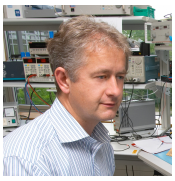

Michael Weirich received the M.Sc. in Physics in 1990 and the Ph.D. in Solid State Physics in 1995 from the 'Universität des Saarlandes', Saarbrücken, Germany. Since 1995 he has worked in R&D of signal processing, analog and power electronics for various companies. At OSRAM GmbH, Munich, Germany he designed electronic ballast for fluorescent lamps and led a team that developed a C based family of ballast with advanced features. Since 2003 he is the head of Fairchild Semiconductor's European application lab in Fürstenfeldbruck, Germany. This lab focuses on the design of power electronics and customer support in this area. Current research interests include high power converters and PSU based on SiC devices as well new topologies for LED lighting.

D.8 Self-oscillating loop based piezoelectric power converter

Patent - Pending

2011 (priority)
US 61/638,883

NIXON PEABODY LLP **PATENT**

Customer No. 70001 **059244-000014PL01**

U.S. PROVISIONAL PATENT APPLICATION

FOR

SELF-OSCILLATING LOOP BASED PIEZOELECTRIC POWER CONVERTER

BY

KASPER SINDING MEYER
MARTIN SCHØLER RØDGAARD
AND
THOMAS ANDERSEN

SELF-OSCILLATING LOOP BASED PIEZOELECTRIC POWER CONVERTER

FIELD OF THE INVENTION

[0001] Aspects of the present disclosure relate to a piezoelectric power converter, and more particularly, to a self-oscillating loop-based piezoelectric power converter.

BACKGROUND OF THE INVENTION

[0002] Piezoelectric transformer based power converters have good potential to substitute traditional magnetics based power converters in numerous voltage or power converting applications such as AC/AC, AC/DC, DC/AC and DC/DC power converter applications. Piezoelectric power converters are capable of providing high isolation voltages and high power conversion efficiencies in a compact package with low EMI radiation. The piezoelectric transformer is normally operated in a narrow frequency band around its fundamental or primary resonance frequency with a matched load coupled to the output of the piezoelectric transformer. The optimum operating frequency or excitation frequency shows strong dependence on different parameters such as temperature, load, fixation and age. Hence, it is a significant challenge to maintain the excitation frequency applied to the input section of the piezoelectric transformer at the optimum frequency during operation of the power converter where the above-mentioned parameter changes. This is particularly pronounced if burst-mode modulation of the input drive signal is utilized because rapid lock-on to the intended excitation frequency is required to avoid large driver losses by intermediate time periods where the input driver fails to operate under ZVS.

[0003] This problem is particularly pronounced for power converters that employ a piezoelectric transformer with native ZVS properties, i.e. with a ZVS factor larger than 100%, and exploit this property to obtain ZVS in an input driver coupled directly to the primary section of the piezoelectric transformer. In this context “directly” means without an external inductor arranged in series or parallel between the input driver and the primary section of the piezoelectric transformer. ZVS operation of the input driver, typically based on a half-bridge or full-bridge MOS transistor circuit, of piezoelectric power converters has traditionally been achieved by adding such an external inductor in series with the input driver. The external inductor ensures that the input of the piezoelectric transformer appears inductive across a relatively large frequency range

such that capacitances at an output node of the input driver can be alternatingly charged and discharged in accordance with the input drive signal without inducing prohibitive power losses.

[0004] However, the external inductor occupies space, adds costs and conducts and radiates EMI in the power converter. It would therefore be advantageous to provide a power converter based on a piezoelectric transformer with native ZVS properties capable of reliable ZVS operation despite changes in operational parameters of the piezoelectric transformer such as temperature, load, fixation and age. This has been achieved in a piezoelectric power converter in accordance with the present invention by the presence of a feedback loop operatively coupled between the output signal at the output electrode of the piezoelectric transformer and the input driver to provide a self-oscillation loop around the primary section of the piezoelectric transformer. Electrical characteristics of the feedback loop are configured such that the excitation frequency of the self-oscillation loop lies within the ZVS operation range of the piezoelectric transformer.

[0005] The IEEE paper by J. Díaz et al. "A Double-Closed Loop DC/DC Converter Based On A Piezoelectric Transformer" describes a piezoelectric power converter which comprises a self-oscillating feedback loop. The input driver is, however, coupled to the input of a piezoelectric transformer via a separate external input inductor to ensure ZVS operation.

SUMMARY OF THE INVENTION

[0006] The present invention relates to a piezoelectric power converter comprising an input driver electrically coupled directly to an input or primary electrode of the piezoelectric transformer without any intervening series or parallel inductor. A feedback loop is operatively coupled between an output voltage of the piezoelectric transformer and the input driver to provide a self-oscillation loop around a primary section of the piezoelectric transformer oscillating at an excitation frequency. Electrical characteristics of the feedback loop are configured to set the excitation frequency of the self-oscillation loop within a zero-voltage-switching (ZVS) operation range of the piezoelectric transformer.

[0007] A first aspect of the invention relates to a piezoelectric power converter comprising a piezoelectric transformer which comprises an input electrode electrically coupled to an input or primary section of the piezoelectric transformer and an output electrode electrically coupled to secondary or output section of the piezoelectric transformer to provide a transformer output

voltage. An input driver is electrically coupled directly to the input electrode of the piezoelectric transformer without any intervening series or parallel inductor to supply an input drive signal to the input electrode. A feedback loop is operatively coupled between the output voltage of the piezoelectric transformer and the input driver to provide a self-oscillation loop around the primary section of the piezoelectric transformer, oscillating at an excitation frequency. Electrical characteristics of the feedback loop are configured to set the excitation frequency of the self-oscillation loop within a ZVS operation range of the piezoelectric transformer.

[0008] In accordance with the present invention, the zero-voltage-switching factor (ZVS factor) of the piezoelectric transformer is larger than 100%, preferably larger than 120%, such as larger than 150% or 200%. This means that the piezoelectric transformer has native ZVS properties or characteristics.

[0009] The ZVS factor is determined at a matched load condition as:

$$ZVS = \frac{\left(k_{eff\_S}^{-2}\right)-1}{\left(k_{eff\_P}^{-2}\right)-1} 0.882 \ ;$$

$k_{eff\_P,}$ being a primary side effective electromechanical coupling factor of the piezoelectric transformer,

$k_{eff\_S,}$ being a secondary piezoelectric transformer effective electromechanical coupling factor, in which:

$$k_{eff\_P} = \sqrt{1 - \frac{f_{res\_p}^2}{f_{anti-res\_p}^2}} \qquad k_{eff\_S} = \sqrt{1 - \frac{f_{res\_s}^2}{f_{anti-res\_s}^2}}$$

f_{res_p} = resonance frequency and frequency of a minimum magnitude of an impedance function at the input electrodes of the piezoelectric transformer with shorted output electrodes,

$f_{anti\text{-}res\_p}$ = anti-resonance frequency and frequency of a maximum magnitude of the impedance function at the input electrodes of the piezoelectric transformer with shorted output electrodes,

f_{res_s} = resonance frequency and frequency of a minimum magnitude of the impedance function at the output electrodes of the piezoelectric transformer with shorted input electrodes,

$f_{anti\text{-}res\_s}$ = anti-resonance frequency and frequency of a maximum magnitude of the impedance function at the output electrodes of the piezoelectric transformer with shorted input electrodes.

[0010] A number of highly useful piezoelectric transformers for the present piezoelectric power converters with both high power conversion efficiencies and native ZVS properties are disclosed in the applicant's co-pending European patent application No. 11176929.5.

[0011] The self-oscillating feedback loop around the native ZVS capable piezoelectric transformer with direct electrical coupling from the input driver to the input electrode without any intervening series or parallel inductor both dispenses with the external inductor. Instead ZVS operation of the input driver is ensured by the inductive behaviour of the piezoelectric transformer within the ZVS operation range of the piezoelectric transformer. Hence, the commonly employed external inductor, which occupies space, adds costs, conducts and radiates EMI as explained above, is avoided. In the direct coupling from the input driver to the input electrode, the inductance of the ordinary external inductor is replaced by the mechanical equivalent inductance already embedded in the vibratory mass of the piezoelectric transformer due to its native ZVS properties. Hence, the radiated EMI from the commonly employed external inductor is largely eliminated. Furthermore, because the ordinary external inductor often employs a ferrite core material the external inductor becomes prone to magnetic saturation from large static or dynamic magnetic fields for example in applications such as MRI scanners, power plants etc. Magnetic saturation of the ferrite core material may cause the piezoelectric power converter to malfunction. This problem is also removed by the eliminated of the ordinary external inductor. The self-oscillating feedback loop furthermore provides a mechanism for maintaining the optimum excitation frequency despite the strong dependence of electrical characteristics of the piezoelectric transformer on environmental parameters such as temperature, load, fixation and age.

[0012] The skilled person will understand that a parasitic wiring or cabling inductance naturally will be associated with the direct electrical coupling between an output of the input driver and the input electrode despite the lack of a separate input inductor. The power converter is preferably designed such that the wiring inductance from the output of the input driver to the input electrode of the piezoelectric transformer is smaller than 500 μH, preferably smaller than 100 μH, even more preferably smaller than 10 μH.

[0013] The electrical characteristics of the feedback loop are preferably configured to set the excitation frequency within the ZVS operation range of the piezoelectric transformer. The bandwidth of the ZVS operation range is typically narrow and located slightly above a fundamental resonance frequency of the piezoelectric transformer depending on specific characteristics of a design of the piezoelectric transformer. The bandwidth of the ZVS operation range of piezoelectric transformers may vary widely between different transformer topologies, modes of operation and physical dimensions. In some embodiments, the piezoelectric transformer is designed or configured with a bandwidth of the ZVS operation which lies between 1 % and 5% of a fundamental or primary resonance frequency of the piezoelectric transformer. In a number of useful embodiments, the electrical characteristics of the feedback loop are configured to set the excitation frequency to a frequency between 75 kHz and 10 MHz such as between 200 kHz and 20 MHz.

[0014] The phase-shift around the feedback loop must be an integer multiple of 360 degrees where the distribution of individual phase shifts between components and circuits of the feedback loop can be effected in numerous ways. The self-oscillation provided by the feedback loop ensures that the excitation frequency automatically tracks changing characteristics of the piezoelectric transformer and electronic circuitry of the input side of the power converter. This effect is particularly pronounced according to a preferred embodiment of the power converter wherein the feedback loop comprises a phase shifting circuit for example a frequency selective filter such as a high-pass, band-pass or a low-pass filter. According to this preferred embodiment, a slope or derivative of a phase response of a transfer function of the piezoelectric transformer is steeper than a slope or derivative of a phase response of the high-pass, band-pass or the low-pass filter within the ZVS operation range of the piezoelectric transformer. The high-pass, band-pass or the low-pass filter is preferably a low order filter such as a first or second order filter which exhibits a relative gentle slope of the phase response. In this way, the slope of the phase response of the piezoelectric transformer becomes much steeper than the slope of the phase response of the frequency selective filter. The predetermined excitation frequency will as a consequence become significantly more sensitive to changes to the frequency response characteristic of the piezoelectric transformer than to changes of the response of the frequency selective filter such that the self-oscillating feedback loop automatically maintains the predetermined excitation frequency at an optimum frequency or within an optimum frequency band.

[0015] According to one embodiment, the feedback loop comprises a cascade of a phase shifter and a comparator. The phase shifter is coupled for receipt of the feedback signal and configured to apply a predetermined phase shift to the feedback signal to provide a phase shifted feedback signal. The comparator is coupled for receipt of the phase shifted feedback signal to generate a square-wave feedback signal at a comparator output. The square-wave feedback signal is coupled to an input of the input driver so as to close the feedback loop.

[0016] The respective phase-shifts induced to the feedback signal by the phase shifter and the comparator may be adjusted in various ways to achieve a certain total phase shift complementing other signal phase shifts around the self-oscillating feedback loop. In one embodiment, the comparator comprises an inverting zero-crossing detector to provide square-wave feedback signal indicating zero-crossings of the phase-shifted feedback signal. In this manner, the inversion introduces a phase shift of at least 180 degrees in the self-oscillating feedback loop. The phase shifter may comprise a frequency selective filter and/or a time delay. The frequency selective filter may comprise a high-pass, band-pass or a low-pass filter with an appropriately tailored phase response. In the alternative, or in addition, the phase shifter may comprise an all-pass type of filter inducing a predetermined phase shift to the self-oscillating feedback loop without any frequency response filtration of the feedback signal.

[0017] The feedback signal to the feedback loop, which is operatively coupled between the output voltage of the piezoelectric transformer and the input driver, may be derived in numerous ways from the output voltage of the piezoelectric transformer. According to one embodiment, the feedback signal of the feedback loop is derived from the transformer output signal at the output electrode of the piezoelectric transformer. In this embodiment the feedback signal is derived directly from the existing output electrode(s) which also supplies power to a DC or AC output voltage node or terminal of the power converter. This embodiment is simple to implement because it uses existing signals and electrodes of the power convertor to provide the feedback signal. However, the feedback signal will be galvanically coupled to the output section of the piezoelectric transformer unless expensive and bulky precautions are taken such as the insertion of isolating optical couplers in the feedback loop. The output section of the piezoelectric transformer may have a very high voltage level for example at mains voltage (110 V to 230 V) or even higher voltages above 1 kV.

[0018] In an advantageous embodiment, the potential safety and regulatory problems caused by the galvanic coupling between the output section and output electrode and the input driver or input side by the feedback signal are avoided by adding a separate feedback output electrode to the output section or sections of the piezoelectric transformer. According to this embodiment, the feedback signal of the feedback loop is derived from a feedback output signal at the feedback output electrode arranged in one or more separate layer(s) of the output section of the piezoelectric transformer to galvanically isolate the feedback output electrode from the output electrode by the electrically insulating piezoceramic material of the transformer. The piezoelectric transformer may generally be configured such that a voltage gain, at the excitation frequency, from the input electrode to the output electrode is larger, substantially equal to, or smaller than a voltage gain from the input electrode to the feedback output electrode. In one embodiment, the voltage gain from the input electrode to the output electrode is between 2 and 50 times larger than the voltage gain from the input electrode to the feedback output electrode. This embodiment is particularly helpful if the output section of the piezoelectric transformer is at a very high voltage level such as at the mains voltage (110 V to 230 V) or higher as mentioned above. The level of the feedback output signal can be stepped down to a manageable level for example between 5 and 10 V such that galvanic isolation and a voltage level that is compatible with a voltage range of the electronic circuitry of the feedback loop is simultaneously provided. According to another embodiment, the voltage gain from the input electrode to the output electrode is between 2 and 50 times smaller than the voltage gain from the input electrode to the feedback output electrode. This embodiment is particularly helpful if the output section of the piezoelectric transformer operates at a relatively low voltage level such as CPU power supplies (e.g. 0.2 V to 5V DC). The level of the feedback output signal can then only be stepped down to a manageable level for example between 5 and 10 V such that galvanic isolation and a voltage level that is compatible with a voltage range of the electronic circuitry of the feedback loop is simultaneously provided.

[0019] In many applications, the feedback output electrode will not be required to deliver any significant power in comparison to the required load power at/from the output electrode. It may therefore be advantageous to design or construct the piezoelectric transformer such a volume of the separate layer of the output section enclosing the feedback output electrode is small-

er than a volume of layers of the output section enclosing the output electrodes, as the power output of an output electrode is proportional to the associated layer volume.

[0020] The skilled person will understand that separate feedback output electrode can be highly useful for galvanic isolation, and other purposes, in piezoelectric power converters which comprise the ordinary series or parallel inductor coupled between the input driver and the input electrode.

[0021] The feedback signal to the feedback loop can also be derived in an indirect manner from the input side of the piezoelectric power converter according to another preferred embodiment of the invention. Due to the lack of the ordinary series or parallel inductor between the input driver and the input electrode, the transformer resonance current cannot be directly monitored or detected at the input side of the power converter. However, the transformer resonance current can be estimated or derived from the input drive signal and a transformer input current. In this embodiment, the feedback signal of the feedback loop is derived by a transformer resonance current estimator from a combination of the input drive signal and the transformer input current running in the primary section of the piezoelectric transformer. This methodology may be applied to build or estimate a continuous transformer resonance current signal. This is preferably accomplished by differentiating the input drive voltage signal before adding/subtracting this signal from the transformer input current signal since the slope of rising and falling edges of the input drive signal indicates the transformer resonance current during time intervals of the input drive signal where the input driver is off. Consequently, the resonance current estimator preferably comprises:

- a first order differentiator coupled to the input drive signal to derive a first order derivative signal of the input drive signal,
- a current sensor, coupled in series with the primary section of the piezoelectric transformer, to supply a sensor signal representative of the transformer input current; and
- a subtractor configured to generate the feedback signal based on a difference between the first order derivative signal and the sensor signal.

[0022] The input current sensor may comprise a resistance arranged in-between a ground connection of the input driver and a ground connection of the piezoelectric transformer to supply a sensor voltage representative of the transformer input current. The first order differentiator may comprise a first order high-pass filter having an input coupled to the input drive signal and

an output supplying the first order derivative signal. A high-pass corner frequency of the first order high-pass filter is preferably larger than a fundamental resonance frequency of the piezoelectric transformer such as at least two times larger or preferably more than 10 times larger. In this manner, it is ensured that the high-pass corner frequency of the first order high-pass filter lies above the excitation frequency because the latter frequency typically is situated proximately to the fundamental resonance frequency of the piezoelectric transformer where the ZVS operation range is located, ensuring that the high-pass filter operates as a true differentiator at the excitation frequency. The subtractor may be implemented in various ways. One embodiment of the subtractor comprises a differential amplifier having a first differential input coupled to the first order derivative signal and the second differential input coupled to the sensor signal. The differential amplifier preferably comprises an operational amplifier either as a separate standard component or as sub-circuit of an ASIC integrating other types of electronic circuitry of the present piezoelectric power converter thereon.

[0023] According to another preferred embodiment of the invention, the piezoelectric power converter comprises a bi-directional switching circuit for reverse power transfer from the load at the output or secondary side of the power converter back to the input side. According to this embodiment, the piezoelectric power converter comprises:

- a bi-directional switching circuit coupled between the output electrode and an output voltage of the power converter,
- a controller adapted to control first and second states of the bi-directional switching circuit based on the input drive signal or the transformer output voltage such that:
- in a first state, forward current is conducted from the output electrode to the output voltage through the bi-directional switching circuit during a first period of a cycle time of the transformer output signal to charge the output voltage,
- in a second state, reverse current is conducted from the output voltage to the output electrode through the bi-directional switching circuit during a second period of the cycle time of the transformer output signal to discharge the output voltage and return power to the primary section of the piezoelectric transformer.

[0024] The presence of the second state wherein reverse current is conducted from the output voltage through the bi-directional switching circuit to the output electrode allows effective output voltage regulation without sacrificing efficiency of the piezoelectric based power converter.

This is because the reverse power is returned to the primary section or side of the piezoelectric transformer. The transmission of reverse current during the second period of the cycle time exploits he inherent bi-directional power transfer property of piezoelectric transformers such that power is transferred in opposite direction to the ordinary one, i.e. forward, power flow in the power converter. Surplus power at the output voltage is transmitted back to the input power source such as a DC supply voltage supplying power to the input driver. According to a preferred embodiment of the invention, the controller is in the second state further configured to control the switching circuit such that both forward current and reverse current is conducted during a single cycle of the transformer output signal. In this embodiment the forward current is conducted during the first period of the cycle time and reverse current is conducted during the second period of the same cycle of the transformer output signal. The second period may have a length corresponding to about one-half or less than the cycle time cycle time of the transformer output signal. The skilled person will appreciate that the degree of charge or discharge of the output voltage may be controlled in a step-wise or substantially continuous manner by a corresponding control of the relative length between the first and second periods of the same cycle of the transformer output signal. In this manner, the controller may provide effective output voltage control through adjustment of the length of the second period of the cycle time. Accordingly, by appropriately balancing the length of the first period of the cycle time relative to the second period of the same cycle, the bi-directional piezoelectric power converter may be adapted to transfer net power to the output voltage or to a load coupled thereto, transfer substantially zero power to the output voltage or transfer a negative power to the output voltage. The skilled person will understand that if the controller sets the length of the second period of the cycle time to zero, the bi-directional piezoelectric power converter conveniently transits from the second state to the first state wherein the bi-directional switching circuit conducts solely forward current so as to charge the output voltage during the first periods of the cycle times. This leads to an increasing level of output voltage e.g. the output voltage becomes more positive or more negative depending on the polarity configuration of the bi-directional switching circuit. In general, the controller may be adapted to terminate the second period of the cycle time, i.e. terminating the reverse conduction of current through the switching circuit, synchronously or asynchronously to the input drive signal or the transformer output signal. The controller preferably comprises an adjustable time delay circuit providing an adjustable duration of the second period

of the cycle time of the transformer output signal such that the amount of reverse power can be controlled. The controller is preferably configured to derive a synchronous state control signal from the input drive signal and apply the synchronous state control signal through the adjustable time delay circuit to a switch control terminal of the second controllable semiconductor switch and/or a switch control terminal of the first controllable semiconductor switch to control respective states of the first and second controllable semiconductor switches. In this manner, the switching circuit is responsive to the synchronous state control signal indicating the termination of the second period of the cycle time. The skilled person will understand that the synchronous state control signal may be derived directly or indirectly from the input drive signal. Indirectly if the synchronous state control signal is derived from another signal in the power converter that is synchronous to the input drive signal such as the transformer output signal. In one such embodiment, the synchronous state control signal is derived from a zero-crossing detector embedded in a self-oscillating feedback loop enclosing input section of the piezoelectric transformer.

[0025] The operation of the power converter during the second state of the bi-directional switching circuit where reverse power is transmitted can be improved in accordance with one embodiment of the invention. When reverse power is transmitted through the power converter the excitation frequency set by the feedback loop decreases. This leads to an increase of the transformer resonance current level and may be counteracted by adjustment of a time delay in the self-oscillating feedback loop. In one embodiment, the feedback loop comprises an adjustable time delay coupled in cascade with the phase shifter and the comparator to adjust the excitation frequency of the feedback loop. This embodiment may further comprise a current detector configured to determine the level of the transformer resonance current and a current limiter adapted to adjust the time delay of the adjustable time delay circuit to limit the transformer resonance current. In this manner an optimal operating point or excitation frequency of the feedback loop can be maintained during both forward power transmission and reverse power transmission of the bi-directional piezoelectric power converter.

[0026] The feedback loop may in certain situations be unable to induce a reliable start of the self-oscillation action due to amongst other factors the non-linear behaviour of the input driver which makes the latter insensitive to low level fluctuations of its input voltage. This may for example the situation if a bandwidth of the phase shifter is so low that noise signal components within the feedback loop are small. Consequently, an advantageous embodiment of the inven-

tion comprises a start-up circuit configured to inject a transient signal into the feedback loop at power-up of the power converter to initiate oscillation at the excitation frequency in the feedback loop. The skilled person will understand that the start-up circuit could be configured in a numerous ways to generate the desired transient signal. The transient signal could comprise a one or more signal pulses of predetermined waveform shape and duration. In another embodiment, the start-up circuit comprises an oscillator coupled into the feedback loop. The oscillator may be configured to generate an essentially continuous transient signal that is removed from the feedback loop by a suitable mechanism once self-oscillation has started. This may for example be controlled by an output impedance of the oscillator which is so large that the continuous transient signal is suppressed or eliminated once self-oscillation is initiated.

BRIEF DESCRIPTION OF THE DRAWINGS

[0027] Preferred embodiments of the invention will be described in more detail in connection with the appended drawings, in which:

[0028] Fig. 1 is a schematic block diagram of a piezoelectric power converter comprising a self-oscillating loop in accordance with a first embodiment of the invention,

[0029] Fig. 2a) is an electrical equivalent circuit of a piezoelectric transformer coupled to an input driver of a piezoelectric power converter in accordance with a first embodiment of the invention,

[0030] Fig. 2b) shown input drive voltage and input current waveforms of the piezoelectric transformer in accordance with the first embodiment of the invention,

[0031] Fig. 3 a detailed schematic block diagram of a transformer resonance current estimator coupled to an input section of a piezoelectric transformer of the piezoelectric power converter in accordance with the first embodiment of the invention,

[0032] Fig. 4 is a schematic block diagram of a piezoelectric power converter comprising a self-oscillating loop in accordance with a second embodiment of the invention,

[0033] Fig. 5 is a detailed schematic block diagram of a transformer output voltage detection circuit coupled to an output section of the piezoelectric transformer of the piezoelectric power converter in accordance with the second embodiment of the invention,

[0034] Fig. 6 is a simplified schematic block diagram of a piezoelectric power converter comprising a self-oscillating loop based on a separate feedback electrode in accordance with a third embodiment of the invention,

[0035] Fig. 7 is a simplified electrical equivalent circuit of the piezoelectric transformer of the piezoelectric power converter in accordance with the third embodiment of the invention; and

[0036] Fig. 8 is a schematic block diagram of a piezoelectric power converter comprising a self-oscillating loop and a bi-directional switching circuit for reverse power transfer in accordance with a fourth embodiment of the invention.

DETAILED DESCRIPTION OF PREFERRED EMBODIMENTS

[0037] The below appended detailed description of embodiments of the present invention comprises various types of self-oscillating loops for DC/DC voltage step-up or voltage step-down power conversion. However, the skilled person will understand that the below described embodiments are highly useful for other types of power converting applications such as AC/AC, AC/DC, DC/AC and DC/DC conversion, in particular conversion requiring high power conversion efficiency and compact dimensions by ZVS operation of the input driver without an external inductor at the input electrode.

[0038] Fig. 1 shows a schematic block diagram of a piezoelectric power converter 100 in accordance with a first embodiment of the invention. The bi-directional piezoelectric power converter 100 comprises a piezoelectric transformer, PT, 104. The piezoelectric transformer, PT, 104 has a first input electrode 105 electrically coupled to an input or primary section of the piezoelectric transformer 104, coupled to the input driver 103 of the piezoelectric power converter and a second input electrode connected to ground, GND. A first output electrode 107a and second output electrode 107b of the piezoelectric transformer 104 are electrically coupled to secondary or output section of the piezoelectric transformer 104 to provide a differential transformer output voltage or signal to a rectification circuit 108. The rectification circuit 108 may comprise a half or full wave rectifier and an output capacitor to provide smoothed DC voltage at the output node or terminal V_{OUT}.

[0039] The piezoelectric power converter 100 additionally comprises an input driver 103 electrically coupled directly to the input electrode 105 without any intervening inductor so as to apply an input drive signal to the input or primary section of the transformer 104. A driver con-

trol circuit 102 generates appropriately timed gate control signals for NMOS transistors M_2 and M_1 of the input driver 103. The input drive signal has a predetermined excitation frequency determined by parameters of a self-oscillating feedback loop operatively coupled between the output voltage of the piezoelectric transformer at output electrodes 107 and 107b and the input driver 103. In the present embodiment, the transformer output voltage is detected indirectly by estimating the transformer resonance current from a combination of the input drive signal supplied at input terminal 105 and a transformer input current running in the primary section of the piezoelectric transformer as explained in detail below in connection with Figs. 2 and 3 showing schematic and signal waveforms of a resonance current detector 118 performing this task. Electrical characteristics of the self-oscillating feedback are configured to set the excitation frequency of the self-oscillation loop within a ZVS operation range of the piezoelectric transformer. The self-oscillating feedback loop comprises a feedback leg 114 coupling a resonance current indicative signal I_{SENSE} which is proportional of the transformer output voltage back to the input driver through a cascade of low-pass filter 120 and a zero-crossing detector 122 such that the loop is closed around the input section of the transformer. The phase-shift around the self-oscillation loop feedback loop or simply feedback loop must be an integer multiple of 360 degree and the respective phase-shifts induced by the resonance current detector 118, the low-pass filter 120 and a zero-crossing detector 122 adjusted in an appropriate manner to achieve this goal.

[0040] It is furthermore desired to maintain a phase shift of approximately 55 degrees between the input drive signal and the transformer resonance current as set by the resonance current detector 118 because this phase difference ensures that the excitation frequency is located within a narrow frequency band above the fundamental resonance frequency of the piezoelectric transformer 104 where native ZVS operation is enabled. Within this narrow frequency band of ZVS operation, the piezoelectric transformer 104 exhibits the above-described ZVS factor larger than 100 % such as larger than 120 % and appears to possess inductive input impedance as seen from the output of the input driver 103. To reach the desired phase shift around the feedback loop on the integer multiple of 360 degrees, the zero-crossing detector 122 may be inverting to induce a further 180 degrees phase shift and a combined time delay of the input driver 103 and the driver control circuit 102 may amount to about 40 degrees of phase shift at the predetermined excitation frequency. These phase shifts add up to about 275 degrees such that the

electrical characteristics of the low-pass filter 120 are designed to induce a phase shift of 75 degrees at the predetermined excitation frequency. This can be achieved by selecting an appropriate cut-off frequency and order of the low-pass filter 120. The skilled person will understand that many other distributions of phase shifts between the circuits of the feedback leg 114 are possible. In one embodiment, the resonance current detector 118 is inverting to add another 180 degrees of phase shift. The low-pass filter 120 could be replaced by a band-pass filter or a pure time delay designed to provide the desired amount of phase shift.

[0041] At the secondary side of the PT 104, a rectifier or rectification circuit 108 is electrically coupled between a differential transformer output signal generated at the output electrodes 107a and 107b coupled to respective output sections of the PT 104. The rectification circuit 108 may be configured to provide half-wave or full-wave rectification of the transformer output signal supplied between the positive output electrode 107a and the negative, or opposite phase, output electrode 107b. The rectification circuit 108 preferably comprise a rectifier capacitor of appropriate capacitance (not shown) configured to generate a positive or negative DC output voltage V_{OUT} across the load resistance R_{LOAD} of the power converter 100. The load may of course comprise a capacitive and/or inductive component in addition to the depicted load resistor R_{LOAD}. During operation of the piezoelectric power converter 100 the level of the DC output voltage V_{OUT} is adjusted or controlled by a control mechanism or loop. The control loop comprises a DC output voltage detection or monitoring circuit 109 which supplies a signal to the output voltage control circuit 110 indicating an instantaneous level of the DC output voltage. A charge control circuit ΔQ compares the measured instantaneous level of the DC output voltage with a reference voltage V_{ref} which for example represents a desired or target DC output voltage of the power converter at V_{OUT}. The charge control circuit determines whether the level of the current DC output voltage is to increase or decrease based on the result of the comparison. The output voltage control circuit 110 generates an Active/Shut-down (A/S) control signal for the gate driver 101 such that the gate driver is disabled if the instantaneous level of the DC output voltage is larger than the reference voltage V_{ref}. If the instantaneous level of the DC output voltage is smaller than the reference voltage V_{ref} the gate driver is enabled and in this burst-mode manner power or energy is transferred to the converter output voltage through the rectification circuit 108.

[0042] Fig. 2a) is an electrical equivalent circuit of the piezoelectric transformer 104 coupled directly to the input driver 103 and to the rectification circuit 108 of the piezoelectric power converter 100 depicted on Fig. 1. As previously mentioned, the transformer output voltage across the first and second output electrodes 107a and 107b is detected indirectly by estimating the transformer resonance current I_L from a combination of the input drive signal V_p at input terminal 105 and the transformer input current I_{in} running through the primary section of the piezoelectric transformer 104. Since the input driver 103 is directly coupled to the input section of the piezoelectric transformer 104 without any external series or parallel inductor, the transformer resonance current cannot be measured through the external series or parallel inductor. The present embodiment of the invention utilizes a resonance current estimator instead to determine or estimate the transformer resonance current indirectly and derive a continuous resonance current signal I_{SENSE} which is supplied to the feedback loop to provide a feedback signal representative of the transformer resonance current. The estimated transformer resonance current is accordingly also representative of the transformer output voltage at the first and second output electrodes 107a and 107b. The resonance current estimator comprises a first order differentiator comprising series coupled capacitor C1 and resistor R1 coupled to the input drive signal V_p. The mid-point voltage V_{diff} at the coupling node between the series coupled capacitor C1 and resistor R1 supplies a first order derivative signal of the input drive signal V_p because a high-pass corner frequency of the first order differentiator is much larger than the fundamental resonance frequency of the piezoelectric transformer 104 such as at least two times larger e.g. 10 times larger.

[0043] The transformer input current I_{in} is detected in the resonance current detector 118 depicted in a detailed schematic diagram on Fig. 3 by a small series resistor R_S acting as a current sensor coupled in series with the primary section of the piezoelectric transformer 104. The series resistor R_S is coupled in a ground line or wire between the ground connection of the primary side of the piezoelectric transformer 104 and the ground connection of the first order differentiator. Hence, a voltage across the series resistor R_S represents, i.e. is proportional to, the transformer input current I_{in}.

[0044] The first order derivative signal V_{diff} and the transformer input I_{in} current signal are supplied to respective inputs of a differential amplifier of the resonance current detector 118. The differential amplifier comprises an operational amplifier 116 and gain setting resistors R2,

R3, R4 and R5 configured such that the gain from each of the inputs can be separately adjusted. The gain from V_{diff} to the resonance current signal I_{SENSE} is adjustable by R4 and R3 and the gain from the transformer input I_{in} current signal is adjustable by R5 and R2 such that convenient scaling between V_{diff} and I_{in} is provided. Furthermore the scaling can also be done trough the selection of R_S, R1 and C1. The function of the resonance current detector 118 is explained by reference to the measured input drive voltage waveform 161 at the lower graph 160 and the transformer input current waveform 151 depicted on the upper graph 150 of Fig. 2 b). The transformer input current waveform 151 is represented by the measured voltage across the series resistor R_S as explained above. The transformer input current I_{in} and the voltage across the series resistor R_S are zero during time periods where the input driver is off, i.e. its dead-time intervals indicated below the graph 160 as t2 and t4, because the output of the input driver at node V_P is charged by the resonance current of the piezoelectric transformer itself. However, the true transformer resonance current I_L is unavailable outside the physical structure of the piezoelectric transformer 104 because a large portion of the resonance current is conducted through the transformer input capacitance represented by parallel capacitor Cd1 of the equivalent diagram of Fig. 2a). However, by differentiating the up and down going transitions of the measured input drive voltage waveform 161 during the dead-time intervals t2 and t4, a scaled representation of the true transformer resonance current I_L is determined. Since the first order derivative signal V_{diff} of the measured input drive voltage waveform 161 is approximately zero (no slope) during on-periods of the input driver 103 as indicated by time periods t1 and t3 the first order derivative does not make any significant contribution to the resonance current signal I_{SENSE} during the latter time periods. During time periods t1 and t3 where the input driver 103 is active and conducting, the transformer resonance current flows through series resistor R_S and therefore generates a proportional sensed voltage which contributes to the resonance current signal $I_{SENSE.}$ This is indicated by the approximate sine shape of the transformer input current waveform 151 during time periods t1 and t3. Hence, the resonance current detector 118 generates a continuous loop feedback signal in form of the resonance current signal I_{SENSE} by combining the first order derivative signal V_{diff} 153 derived from the input voltage V_P 161 and the transformer input current I_{in} measured across the sense/series resistor R_S 151.

[0045] Since the resonance current signal I_{SENSE} for the feedback loop is generated from the input section of the piezoelectric transformer 104, the feedback signal is galvanic insulated from

the output section of the piezoelectric transformer 104. Hence, if the output section supplies high voltage signals because of the amplification characteristics of the piezoelectric transformer 104, the primary section is isolated from the high voltages enhancing safety and helps the power converter in complying with high voltage regulatory requirements.

[0046] Fig. 4 is a schematic block diagram of a piezoelectric power converter 400 comprising a self-oscillating loop in accordance with a second embodiment of the invention. The piezoelectric power converter 400 shares a large number of electrical characteristics and features with the above described first embodiment of the power converter and corresponding features have accordingly been provided with corresponding reference numerals to ease comparison. However, the way the feedback signal for the feedback leg 414 is derived from the piezoelectric transformer 404 differs in the present embodiment compared to the first embodiment. In the present embodiment, a differential transformer output voltage or signal for the feedback loop is derived from a first output electrode 407a and second output electrode 407b of the piezoelectric transformer 404. The first and second output electrodes 407a, 407b are in addition electrically coupled to respective secondary or output sections of the piezoelectric transformer 404 to provide the differential transformer output voltage to a rectification circuit 408. The rectification circuit 408 may comprise a half or full wave rectifier and an output capacitor to provide smoothed DC voltage at the output node or terminal V_{OUT}. An output voltage detection circuit 418 receives the differential transformer output voltage and generates a single-ended or differential sense signal, V_{SENS} which is transmitted to a low-pass filter 420 with similar characteristics to the low-pass filter of the first embodiment discussed above. Since, a potentially high transformer output voltage is fed back to the input section or primary side of the converter 400 there is not any galvanic isolation between the output side/voltage and the input side. However, in one preferred embodiment, the output voltage detection circuit 418 comprises a pair of small series capacitors that at least breaks any DC current path between the output side/voltage and the input side as described below in connection with Fig. 5. The skilled person will notice that the output voltage detection circuit 418 can be made less complex in the present embodiment compared to the resonance current detector 118 coupled to the primary transformer side of the piezoelectric transformer 104 in the first embodiment because a continuous transformer output voltage signal representing the transformer resonance current is directly available for the self-oscillating feedback loop in the present embodiment of the converter.

[0047] Fig. 5 is a detailed schematic block diagram of the transformer output voltage detection circuit 418 coupled to the output section of the piezoelectric transformer 404 (PT) of the piezoelectric power converter schematically depicted on Fig. 4. The rectifier 408 and the input driver 403 are also schematically indicated to ease comparison. The transformer output voltage detection circuit 418 comprises a first pF sized series capacitor C1 coupled in series with the first output electrode 407a (S1) and a second pF sized series capacitor C1 coupled in series with the second output electrode 407b (S2). A network of resistors R3 and R1 are configured to couple one phase of the transformer output signal from the series capacitor C1 to a matched pair of current mirror coupled transistors Q1. A corresponding coupling arrangement is connected to the other series capacitor C2. In effect, the single-ended feedback signal V_{SENS} is derived from the differential transformer output voltage. The feedback signal V_{SENS} is essentially a square wave signal in phase with the differential transformer output voltage. This feedback signal V_{SENS} is subsequently applied to the feedback leg 414 and phased shifted trough the low-pass filter 420 with similar characteristics to the low-pass filter of the first embodiment discussed above.

[0048] Fig. 6 is a simplified schematic block diagram of a piezoelectric power converter 600 comprising a self-oscillating loop based on a separate feedback output electrode 607c for supplying a feedback output signal to the self-oscillating loop in accordance with a third embodiment of the invention. The piezoelectric power converter 600 shares a large number of electrical characteristics and features with the above described second embodiment of the power converter 400 and corresponding features have accordingly been provided with corresponding reference numerals to ease comparison. However, the way the feedback signal for the feedback leg 614 is derived from the piezoelectric transformer 604 differs in the present embodiment compared to the second embodiment. In the present embodiment, a separate feedback output electrode 607c supplies a feedback output signal Fb representative of the differential transformer output voltage across the first and second output electrodes 607a, 607b to the output voltage detection circuit 618. The first and second output electrodes 607a, 607b electrically coupled to respective secondary or output sections of the piezoelectric transformer 604 and the differential transformer output voltage is transmitted to a rectification circuit 608 in a manner similar to the second embodiment described above. The rectification circuit 608 may accordingly comprise a half or full

wave rectifier coupled to an output capacitor(s) to provide a smoothed DC voltage at the output node or terminal V_{OUT}.

[0049] In the present embodiment, the piezoelectric transformer 604 is fabricated with the separate feedback output electrode 607c arranged or embedded in a separate layer of the output or secondary section of the piezoelectric transformer 604. The feedback signal supplied through the feedback path at the separate output electrode 607c is thereby galvanically isolated from the output sections or sides, output voltages such as V_{OUT} and electronic circuitry of the secondary side of the piezoelectric power converter 600. The skilled person will understand that the piezoelectric transformer 604 may comprise several separate feedback electrodes for example a dedicated feedback electrode in each of the output sections of the piezoelectric transformer 604 such that the illustrated feedback output signal Fb may comprise a differential feedback signal. A voltage gain, at the excitation frequency, from the input electrode 605 to the differential transformer signal across the first and second output electrodes 607a, 607b may be essentially equal to, larger than, or smaller than a voltage gain from the input electrode 605 to the feedback output electrode(s) 607c for example between 2 and 50 times larger or between 2 and 50 times smaller. In step up voltage conversion applications of the present piezoelectric power converter 600, a smaller voltage gain to the feedback output electrode(s) 607c may be preferable such that galvanic isolation and an appropriate voltage level for electronic components of the output voltage detector 618 simultaneously are achieved. Even if the voltage gain, at the excitation frequency, from the input electrode 605 to the differential transformer signal across the first and second output electrodes 607a, 607b is essentially equal to the voltage gain from the input electrode 605 to the feedback output electrode(s) 607c, the piezoelectric power converter 600 benefits from the galvanic isolation between the input side and output side circuitry.

[0050] According to one such embodiment, a volume of the separate layer of the output section which encloses the feedback output electrode 607c is smaller than a volume of layers of the output section(s) enclosing the output electrodes 607a, 607b. This can be achieved by embedding the feedback output electrodes i to a small portion of the secondary PT section, as it should only occupy a very small part of the output PT section (or input PT section if feedback is taken from the primary side) and will therefore not distort or degrade performance of the output section significantly. Depending on the specific piezoelectric transformer design and structure, embedding the feedback output electrode can be relatively straight-forward to implement. Embed-

ding can also be very convenient if the voltage level of the output section is appropriate for electronic components of the output voltage detector 618, as the feedback output electrode 607c will possess a similar voltage level, if small parts of the existing electrodes in the output section are used, so the feedback output electrodes have the same layer thickness.

[0051] The feedback output electrode 607c can also be implemented as a separate section of the piezoelectric transformer 604 if this is more convenient, practical or the transformer design does not allow embedding the feedback output electrode. In any case, it is preferred that the separate feedback section of the piezoelectric transformer occupies a very small part of the entire piezoelectric transformer 604 structure without distorting or degrading the transformer performance as described above. Depending on the piezoelectric transformer design and structure, a separate output section may from a practical perspective be simpler to implement than embedding. The separate output section may also be more convenient for piezoelectric transformer designs where none of the output or secondary transformer sections has an appropriate voltage level for the electronic components of the output voltage detector 618.

[0052] Fig. 7 illustrates a simplified electrical equivalent diagram inside dotted box 604 of the piezoelectric transformer 604 of the piezoelectric power converter 600 in accordance with the third embodiment of the invention. The simplified electrical equivalent diagram comprises a pair of separate secondary windings where the load is coupled to the upper secondary winding which also provides the positive DC output voltage V_{OUT}. The rectifier has been left out of the diagram for simplicity. The lower secondary winding corresponds to the separate feedback output electrode 607c and provides a feedback output signal V_{FB} to the output voltage detection circuit 618. As illustrated on the drawing, the lower secondary winding is galvanically isolated from the upper secondary winding and therefore not used to supply power to the load. Hence, the volume of the output section occupied by the separate feedback output electrode 607c can be much smaller than the volume of the output section(s) enclosing the output electrodes 607a, 607b.

[0053] Fig. 8 is a schematic block diagram of a piezoelectric power converter 800 comprising a self-oscillating loop and a bi-directional switching circuit 808 for reverse power transfer in accordance with a fourth embodiment of the invention. The piezoelectric power converter 800 shares a large number of electrical characteristics and features with the above described third embodiment of the power converter 600, in particular a separate feedback output electrode 807c

arranged or embedded in a separate layer of the output or secondary section of the piezoelectric transformer 804. The feedback signal from the feedback output electrode 807c is likewise supplied to the output voltage detection circuit 818 and further through a feedback path of the primary side such that the primary side circuitry becomes galvanic isolated from the secondary side.

[0054] At the secondary side of the PT 804, the bi-directional switching circuit 808 is electrically coupled between a single-ended transformer output signal generated at the output electrode 807 of the PT 804 and a positive DC output voltage V_{OUT} applied across a load capacitor C_{LOAD} of the power converter 800. The load may of course comprise a resistive and/or inductive component in addition to the depicted load capacitance C_{LOAD}. A controller or control circuit is adapted to control forward current conduction from the output electrode 807 to V_{OUT} through the bi-directional switching circuit 808 during a first period of the cycle time of the transformer output signal. The positive DC output voltage V_{OUT} is accordingly charged during the first period of the cycle time. This transformer output signal, oscillating at the excitation frequency set by the self-oscillating feedback loop around the feedback electrode 807c, is applied to a midpoint node between series coupled NMOS transistors M_4 and M_3 of the bi-directional switching circuit 808. The output section of the PT 804, oscillating at the excitation frequency, behaves largely as a current source injecting AC current into the midpoint node between series coupled M_4 and M_3 to generate the transformer output signal or voltage. Furthermore, the controller is adapted to control a second period of the cycle time of the transformer output signal wherein reverse current is conducted through the bi-directional switching circuit 808 to the output electrode 807 of the PT 804 such that V_{OUT} is discharged during the second period of the cycle time. During the second period of the cycle time power is returned to the primary section of the piezoelectric transformer through the output electrode 807 of the PT.

The skilled person will appreciate that M_3 and M_4 function as respective controllable semiconductor switches each exhibiting low resistance between an inlet and an outlet node (i.e. drain and source terminals) in the on-state and very large resistance in the off-state or non-conducting state. The on-resistance of each of M_3 and M_4 in its on-state/conducting state may vary considerably according to requirements of a particular application, in particular the voltage level at the DC output voltage V_{OUT} or load impedance. In the present high-voltage embodiment of the invention, each of the M_3 and M_4 is preferably selected such that its on-resistance lies between 50

and 1000 ohm such as between 250 and 500 ohm. The positive DC supply voltage V_{DD} may vary widely in accordance with the requirements of a particular application. In the present embodiment of the invention, the positive DC supply voltage V_{DD} is preferably selected to a voltage between 20 and 40 volt such as about 24 volt.

[0055] The bi-directional switching circuit 808 comprises a high-side semiconductor diode D_4 arranged or coupled across drain and source terminals of M_4 so as to conduct the forward current to the DC output voltage V_{OUT} in a first state of the bi-directional switching circuit 808. A low-side semiconductor diode D_3 is in a similar manner coupled across drain and source terminals of M_3 so as to conduct the reverse current through the output electrode 807 and output section of the PT 804 during at least a portion of the first state. In the first state, the forward current is conducted from the output electrode 807 of the PT 804 through the bi-directional switching circuit 808 to the DC output voltage V_{OUT} during a first period of a cycle time of the transformer output signal to charge the output voltage. This is accomplished by switching the high-side NMOS transistor M_4 to its on-state or conducting state by a self-powered high-side driver 806 which forms part of the controller. The self-powered high-side driver 806 or self-powered driver 806 is coupled between the control or gate terminal of M_4 and the output electrode 807 which supplies the transformer output signal. The timing of the state switching of M_4 is determined by the detection of forward current in D_4 by a current sensor (not shown) contained in the self-powered driver 806. This current sensor is preferably arranged in series with the high-side semiconductor diode D_4. In response to detection of forward current in D_4 the self-powered driver 806 switches M_4 to its on-state which effectively clamps D_4 such that a majority of the forward current flowing through the parallel connection of M_4 and D_4 to the DC output voltage V_{OUT} in reality flows through M_4. On the other hand, during a negative half-cycle of the transformer output signal in the first state of the bi-directional switching circuit 808, D_4 is reverse biased and M_4 switched to its off-state at expiry of a timer period setting of an associated timer circuit (not shown). However, current is now conducted from the negative supply rail, i.e. GND in the present embodiment, to the output electrode 807 of the PT 804 through the parallel connection of M_3 and D_3. Initially, D_3 will start to conduct forward current once it becomes forward biased by the negative transformer output voltage. M_3 is on the other hand, switched to its on-state or conducting state by a low-side driver 821 which forms part of the controller. The low-side driver 821 is coupled to the gate terminal of M_3 and configured to switch M_3 from its off-

state to its on-state and vice versa. However, while the timing of the state switching of M_3 from its off-state to the on-state is determined in a manner similar to M_4, the opposite state switching of M_3 is effected synchronously to input drive signal as explained below. M_3 is switched from the off-state to the on-state by a detection of forward current in D_3 by a current sensor (not shown) contained in the low-side driver 821. This current sensor is arranged in series with the low-side semiconductor diode D_3. At the detection of forward current in D_3 the low-side driver 821 switches M_3 to its on-state which effectively clamps D_3 such that a majority of the forward current flowing through the parallel connection of M_3 and D_3 in reality flows through M_3.

[0056] Consequently, in the first state the bi-directional switching circuit 808 functions as a half-wave rectifier or voltage doubler of the transformer output signal such that forward current is conducted from the output electrode 807 of the PT 804 through the high-side NMOS transistor M_4 and semiconductor diode D_4 to the DC output voltage V_{OUT} to charge V_{OUT}. In the negative half-periods of the transformer output signal, current is circulated around the secondary section of the PT 804 without charging the DC output voltage in the current embodiment which uses the half-wave rectification provided by the present bi-directional switching circuit 808. In comparison to a traditional diode-based half-wave rectifier, the bi-directional switching circuit 808 additionally comprises the NMOS transistors M_4 and M_3 of the bi-directional switching circuit 808 arranged for clamping of the high and low-side semiconductor diodes D_4 and D_3. During a second state and during a third state of the bi-directional switching circuit 808, the NMOS transistors M_3 and M_4 are controlled by the controller such that a flow of reverse power is enabled. Due to the inherent bi-directional transfer property of the PT 804 power applied to the secondary section through the output electrode 807 is transferred to the input section of the PT 804 in effect transferring power in opposite direction to the normal flow of power of the power converter 800.

[0057] In connection with the reverse current conduction during the second period of the cycle time, state switching of M_3 is controlled by the low-side driver 821 coupled to the gate terminal of M_3. The low-side driver 821 is responsive to a synchronous state control signal derived from the input drive signal supplied by an adjustable time delay circuit, control ΔT, of a phase controller 811. The phase controller comprises the adjustable time delay circuit, control ΔT, and a fixed time delay, ΔT circuit. The phase controller 811 receives s zero-crossing detector output signal 819 which switches states synchronously to the input drive signal and the transformer

output signal because this signal is derived from the self-oscillating feedback loop. Since the input drive signal and the transformer output signal oscillate synchronously to each other, the time delay imposed by the phase controller 811 to the zero-crossing detector output signal 819 sets a length or duration of the second period of the cycle time of the transformer output signal. M_3 is allowed to continue conducting current for the duration of the second period of the cycle time until the state transition of the synchronous state control signal turns off M_3 of the low-side driver 821. While the corresponding state switching of the high-side NMOS transistor M_4 from its on-state to its off-state in one embodiment is controlled by the synchronous state control signal albeit phase shifted about 180 degrees, the present embodiment of the invention uses a different turn-off mechanism provided the self-powered high-side driver 806. The self-powering of the high-side driver 806 is configured to terminate a reverse current conducting period of M_4 based on an internally generated state control signal supplied by an internal timer rather than the above-described synchronous state control signal supplied by the adjustable time delay circuit, control ΔT. The self-powered property of the high-side driver 806 is highly advantageous for high-voltage output PT based power converters where the DC output voltage may be above 1 kV. The self-powering property of the high-side driver 806 circumvents the need for raising the zero-crossing detector output signal 819 to a very high voltage level, i.e. matching the level of the DC output voltage, before being supplied to the high-side driver 806 to appropriately control the gate terminal of M_4. The skilled person will recognize that the gate terminal of M_4 must be raised to a level above the level of the DC output voltage signal to switch M_4 to its on-state. The self-powered high-side driver 806 is electrically coupled between the gate terminal of M_4 and the output electrode 807 carrying the transformer output voltage. During operation, the bi-directional piezoelectric power converter 800 comprises two distinct mechanisms for adjusting the level of the DC output voltage V_{OUT}. A first mechanism uses a DC output voltage detection or monitoring circuit 809 which supplies a signal to the output voltage control circuit 810 of the controller indicating the instantaneous level of the DC output voltage. A charge control circuit ΔQ compares the instantaneous level of the DC output voltage with a reference voltage which for example represents a desired or target DC output voltage of the power converter. The charge control circuit determines whether the current DC output voltage is to be increased or decreased based on this comparison and adjusts at least one of: {a modulation of a pulse width modulated input drive signal, a carrier frequency of the pulse width modulated input drive signal, a burst

frequency of a burst modulated input drive signal} in appropriate direction to obtain the desired adjustment of the DC output voltage. A second mechanism for adjusting the level of the DC output voltage V_{OUT} also uses the level signal from the DC output voltage detection circuit 809. In this instance the output voltage control circuit 810 adjusts the duration of the second period of the cycle time of the transformer output signal where M_3 conducts reverse current through the adjustable time delay circuit, control ΔT, of the phase controller 811. The corresponding adjustment of the second period of the cycle time as regards M_4 is preferably made by delaying the triggering time or point of the timer circuit included in the self-contained high-side driver 806. The delay of the triggering time of the timer circuit may be controlled dynamically during operation of the bi-directional power converter 800 by the controller by adjusting a delay of an adjustable time delay circuit, control ΔT, to reach a desired or target duration of the second period of the cycle time of the transformer output signal. The adjustable time delay circuit, control ΔT, allows the controller to adjust the duration of the second period of the cycle time of the transformer output signal wherein reverse current is conducted by the bi-directional switching circuit through the output electrode 807 back to the primary side of the PT 804. By this adjustment of the duration of the second period of the cycle time, the amount of generated reverse power can be effectively controlled allowing for the desired adjustment of the level of the DC output voltage V_{OUT} while conserving power.

[0058] The skilled person will appreciate that the degree of charge or discharge of the V_{OUT} may be controlled in a step-wise or substantially continuous manner by a corresponding control of the duration of the second period of the cycle time such that the level of V_{OUT} may be continuously increased or reduced as desired. The skilled person will understand that if the duration of the second period of the cycle time is set to zero by the controller, the bi-directional piezoelectric power converter 800 may be adapted to exclusively operate in the first state where the switching circuit charges the positive DC output voltage during the first period of cycle times of the transformer output signal. In this state, the NMOS transistors M_3 and M_4 are only conducting during the first period of the cycle time so to actively clamp the low-side and high-side semiconductor diodes D_3 and D_4, respectively.

[0059] The self-oscillating feedback loop comprising comprises a resonance current control circuit 812 comprising a peak current detector 826 coupled to a current limiter 828. The resonance current control circuit 812 is configured to adjust a time delay of the adjustable time de-

lay circuit 824 arranged in the feedback leg 814. The resonance current level of the piezoelectric transformer 804 is determined based on the output signal of the output voltage detector 818, or, alternatively, from an output of a low-pass filter 820 coupled to the output voltage detector 818. The output voltage detector 818 may advantageously comprise a simple resistive load applied to the feedback signal from the feedback output electrode 807c. In this situation, the resonance current level of the piezoelectric transformer can be determined in a straightforward manner by the peak current detector 826 from the level of the feedback signal and the known resistance of the resistive load. The low-pass filter 820 may have similar electrical characteristics to the low-pass filter of the first embodiment discussed above. The zero-crossing detector 822 receives a low-pass filtered signal from the low-pass filter 820 and provides an essentially square wave shaped signal indicating zero-crossings of the filtered signal which possesses an approximate sine shaped waveform. The square wave signal is transmitted to an adjustable time delay circuit 824 which introduces a variable phase shift in the self-oscillating feedback loop such that the predetermined excitation frequency can be adjusted. An output signal of the adjustable time delay circuit 824 is coupled to the drive control circuit 802 such as to close the self-oscillating feedback loop around an input driver 803. A resonance current control circuit 812 detects a peak current from the output signal of the output signal of the voltage detector 818 as described above and adjusts a time delay of the adjustable time delay circuit 824 based thereon. This is useful to compensate for an increase of ac resonance current under reverse power transmission through the piezoelectric power converter, e.g. in the second state of the bi-directional switching circuit 808. The ac resonance current in the piezoelectric transformer increases under reverse power transmission and this condition is detected by the peak current detector 826 of the resonance current control circuit 812. The effect is compensated by limiting the ac resonance current by the current limiter 828 which makes an appropriate adjustment of the time delay in the adjustable time delay circuit 824 such that an optimal operation point of the self-oscillating feedback loop can be maintained during both forward power transmission and reverse power transmission of the bi-directional piezoelectric power converter 800. In the present embodiment of the invention where the input driver 803 is coupled directly to the input electrode 805 without any series or parallel inductor, the piezoelectric transformer 104 preferably possess a ZVS factor larger than 100 % such as larger than 120 %. In this manner ZVS operation of the input driver 103 is enabled both in a first state and a second state of a bi-directional switching circuit

808. The ZVS operation of the input driver 103 improves the power conversion efficiency of the bi-directional piezoelectric power converter 800. The predetermined excitation frequency is preferably selected in the manner already discussed above in connection with the first embodiment of the invention. The use of the self-oscillating feedback loop has considerable advantages because, the predetermined excitation frequency automatically tracks changing characteristics of the piezoelectric transformer 804 and electronic circuitry of the input side of the power converter like the drive control circuit 802. These characteristics will typically change across operation temperature and age but the self-oscillating feedback loop ensures changes are tracked by the excitation frequency because a slope of the phase response of the piezoelectric transformer 804 is typically much steeper than a slope of a phase response of the low-pass filter 820. In this manner, the predetermined excitation frequency will be significantly more sensitive to changes in frequency response characteristic of the piezoelectric transformer 804 such that the self-oscillating feedback loop automatically maintains the predetermined excitation frequency at an optimum frequency or within an optimum frequency band such as in the ZVS operation band of the piezoelectric transformer 804.

CLAIMS

1. A piezoelectric power converter comprising:
   - a piezoelectric transformer comprising an input electrode electrically coupled to an input or primary section of the piezoelectric transformer and an output electrode electrically coupled to secondary or output section of the piezoelectric transformer to provide a transformer output voltage,
   - an input driver electrically coupled directly to the input electrode without any intervening series or parallel inductor to supply an input drive signal to the input electrode,
   - a feedback loop operatively coupled between the output voltage of the piezoelectric transformer and the input driver to provide a self-oscillation loop around the primary section of the piezoelectric transformer, oscillating at an excitation frequency, wherein:
   - electrical characteristics of the feedback loop are configured to set the excitation frequency of the self-oscillation loop within a ZVS operation range of the piezoelectric transformer.

2. A piezoelectric power converter according to claim 1, wherein a feedback signal of the feedback loop is derived from the transformer output signal at the output electrode of the piezoelectric transformer.

3. A piezoelectric power converter according to claim 1, wherein a feedback signal of the feedback loop is derived from a feedback output signal at a feedback output electrode arranged in one or more separate layer(s) of the output section of the piezoelectric transformer to galvanic isolate the feedback output electrode from the output electrode.

4. A piezoelectric power converter according to claim 4, wherein a volume of the separate layer(s) of the output section enclosing the feedback output electrode is smaller than a volume of layers of the output section enclosing the output electrode.

5. A piezoelectric power converter according to claim 3, wherein a voltage gain, at the excitation frequency, from the input electrode to the output electrode is larger or smaller than a

voltage gain from the input electrode to the feedback output electrode, preferably between 2 and 50 times larger or between 2 and 50 times smaller.

6. A piezoelectric power converter according to claim 1, wherein a feedback signal of the feedback loop is derived by a transformer resonance current estimator from a combination of the input drive signal and a transformer input current running in the primary section of the piezoelectric transformer.

7. A piezoelectric power converter according to claim 6, wherein the resonance current estimator comprises:
- a first order differentiator coupled to the input drive signal to derive a first order derivative signal of the input drive signal,
- a current sensor, coupled in series with the primary section of the piezoelectric transformer, to supply a sensor signal representative of the transformer input current; and
- a subtractor configured to generate the feedback signal based on a difference between the first order derivative signal and the sensor signal.

8. A piezoelectric power converter according to claim 6, wherein the first order differentiator comprises a first order high-pass filter having an input coupled to the input drive signal and an output supplying the first order derivative signal;
wherein a high-pass corner frequency of the first order high-pass filter is larger than a fundamental resonance frequency of the piezoelectric transformer such as at least two times larger or preferably more than 10 times larger.

9. A piezoelectric power converter according to claim 6 or 7, wherein the subtractor comprises a differential amplifier having a first differential input coupled to the first order derivative signal and the second differential input coupled to the sensor signal.

10. A piezoelectric power converter according to claim 5 or 6, wherein the input current sensor comprises a resistance arranged in-between a ground connection of the input driver and a ground connection of the piezoelectric transformer.

11. A piezoelectric power converter according to any of claims 2-9, wherein the feedback loop comprises a cascade of:
- a phase shifter coupled for receipt of the feedback signal to apply a predetermined phase shift to the feedback signal to provide a phase shifted feedback signal,
- a comparator coupled for receipt of the phase shifted feedback signal to generate a square-wave feedback signal at a comparator output; wherein the square-wave feedback signal is coupled to an input of the input driver so as to close the feedback loop.

12. A piezoelectric power converter according to claim 11, wherein the phase shifter comprises a high-pass, band-pass, low-pass filter or a time delay.

13. A piezoelectric power converter according to claim 10 or 11, wherein the comparator comprises an inverting zero-crossing detector to provide square-wave feedback signal indicating zero-crossings of the phase-shifted feedback signal.

14. A piezoelectric power converter according to any of the preceding claims, comprising:
- a bi-directional switching circuit coupled between the output electrode and an output voltage of the power converter,
- a controller adapted to control first and second states of the bi-directional switching circuit based on the input drive signal or the transformer output voltage such that:
- in a first state, forward current is conducted from the output electrode to the output voltage through the bi-directional switching circuit during a first period of a cycle time of the transformer output signal to charge the output voltage,
- in a second state, reverse current is conducted from the output voltage to the output electrode through the bi-directional switching circuit during a second period of the cycle time of the transformer output signal to discharge the output voltage and return power to the primary section of the piezoelectric transformer.

15. A piezoelectric power converter according to claim 14, wherein the controller in the second state is further configured to control the switching circuit such that:

- both forward current and reverse current is conducted during a single cycle of the transformer output signal.

16. A piezoelectric power converter according to claim 14 or 15, wherein the switching circuit comprises a half-wave rectifier or a full-wave rectifier operatively coupled to the output electrode.

17. A piezoelectric power converter according to any of claim 14-16, wherein the feedback loop comprises an adjustable time delay coupled in cascade with the phase shifter and the comparator to adjust the excitation frequency of the self-oscillating loop.

18. A piezoelectric power converter according to claim 17, wherein the feedback loop comprises:
    - a current detector configured to determine a level of a transformer resonance current resonance of the piezoelectric transformer,
    - a current limiter adapted to adjust a time delay of the adjustable time delay circuit to limit the transformer resonance current.

19. A piezoelectric power converter according to any claims 12-18, wherein a slope or derivative of a phase response of a transfer function of the piezoelectric transformer is steeper than slope or derivative of a phase response of the band-pass, high-pass or low-pass filter within the ZVS operation range of the piezoelectric transformer.

20. A piezoelectric transformer according to any of the preceding claims, comprising a piezoelectric transformer with a zero-voltage switching factor (ZVS factor) larger than 100%, preferably larger than 120%, such as larger than 150% or 200%;

    in which the ZVS factor is determined at a matched load condition as:

$$ZVS = \frac{\left(k_{eff\_S}^{-2}\right)-1}{\left(k_{eff\_P}^{-2}\right)-1} 0.882 \text{ ;}$$

$k_{eff\_P,}$ being a primary side effective electromechanical coupling factor of the piezoelectric transformer,

$k_{eff\_S,}$ being a secondary piezoelectric transformer effective electromechanical coupling factor, in which:

$$k_{eff\_P} = \sqrt{1 - \frac{f_{res\_p}^2}{f_{anti-res\_p}^2}} \qquad k_{eff\_S} = \sqrt{1 - \frac{f_{res\_s}^2}{f_{anti-res\_s}^2}}$$

f_{res_p} = resonance frequency and frequency of a minimum magnitude of an impedance function at the input electrodes of the piezoelectric transformer with shorted output electrodes,

$f_{anti\text{-}res\_p}$ = anti-resonance frequency and frequency of a maximum magnitude of the impedance function at the input electrodes of the piezoelectric transformer with shorted output electrodes,

f_{res_s} = resonance frequency and frequency of a minimum magnitude of the impedance function at the output electrodes of the piezoelectric transformer with shorted input electrodes,

$f_{anti\text{-}res\_s}$ = anti-resonance frequency and frequency of a maximum magnitude of the impedance function at the output electrodes of the piezoelectric transformer with shorted input electrodes.

21. A piezoelectric power converter according to any of the preceding claims, wherein a bandwidth of the ZVS operation range of the piezoelectric transformer lies between 1% and 5% of a fundamental or primary resonance frequency of the piezoelectric transformer.

22. A piezoelectric power converter according to any of the preceding claims, wherein a wiring inductance at the output of the input driver to the input electrode is smaller than 500 µH, preferably smaller than 100 µH, even more preferably smaller than 10 µH.

23. A piezoelectric power converter according to any of the preceding claims, comprising a start-up circuit configured to inject a transient signal into the feedback loop at power-up of

the power converter to initiate oscillation at the excitation frequency in the feedback loop.

24. A piezoelectric power converter according to claim 23, wherein the start-up circuit comprises an oscillator coupled into the feedback loop.

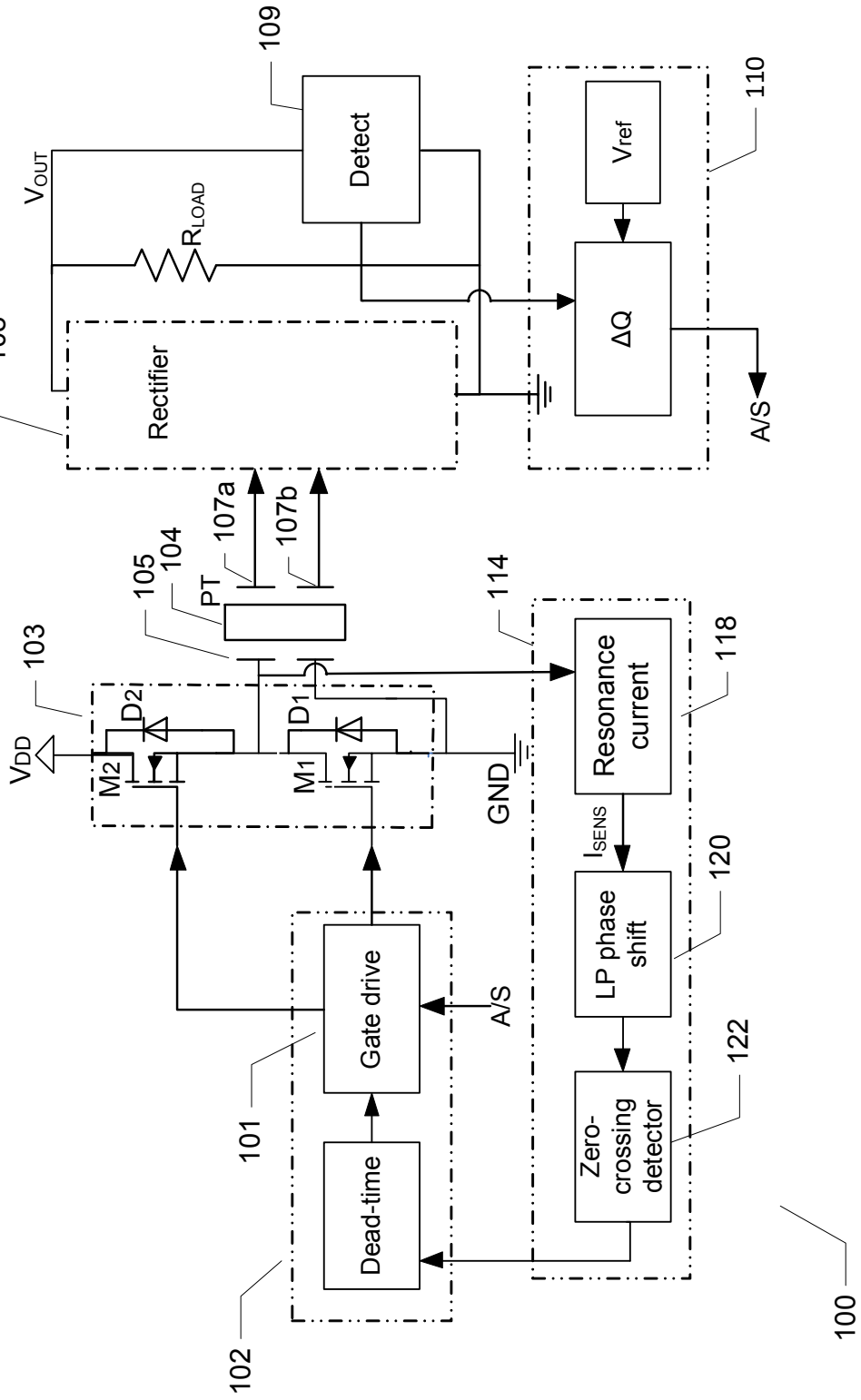
109
Detect
110
Vref
VOUT
RLOAD
ΔQ
A/S
108
Rectifier
107a
107b
104
105
PT
114
103
D2
D1
VDD
M2
M1
GND
Resonance current
118
ISENS
120
LP phase shift
Gate drive
A/S
122
Zero-crossing detector
101
Dead-time
102
100

Fig. 1

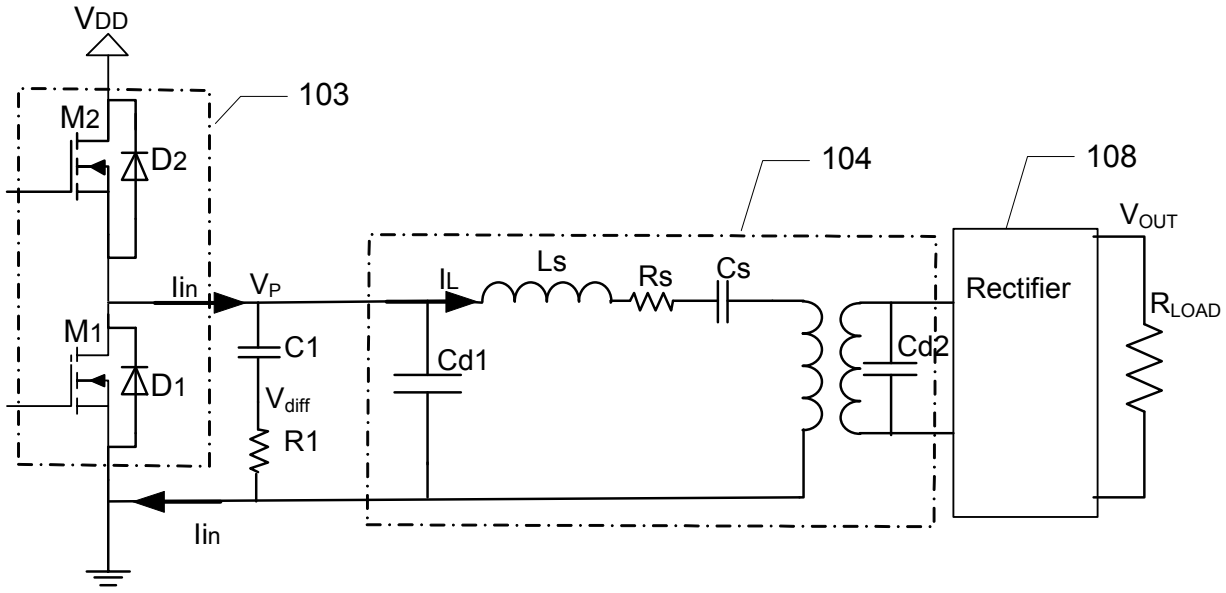
VDD
103
M2
D2
M1
D1
Iin
VP
C1
Vdiff
R1
Iin
104
IL
Ls
Rs
Cs
Cd1
Cd2
108
Rectifier
VOUT
RLOAD

a)

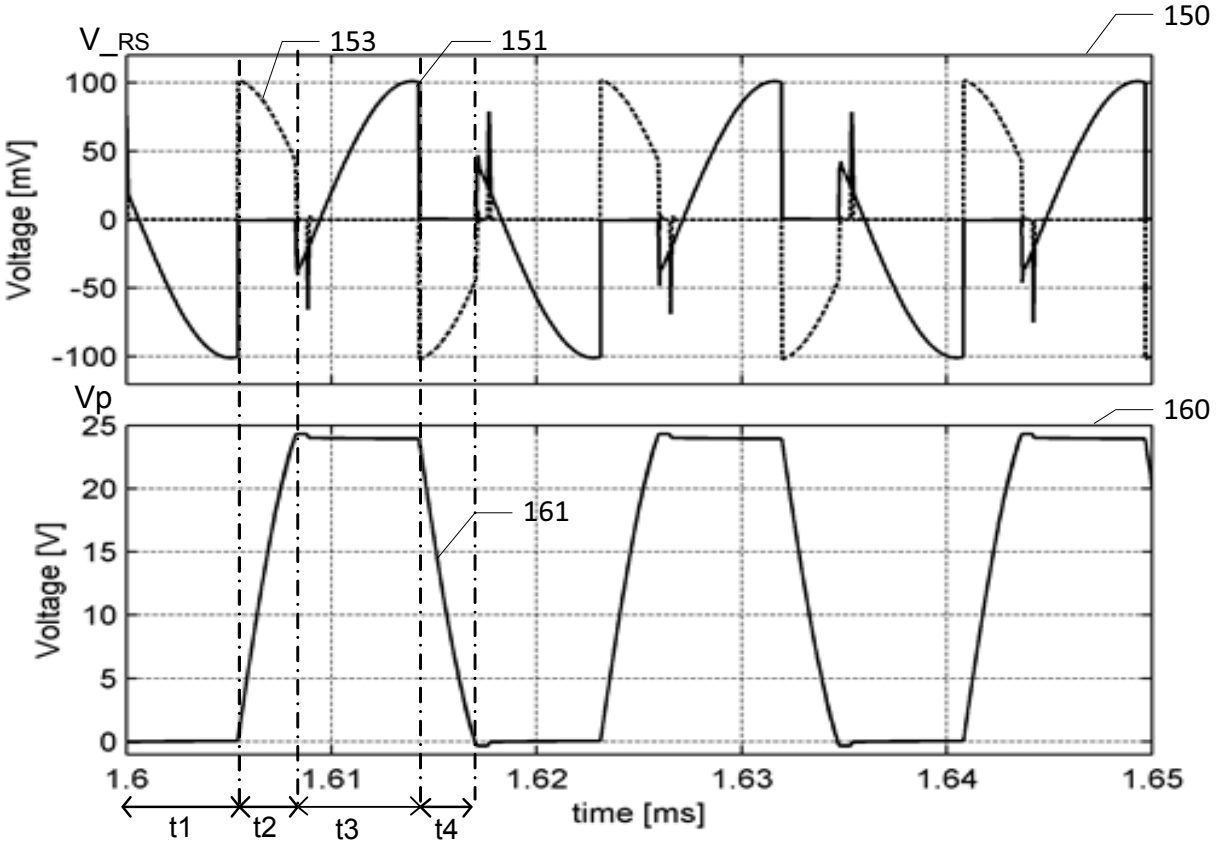
150
V_RS
153
151
100
50
0
-50
-100
Voltage [mV]
Vp
160
161
25
20
15
10
5
0
Voltage [V]
1.6
1.61
1.62
1.63
1.64
1.65
time [ms]
t1
t2
t3
t4

b)

Fig. 2

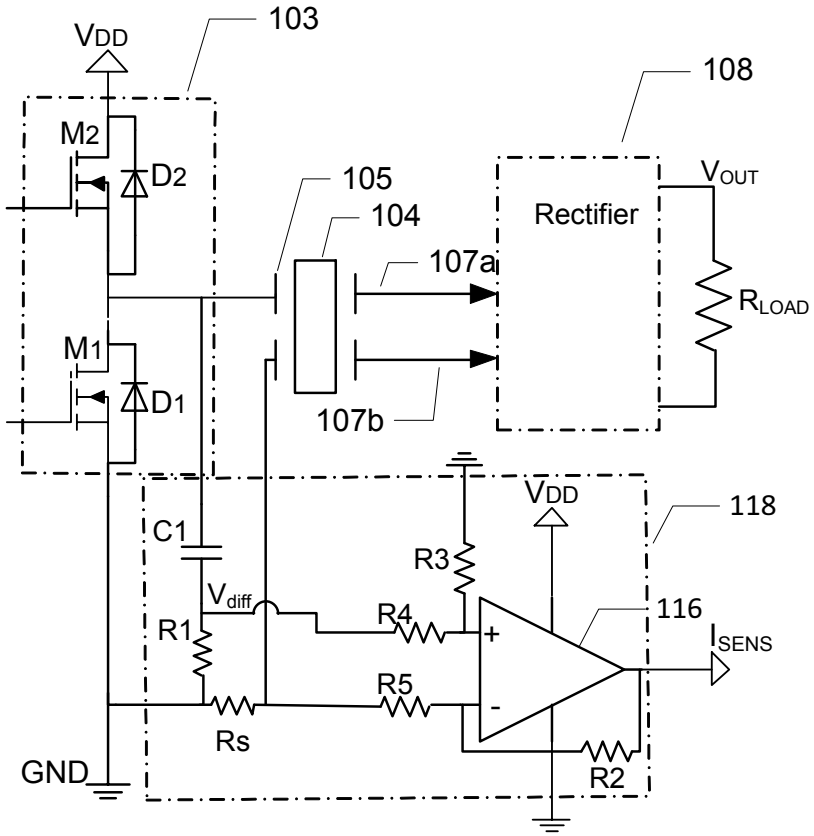
VDD
103
108
M2
D2
105
104
Rectifier
VOUT
107a
RLOAD
M1
D1
107b
VDD
118
C1
R3
Vdiff
R1
R4
116
+
ISENS
R5
-
Rs
GND
R2

Fig. 3

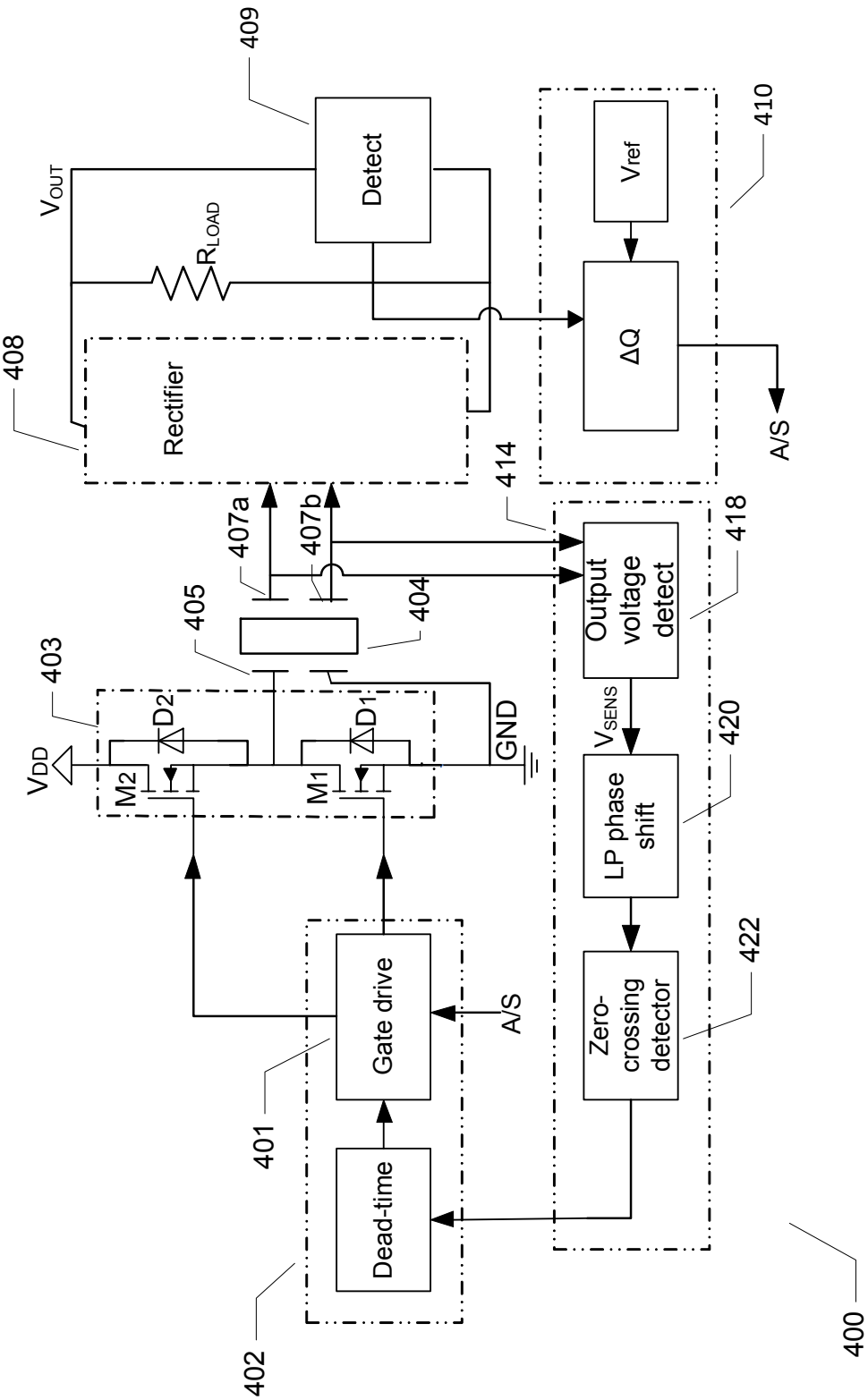
409
Detect
V_{OUT}
R_{LOAD}
408
Rectifier
410
Vref
ΔQ
A/S
414
407a
407b
404
405
403
418
Output voltage detect
V_{SENS}
420
LP phase shift
422
Zero-crossing detector
D2
D1
V_{DD}
M2
M1
GND
Gate drive
A/S
401
Dead-time
402
400

Fig. 4

5/8

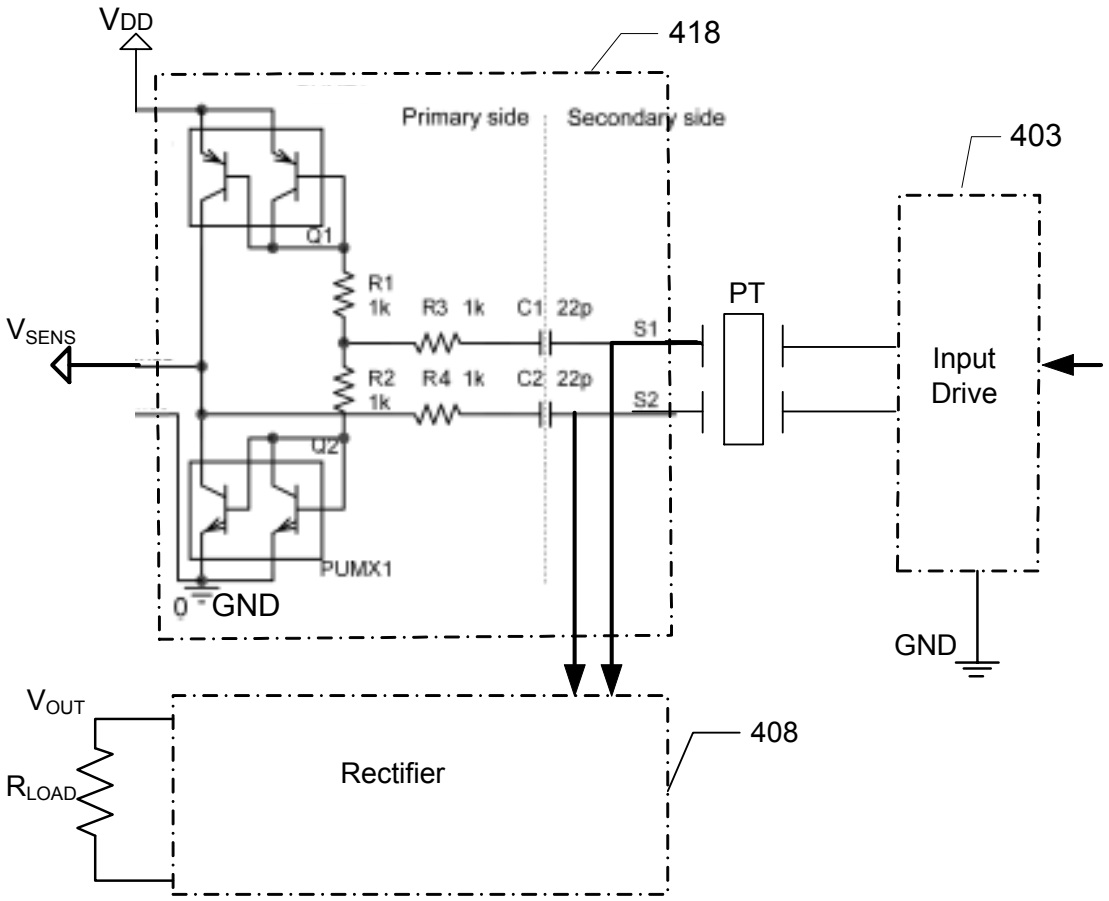
VDD
418
Primary side
Secondary side
403
Q1
R1
1k
R3 1k
C1 22p
PT
VSENS
S1
R2
1k
R4 1k
C2 22p
S2
Input
Drive
Q2
PUMX1
0
GND
GND
VOUT
RLOAD
Rectifier
408

Fig. 5

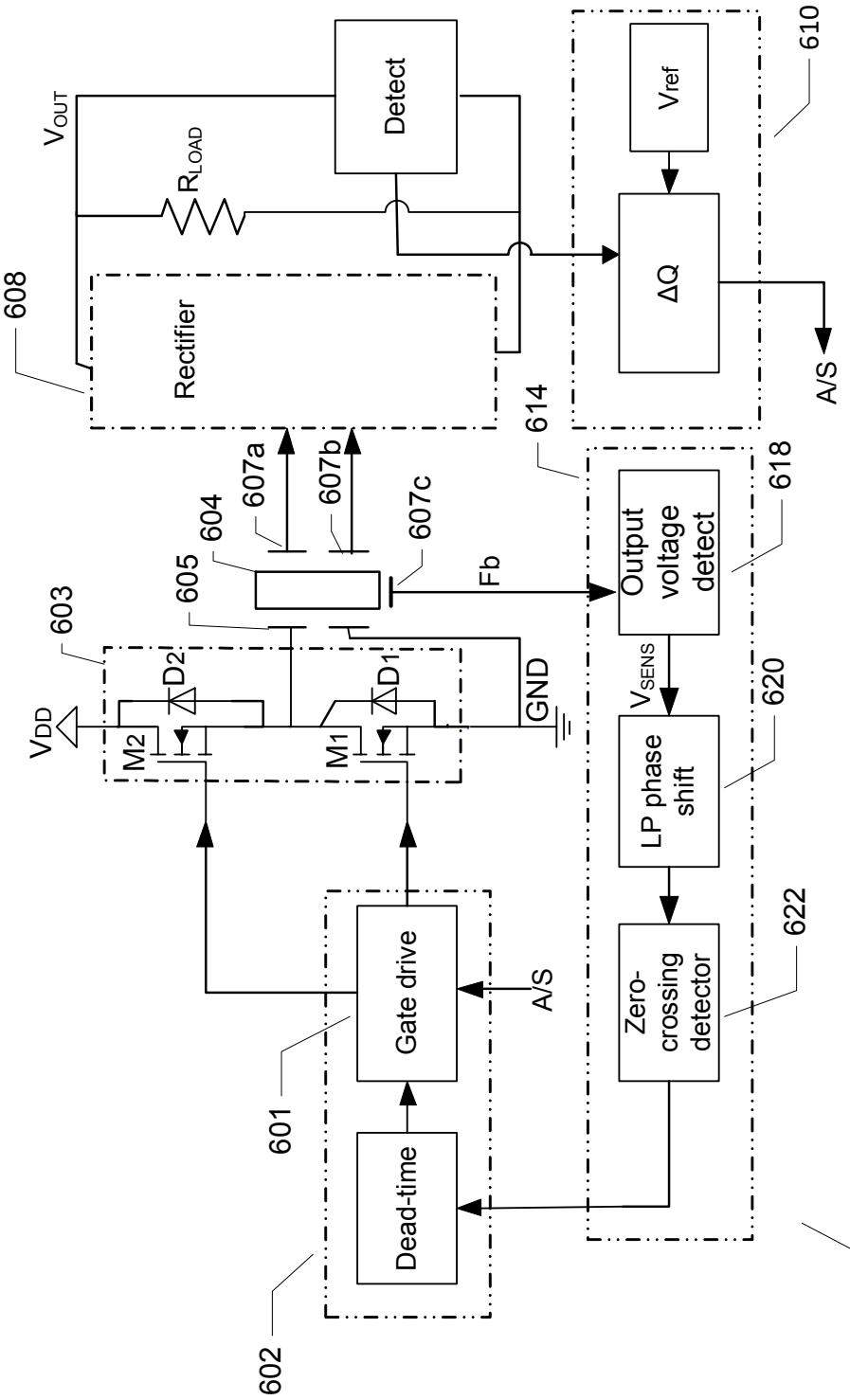
Detect
V_{OUT}
R_{LOAD}
Rectifier
608
Vref
610
ΔQ
A/S
614
607a
607b
607c
604
605
Fb
Output voltage detect
618
603
D2
D1
V_{DD}
M2
M1
GND
V_{SENS}
620
LP phase shift
Gate drive
A/S
601
Zero-crossing detector
622
Dead-time
602
600

Fig. 6

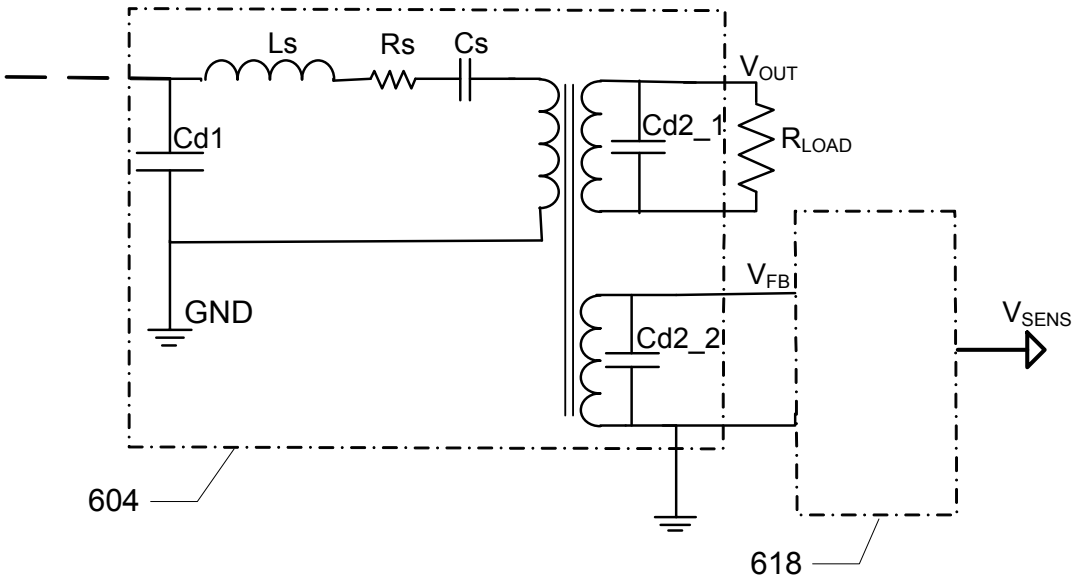

Fig. 7

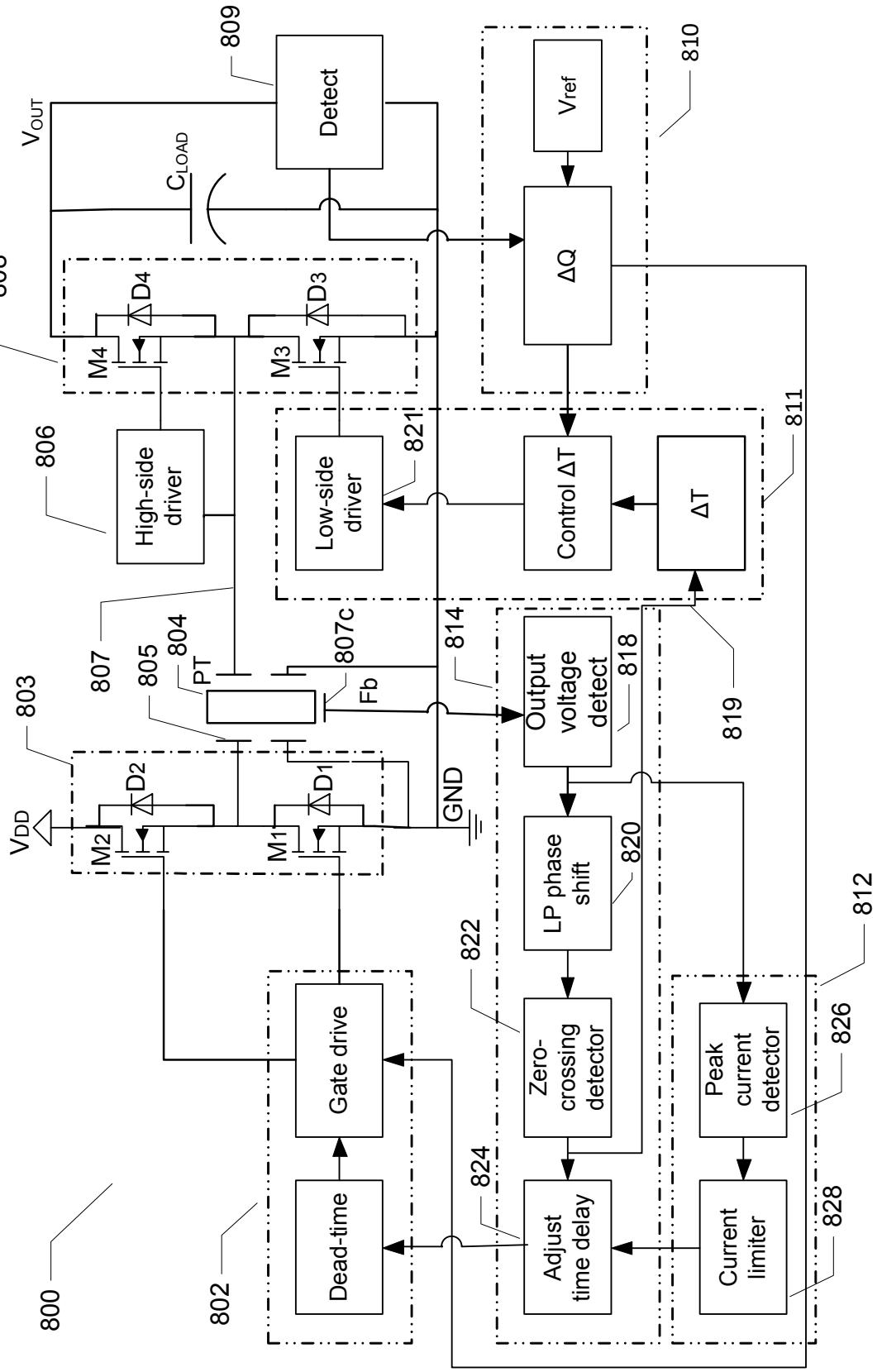
800
802
803
804
805
806
807
807c
808
809
810
811
812
814
818
819
820
821
822
824
826
828
Detect
Vref
ΔQ
Control ΔT
ΔT
High-side driver
Low-side driver
Output voltage detect
LP phase shift
Zero-crossing detector
Peak current detector
Gate drive
Dead-time
Adjust time delay
Current limiter
VOUT
CLOAD
VDD
GND
PT
Fb
D1
D2
D3
D4
M1
M2
M3
M4

Fig. 8

D.9 Piezoelectric power converter with bi-directional power transfer

Patent - Pending

2011 (priority)
EP11192356
US 61/567,924

NIXON PEABODY LLP
Customer No. 70001

PATENT
059244-11PL01

U.S. PROVISIONAL PATENT APPLICATION

FOR

PIEZOELECTRIC POWER CONVERTER WITH BI-DIRECTIONAL POWER TRANSFER

BY

MICHAEL ANDREAS ESBERN ANDERSEN

KASPAR SINDING MEYER

MARTIN SCHØLER RØDGAARD

AND

THOMAS ANDERSEN

PIEZOELECTRIC POWER CONVERTER WITH BI-DIRECTIONAL POWER TRANSFER

COPYRIGHT

FIELD OF THE PRESENT DISCLOSURE

[0002] The present invention relates to a bi-directional piezoelectric power converter comprising a piezoelectric transformer. The piezoelectric transformer comprises an input electrode electrically coupled to a primary section of the piezoelectric transformer and an output electrode electrically coupled to an output section of the piezoelectric transformer to provide a transformer output signal. A bi-directional switching circuit is coupled between the output electrode and a DC or AC output voltage of the power converter. Forward and reverse current conducting periods of the bi-directional switching circuit is based on the input drive signal or the transformer output signal such that a forward current is conducted from the output electrode through the bi-directional switching circuit to the DC or AC output voltage in a first state to charge the DC or AC output voltage. In a second state, a reverse current is conducted through the bi-directional switching circuit from the DC or AC output voltage to the output electrode to discharge the DC or AC output voltage and return power to the primary section of the piezoelectric transformer.

BACKGROUND

[0003] Traditional piezoelectric transformer based power converters are only capable of supplying power in one direction, from an input voltage/power source to a DC or AC output of the power converter. Furthermore, the piezoelectric transformer is normally operated in a narrow frequency band around its fundamental or primary resonance frequency with a matched load coupled to the output of the piezoelectric transformer. This is required to optimize power conversion efficiency of the power converter. The small optimum frequency band of operation and the need for a matched load make it difficult to provide output voltage regulation without sacrificing

efficiency of the piezoelectric based power converter. Instead of transferring surplus power to the load coupled to the secondary side of the power converter, the present power converter enables reverse transmission of power back to the input source to conserve energy.

[0004] Likewise in situations where the excitation frequency is substantially fixed, traditional output voltage control techniques based frequency modulation or pulse width modulation of the input drive signal cannot easily be adapted to control a DC or AC output voltage of the converter without causing considerable deterioration of the power conversion efficiency of the power converter.

[0005] Another challenge in the design of traditional piezoelectric transformer based power converters is to obtain zero-voltage-switching (ZVS) in an input driver, typically based on a half-bridge or full-bridge MOS transistor circuit, coupled to a primary or input section of the piezoelectric transformer. ZVS operation of piezoelectric transformers has traditionally been achieved by adding an external inductor in series or in parallel with the primary or input section of the piezoelectric transformer. The external inductor ensures that the input of the piezoelectric transformer appears inductive across a certain frequency range and such that an output node of the input driver can be charged/discharged in accordance with the input drive signal without inducing prohibitive power losses. However, the external inductor occupies space, adds costs and conducts and radiates EMI in the power converter. It would therefore be advantageous to provide a piezoelectric transformer based power converters capable of ZVS operation with good power conversion efficiency without the ordinary external inductor. ZVS operation of piezoelectric transformers is supported in accordance with one aspect of the invention by increasing an apparent ZVS factor of piezoelectric transformer of a power converter by conducting reverse current from the DC or AC output voltage to the secondary section of the piezoelectric transformer as described in further detail below. This methodology increases the apparent ZVS factor of a piezoelectric transformer which can be useful to transform a piezoelectric transformer design or construction without inherent ZVS capability to one with ZVS capability. In addition, even piezoelectric transformer designs with inherent ZVS capability, i.e. a ZVS factor above 100 %, can benefit from a further increase of apparent ZVS factor because it enlarges or broadens the frequency band supporting ZVS operation.

SUMMARY

[0006] A first aspect of the invention relates to a bi-directional piezoelectric power converter comprising:

- a piezoelectric transformer comprising an input electrode electrically coupled to an input or primary section of the piezoelectric transformer and an output electrode electrically coupled to secondary or output section of the piezoelectric transformer to provide a transformer output signal. An input driver of the bi-directional piezoelectric power converter is electrically coupled to the input electrode and arranged to supply an input drive signal with a predetermined excitation frequency to the input electrode. A bi-directional switching circuit is coupled between the output electrode and an output voltage of the converter and a controller is adapted to control first and second states of the bi-directional switching circuit based on the input drive signal or the transformer output signal such that:
- in a first state, forward current is conducted from the output electrode to the output voltage through the bi-directional switching circuit during a first period of a cycle time of the transformer output signal to charge the output voltage,
- in a second state, reverse current is conducted from the output voltage to the output electrode through the bi-directional switching circuit during a second period of the cycle time of the transformer output signal to discharge the output voltage and return power to the primary section of the piezoelectric transformer.

[0007] The presence of the second state wherein reverse current is conducted from the output voltage through the bi-directional switching circuit to the output electrode allows effective output voltage regulation without sacrificing efficiency of the piezoelectric based power converter because power is returned to the primary section of the piezoelectric transformer. The transmission of reverse current during the second period of the cycle time exploits an inherent bi-directional power transfer property of piezoelectric transformers such that power is transferred in opposite direction to the ordinary, i.e. forward, power flow in the power converter. Surplus power at the output voltage is transmitted back to the input power source such as a DC supply voltage supplying power to the input driver. According to a preferred embodiment of the invention, the controller is in the second state further configured to control the switching circuit such that both forward current and reverse current is conducted during a single cycle of the transformer output signal. In this embodiment the forward current is conducted during the first period of the

cycle time and reverse current is conducted during the second period of the same cycle of the transformer output signal. The second period may have a length corresponding to about one-half or less than the cycle time cycle time of the transformer output signal. The skilled person will appreciate that the degree of charge or discharge of the output voltage may be controlled in a step-wise or substantially continuous manner by a corresponding control of the relative length between the first and second periods of the same cycle of the transformer output signal. In this manner, the controller may provide effective output voltage control through adjustment of the length of the second period of the cycle time. Accordingly, by appropriately balancing the length of the first period of the cycle time relative to the second period of the same cycle, the bi-directional piezoelectric power converter may be adapted to transfer net power to the output voltage or to a load coupled thereto, transfer substantially zero power to the output voltage or transfer a negative power to the output voltage. The skilled person will understand that if the controller sets the length of the second period of the cycle time to zero, the bi-directional piezoelectric power converter conveniently transits from the second state to the first state wherein the bi-directional switching circuit conducts solely forward current so as to charge the output voltage during the first periods of the cycle times. This leads to an increasing level of output voltage e.g. the output voltage becomes more positive or more negative depending on the polarity configuration of the bi-directional switching circuit. In general, the controller may be adapted to terminate the second period of the cycle time, i.e. terminating the reverse conduction of current through the switching circuit, synchronously or asynchronously to the input drive signal or the transformer output signal. The controller preferably comprises an adjustable time delay circuit providing an adjustable duration of the second period of the cycle time of the transformer output signal such that the amount of reverse power can be controlled. The controller is preferably configured to derive a synchronous state control signal from the input drive signal and apply the synchronous state control signal through the adjustable time delay circuit to a switch control terminal of a second controllable semiconductor switch and/or a switch control terminal of the first controllable semiconductor switch of the switching circuit to control respective states of the first and second controllable semiconductor switches. In this manner, the switching circuit is responsive to the synchronous state control signal indicating the termination of the second period of the cycle time. The skilled person will understand that the synchronous state control signal may be derived directly or indirectly from the input drive signal. Indirectly if the synchronous state control signal

is derived from another signal in the power converter that is synchronous to the input drive signal such as the transformer output signal. In one such embodiment, the synchronous state control signal is derived from a zero-crossing detector embedded in a self-oscillating feedback loop enclosing input section of the piezoelectric transformer.

[0008] According to a preferred embodiment of the invention, the controller is adapted to sense a current through, or a voltage across, an electrical component of the bi-directional switching circuit. The controller initiates the forward current conduction in the first period of the cycle time in response to a sensed current or voltage so as to asynchronously initiate the forward current conduction. This embodiment simplifies the generation of an appropriately timed control signal or signals for the controller to the bi-directional switching circuit because the forward current conduction is automatically started without any need for a synchronous signal to indicate the correct phase of the transformer output signal. The electrical component may comprise a transistor, a diode or a resistor. In one embodiment, the electrical component comprises a series resistor coupled is series with a semiconductor diode coupled between the transformer output voltage and the output voltage. In this embodiment, the controller may be adapted to detect a flow of forward current by monitoring the polarity of a voltage drop across the series resistor since this polarity indicates the direction of current flow from the transformer output electrode to the output voltage. The flow of forward current through the switching circuit automatically starts when the transformer output signal exceeds the output voltage with approximately one diode voltage drop.

[0009] The predetermined excitation frequency is preferably selected or adjusted to a frequency which proximate to, or slightly above, a fundamental resonance frequency of the piezoelectric transformer depending on how the input driver is coupled to the input electrode of the primary section of the piezoelectric transformer. If the input driver is coupled to the primary section through a series/parallel inductor, the predetermined excitation frequency is preferably placed in proximity of the fundamental resonance frequency. The series/parallel inductor is adapted to provide so-called zero voltage switching (ZVS operation) of the input driver. If the input driver on the other hand is directly coupled to the input electrode of the piezoelectric transformer, i.e. without any series/parallel inductor, the predetermined excitation frequency is preferably placed within a selected frequency band or range placed slightly above the fundamental resonance frequency where the piezoelectric transformer may exhibit an intrinsic inductive input

impedance, i.e. possess a ZVS factor larger than 100 % such as larger than 120 % according to the below defined definition of the ZVS factor. The inductive input impedance in the selected frequency band or range enables ZVS operation of the input driver even in the first state of the bi-directional switching circuit so as to eliminate switching losses in the input driver. The setting of the predetermined excitation frequency depends on the fundamental resonance frequency of the piezoelectric transformer which may vary widely depending on its mode of operation and its physical dimensions. However, in a number of useful embodiments, the predetermined excitation frequency lies between 40 kHz and 1 MHz such as between 50 kHz and 200 kHz.

[0010] The bi-directional switching circuit preferably comprises one or more controllable semiconductor switches adapted to conduct the forward current from the output electrode to the output voltage during the first period of the cycle time. The one or more controllable semiconductor switches likewise conducts reverse current from the output voltage to the output electrode in the second state. The one or more controllable semiconductor switches preferably comprise(s) a semiconductor selected from the group of {MOSFET (metal-oxide-semiconductor field effect transistor), IGBT (insulated-gate bipolar transistor), bipolar transistor, Gate Turn-off thyristor (GTO)}. According to a preferred embodiment, each of the one or more controllable semiconductor switches preferably comprises a MOS transistor, such as a NMOS (n-channel metal oxide semiconductor) transistor, which is capable of bi-directional current flow between its source and drain terminals with a small on-resistance during both forward and reverse current conduction. The on-states and off-states of each of the MOS transistors are controllable by appropriate control of the drive voltage on a gate terminal of the MOS transistor. One embodiment based on the one or more controllable semiconductor switches comprises a first controllable semiconductor switch arranged between the output electrode and the output voltage and a second controllable semiconductor switch arranged between the output electrode and a negative supply voltage. The negatives supply voltage may be ground reference of the power converter. The controller is configured to alternatingly switch the first and second controllable semiconductor switches to respective on-states and off-states in a non-overlapping manner to control the forward and reverse current conduction. In the first state, this embodiment provides half-wave rectification of the transformer output signal by conducting the forward current to the output voltage through the first controllable semiconductor switch when transformer current out of the output electrode is positive. When the transformer current out of the output electrode is negative the second control-

lable semiconductor switch conducts and circulates current through the secondary side of the piezoelectric transformer. The skilled person will understand that the bi-directional switching circuit may comprise a full-wave rectification circuit such that a third controllable semiconductor switch is arranged between a second output electrode of the secondary side of the piezoelectric transformer and the output voltage and a fourth controllable semiconductor switch arranged between the second output electrode and the negative supply voltage.

[0011] According to an embodiment of the bi-directional piezoelectric power converter, the bi-directional switching circuit further comprises a first semiconductor diode coupled across inlet and outlet nodes of the first controllable semiconductor switch, e.g. drain and source terminals of the MOS transistor, to conduct forward current to the output voltage during at least a portion of a first period of the cycle time. A second semiconductor diode may be coupled across inlet and outlet nodes of the second controllable semiconductor switch, e.g. drain and source terminals of another MOS transistor, to conduct current during at least a portion of the cycle time of the transformer output signal. The first semiconductor diode or the second semiconductor diode may comprise a body/substrate diode integrally formed with the first or the second semiconductor switch, respectively. This reduces semiconductor substrate area consumption on a semiconductor die or substrate onto which the power converter may be integrated.

[0012] The on-set of flow of forward current through the first semiconductor diode is a convenient detection mechanism for the controller to asynchronously determine when the first controllable semiconductor switch must be switched to its on-state. In this manner, the controller may be configured to sense the forward current through, or the forward voltage across, the first semiconductor diode; and switch the first controllable semiconductor switch to its on-state in response to a sensed forward current or voltage so as to actively clamp the first semiconductor diode during the first period of the cycle time. In this manner, the first semiconductor diode conducts forward current to the output voltage during the portion of the first period of the cycle time and the first controllable semiconductor switch conducts the forward current during a major portion of the first period of the cycle time due to its lower impedance/forward voltage drop once activated.

[0013] According to another preferred embodiment of the invention, the controller comprises a self-powered driver coupled between the switch control terminal of the first controllable semiconductor switch and the output electrode of the output section. Furthermore, the self-

powered driver comprises a timer circuit configured to control the state of the first semiconductor switch in accordance with a timer period setting wherein the timer period setting is based on the cycle time of the transformer output signal. The termination of the second period of the cycle time is therefore controlled by the timer period setting rather than the previously discussed synchronous state control signal. The coupling of the self-powered or autonomous driver allows the driver to float and follow an instantaneous voltage of output electrode of the piezoelectric transformer. Since the instantaneous voltage of output electrode may rise to a level of several hundred volt or even several kilovolt for high-voltage piezoelectric power converters the lack of any need for supplying a switch control signal at the same voltage level to the self-powered driver for terminating the second period of the cycle time is a significant advantage. The self-powered driver preferably comprises a local energy storage component supplying power to the self-powered driver and a rectifying element is coupled between the local energy storage component and a power supply voltage of the power converter to energize the local energy storage component. The local energy storage component may comprise a capacitor or a rechargeable battery that is charged or energized during time intervals wherein the instantaneous voltage at output electrode is relatively small such as below a DC supply voltage of the power converter. The DC supply voltage may be a positive DC supply voltage between 10 and 50 volt such as about 24 volt. During time intervals wherein the instantaneous voltage at output electrode has a high magnitude such as above a positive DC supply voltage or below a negative DC supply voltage of the power converter, the local energy storage component is charged and delivers a local supply voltage to the self-powered driver including the timer circuit allowing these to operate as described above. The rectifying element preferably comprises a high-voltage diode having a break-down voltage larger than 200 V, or more preferably larger than 500 V or larger than 1000 V. In the latter embodiment, the high-voltage diode is preferably the only galvanic connection between the self-powered driver and the power supply voltages or rail of the power converter. The high-voltage diode is reverse biased during time intervals where the instantaneous voltage at output electrode has a high magnitude as described above such that the local energy storage component is the exclusive source of power for the self-powered driver during such time intervals. In one embodiment, the self-powered driver is configured to start the timer in response to a change of bias state of the rectifying element. Consequently, when the instantaneous voltage at output electrode exceeds the local supply voltage, the timer automatically initiates the second period of the cycle

time and sets this period substantially equal to the timer period setting. The timer period setting is preferably equal to 50 % of the cycle time of the transformer output signal but may be less in other embodiments such as less than 20 % or 10 % of the cycle time of the transformer output signal.

[0014] Power converters are often required to provide a specified or target AC or DC voltage as the output voltage within certain bounds or limits which generally require voltage regulation at the load. The present piezoelectric power converter is capable of providing output voltage regulation without sacrificing power conversion efficiency by transferring power back to the input energy source during the second period of the cycle time where the output voltage is discharged as previously described. The controller may be configured to control the switching between the first and second states of the bi-directional switching circuit based on a difference between the output voltage and a predetermined AC or DC reference voltage where the latter is the target AC or DC voltage. If the AC or DC reference voltage is larger than the current output voltage of the piezoelectric power converter, the controller may adapt the bi-directional switching circuit to exclusively operate in the first state to increase the output voltage. On the other hand if the current output voltage of the piezoelectric power converter is smaller the AC or DC reference voltage, the controller may adapt the bi-directional switching circuit to operate in the second state to decrease or discharge the output voltage during the second time periods of the cycle time and at the same time return power to the input power source through the primary section of the piezoelectric transformer.

[0015] In one embodiment, the predetermined excitation frequency of the input drive signal is set by a self-oscillating feedback loop arranged around the input driver and the piezoelectric transformer. The use of the self-oscillating feedback loop to set the predetermined excitation frequency or excitation frequency has considerable advantages because the excitation frequency automatically tracks changing characteristics of the piezoelectric transformer itself and electronic circuitry of the input driver. These characteristics will typically change across operation temperature and age of the piezoelectric power converter, but the feedback loop ensures such changes are tracked by the excitation frequency so as to maintain the excitation frequency at an optimum frequency or within an optimum frequency band. The optimum frequency band may be a frequency range wherein the piezoelectric transformer exhibits inductive behaviour with a ZVS factor higher than 100 % such that ZVS operation of the input driver can be achieved

even in the first state of the bi-directional switching circuit. In one embodiment the self-oscillating feedback loop comprises an adjustable time delay configured to adjust a phase response of the self-oscillating feedback loop whereby the predetermined excitation frequency is adjusted. . This is particularly useful in connection with the present bi-directional piezoelectric power converter wherein the impedance characteristics of the piezoelectric transformer changes at and proximate to the fundamental resonance frequency in response to the level of reverse power transmission. When reverse power is transmitted through the power converter, e.g. during the second state of the bi-directional switching circuit, the excitation frequency set by the self-oscillating feedback loop decreases and the ac resonance current in the piezoelectric transformer increases. This effect can be detected by a resonance current control circuit and compensated by an appropriate adjustment of the delay of the adjustable time delay such that an optimal operation point of the self-oscillating feedback loop can be maintained during both forward power transmission and reverse power transmission of the bi-directional piezoelectric power converter.

[0016] A second aspect of the invention relates to a piezoelectric power converter comprising:

- a piezoelectric transformer comprising an input electrode electrically coupled to an input or primary section of the piezoelectric transformer and an output electrode electrically coupled to secondary or output section of the piezoelectric transformer to provide a transformer output voltage,
- an input driver electrically coupled directly to the input electrode and arranged to supply an input drive signal to the input electrode,
- a feedback loop operatively coupled between the output electrode of the piezoelectric transformer and the input driver to provide a self-oscillation loop around the input section of the piezoelectric transformer oscillating at an excitation frequency. The electrical characteristics of the feedback loop are preferably configured to set the excitation frequency of the self-oscillation loop within a ZVS operation range of the piezoelectric transformer.

[0017] The piezoelectric power converter according to this second aspect of the invention benefits from the above-described advantages of the self-oscillating feedback loop arranged around the input driver and the piezoelectric transformer. The piezoelectric transformer preferably has a zero-voltage switching factor (ZVS factor) larger than 1.0 or 100 %, preferably larger than 1.2 or 120%, such as larger than 1.5 or 150%, or larger than 2.0 or 200 %;

[0018] in which the ZVS factor is determined at a matched load condition as:

$$ZVS = \frac{k_{eff\_S}^{-2} - 1}{k_{eff\_P}^{-2} - 1}\ 0.882 \quad (1)$$

[0019] $k_{eff\_P,}$ being a primary side effective electromechanical coupling factor of the piezoelectric transformer,

[0020] $k_{eff_S,}$being a secondary piezoelectric transformer effective electromechanical coupling factor, in which:

$$k_{eff\_P} = \sqrt{1 - \frac{f_{res\_p}^2}{f_{anti-res\_p}^2}} \qquad k_{eff\_S} = \sqrt{1 - \frac{f_{res\_s}^2}{f_{anti-res\_s}^2}}$$

[0021] f_{res_p} = a minimum magnitude of an impedance function at the input electrode of the piezoelectric transformer with shorted first and second output electrodes,

[0022] $f_{anti\_res\_p}$ = a maximum magnitude of the impedance function at the input electrode of the piezoelectric transformer with shorted first and second output electrodes,

[0023] f_{res_s} = a minimum magnitude of the impedance function at the first and second output electrodes of the piezoelectric transformer with shorted input electrodes,

[0024] $f_{anti\_res\_s}$ = a maximum magnitude of the impedance function at the first and second output electrode of the piezoelectric transformer with shorted input electrodes.

[0025] A third aspect of the invention relates to a method of increasing an apparent ZVS factor of a piezoelectric transformer of a power converter. The method comprising steps of:

- applying an input drive signal with a predetermined excitation frequency to an input electrode of the piezoelectric transformer,
- providing a bi-directional switching circuit coupled between a secondary or output section of the piezoelectric transformer and an output voltage of the power converter,
- conducting, in a first state, forward current from the output section to the output voltage through the bi-directional switching circuit during a first period of a cycle time of the transformer output signal to charge the output voltage,

- conducting, in a second state, reverse current from the output voltage to the output section through the bi-directional switching circuit during a second period of the cycle time of the transformer output signal to discharge the output voltage,

- adjusting the apparent ZVS factor of the piezoelectric transformer by adjusting a length of the second period of the cycle time.

[0026] As described above, when reverse power is transmitted through the power converter during the second period of the cycle time of the transformer output signal, the ac resonance current in the piezoelectric transformer increases in response thereto such that it appears more inductive as seen from the input driver coupled to the primary side of the piezoelectric transformer. The increase of apparent transformer input inductance is caused by the increasing energy storage capability of the piezoelectric transformer. This increase of apparent inductance of the piezoelectric transformer is highly useful to reduce the overall size and EMI radiation of the piezoelectric power converter. The higher apparent inductance of the piezoelectric transformer itself allows the input driver to be coupled directly to input electrode of the primary section without any of the normally used series or parallel inductors and still maintain zero-voltage switching conditions in the input driver, i.e. ZVS operation. Thereby, the present methodology of increasing the apparent ZVS factor of the piezoelectric transformer, and the corresponding bi-directional piezoelectric power converter, can utilize piezoelectric transformer types without native ZVS capability, i.e. having a ZVS factor below 100 %, and still allow ZVS operation of the input driver. The length of the second period of the cycle time may accordingly be adjusted to a value which provides ZVS operation of the input driver during operation of the power converter in the second state of the switching circuit.

[0027] A preferred embodiment of the present methodology comprises a further step of:

- conducting both forward current and reverse current during a single cycle of the transformer output signal. As previously explained, the net power transferred to the output voltage may be controlled in either a step-wise or in a substantially continuous manner by a corresponding control of the relative length between the first and second periods of the same cycle of the transformer output signal such that energy efficient and accurate output voltage regulation is possible. Since the amount of reversely transmitted power or energy through the piezoelectric transformer can be varied by adjusting the length of the second period of the cycle of the transformer output

signal the apparent ZVS factor of the piezoelectric transformer can be efficiently and accurately controlled.

BRIEF DESCRIPTION OF THE DRAWINGS

[0028] Preferred embodiments of the invention will be described in more detail in connection with the appended drawings, in which:

[0029] Fig. 1 is a schematic block diagram of a bi-directional piezoelectric power converter in accordance with a first embodiment of the invention,

[0030] Fig. 2 is a schematic block diagram of a self-powered high-side driver for a bi-directional piezoelectric power converter,

[0031] Fig. 3 is a schematic block diagram of a bi-directional piezoelectric power converter in accordance with a second embodiment of the invention,

[0032] Figs. 4a) – d) depict measured forward and reverse current waveforms through a bi-directional switching circuit at four different output power settings of the piezoelectric power converter depicted in Fig. 1,

[0033] Fig. 4e) shows measured forward and reverse power figures through the bi-directional piezoelectric power converter over a time period where these quantities are adjusted during operation of the power converter,

[0034] Fig. 5 is a schematic block diagram of a generic bi-directional switching circuit,

[0035] Fig. 6 is a schematic block diagram of a bi-directional switching circuit configured for half-wave rectification with either positive or negative DC output voltage; and

[0036] Fig. 7 is a schematic block diagram of a bi-directional switching circuit configured for full-wave rectification with positive DC output voltage.

DETAILED DESCRIPTION

[0037] The below appended detailed description of embodiments of the present invention relate to bi-directional piezoelectric power converters for voltage step-up or voltage multiplication aimed at generating high DC output voltages such as output voltages from several hundred Volts to several thousand Volts. However, the skilled person will understand that the below de-

scribed embodiments are highly useful for other types of applications such as step-down and low voltage power converters requiring high power conversion efficiency.

[0038] Fig. 1 shows a schematic block diagram of a bi-directional piezoelectric power converter 100 in accordance with a first embodiment of the invention. The bi-directional piezoelectric power converter 100 comprises a piezoelectric transformer, PT, 104. The piezoelectric transformer, PT, 104 has a first input electrode 105 electrically coupled to an input or primary section of the bi-directional piezoelectric power converter 100 and a second input electrode connected to ground, GND. A first output electrode 107 of the piezoelectric transformer 104 is electrically coupled to secondary or output section of the piezoelectric transformer 104 to provide a transformer output signal and a second output electrode is connected to ground, GND, like the second input electrode. The bi-directional piezoelectric power converter 100 additionally comprises an input driver 103 electrically coupled directly to the input electrode 105 so as to apply an input drive signal to the input or primary section. A driver control circuit 102 generates appropriately timed gate control signals for NMOS transistors M_2 and M_1 of the input driver 103. The input drive signal has a predetermined excitation frequency determined by parameters of a self-oscillating feedback loop arranged around or enclosing the input driver 103 and the piezoelectric transformer 104. The self-oscillating feedback loop comprises a feedback leg 114 coupling a resonance oscillation signal, having a frequency equal to the predetermined excitation frequency, detected in the piezoelectric transformer structure back to the driver control circuit 102. The self-oscillating feedback loop comprises a resonance current control circuit 112 comprising a peak current detector 126 coupled to a current limiter 128. The resonance current control circuit 112 is configured to adjust a time delay of the adjustable time delay circuit 124 arranged in the feedback leg 114. An AC resonance current in the piezoelectric transformer 104 is detected by a resonance current detector 118 coupled to either the primary side or secondary side of the piezoelectric transformer 104. A resonance current signal supplied by the detector 118 is transmitted to a low-pass or band-pass filter 120 which provides additional phase shift through the feedback loop and may attenuate or suppress certain harmonics components of the fundamental resonance frequency of the piezoelectric transformer 104. A zero-crossing detector 122 receives a filtered signal from the low-pass or band-pass filter 120 and provides an essentially square wave shaped signal indicating zero-crossings of the filtered signal which has an approximate sine shaped waveform. The square wave signal is transmitted to an adjustable time delay

circuit 124 which introduces a variable phase in the self-oscillating feedback loop such that the predetermined excitation frequency can be adjusted. An output signal of the adjustable time delay circuit 124 is coupled to the drive control circuit 102 such as to close the self-oscillating feedback loop around the input driver 103. A resonance current control circuit 112 detects a peak current from the output signal of the low-pass or band-pass filter 120 and adjusts a time delay of the adjustable time delay circuit 124 based thereon. This is useful to compensate for a decrease of the excitation frequency set by the self-oscillating feedback loop under reverse power transmission through the piezoelectric power converter, e.g. in the second state of the bi-directional switching circuit. The ac resonance current in the piezoelectric transformer increases under reverse power transmission and the change is detected by a peak current detector 126 of the resonance current control circuit 112. The effect is compensated by limiting the ac resonance current by the current limiter 128 which makes an appropriate adjustment of the time delay in the adjustable time delay circuit 124 such that an optimal operation point of the self-oscillating feedback loop can be maintained during both forward power transmission and reverse power transmission of the bi-directional piezoelectric power converter 100.

[0039] In the present embodiment of the invention where the input driver 103 is coupled directly to the input electrode 105 without any series or parallel inductor, the piezoelectric transformer 104 preferably possess a ZVS factor larger than 100 % such as larger than 120 %. In this manner ZVS operation of the input driver 103 is enabled both in a first state and a second state of a bi-directional switching circuit 108. The ZVS operation of the input driver 103 improves the power conversion efficiency of the bi-directional piezoelectric power converter 100. The predetermined excitation frequency is preferably selected or set to lie slightly above a fundamental resonance frequency of the piezoelectric transformer 104 within a frequency band or range where the piezoelectric transformer 104 exhibits the above-described ZVS factor larger than 100 % and appears possess inductive input impedance. The feedback leg 114 is coupled to the resonance current control circuit 112 that detects and limits the ac current flowing inside the piezoelectric transformer 104 as explained in further detail above. The use of the self-oscillating feedback loop has considerable advantages because, the predetermined excitation frequency automatically tracks changing characteristics of the piezoelectric transformer 104 and electronic circuitry of the input side of the power converter like the drive control circuit 102. These characteristics will typically change across operation temperature and age but the self-oscillating feedback loop

ensures changes are tracked by the excitation frequency because a slope of the phase response of the piezoelectric transformer 104 is typically much steeper than a slope of a phase response of the low-pass or band-pass filter 120. In this manner, the predetermined excitation frequency will largely be sensitive only to changes of electrical characteristics of the piezoelectric transformer 104 such that the self-oscillating feedback loop automatically maintains the predetermined excitation frequency at an optimum frequency or within an optimum frequency band such as in the ZVS operation range or frequency band of the piezoelectric transformer 104.

[0040] At the secondary side of the PT 104, a bi-directional switching circuit 108 is electrically coupled between a transformer output signal generated at the output electrode 107 of the PT 104 and a positive DC output voltage V_{OUT} applied across a load capacitor C_{LOAD} of the power converter 100. The load may of course comprise a resistive and/or inductive component in addition to the depicted load capacitance C_{LOAD}. A controller or control circuit is adapted to control forward current conduction from the output electrode 107 to V_{OUT} through the bi-directional switching circuit 108 during a first period of the cycle time of the transformer output signal. The positive DC output voltage V_{OUT} is accordingly charged during the first period of the cycle time. This transformer output signal, oscillating at the excitation frequency of the input signal, is applied to a midpoint node between series coupled NMOS transistors M_4 and M_3 of the bi-directional switching circuit 108. The output section of the PT 104, oscillating at the excitation frequency, behaves largely as a current source injecting AC current into the midpoint node between series coupled M_4 and M_3 to generate the transformer output signal or voltage. Furthermore, the controller is adapted to control a second period of the cycle time of the transformer output signal wherein reverse current is conducted through the bi-directional switching circuit 108 to the output electrode 107 of the PT such that V_{OUT} is discharged during the second period of the cycle time. During the second period of the cycle time power is returned to the primary section of the piezoelectric transformer through the output electrode 107 of the PT.

[0041] The skilled person will appreciate that M_3 and M_4 function as respective controllable semiconductor switches each exhibiting low resistance between an inlet and an outlet node (i.e. drain and source terminals) in the on-state and very large resistance in the off-state or non-conducting state. The on-resistance of each of M_3 and M_4 in its on-state/conducting state may vary considerably according to requirements of a particular application, in particular the voltage level at the DC output voltage V_{OUT} or load impedance. In the present high-voltage embodiment

of the invention, each of the M_3 and M_4 is preferably selected such that its on-resistance lies between 50 and 1000 ohm such as between 250 and 500 ohm. The positive DC supply voltage V_{DD} may vary widely in accordance with the requirements of a particular application. In the present embodiment of the invention, the positive DC supply voltage V_{DD} is preferably selected to a voltage between 20 and 40 volt such as about 24 volt.

[0042] The bi-directional switching circuit 108 comprises a high-side semiconductor diode D_4 arranged or coupled across drain and source terminals of M_4 so as to conduct the forward current to the DC output voltage V_{OUT} in a first state of the bi-directional switching circuit 108. A low-side semiconductor diode D_3 is in a similar manner coupled across drain and source terminals of M_3 so as to conduct the reverse current through the output electrode 107 and output section of the PT 104 during at least a portion of the first state. In the first state, the forward current is conducted from the output electrode 107 of the PT 104 through the bi-directional switching circuit 108 to the DC output voltage V_{OUT} during a first period of a cycle time of the transformer output signal to charge the output voltage. This is accomplished by switching the high-side NMOS transistor M_4 to its on-state or conducting state by a self-powered high-side driver 106 which forms part of the controller. The self-powered high-side driver 106 or self-powered driver 106 is coupled between the control or gate terminal of M_4 and the output electrode 107 which supplies the transformer output signal. The timing of the state switching of M_4 is determined by the detection of forward current in D_4 by a current sensor (not shown) contained in the self-powered driver 106. This current sensor is preferably arranged in series with the high-side semiconductor diode D_4. In response to detection of forward current in D_4 the self-powered driver 106 switches M_4 to its on-state which effectively clamps D_4 such that a majority of the forward current flowing through the parallel connection of M_4 and D_4 to the DC output voltage V_{OUT} in reality flows through M_4. On the other hand, during a negative half-cycle of the transformer output signal in the first state of the bi-directional switching circuit 108, D_4 is reverse biased and M_4 switched to its off-state at expiry of a timer period setting of the timer circuit 205 (refer to Fig. 2) as explained below in additional detail. However, current is now conducted from the negative supply rail, i.e. GND in the present embodiment, to the output electrode 107 of the PT 104 through the parallel connection of M_3 and D_3. Initially, D_3 will start to conduct forward current once it becomes forward biased by the negative transformer output voltage. M_3 is on the other hand, switched to its on-state or conducting state by a low-side driver 121 which forms part

of the controller. The low-side driver 121 is coupled to the gate terminal of M_3 and configured to switch M_3 from its off-state to its on-state and vice versa. However, while the timing of the state switching of M_3 from its off-state to the on-state is determined in a manner similar to M_4, the opposite state switching of M_3 is effected synchronously to input drive signal as explained below. M_3 is switched from the off-state to the on-state by a detection of forward current in D_3 by a current sensor (not shown) contained in the low-side driver 121. This current sensor is arranged in series with the low-side semiconductor diode D_3. At the detection of forward current in D_3 the low-side driver 121 switches M_3 to its on-state which effectively clamps D_3 such that a majority of the forward current flowing through the parallel connection of M_3 and D_3 in reality flows through M_3.

[0043] Consequently, in the first state the bi-directional switching circuit 108 functions as a half-wave rectifier or voltage doubler of the transformer output signal such that forward current is conducted from the output electrode 107 of the PT 104 through the high-side NMOS transistor M_4 and semiconductor diode D_4 to the DC output voltage V_{OUT} to charge V_{OUT}. In the negative half-periods of the transformer output signal, current is circulated around the secondary section of the PT 104 without charging the DC output voltage in the current embodiment which uses the half-wave rectification provided by the present bi-directional switching circuit 108. In comparison to a traditional diode-based half-wave rectifier, the bi-directional switching circuit 108 additionally comprises the NMOS transistors M_4 and M_3 of the bi-directional switching circuit 108 arranged for clamping of the high and low-side semiconductor diodes D_4 and D_3. During a second state and during a third state of the bi-directional switching circuit 108, the NMOS transistors M_3 and M_4 are controlled by the controller such that a flow of reverse power is enabled. The reverse current is conducted through the bi-directional switching circuit 108 from the DC output voltage V_{OUT} to the output electrode 107 of the PT 104 during a second period of the cycle time of the transformer output signal so as to discharge V_{OUT}. Due to the inherent bi-directional transfer property of the PT 104 power applied to the secondary section through the output electrode 107 is transferred to the input section of the PT 104 in effect transferring power in opposite direction to the normal flow of power of the power converter 100.

[0044] In connection with the reverse current conduction during the second period of the cycle time, state switching of M_3 is controlled by the low-side driver 121 coupled to the gate terminal of M_3. The low-side driver 121 is responsive to a synchronous state control signal de-

rived from the input drive signal supplied by an adjustable time delay circuit, control ΔT, of a phase controller 111. The phase controller comprises the adjustable time delay circuit, control ΔT, and a fixed time delay, ΔT circuit. The phase controller 111 receives the previously mentioned zero-crossing detector output signal 119 which switches states synchronously to the input drive signal and the transformer output signal because this signal is generated inside the self-oscillating feedback loop. Since the input drive signal and the transformer output signal oscillate synchronously to each other, the time delay imposed by the phase controller 111 to the zero-crossing detector output signal 119 sets a length or duration of the second period of the cycle time of the transformer output signal. M_3 is allowed to continue conducting current for the duration of the second period of the cycle time until the state transition of the synchronous state control signal turns off M_3 of the low-side driver 121. While the corresponding state switching of the high-side NMOS transistor M_4 from its on-state to its off-state in one embodiment is controlled by the synchronous state control signal albeit phase shifted about 180 degrees, the present embodiment of the invention uses a different turn-off mechanism provided by the self-powered high-side driver 106. The self-powering of the high-side driver 106 is configured to terminate a reverse current conducting period of M_4 based on an internally generated state control signal supplied by an internal timer rather than the above-described synchronous state control signal supplied by the adjustable time delay circuit, control ΔT. The self-powered property of the high-side driver 106 is highly advantageous for high-voltage output PT based power converters where the DC output voltage may be above 1 kV. The self-powering property of the high-side driver 106 circumvents the need for raising the zero-crossing detector output signal 119 to a very high voltage level, i.e. matching the level of the DC output voltage, before being supplied to the high-side driver 106 to appropriately control the gate terminal of M_4. The skilled person will recognize that the gate terminal of M_4 must be raised to a level above the level of the DC output voltage signal to switch M_4 to its on-state. The self-powered high-side driver 106 is electrically coupled between the gate terminal of M_4 and the output electrode 107 carrying the transformer output voltage as explained in further detail below in connection with Fig. 2.

[0045] During operation, the bi-directional piezoelectric power converter 100 comprises two distinct mechanisms for adjusting the level of the DC output voltage V_{OUT}. A first mechanism uses a DC output voltage detection or monitoring circuit 109 which supplies a signal to the output voltage control circuit 110 of the controller indicating the instantaneous level of the DC

output voltage. A charge control circuit ΔQ compares the instantaneous level of the DC output voltage with a reference voltage which for example represents a desired or target DC output voltage of the power converter. The charge control circuit determines whether the current DC output voltage is to be increased or decreased based on this comparison and adjusts at least one of: {a modulation of a pulse width modulated input drive signal, a carrier frequency of the pulse width modulated input drive signal, a burst frequency of a burst modulated input drive signal} in appropriate direction to obtain the desired adjustment of the DC output voltage. A second mechanism for adjusting the level of the DC output voltage V_{OUT} also uses the level signal from the DC output voltage detection circuit 109. In this instance the output voltage control circuit 110 adjusts the duration of the second period of the cycle time of the transformer output signal where M_3 conducts reverse current through the adjustable time delay circuit, control ΔT, of the phase controller 111. The corresponding adjustment of the second period of the cycle time as regards M_4 is preferably made by delaying the triggering time or point of a timer circuit included in the self-contained high-side driver 106 as explained below in connection with Fig. 2. The delay of the triggering time of the timer circuit may be controlled dynamically during operation of the bi-directional power converter 100 by the controller by adjusting a delay of an adjustable time delay circuit, control ΔT, to reach a desired or target duration of the second period of the cycle time of the transformer output signal. The adjustable time delay circuit, control ΔT, allows the controller to adjust the duration of the second period of the cycle time of the transformer output signal wherein reverse current is conducted by the bi-directional switching circuit through the output electrode 107 back to the primary side of the PT 104. By this adjustment of the duration of the second period of the cycle time, the amount of reverse power can be effectively controlled allowing for the desired adjustment of the level of the DC output voltage V_{OUT} while conserving power.

[0046] The skilled person will appreciate that the degree of charge or discharge of the V_{OUT} may be controlled in a step-wise or substantially continuous manner by a corresponding control of the duration of the second period of the cycle time such that the level of V_{OUT} may be continuously increased or reduced as desired. Furthermore, the length of the second period of the cycle time of the high-side NMOS transistor M_4 may be adapted to track the same for M_3 as explained below in connection with the detailed description of the operation of the self-powered high side driver 106. The skilled person will understand that if the duration of the second period

of the cycle time is set to zero by the controller, the bi-directional piezoelectric power converter 100 may be adapted to exclusively operate the first state where the switching circuit charges the positive DC output voltage during the first period of cycle times of the transformer output signal. In this state, the NMOS transistors M_3 and M_4 are only conducting during the first period of the cycle time so to actively clamp the low-side and high-side semiconductor diodes D_3 and D_4, respectively.

[0047] Fig. 2 is a schematic circuit diagram of the design of the self-powered high-side driver 106. The self-powered driver 106 comprising the above-mentioned timer circuit 205 or timer 205 coupled to the gate terminal of NMOS transistor M_4 through gate driver 207 so as to control the duration of its on-state, and possibly an off-state, of M_4 in accordance with a timer period defined by a timer period setting. The timer period or timer delay is preferably adjusted to about 50 % of the cycle of the transformer output signal as set by the excitation frequency controlled by the self-oscillating feedback loop. The self-powered driver 106 comprises a rectifying element in form of high-voltage diode 201 coupled in series with a pair of anti-parallel diodes D_{1a} and D_{1b} which are coupled to a local supply capacitor 203 C_{local}. The local supply capacitor 203 is acting as a rechargeable energy storage component which is charged (as indicated by charge current I_{boot}) with energy from the positive DC supply voltage V_{DD} during conduction periods of the high-voltage diode 201. The voltage V_{local} on the local supply capacitor 203 C_{local} is coupled to voltage supply lines of the circuit blocks of the self-powered high-side driver 106 to supply operating power to these circuits during time periods where the self-powered driver 106 is decoupled from the residual portion of the power converter as described below. A Reset input R of the timer circuit 205 is coupled to a voltage level V_R at a circuit node in-between the high-voltage diode 201 and the anti-parallel diodes D_{1a} and D_{1b}. When the transformer output voltage at the output electrode 107 of the PT is raised above GND because the low-side NMOS transistor M_3 has been switched to its non-conducting state the AC current supplied by the PT through the output electrode 107 raises the voltage at the midpoint node between series coupled NMOS transistors M_4 and M_3 eventually leading to a forward biasing of the semiconductor di-

ode D_4, the voltage level at V_R will fall from approximately V_{DD} towards the local zero potential on node 107, Gnd_local. When the voltage level at V_R has dropped down to the local zero potential, the high-voltage diode 201 becomes reverse biased. The timer circuit 205 is triggered because V_R is conveyed to the Reset input R of the timer circuit 205. The output of the timer circuit 205 switches to its off state after expiry of the timer period, i.e. about one-half of the cycle time of the transformer output signal in the present embodiment. This state transition is then immediately conveyed to the gate input of M_4 by the gate driver 207. In response M_4 is accordingly switched to its off-state. Consequently, the state switching of M_3 from on-state to the off-state determines when the transformer output voltage at the output electrode 107 begins to increase from the ground level triggering the timer circuit 205 and initiating the timer period according to the timer period setting. Because, the state switching of M_3 from its on-state to its off-state is controlled by the above-described synchronous state control signal supplied by the adjustable time delay circuit, control ΔT, the turn-off timing or instant of M_3 indirectly controls or sets the delayed turn-off timing of M_4. Consequently, by adjustment of the time delay provided by the time delay circuit, control ΔT, the controller is able to adjust the length of the second period of the cycle time of the high-side NMOS transistor M_4 where reverse current is conducted. The current sense circuit is adapted to sense a forward current running through the semiconductor diode D_4 by monitoring a voltage drop across a sense resistor R and turn on M_4 through the gate driver 207 in response to a detection of forward current such that M_4 effectively clamps the semiconductor diode D_4 during the first period of the cycle time of the transformer output signal to establish a low-impedance path for the conduction of forward current through the bi-directional switching circuit to V_{OUT} to charge V_{OUT}.

[0048] Fig. 3 shows a schematic block diagram of a bi-directional piezoelectric power converter 300 in accordance with a second embodiment of the invention. Corresponding features have been provided with corresponding reference numerals in the first and second embodiments of the bi-directional piezoelectric power converter to ease comparison. Generally, the bi-directional piezoelectric power converter 300 has similar characteristics and features as those

explained in connection with the first embodiment, but the way the predetermined excitation frequency at the input driver 302 is set differs. In the first embodiment, the predetermined excitation frequency was set by loop parameters, including parameters of the PT 104, of the self-oscillating feedback loop formed around the piezoelectric transformer. However, in the present embodiment, the predetermined excitation frequency is set by an independent frequency generator or oscillator 317. The predetermined excitation frequency is preferably set to a value within a frequency range where the PT 304 exhibits inductive input impedance. Such inductive input impedance enables ZVS operation of the input driver 303 to improve its power conversion efficiency as explained above.

[0049] Figs. 4a) – d) depict measured forward and reverse current waveforms through the bi-directional switching circuit 108 during delivery of a positive, zero and negative net output power to the load capacitor $C_{LOAD.}$ The y-axis of all the upper graphs 402 depicts current in mA and the x-axes time in milliseconds such that the x-axis spans over a time period of about 100 μS. The dotted curve 403 of each of the upper graphs 402 of Figs. 4a)-d) shows measured current through the parallel connection of M_4 and D_4 to the DC output voltage V_{OUT} (refer to Fig. 1) such that V_{OUT} is charged during positive half-periods of the transformer output signal on the electrode 107. The full line curves 405 of the same graphs 402 of Figs. 4a)–d) show measured current through the parallel connection of M_3 and D_3 where current is conducted in opposite or negative half-periods of the cycle time of the transformer output signal. In the negative half-periods of the transformer output signal, the current is circulated around the secondary section of the PT 104 without charging the DC output voltage. The lower graphs 401 of Figs. 4a)-d) show the input drive voltage waveform 407 at the first input electrode 105 which is coupled to the input section of the PT. The y-axis of the lower graphs 401 depicts the input drive voltage in volt. The skilled person will understand that the corresponding transformer output voltage at the electrode 107 may have peak values above several hundred or even several kV due to the voltage gain of the PT 104.

[0050] In the depicted operation mode in Fig. 4a), the bi-directional switching circuit operates essentially in its first state where the circuit essentially acts as a traditional half-wave rectifier. The DC output voltage V_{OUT} is charged by the forward current running through the high-side rectifying element, comprising the parallel connection of M_4 and $D_{4,}$ to the DC output voltage in every positive half-period of the transformer output voltage. The current through the

parallel connection of M_4 and D_4 runs forward during the first period 403f of each of the cycle times of the transformer output signal as indicated schematically on the dotted current waveform curve 403. A positive net output power of 2.6 W is delivered to the load capacitor $C_{LOAD.}$

[0051] In Fig. 4b), the bi-directional switching circuit 108 has been switched to its second state and the positive output power to load capacitor C_{LOAD} is reduced from the above 2.6 W to 1.4 W by reverse conduction of power to the input side of the PT. This is visible by inspection of the dotted curve 403 of the upper graph 402 of Fig. 4b) which shows measured current through the high-side rectifying element, comprising the parallel connection of M_4 and $D_{4,}$ to the DC output voltage. The current through the parallel connection of M_4 and D_4 runs forward during a first period 403f of the cycle time of the transformer output signal such that the DC output voltage is charged. However, during a second period 403r of the same cycle of the transformer output signal, the current through the parallel connection of M_4 and D_4 runs in an opposite direction and becomes negative such that the DC output voltage is discharged rather than charged. The second period of the cycle of the transformer output signal, where reverse current is conducted, is introduced or caused by a delayed or phase-shifted turn-off timing of the NMOS transistor M_4 through the adjustable time delay circuit, control ΔT, of the phase controller 111 as previously explained. By comparison of the areas underneath the current waveform 403 during the first and second periods 403f, 403r of the same cycle of the transformer output signal it is apparent that net positive charge or power is transferred to the DC output voltage under the chosen conditions which is consistent with the measured positive output power of 1.4 W.

[0052] In Fig. 4c), the bi-directional switching circuit 108 also operates in its second state as was the case in Fig. 4b). However, the output power to the load capacitor C_{LOAD} is reduced from the above 1.4 W to 0.0 W by an increased delay of the turn-off timing of the NMOS transistor M_4 as explained above in connection with Fig. 2. The increased time shift leads to a longer duration of the second period of the transformer output signal where reverse current is conducted through M_4 such the DC output voltage is further discharged compared to the situation in Fig. 4b). This is visible by inspection of the dotted curve 403 of the upper graph 402 of Fig. 4c) which shows measured current through the high-side rectifying element, comprising the parallel connection of M_4 and $D_{4,}$ to the DC output voltage during consecutive cycle times of the

transformer output voltage. The current through the parallel connection of M_4 and D_4 runs forward during a first period 403f of the cycle time of the transformer output signal such that the DC output voltage is charged. However, during a second period 403r of the same cycle of the transformer output signal, the current through the parallel connection of M_4 and D_4 becomes negative as explained above such that the DC output voltage is discharged rather than charged in the second time period. By comparison of the areas underneath the current waveform 403 during the first and second periods 403f, 403r of the same cycle of the transformer output signal it is readily apparent that approximately zero net charge or zero net power is transferred to the DC output voltage during a cycle time of the transformer output voltage under the chosen conditions. This observation is also consistent with the measured output power of 0.0 W.

[0053] Finally, in Fig. 4d), the bi-directional switching circuit 108 continues to operate in the second state as was the case in Figs. 4b) and c). However, the net output power to the load capacitor C_{LOAD} is now negative at -2.4 W rather than positive or zero. This has been achieved by a further increase of the delay of the turn-off timing of the NMOS transistor M_4 as explained above in connection with Fig. 2. The increased time shift leads to a longer duration of the second period of the transformer output signal where reverse current is conducted through M_4 such the DC output voltage is further discharged compared to the situation in Fig. 4c). This is visible by inspection of the dotted curve 403 of the upper graph 402 of Fig. 4d) which shows measured current through the high-side rectifying element, comprising the parallel connection of M_4 and D_4 to the DC output voltage during consecutive cycle times of the transformer output voltage. The first period 403f of the cycle time of the transformer output signal is very small such that only a single short spike of forward current through the parallel connection of M_4 and D_4 is visible making the amount of charge or forward current transferred to the DC output voltage nearly zero during the first period 403f. However, the second period 403r has nearly a duration of an entire half-period of the cycle time or period of the transformer output signal such that a large amount of reverse current is conducted through the parallel connection of M_4 and D_4 leading to a substantial discharge of the DC output voltage. Consequently, by comparison of the areas underneath the current waveform 403 during the first and second periods 403f, 403r of the same cycle

of the transformer output signal it is readily apparent that substantial amount of negative net charge or negative net power is transferred to the DC output voltage during a cycle time of the transformer output voltage under the chosen conditions. This observation is also consistent with the measured output power of -2.4 W.

[0054] Fig. 4e) shows measured forward and reverse power figures through the bi-directional piezoelectric power converter over a time period of approximately 6 milliseconds where these quantities are dynamically adjusted in opposite direction during operation of the piezoelectric power converter. The upper graph 412 shows corresponding values of measured input power, curve 415, and output power, curve 416, over time. The lower graph 411 shows the delay of the turn-off timing of the NMOS transistor M_4 which is controlled by the turn-off timing of the low-side NMOS transistor M_3 through the adjustable time delay circuit, control ΔT, of the phase controller 111 as previously explained. The y-axis of the lower graph 411 depicts this time delay in μS. As illustrated, the controller of the present piezoelectric power converter enables both full forward transmission of power from the input to the output as illustrated at a time delay value of zero μS. In this operation state, substantially all input power of approximately 2.6 W is transferred to the load capacitor $C_{LOAD.}$ When the time delay is gradually increased from about 1 μS to about 6 μS over time depicted along the x-axis from about 6 mS to about 8 mS, the input power gradually becomes less and less positive and finally negative indicating that a continuously increasing amount of power is transmitted in reverse direction from the output voltage and back to the primary section of the piezoelectric transformer. The measured output power curve 416 has a mating shape indicating that a gradually decreasing output power and finally a negative output power is supplied to the load capacitor $C_{load.}$ Hence the load capacitor is discharged by reverse power transmission back to the primary section of the piezoelectric transformer. The skilled person will appreciate the efficient and flexible way the present bi-directional piezoelectric power converter can be adapted for both forward and reverse transmission of power by control of the first and second states of the bi-directional switching circuit. This property enables energy efficient and accurate output voltage regulation.

[0055] Fig. 5 is a schematic block diagram of a generic and highly versatile bi-directional switching circuit 508 coupled to a PT 504. The bi-directional switching circuit 508 can be programmed to provide a positive or negative output voltage across the load capacitor C_{load} and to

provide half-wave or full-wave rectification of the transformer output signal supplied between the positive output electrode 507 and a negative, or opposite phase, output electrode 507b. The different modes of operation can be obtained through appropriate programming or setting of respective control voltages on the gate terminals of the NMOS transistors M4A, M4B, M3A, M3B, M6A, M6B, M5A and M5B. The transformer output signal at the positive output electrode 507 is applied to a midpoint node of a first branch of cascaded NMOS transistors M4A, M4B, M3A and M3B wherein an upper leg or high-side leg comprises M4A and M4B while a lower leg comprises cascaded NMOS transistors M3A and M3B. The oppositely phased transformer output signal at the negative output electrode 507b is applied to a midpoint node of a second branch of cascaded NMOS transistors M6A, M6B, M5A and M5B wherein an upper leg or high-side leg comprises M6A and M6B while a lower leg comprises cascaded NMOS transistors M5A and M5B. The secondary side of the PT 504 acts as a current source through the positive and negative output electrodes 507, 507b, respectively.

[0056] With NMOS transistors M4A, M4B and NMOS transistors M5A, M5B in their respective on-states/conducting states, a positive output voltage V_{OUT} is applied to the output electrodes 507, 507b irrespective of the polarity of the current delivered by the secondary side of the PT 504 through the positive and negative output electrodes 507, 507b, respectively. With NMOS transistors M4A, M4B and NMOS transistors M6A, M6B in their respective on-states/conducting states, zero volts is applied to the output electrodes 507,507b irrespective of the polarity of the current delivered by the secondary side of the PT 504 through the positive and negative output electrodes 507, 507b, respectively. With NMOS transistors M3A, M3B and NMOS transistors M6A, M6B in their respective on-states/conducting states, a negative DC output voltage V_{OUT} is applied to the output electrodes 507,507b irrespective of the polarity of the current delivered by the secondary side of the PT 504 through the positive and negative output electrodes 507, 507b, respectively.

[0057] In this manner, the bi-directional switching circuit 508 enables a controlled bi-directional flow of power through the PT 504 for output voltages of any polarity. Some of the different modes of operation are described below in further detail.

[0058] Fig. 6 is a schematic block diagram of a bi-directional switching circuit 608 configured for half-wave rectification of the transformer output signal supplied between the positive and negative output electrode 607 and 607b, respectively. The present bi-directional switching

circuit 608 is capable of providing both positive and negative output voltages at V_{OUT} by appropriate programming or adaptation. By constantly holding the NMOS transistors M4B, M3B in their respective on-states or conducting states during operation of the switching circuit 608, M4A and M3A will act as a half-wave rectifier generating a positive voltage at V_{OUT} by adapting the control signals for these NMOS transistors in the manner described above in connection with the first embodiment of the invention. This mode of operation of the bi-directional switching circuit 608 is accordingly similar to the operation of the bi-directional switching circuit 308 described previously under the first embodiment of the invention. The bi-directional switching circuit 608 can however also be programmed to provide a negative output voltage at V_{OUT} by setting the NMOS transistors M4A and M3A constantly to their on-states. In this alternative mode of operation, M4B and M3B will act as a half-wave rectifier generating a negative DC output voltage when appropriate control signals are applied to their respective gate inputs.

[0059] The secondary side of the PT 604 acts as a current source through the positive and negative output electrodes 607, 607b, respectively as previously explained. With NMOS transistors M4A, M4B switched to their respective on-states/conducting states, a positive output voltage V_{OUT} is applied to the output electrodes 607 irrespective of the polarity of the current delivered by the secondary side of the PT 604 through the positive output electrode 607. With NMOS transistors M3A, M3B switched to their respective on-states/conducting states, zero volts is applied to the output electrodes 607 irrespective of the polarity of the current delivered by the secondary side of the PT 604 through the positive output electrode 607. In this manner, the bi-directional switching circuit 608 enables a controlled bi-directional flow of power through the PT 604 for positive output voltages at V_{OUT} in a first state and controlled bi-directional flow of power through the PT 604 for negative output voltages at V_{OUT} in a second state.

[0060] Fig. 7 is a schematic block diagram of a bi-directional switching circuit 708 configured for full-wave rectification of the transformer output signal supplied between the positive and negative output electrode 707 and 707b, respectively. The bi-directional switching circuit 708 is configured to generate a positive output voltage across the load capacitor e.g. a positive DC voltage. The secondary side of the PT 704 acts as a current source through the positive and negative output electrodes 707, 707b, respectively as previously explained. With NMOS transistors M4A, M5A switched to their respective on-states/conducting states, the voltage V_{OUT} is applied to the output electrodes 707, 707b irrespective of the polarity of the current delivered by

30

the secondary side of the PT 704 through the output electrodes 707, 707b. With NMOS transistors M4A, M6A switched to their respective on-states/conducting states, or NMOS transistors M3A, M5A switched to their respective on-states/conducting states, zero volts is applied to the output electrodes 707, 707b irrespective of the polarity of the current delivered by the secondary side of the PT 704 through the output electrodes 707, 707b. With NMOS transistors M3A, M6A switched to their respective on-states/conducting states, minus V_{OUT} ($-V_{OUT}$) is applied to the output electrodes 707, 707b irrespective of the polarity of the ac current delivered by the secondary side of the PT 704 through the output electrodes 707, 707b.

CLAIMS

1. A bi-directional piezoelectric power converter comprising:

- a piezoelectric transformer comprising an input electrode electrically coupled to an input or primary section of the piezoelectric transformer and an output electrode electrically coupled to secondary or output section of the piezoelectric transformer to provide a transformer output signal,

- an input driver electrically coupled to the input electrode and arranged to supply an input drive signal with a predetermined excitation frequency to the input electrode,

- a bi-directional switching circuit coupled between the output electrode and an output voltage of the converter,

- a controller adapted to control first and second states of the bi-directional switching circuit based on the input drive signal or the transformer output signal such that:

- in a first state, forward current is conducted from the output electrode to the output voltage through the bi-directional switching circuit during a first period of a cycle time of the transformer output signal to charge the output voltage,

- in a second state, reverse current is conducted from the output voltage to the output electrode through the bi-directional switching circuit during a second period of the cycle time of the transformer output signal to discharge the output voltage and return power to the primary section of the piezoelectric transformer.

2. A bi-directional piezoelectric power converter according to claim 1, wherein the controller in the second state is further configured to control the switching circuit such that:

- both forward current and reverse current is conducted during a single cycle of the transformer output signal.

3. A bi-directional piezoelectric power converter according to claim 1 or 2, wherein the controller is adapted to terminate the second period of the cycle time synchronously to the input drive signal or synchronously to the transformer output signal.

4. A bi-directional piezoelectric power converter according to any of claims 1-3, wherein the controller is adapted to initiate the first period of the cycle time synchronously to the input drive signal or synchronously to the transformer output signal.

5. A bi-directional piezoelectric power converter according to any of claims 1-3, wherein the controller is adapted to:

- sense a current in, or a voltage across, an electrical component of the bi-directional switching circuit,
- initiate the forward current conduction in the first period of the cycle time in response to a sensed current or voltage so as to asynchronously initiate the forward current conduction.

6. A bi-directional piezoelectric power converter according to any of the preceding claims, wherein the bi-directional switching circuit comprises:

- a first controllable semiconductor switch arranged between the output electrode and the output voltage,
- a second controllable semiconductor switch arranged between the output electrode and a negative supply voltage; wherein the controller is configured to alternatingly switch the first and second controllable semiconductor switches to respective on-states and off-states in a non-overlapping manner to control the forward and reverse current conduction.

7 A bi-directional piezoelectric power converter according to claim 6, wherein the bi-directional switching circuit further comprises:

- a first semiconductor diode coupled across inlet and outlet nodes of the first controllable semiconductor switch to conduct forward current to the output voltage during at least a portion of the first period of the cycle time.

8. A bi-directional piezoelectric power converter according to claim 7, wherein the controller is configured to sense the forward current through, or the forward voltage across, the first semiconductor diode; and

- switch the first controllable semiconductor switch to the on-state in response to a sensed forward current or voltage so as to actively clamp the first semiconductor diode during the first period of the cycle time.

9. A bi-directional piezoelectric power converter according to any of the preceding claims, wherein the controller comprises an adjustable time delay circuit providing an adjustable duration of the second period of the cycle time of the transformer output signal.

10. A bi-directional piezoelectric power converter according to claim 9, wherein the controller is configured to derive a synchronous state control signal from the input drive signal; and

- apply the synchronous state control signal through the adjustable time delay circuit to a switch control terminal of the second controllable semiconductor switch and/or a switch control terminal of the first controllable semiconductor switch to control respective states of the first and second controllable semiconductor switches.

11. A bi-directional piezoelectric power converter according to claim 10, wherein the controller comprises:

- a self-powered driver coupled between the switch control terminal of the first controllable semiconductor switch and the output electrode of the output section;

- the self-powered driver comprising a timer circuit configured to control the state of the first semiconductor switch in accordance with a timer period setting; said timer period setting being based on the cycle time of the transformer output signal.

12. A bi-directional piezoelectric power converter according to claim 11, wherein the self-powered driver comprises a local energy storage component supplying power to the self-powered driver; and

- a rectifying element coupled between the local energy storage component and a power supply voltage of the power converter to energize the local energy storage component.

13. A bi-directional piezoelectric power converter according to claim 12, wherein the rectifying element comprises a high-voltage diode having a break-down voltage larger than 200 V, or more preferably larger than 500 V or larger than 1000 V.

14. A bi-directional piezoelectric power converter according to claim 12 or 13, wherein the self-powered driver is configured to start the timer in response to a change of bias state of the rectifying element.

15. A bi-directional piezoelectric power converter according to claim 13 or 14, wherein the timer period setting substantially equals 50 % of the cycle time the of the transformer output signal.

16. A bi-directional piezoelectric power converter according to any of claims 6-15, wherein the first and/or the second semiconductor switch comprises a semiconductor selected from the group of {MOSFET, IGBT, bipolar transistor, Gate Turn-off thyristor (GTO)}.

17. A bi-directional piezoelectric power converter according to any of claims 6-15, wherein the first semiconductor diode and/or the second semiconductor diode comprises a body/substrate diode integrally formed with the first or the second semiconductor switch, respectively.

18. A bi-directional piezoelectric power converter according to any of the preceding claims, wherein the controller is configured to controlling the switching between the first state and the second state based on a difference between the output voltage and a predetermined AC or DC reference voltage.

19. A bi-directional piezoelectric power converter according to any of the preceding claims, comprising a self-oscillating feedback loop arranged around the input driver and the piezoelectric

transformer, wherein the self-oscillating feedback loop is adapted to set the predetermined excitation frequency of the input drive signal.

20. A bi-directional piezoelectric power converter according to claim 19, wherein the self-oscillating feedback loop comprises an adjustable time delay configured to adjust a phase response of the self-oscillating feedback loop whereby the predetermined excitation frequency is adjusted.

21. A bi-directional piezoelectric power converter according to claim 19 or 20, wherein the self-oscillating feedback loop comprises a zero-crossing detector configured to supply a synchronization signal to the controller, said synchronization signal being synchronous to the input drive signal or the transformer output signal.

22. A method of increasing an apparent ZVS factor of a piezoelectric transformer of a power converter, comprising steps of:

- applying an input drive signal with a predetermined excitation frequency to an input electrode of the piezoelectric transformer,
- providing a bi-directional switching circuit coupled between a secondary or output section of the piezoelectric transformer and an output voltage of the power converter,
- conducting, in a first state, forward current from the output section to the output voltage through the bi-directional switching circuit during a first period of a cycle time of the transformer output signal to charge the output voltage,
- conducting, in a second state, reverse current from the output voltage to the output section through the bi-directional switching circuit during a second period of the cycle time of the transformer output signal to discharge the output voltage,
- adjusting the apparent ZVS factor of the piezoelectric transformer by adjusting a length of the second period of the cycle time.

23. A method of increasing an apparent ZVS factor of a piezoelectric transformer of a power converter, comprising a further step of:

- conducting both forward current and reverse current during a single cycle of the transformer output signal.

ABSTRACT

A bi-directional piezoelectric power converter comprising a piezoelectric transformer. The piezoelectric transformer comprises an input electrode electrically coupled to a primary section of the piezoelectric transformer and an output electrode electrically coupled to an output section of the piezoelectric transformer to provide a transformer output signal. A bi-directional switching circuit is coupled between the output electrode and a DC or AC output voltage of the power converter. Forward and reverse current conducting periods of the bi-directional switching circuit is based on the input drive signal or the transformer output signal such that a forward current is conducted from the output electrode through the bi-directional switching circuit to the DC or AC output voltage in a first state to charge the DC or AC output voltage. In a second state, a reverse current is conducted through the bi-directional switching circuit from the DC or AC output voltage to the output electrode to discharge the DC or AC output voltage and return power to the primary section of the piezoelectric transformer.

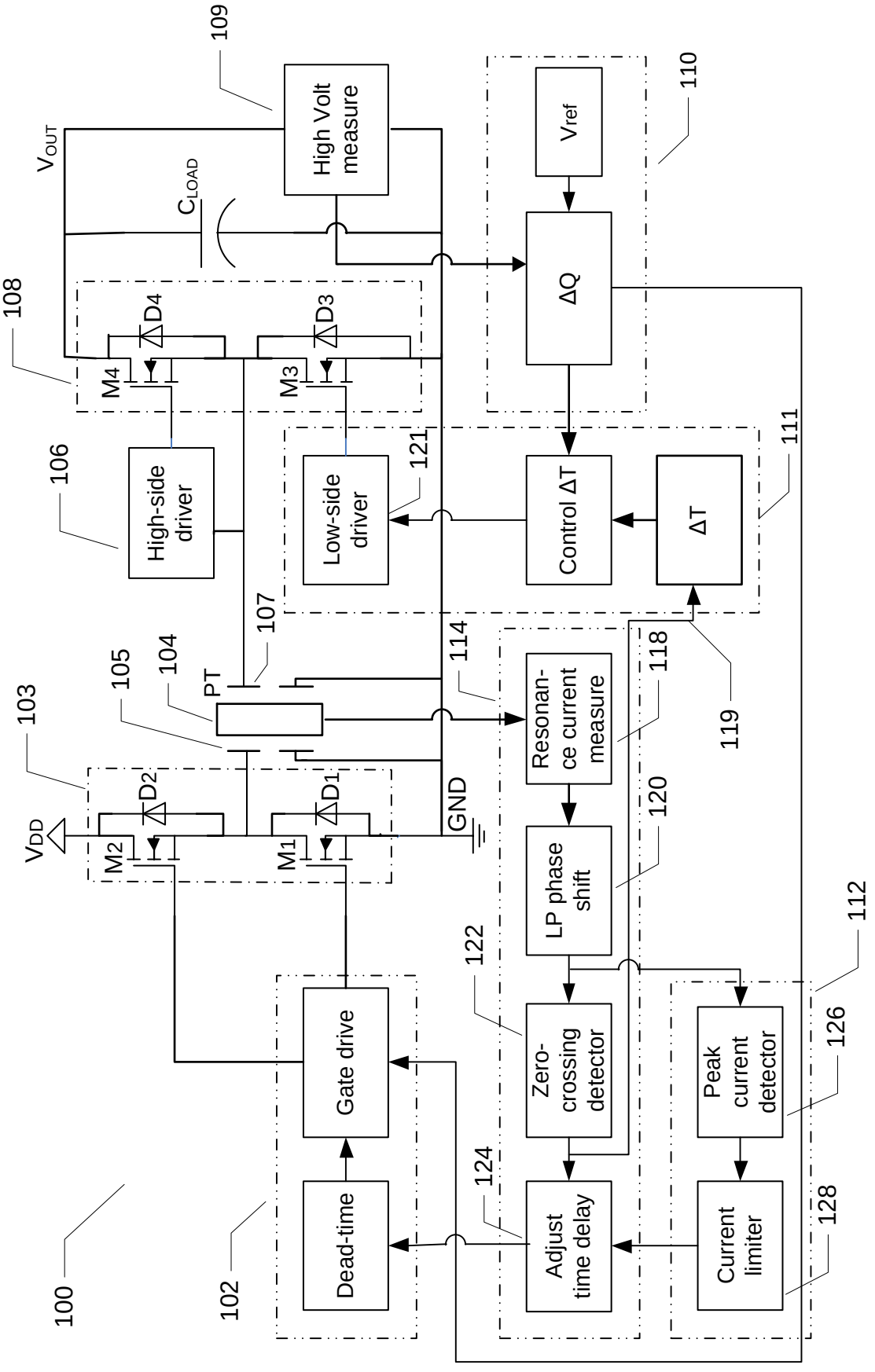
109
High Volt measure
V_{OUT}
C_{LOAD}
110
V_{ref}
ΔQ
108
D4
D3
M4
M3
106
High-side driver
Low-side driver
121
Control ΔT
ΔT
111
107
105
104
PT
114
Resonan-ce current measure
118
103
119
D2
D1
V_{DD}
M2
M1
GND
120
LP phase shift
122
112
Gate drive
Zero-crossing detector
Peak current detector
126
124
Dead-time
Adjust time delay
Current limiter
128
100
102

Fig. 1

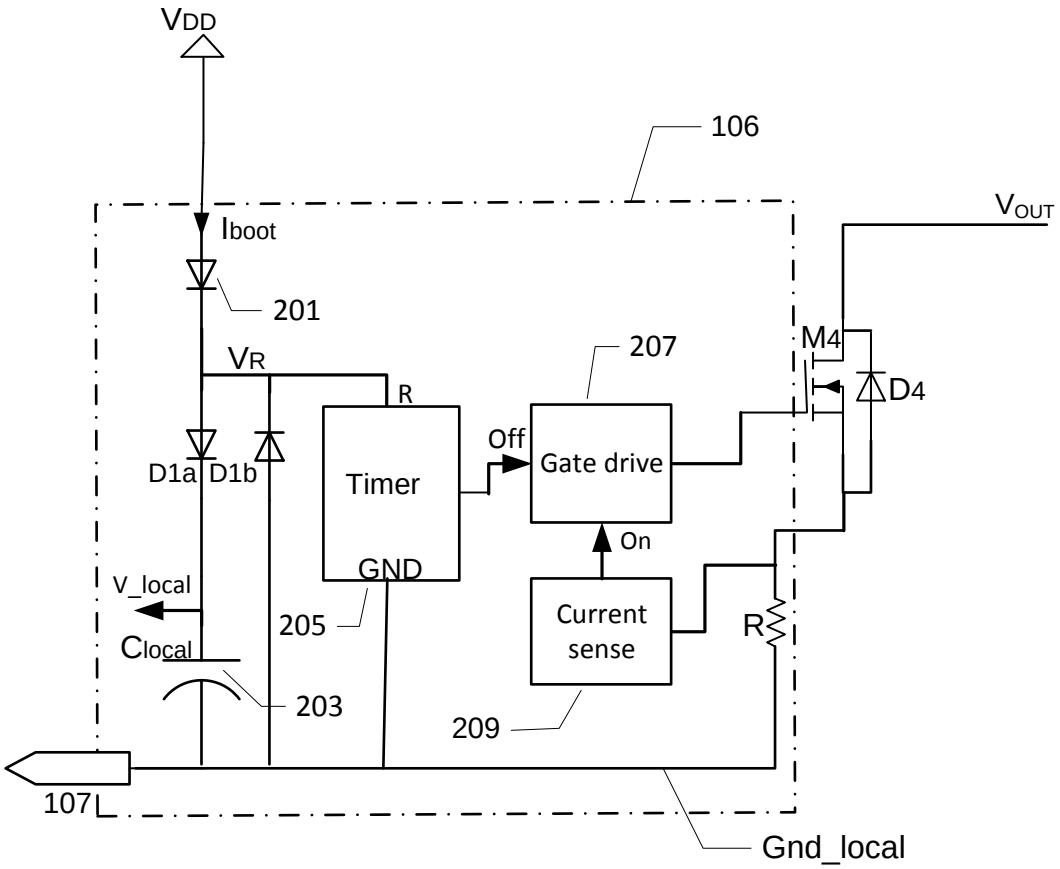
VDD
106
VOUT
Iboot
201
VR
207
M4
R
D4
D1a
D1b
Timer
Off
Gate drive
On
GND
V_local
205
Current sense
R
Clocal
203
209
107
Gnd_local

Fig. 2

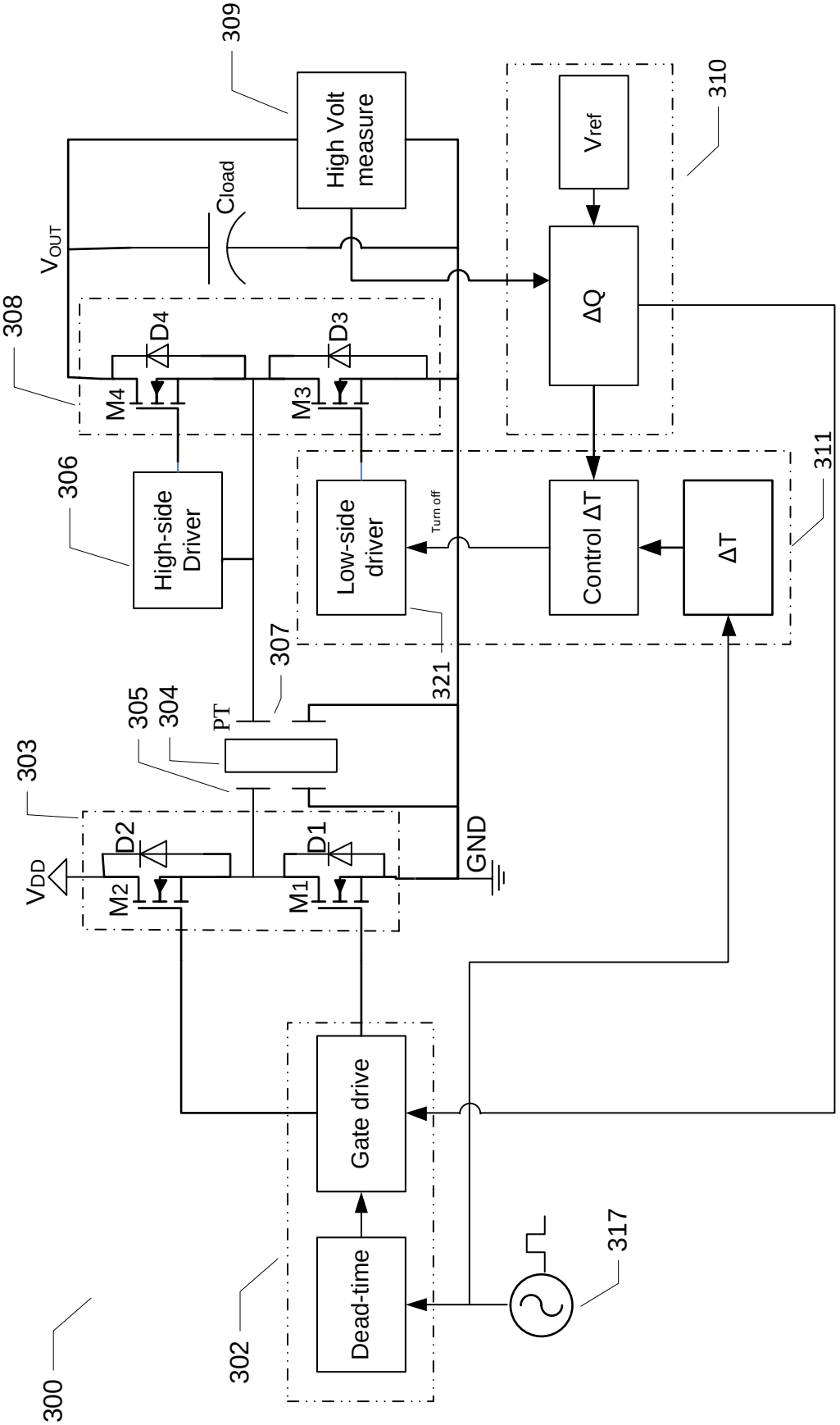
309
High Volt measure
Vref
310
Cload
VOUT
ΔQ
308
D4
D3
M4
M3
306
High-side Driver
Low-side driver
Turn off
Control ΔT
ΔT
311
307
321
305
304
PT
303
D2
D1
VDD
M2
M1
GND
Gate drive
Dead-time
317
302
300

Fig. 3

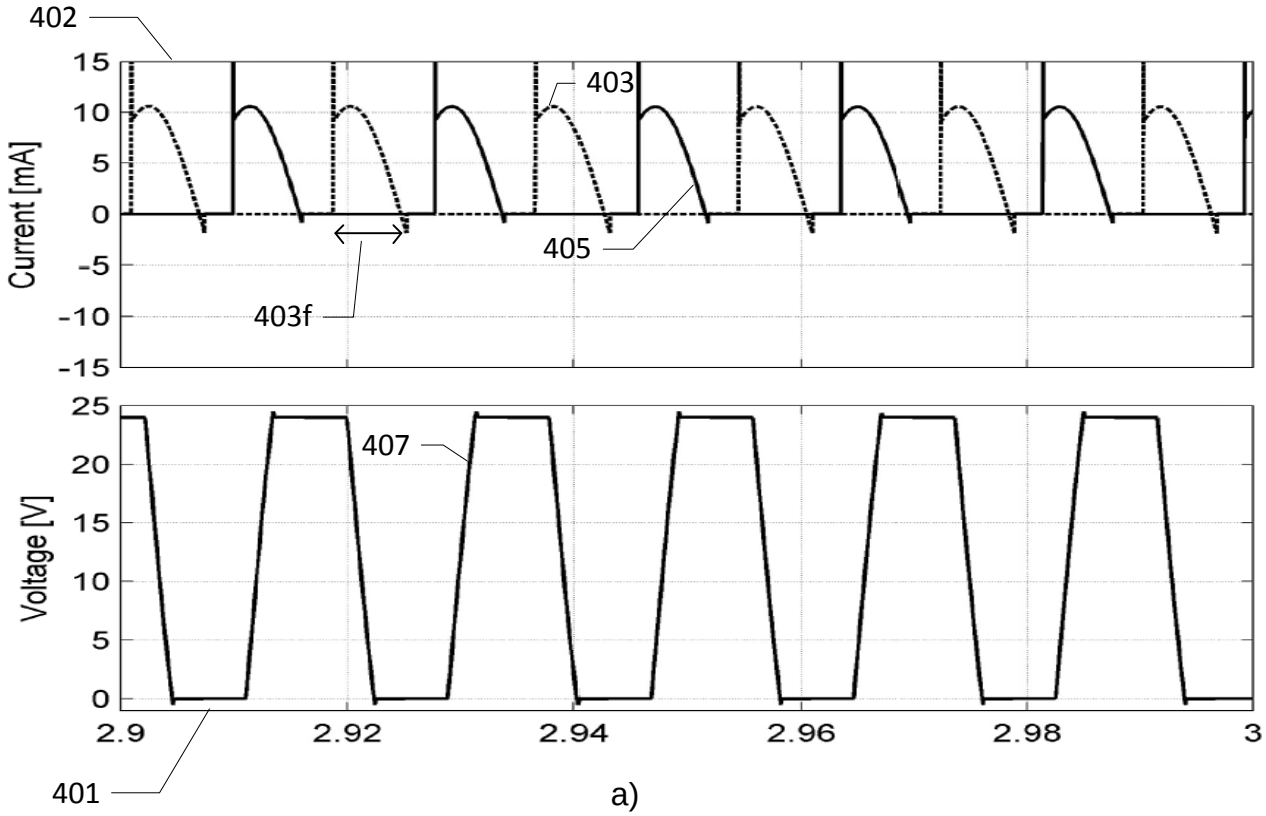
402
403
405
403f
407
401
Current [mA]
Voltage [V]
15
10
5
0
-5
-10
-15
25
20
15
10
5
0
2.9
2.92
2.94
2.96
2.98
3

a)

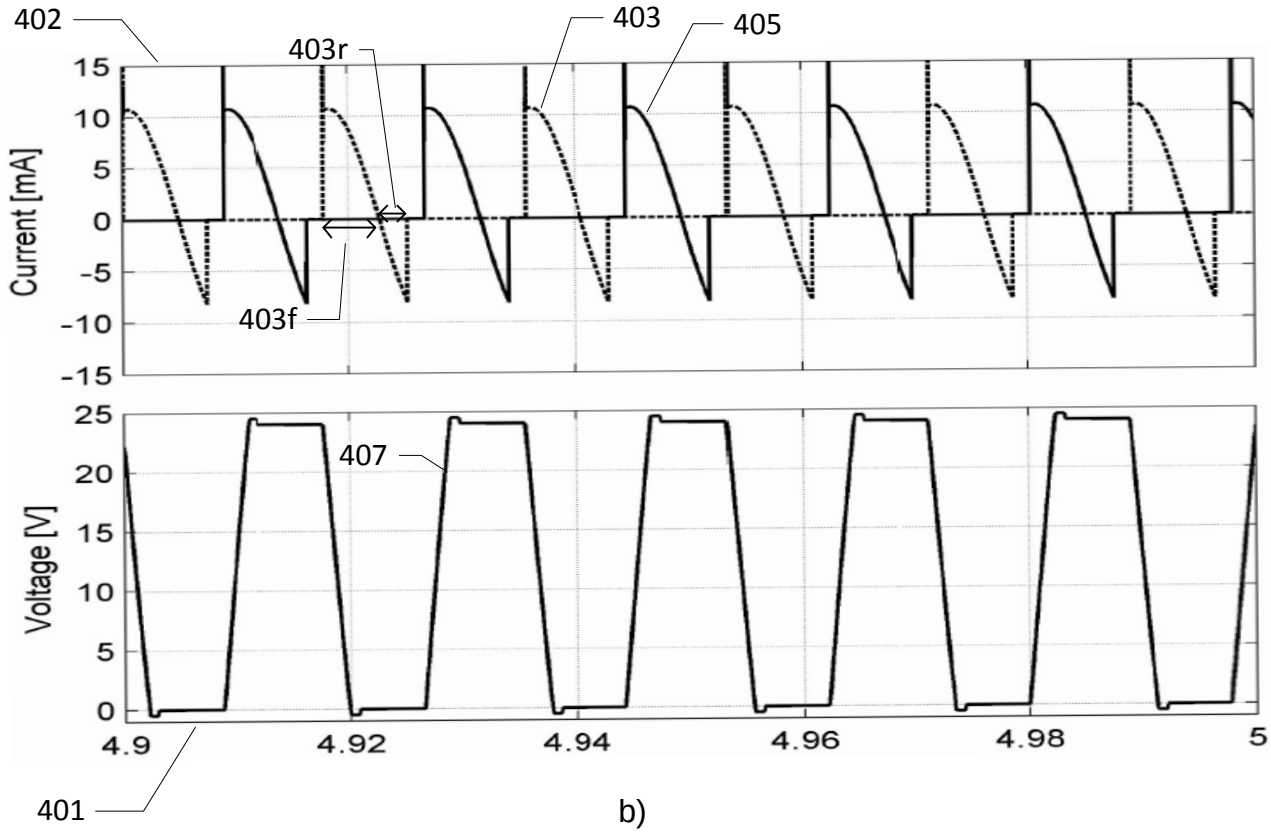
402
403r
403
405
403f
407
401
Current [mA]
Voltage [V]
15
10
5
0
-5
-10
-15
25
20
15
10
5
0
4.9
4.92
4.94
4.96
4.98
5

b)

Fig.4a)-b)

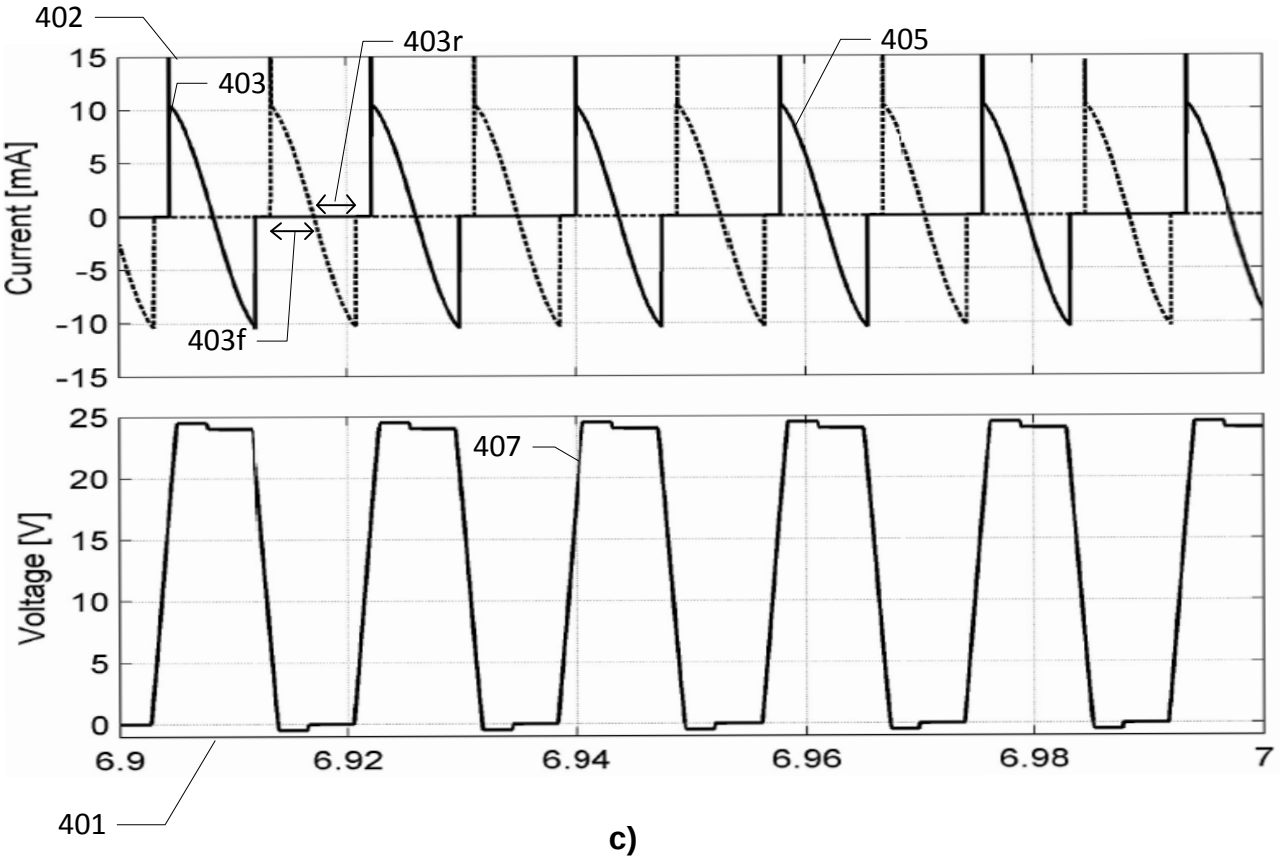
402
403r
405
403
Current [mA]
403f
407
Voltage [V]
401
c)

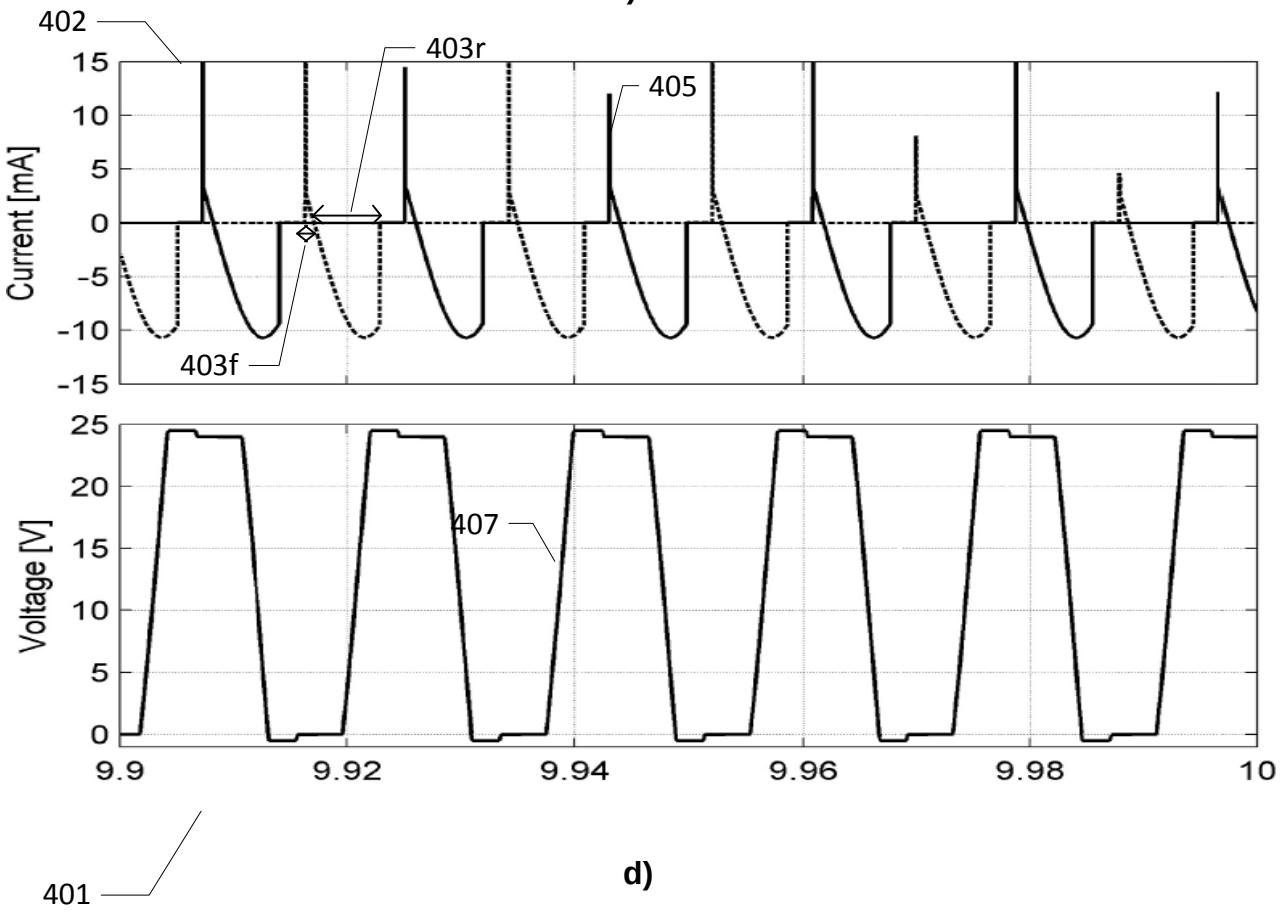
402
403r
405
Current [mA]
403f
407
Voltage [V]
401
d)

Fig. 4 c)-d)

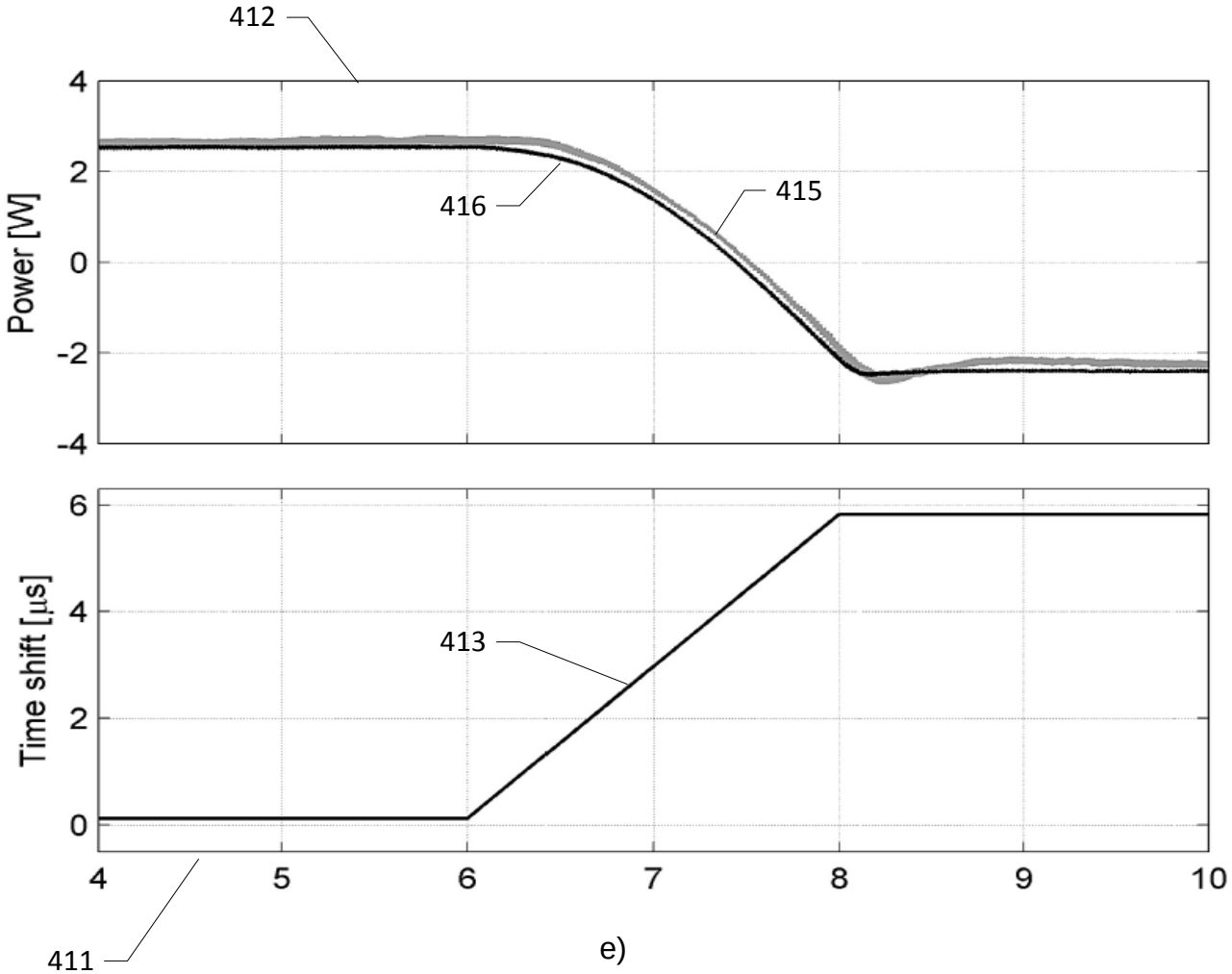
412
416
415
Power [W]
4
2
0
-2
-4
Time shift [µs]
6
4
2
0
413
4
5
6
7
8
9
10
411
e)

Fig. 4 e)

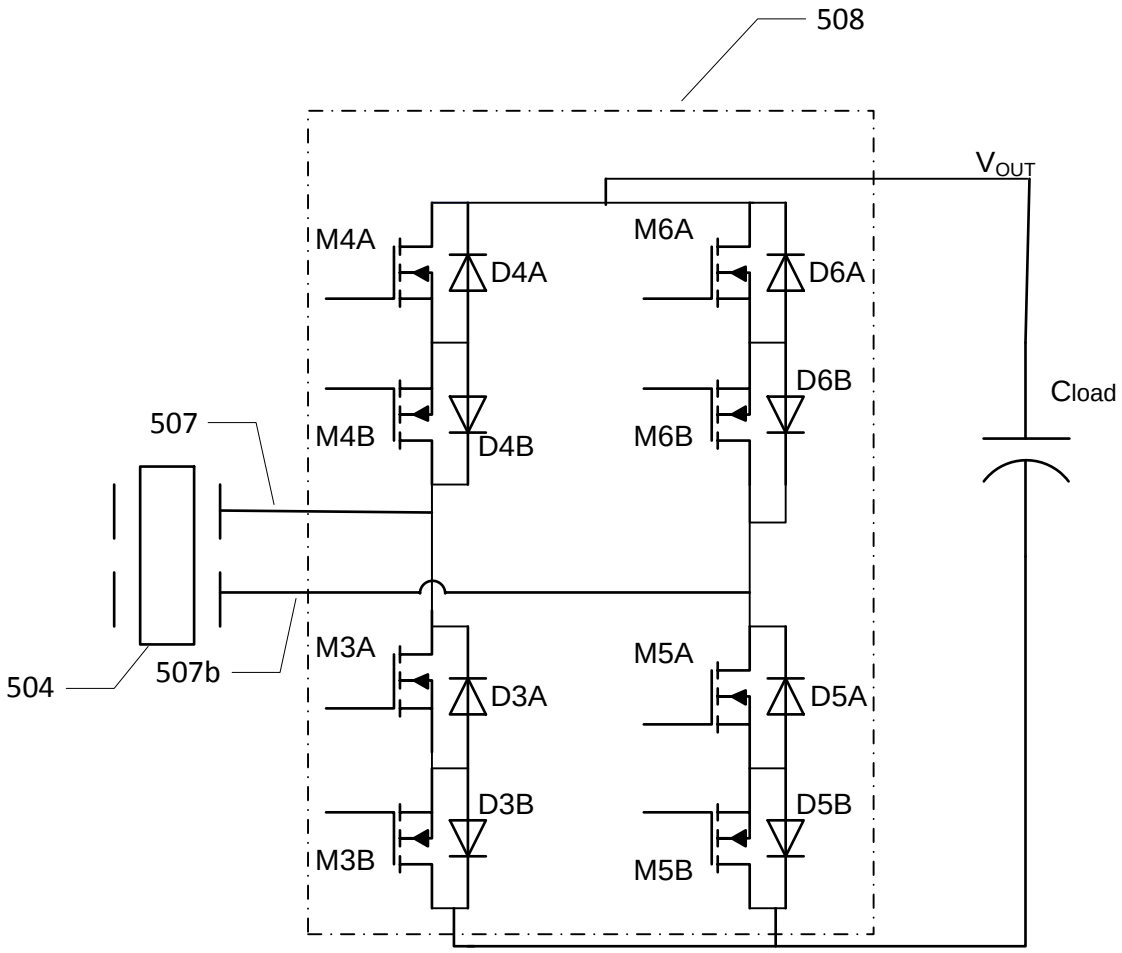
508
V_{OUT}
M4A
D4A
M6A
D6A
D6B
Cload
507
M4B
D4B
M6B
M3A
D3A
M5A
D5A
504
507b
D3B
D5B
M3B
M5B

Fig. 5

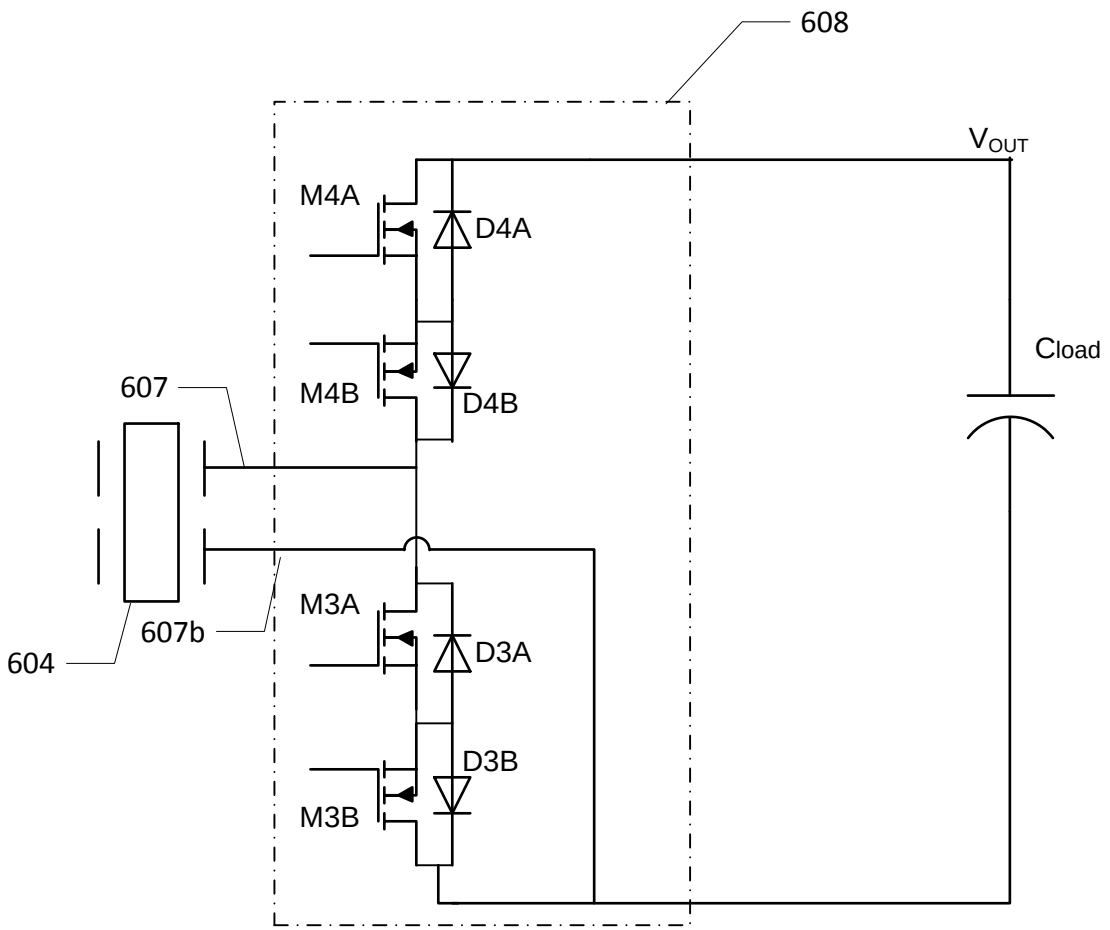

Fig. 6

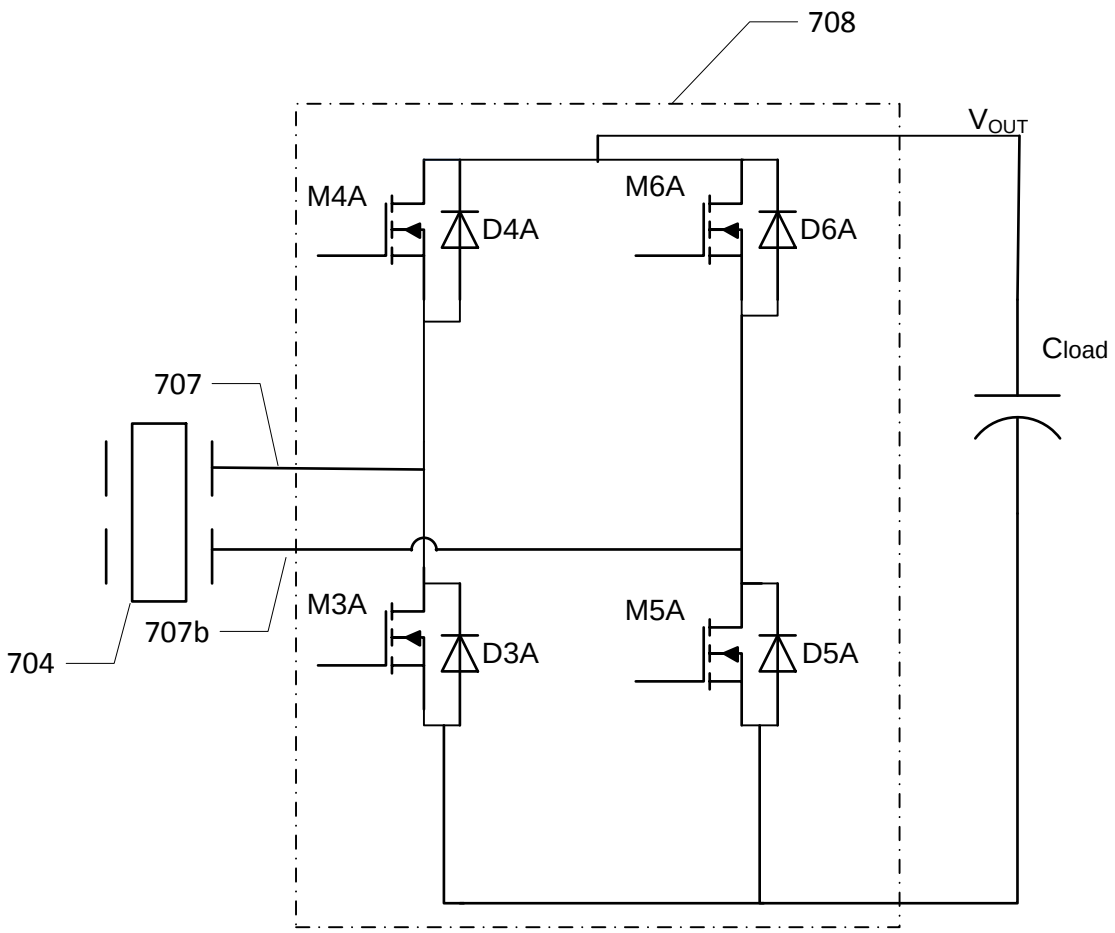

Fig. 7

www.elektro.dtu.dk
Department of Electrical Engineering
Electronics Group
Technical University of Denmark
Ørsteds Plads
Building 348
DK-2800 Kgs. Lyngby
Denmark
Tel: (+45) 45 25 38 00
Fax: (+45) 45 93 16 34
Email: info@elektro.dtu.dk

ISBN: 978-87-92465-69-6